February 2010

UNIVERSITY OF CANTERBURY
Te Whare Wānanga o Waitaha
CHRISTCHURCH NEW ZEALAND

Photo-activated Cytotoxins

A thesis submitted in partial fulfilment of the requirements
for the Degree of

Doctor of Philosophy in Chemistry

in the University of Canterbury

by

Alan Murray Downward

Acknowledgements

There are many people to whom I wish to extend my thanks and acknowledge the role they played during the course of my study. I would like to begin by thanking my supervisor Richard Hartshorn, for his support, advice and guidance during these last four years. Also thank you to the past and present members of the Hartshorn group.

Many thanks also go to the technical staff of the department, in particular Rob McGregor, Wayne MacKay and Marie Squire. For their assistance with X-ray crystallography, I need to thank Ward Robinson, Chris Fitchett, Chris Hawes, Jeni Burgess and Matt Polson. Thank you to Gill Ellis for running the cytotoxicity assays.

To my friends and family, your support has been treasured.

Finally I would like to acknowledge Tigist Dereje, who has only ever shown me love and support throughout the duration of my study.

Table of Contents

Abbreviations

A	absorbance
bheen	N,N′-bis(2-hydroxyethyl)ethane-1,2-diamine
bpy	2,2′-bipyridine
ceen	*N*-(2-chloroethyl)ethane-1,2-diamine
cisplatin	*cis*-diamminedichloroplatinum(II)
conc	concentrated
cyclam	1,4,8,11-tetraazacyclotetradecane
dil	dilute
DDD	dichlorodiphenyldichloroethane
DDT	dichlorodiphenyltrichloroethane
DMF	*N*,*N*-dimethylformamide
DMSO	dimethylsulfoxide
DNA	deoxyribonucleic acid
dpq	2,3-di(pyridin-2-yl)quinozaline
E. coli	*Escherichia coli*
en	ethane-1,2-diamine
ESI-MS	electrospray ionisation mass spectrometry
fac	facial
FTIR	Fourier transform infrared spectroscopy
gCOSY	gradient selected correlation spectroscopy
GS	ground state
heen	*N*-(2-hydroxyethyl)ethane-1,2-diamine

HSQCAD	heteronuclear single quantum coherence adiabatic
IC_{50}	half maximal inhibitory concentration
IR	infra-red
ISC	intersystem crossing
LMCT	ligand-to-metal-charge-transfer
M	moles per litre
^{3}MC	metal-centred triplet state
mer	meridional
MLCT	metal-to-ligand-charge-transfer
^{1}MLCT	metal-to-ligand-charge-transfer singlet state
^{3}MLCT	metal-to-ligand-charge-transfer triplet state
MMCT	metal-to-metal-charge-transfer
NMR	nuclear magnetic resonance
NOE	nuclear Overhauser enhancement
NOESY	nuclear Overhauser enhancement spectroscopy
phen	1,10-phenanthroline
phendione	1,10-phenanthroline-5,6-dione
phtp	3-(1,10-phenanthrolin-2-yl)-[1,2,4]triazino[6,5-f][1,10]phenanthroline
ppm	parts per million
py	pyridine
pytp	3-(pyridin-2-yl)-[1,2,4]triazino[5,6-f][1,10]phenanthroline
pytz	3,6-di(pyridin-2-yl)-1,2,4,5-tetrazine
pztp	3-(pyrazin-2-yl)-[1,2,4]triazino[5,6-f][1,10]phenanthroline

pztz	3,6-di(pyrazin-2-yl)-1,2,4,5-tetrazine
tbbpy	4,4′-di-*tert*-butyl-2,2′-bipyridine
OTf	trifluoromethanesulfonate
THF	tetrahydrofuran
TMPS	sodium 3-(trimethylsilyl)-1-propane sulfonate
TMS	tetramethylsilane
tpphz	tetrapyrido[3,2-a:2′,3′-c:3″,2″-h:2‴,3‴-j]phenazine (tpphz)
tpy	2,2′:6′,2″-terpyridine
tren	tris(2-aminoethyl)amine
ttp	4-(*p*-tolyl)-2,2′:6′2″-terpyridine
UV	ultraviolet
vis	visible

List of Figures

List of Tables

Abstract

The thesis addresses the potential application of ruthenium(II)-cobalt(III) heterodinuclear complexes as a new selective cancer treatment. The selectivity is to be achieved through the use of visible light to trigger activation of the drug.

The majority of work conducted relates to the design and synthesis of the bridging ligand for the final ruthenium(II)-cobalt(III) heterodinuclear complex. In Chapter 2, a potential bridging ligand based on a functionalised terpyridine is described. The intention was to bind the ruthenium(II) metal centre to the terpyridine end of the bridging ligand and have a secondary binding domain available for coordination of the cobalt(III) metal centre. However, a reductive step in the synthetic pathway failed to produce the desired product and this potential bridging ligand had to be abandoned.

In Chapter 3, two series of bridging ligands are described. The first of these series is based on Jurgen Sauer's 'LEGO' system. In addition to describing the free synthesis of these ligands, their synthesis on a ruthenium(II) metal centre is described. The second series is based on disubstituted-1,2,4,5-tetrazines. These compounds are only able to be directly synthesised as the non-coordinated ligand. Coordination of these ligands to a single ruthenium(II) metal centre is then described. Ruthenium(II) complexes of both ligand series are then exposed to several transition metals and their ability to coordinate a second metal centre investigated.

The formation of ruthenium(II)-cobalt(III) heterodinuclear complexes, using the ligand series detailed in Chapter 3, is described in Chapter 4. These complexes are formed by reacting the ruthenium(II) complex of the bridging ligand with either $[Co(en)_2(OTf)_2](OTf)$ or $[Co(tren)(OTf)_2](OTf)$. These heterodinuclear complexes exhibit photo-activated ligand release, which makes them candidates for development as a potential cancer treatment.

Abstract

The non-bridging ligands coordinated to the cobalt(III) metal centre in Chapter 4 were not cytotoxic. In order to make the system biologically active these ligands need to be changed. Chapter 5 describes how nitrogen mustards (a class of cytotoxic DNA alkylators) could be introduced as the non-bridging ligands. This involves the synthetic strategy of forming the cobalt(III) complex of the alcohol precursor of a nitrogen mustard. This precursor complex is then converted into the nitrogen mustard complex and coordinated to the ruthenium(II) bound bridging ligand.

The synthetic strategies outlined in this thesis can be applied to a wide range of potential bridging ligands and could potentially lead to a large number of ruthenium(II)-cobalt(III) heterodinuclear complexes being synthesised.

One journal article based on this research has been accepted for publication, in the Australian Journal of Chemistry. Three more articles are in preparation.

Chapter 1: Introduction

1.1. Introduction

During 2005 there were 18,610 new cancer registrations and 7,971 deaths from cancer recorded in New Zealand.[1] This means that in 2005 cancer accounted for 29.4 % of all deaths and was the leading cause of death in New Zealand. This makes research into new methods of cancer treatment both topical and important.

The development of new cancer treatments provides medical practitioners with more options when treating a cancerous growth. Additional benefit may also be gained through a decrease in the negative side effects generally associated with cancer treatments.

1.2. Differences between Malignant Tumours and Healthy Tissue

A tumour is an abnormal tissue growth or mass that serves no useful purpose. In the case of a malignant tumour there is rapid growth of the mass and destruction of normal cells. The tumour may also spread to other parts of the body and is life threatening. The rapid growth causes the structure of the tumour to be highly irregular; blood vessels within the mass are a mixture of those that originally belonged to healthy tissue that the tumour invaded, and the tumour's own microvessels. Therefore the blood vessels within the tumour are highly irregular, tortuous and develop abnormalities such as arterio-venous shunts, blind ends, a lack of smooth muscle, and incomplete endothelial linings and basement membranes. The end result is that the tumour has poor vasculature throughout and the vessels are 'leaky' when compared to blood vessels in normal tissue.[2]

The poor vasculature results in insufficient amounts of oxygen being able to diffuse to all cells in the tumour and the formation of hypoxic and even necrotic regions (Figure 1.1).

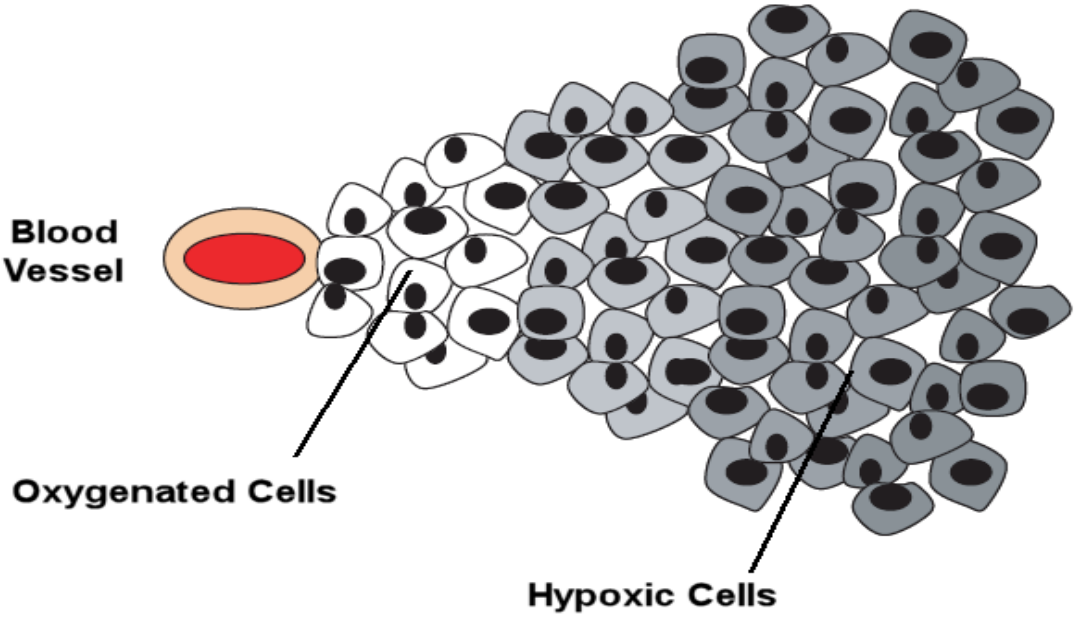

Figure 1.1 Hypoxia in tumours, the more hypoxic regions are shaded darker[3]

In addition to a decrease in oxygen levels associated with an increase in distance to nearest blood vessel, there is also a decrease in pH. It is believed that the main reason for this decrease in pH is the hydrolysis of adenosine triphosphate.[4, 5] Unfortunately some drugs, such as doxorubicin, are absorbed less readily and are less cytotoxic at lower pH.[6] This means that these treatments are less effective against the hypoxic regions of the tumour. In addition to this, because the drug needs to diffuse further to reach these areas the dose received is also lower. Unfortunately, exposure to non-lethal concentrations of a chemotherapeutic agent can also result in the development of resistant tumours.

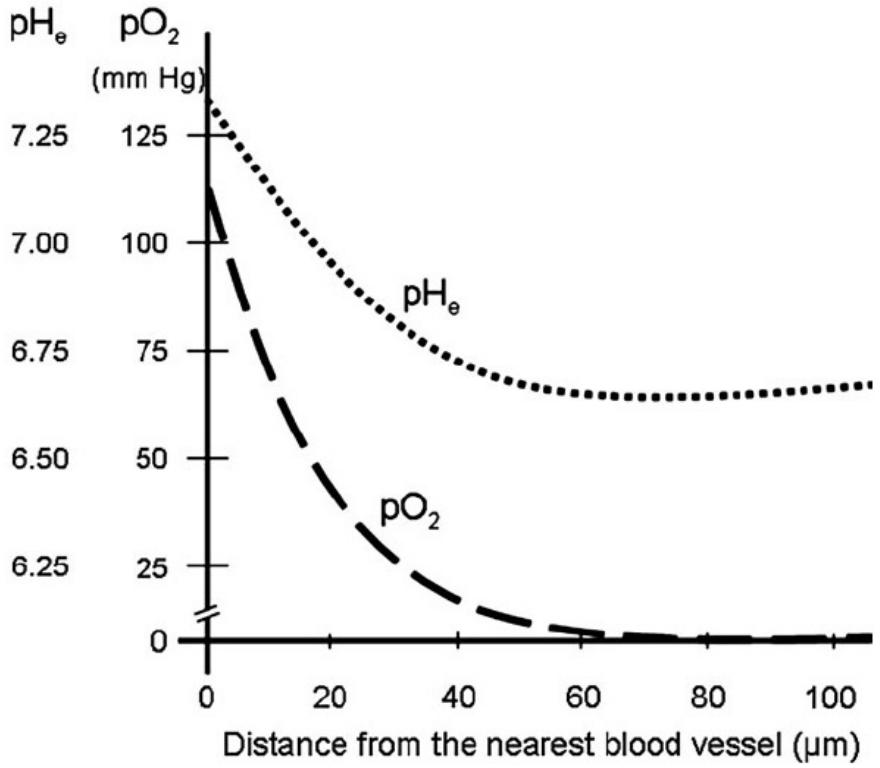

Figure 1.2 Oxygen concentration and pH in relation to distance to nearest blood vessel[7]

A further consideration when targeting a cancerous growth is the leaky vasculature. The incomplete endothelial lining and basement membranes result in the tumour vessels being more permeable to large molecules. It has been observed that these defects result in the tumour being permeable by liposomes 400 nm in diameter, but not by liposomes 600 nm in diameter.[8] This suggests that the average size of the pores in tumour vessels is between 400 and 600 nm. It is possible that the pore size is smaller than this and that the liposomes are deforming to pass through. However, prior measurements of the average pore size in rat liver tissue using a scanning electron microscope found that the periportal fenestrae (pores around the portal veins) have an average diameter of 106 nm. The same study found that the hepatocytes will take up liposomes up to around 100 nm in diameter and that larger liposomes are taken up by the macrophagic Kupffer cells.[9] These observations are consistent with the

proposal that pore diameter can be estimated to be the same as the diameter of the largest liposome that can pass through.

These differences between healthy tissue and malignant tumours provide both an impediment to effective treatment, as well as a possible basis for targeting the cancerous growth through chemotherapy.

1.3. Origins of Chemotherapy

Chemotherapy is the use of highly toxic drugs to treat or control cancer cells, either by interfering with their growth or preventing their reproduction.[10] The origins of modern chemotherapeutic agents date back to the First World War. Mustard gas was used as a chemical warfare agent, causing severe irritation to the skin, eyes, and respiratory system and resulting in blistering and skin ulcers. However, after the war ended, it was discovered that in addition to its vesicant properties, mustard gas was toxic towards blood and bone marrow.[11] The active ingredient of mustard gas is the sulfur mustard bis(2-chloroethyl)sulfide, a colourless odourless liquid in its pure form. However, the impure form is coloured, usually yellow, and has an odour resembling mustard plants, hence the name.

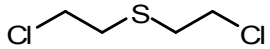

Figure 1.3 bis(2-chloroethyl)sulfide (mustard gas)

The 1925 Geneva Protocol banned the war time use of toxic gases. However, this did not stop military studies with the gas from continuing. In 1946, after the end of the Second World War, Goodman et al[12] revealed that they had been conducting war time studies involving the effects of nitrogen mustards on lymphomas. The publication of their results had to be delayed because of war time secrecy and when finally published gave medical practitioners a method of treatment besides surgery and radiation therapy.[13] In addition to

providing medical practitioners with a new treatment regime, the publication gave rise to the concept that a chemical which shows toxicity towards normal tissues could potentially be used in the treatment of neoplastic disease.

The drug Mitotane (**1.1**), used in the treatment of adrenocortical carcinoma, is another example of observed toxicity towards normal cells resulting in the discovery of an effective treatment for abnormal cells. Nelson and Woodard,[14] while evaluating the toxicity of insecticides, observed that crude dichlorodiphenyldichloroethane (DDD) caused atrophy of the adrenal cortex. DDD, which is very similar to the insecticide DDT (**1.2**) (dichlorodiphenyltrichloroethane), was then studied for use as a chemotherapeutic agent. The active compounds were found to be the *o,p′* isomers of DDD, which are now marketed as the drug Mitotane (Figure 1.4).[15]

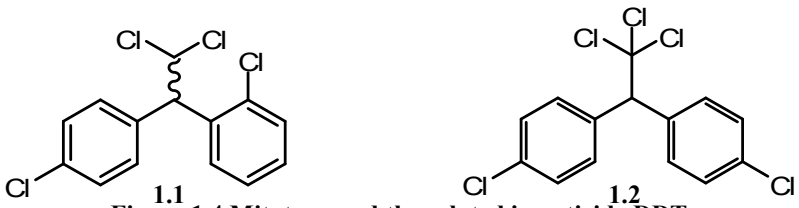

1.1 **1.2**

Figure 1.4 Mitotane and the related insecticide DDT

Because of the well established history of poisoning associated with metal based treatments, especially with heavy metals, many prejudices had to be overcome before the field of medicinal metal complexes would come into its own. One of the earliest metal containing treatments for cancer, dating back to 1786, was a 1% solution of potassium arsenite known as Fowler's solution. This is a highly toxic solution which causes cirrhosis of the liver as well as other cancers to form.[16]

The origins of the first successful metal based chemotherapeutic agents lie not in war or toxicity trials but rather in serendipity. Barnett Rosenberg, while examining the influence of an electric field on bacterial growth, observed that the *E. coli* bacteria grew up to 300 times

their own length without cell division. The platinum electrodes being used in these studies were submerged in an electrolyte solution containing ammonium chloride. This resulted in the formation a range of platinum species, including ammonium hexachloroplatinate(IV), which could be then photochemically converted into *cis*-diamminetetrachloroplatinum(IV). Through additional experiments with platinum complexes and *E. coli*, Rosenberg was able to demonstrate that it was *cis*-diamminetetrachloroplatinum(IV) that was causing the abnormal cell growth (Figure 1.5). [17, 18]

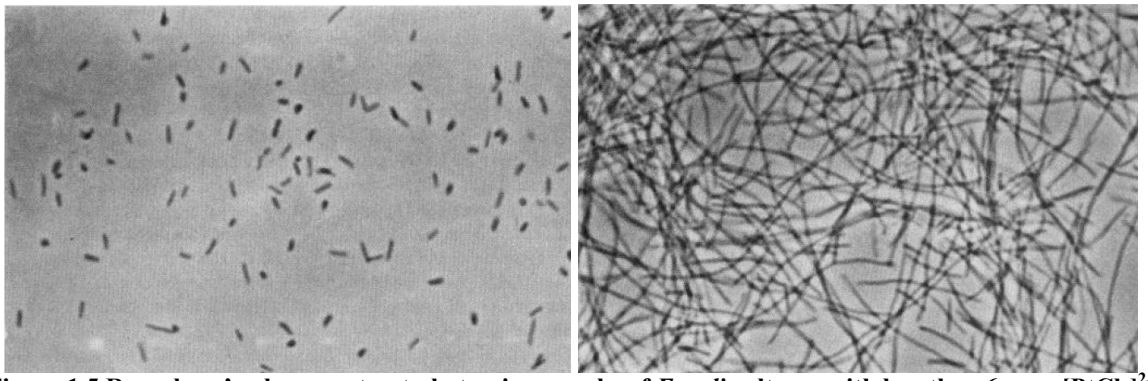

Figure 1.5 Rosenberg's phase contrast photomicrographs of *E. coli* cultures with less than 6 ppm $[PtCl_6]^{2-}$ and with 8 ppm *cis*-$[PtCl_4(NH_3)_2]$

Following on from this, Rosenberg synthesised a range of simple platinum complexes, including *cis*-diamminedichloroplatinum(II) (cisplatin). Using these complexes he was able to achieve a reduction in tumour weight and increase the lifespan of the animal test subjects.[19] Cisplatin is still used today and is highly effective against testicular and ovarian carcinomas as well as bladder, head and neck tumours.[16]

Thanks to the work of Rosenberg, the reluctance to use metals in the treatment of disease was overcome and the field of metal-based chemotherapy was opened up. Today a wide range of compounds containing metals such as ruthenium, gold, gallium, titanium, tin, iron and cobalt are used and/or examined as possible cancer treatments.

1.4. Effect of Chemotherapeutic Agents on DNA

Most chemotherapeutic agents interact with DNA in some manner. These interactions can be either indirect or direct. Indirect interactions involve interference with the precursors and biochemical apparatus necessary for DNA synthesis while direct interactions can be summarised as occurring through intercalation, outer-sphere binding, inner-sphere binding and strand breakage.

Intercalation involves the insertion of a planar molecule between two DNA base pairs; this process is primarily driven by π stacking and electrostatic interactions.[20] This binding mode distorts the DNA structure; however, the actual mechanism by which intercalating chemotherapeutic agents operate is through strand breakages resulting from the inhibition of the religation step of DNA topoisomerase II.[20, 21]

Outer sphere binding occurs through the interaction of the negatively charged backbone of the DNA double helix and positively charged molecules.[22] It has been well established that octahedral cobalt(III) complexes are capable of these types of interactions.[23]

Inner sphere binding involves the formation of covalent bonds to the bases of DNA. This interaction is a very common between transition metals and DNA.[22]

Strand breakage can occur for a variety of reasons. As mentioned previously, intercalation can cause strand breakage through its interaction with DNA topoisomerase II. In addition to this, strand breakage can occur through redox and hydrolytic reactions.

1.4.1. Nitrogen Mustards

Nitrogen mustards are a class of DNA alkylating agents and were the first clinically effective cancer chemotherapeutic agents. The first nitrogen mustard drug was mechlorethamine and it is still in use today (Figure 1.6).

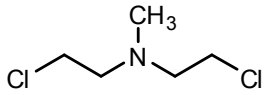

Figure 1.6 Mechlorethamine

Mechlorethamine's major clinical use is in the treatment of Hodgkin's disease. The cytotoxicity results from its ability to crosslink DNA. All nitrogen mustards either mono-alkylate or crosslink DNA and this can often trigger apoptosis. This alkylation occurs in a two step process. First a cationic cyclic intermediate is formed by the lone pair on the nitrogen atom displacing a chloride ion, followed by nucleophilic attack from DNA onto the cyclic intermediate (Figure 1.7).

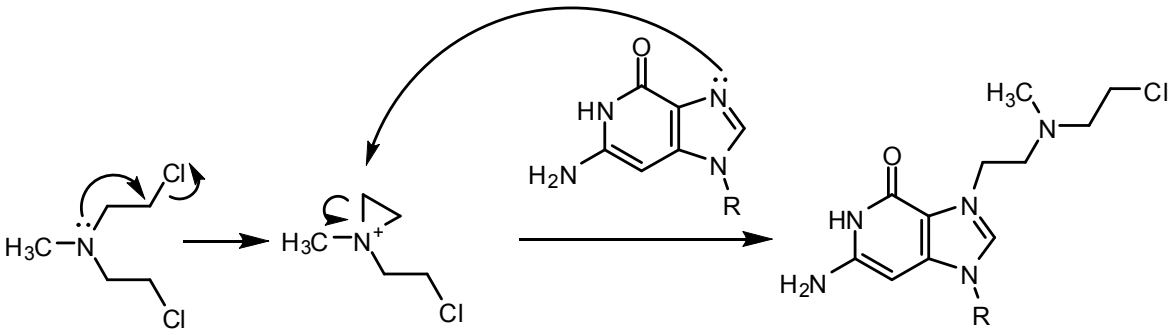

Figure 1.7 Alkylation of DNA by a nitrogen mustard

The biggest problem associated with nitrogen mustards is their lack of specificity for cancerous growths. Instead, they result in a high degree of DNA alkylation in the major groove at the N7 position of guanine.[24] In order to try and improve the selectivity of nitrogen mustards there has been a lot of work conducted on the development of prodrugs; compounds that will be selectively transformed into nitrogen mustards after administration.

1.4.2. Cisplatin

Cisplatin is the gold standard of metal based chemotherapeutic agents. Its activity was first discovered in 1969, and it has since become established as a highly effective drug for the treatment of testicular tumours (Figure 1.8), ovarian carcinomas, bladder tumours and head and neck cancer. In addition to this, it has also shown activity towards lung cancers, lymphomas, breast cancer, and oesophageal cancer as well as several other tumour types.[25]

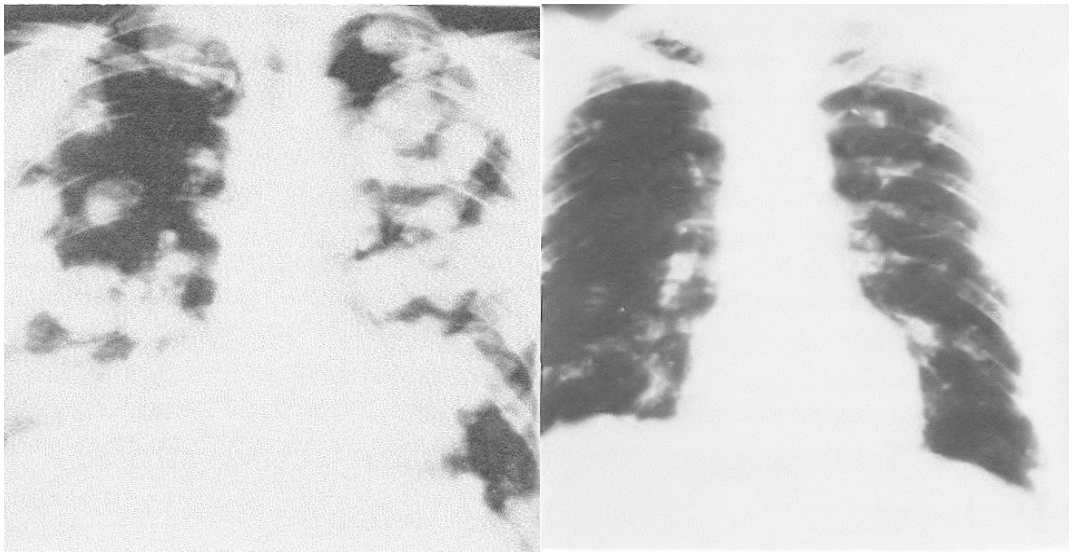

Figure 1.8 Lung metastases of a testicular cancer patient before and after receiving 4 cycles of cisplatin-containing chemotherapy[16]

An additional benefit of cisplatin is the marked synergy shown when combined with other chemotherapeutic agents; thus enabling more flexibility in the design of drug regimens. The major disadvantage associated with the use of cisplatin is the persistence of severe toxic side effects.[26] A review of 32 chemotherapeutic agents for nephrotoxicity found that cisplatin posed the highest risk.[27] This risk can be minimised by the use of hydration, diuretics and sulfur nucleophiles, as this lowers the concentration of the active drug in the kidneys.

Because of the success of cisplatin, a lot of work has gone into testing analogous chemicals to develop structure-activity relationships. The primary aim of these studies is to

develop active complexes that are less toxic than cisplatin; an example of such a drug is carboplatin (Figure 1.9).

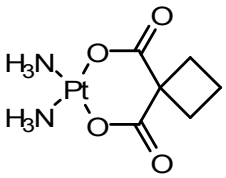

Figure 1.9 Carboplatin

The toxic side effects of carboplatin are much milder than those associated with cisplatin; there is no neurotoxicity, gastrointestinal effects are milder and there is considerably less damage to the kidneys. Because of the reduced nephrotoxicity, and therefore lack of need for hydration, carboplatin can be administered on an outpatient basis.

The platinum-based chemotherapeutic agents all interact with DNA in the same manner. The first step is aquation, where at least one of the leaving groups is replaced with water. The platinum then binds to DNA, initially forming a monofunctional adduct. Platinum binding to DNA is irreversible and as such any observed selectivity must arise through preassociation and kinetic control. The platinum then binds to the DNA a second time, possibly after a second aquation step, resulting in the formation of both interstrand and intrastrand bifunctional adducts. This cross-linking results in the deformation of the DNA strand and ultimately results in cell death, most probably *via* apoptosis.[28]

1.4.3. Ruthenium Complexes

Platinum group transition metals have a relatively high affinity for the lone pairs on most nitrogen ligands; this includes those which occur in important classes of biomolecules such as proteins and nucleic acids. The wide variety of complexes capable of being formed makes ruthenium a very promising chemotherapeutic agent.[29]

The observed mutagenic effects of ruthenium complexes indicated to early researchers that DNA was the target molecule for ruthenium based anticarcinogens and provided a valuable working hypothesis for the design of new drugs.[30] Since then, ruthenium complexes have been shown to interact with DNA through a variety of mechanisms such as coordination to the base pairs, or as a groove binder, metallointercalator (complexes that unwind DNA in order to π-stack between two base pairs) or metalloinsertor (complexes that eject the bases of a single base-pair, with their planar ligand acting as a π -stacking replacement in the DNA base stack) (Figure 1.10). The type of interaction is determined by the coordinated ligands. Ruthenium complexes with monodentate ligands, such as $[Ru(NH_3)_5Cl]Cl_2$, coordinate to DNA. However, the formation of coordination bonds between nucleic acids and cationic ruthenium compounds is likely to be preceded by electrostatic interactions, such as outer sphere binding to the negatively charged phosphate backbone. Ruthenium(II) complexes with three bidentate aromatic ligands are more likely to non-covalently interact with DNA. Depending on the ligands that are coordinated to the ruthenium centre, the complex may be chiral, and this chirality can in turn affect the way that the metal interacts with the DNA.[31, 32]

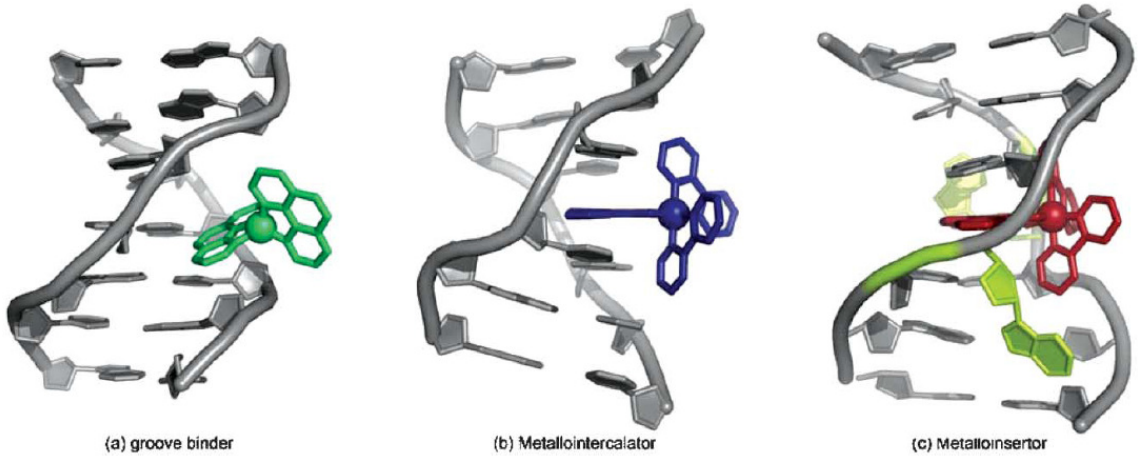

Figure 1.10 Non covalent binding modes of metal complexes to DNA[32]

It has also been shown that many diruthenium complexes will associate with non-duplex DNA and RNA structures such as bulges, junctions and hairpin loops. These studies have shown that the nature of the bridging ligand, flexible or rigid, as well as the terminal ligands and their coordination geometry all affect the selectivity of the complex for a specific feature.[33]

There are several key differences between ruthenium and most of the platinum based anticancer drugs. Firstly, ruthenium complexes are usually six coordinate with an octahedral geometry as opposed to the square planar arrangement of platinum(II) complexes. Secondly, the facility with which electron transfer takes place for ruthenium(II)-ruthenium(III) as opposed to platinum(II)-platinum(IV), which undergoes both a change in coordination number and bond distance, means that ruthenium complexes are more capable of causing strand cleavage through a redox pathway. Finally, ruthenium compounds are known to be less toxic than their platinum counterparts.[34]

Two ruthenium-based anticancer drugs, NAMI-A and KP1019 (Figure 1.11), have successfully completed phase I clinical trials for the treatment of metastatic tumours and colon cancers. It is believed that these drugs select for cancerous tissue by mimicking iron ions. Since rapidly dividing cells have a greater demand for iron, this results in the ruthenium complexes being more effectively delivered. In the case of NAMI-A, the dose-limiting toxicity was the formation of painful blisters, while KP1019 had comparatively mild side effects. Although the mechanism of cytotoxic action is not known, it is believed to involve activation of the complex by reduction from ruthenium(III) to ruthenium(II) inside the tumour.[34, 35, 36]

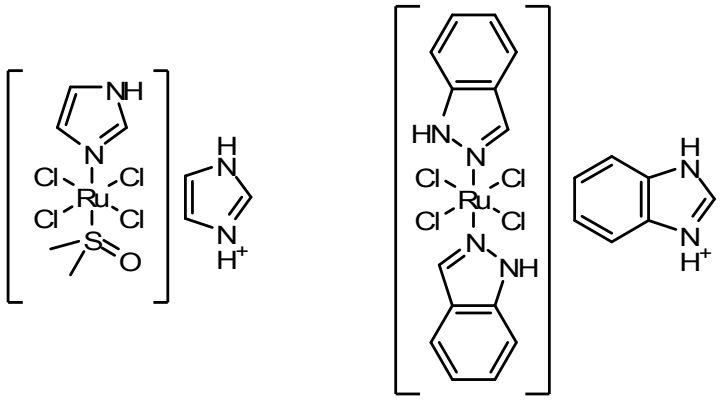

NAMI-A KP1019

Figure 1.11 Structure of NAMI-A and KP1019

1.5. Targeted Treatment of Cancerous Cells

Since chemotherapy uses highly toxic chemicals, the targeting of cancerous cells in preference to non-cancerous cells is essential for developing successful treatments. In order to achieve this selectivity, most traditional treatments have focused on exploiting the differences between healthy and cancerous cells. For most chemotherapeutic agents the primary form of discrimination is achieved by targeting the rapid proliferation of the cancerous cells.[2, 3, 37]

However, there are limitations associated with this type of selectivity. The dosage is limited by the cytotoxic effects of the drug on normal cells, especially bone marrow, hair follicles, and epithelial cells lining the gastrointestinal tract.[2] Over time, tumours can develop a resistance to the drug, which can arise through mutations, changes in uptake, metabolism, or the limited ability of the drug to penetrate the tumour.[7] Also, not all tumours, or parts of tumours, are fast growing and may not be targeted by traditional chemotherapy agents.

One way to circumvent the problems associated with chemotherapy is through the development of prodrugs, compounds that become active after administration. The advantage of using a prodrug is that it can lead to optimisation of the absorption, distribution and metabolism of the active compound. In addition, the use of prodrugs often results in an

increase in selectivity towards the intended target, which can reduce the negative side effects associated with treatment.

An example of a prodrug currently being used in chemotherapy is cyclophosphamide. Cyclophosphamide is oxidized in the liver by the mixed function oxidase system[38] into 4-hydroxycyclophosphamide, and the ring opened aldophosphamide. The biologically active nitrogen mustard phosphoramide is then produced by a β elimination of the aldophosphamide (Figure 1.12).[39, 40] This mustard then alkylates and crosslinks DNA and this ultimately leads to apoptosis.

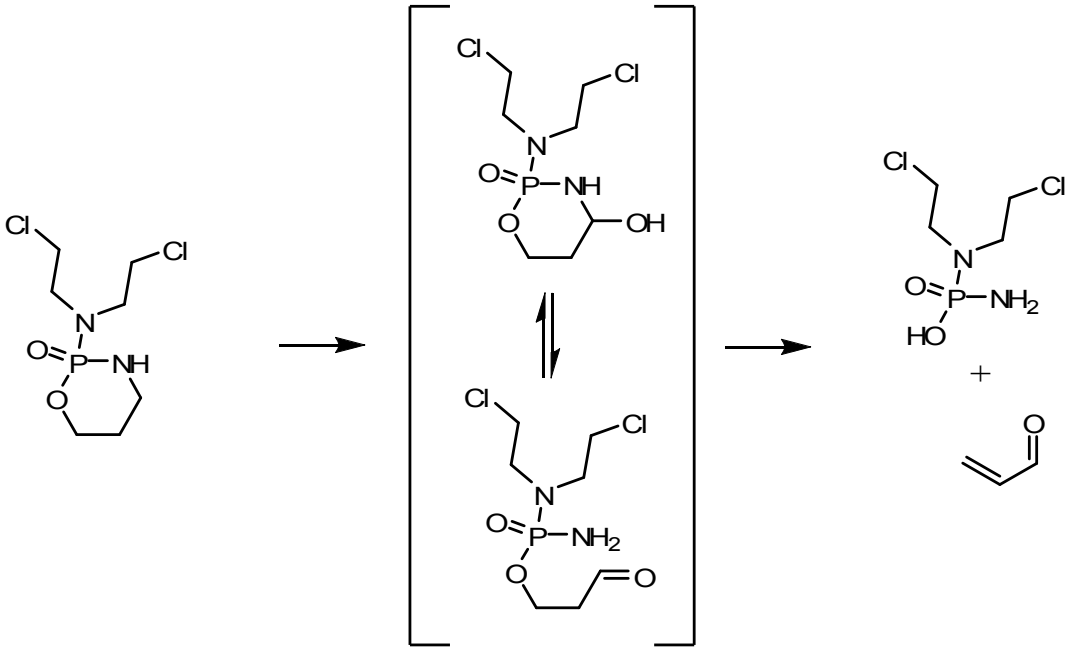

Figure 1.12 Conversion of the prodrug cyclophosphamide into the phosphoramide mustard alkylating agent

Unfortunately most prodrugs activate non-specifically, usually in the liver, and as such are still limited by their negative effects on healthy tissue. In order to develop a truly selective treatment, more of the differences between cancerous and non-cancerous cells need to be exploited.

Prodrugs which become active by a reductive mechanism and can be easily back oxidised by molecular oxygen should show an increase in selectivity for the hypoxic regions of tumours, where the concentration of oxygen is lower. Tirapazamine (3-aminobenzo[1,2,4]triazine-1,4-di-*N*-oxide), which shows a 2 to 3 fold selectivity for hypoxic regions *in vivo*, promises to be the first hypoxia selective drug with clinical applications and is currently undergoing stage III trials. The drug is activated by an enzymatic one electron reduction, forming a radical intermediate which, if not back oxidised, causes DNA breakages (Figure 1.13).[37] However, limitations such as lower hypoxia selectivity *in vivo* compared to *in vitro* mean that the usefulness of tirapazamine could be more related to its use as a lead compound for future hypoxia selective drugs, rather than as a final treatment.[41]

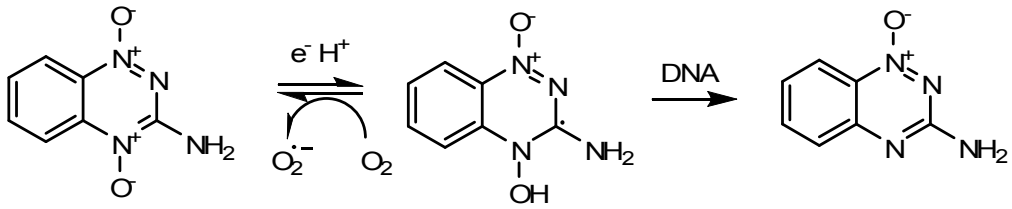

Figure 1.13 Activation of tirapazamine by a reductive mechanism

Another way to target the hypoxic region of the tumour is through the use of pH sensitive drugs. The exact effect of pH is complicated because pH can influence the transport, uptake and metabolism of a drug.[4] However, neutral species are often more readily taken up by cells than charged species and, if the pK_a of the drug is low, then it will be more readily absorbed at low pH. Chlorambucil, 4-[bis(2-chloroethyl)amino]benzenebutanoic acid (Figure 1.14), is an example of such a drug. With a pK_a of 5.8, chlorambucil exists primarily in the deprotonated form at physiological pH, but at lower pH the neutral form will be prevalent, resulting in an increase in uptake.[3]

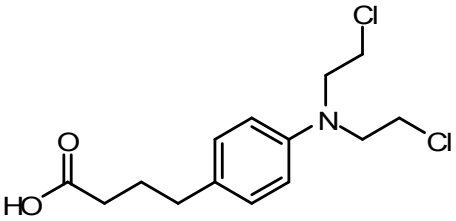

Figure 1.14 Chlorambucil

Because tumours have leaky vasculature, another way to specifically target them is through the use of drug-carrying nanoparticles or liposomes. The drug doxorubicin (Figure 1.15) is used in the treatment of a variety of neoplastic diseases, and the liposomal formulation has also been approved for use in the treatment of ovarian cancer under the name DOXIL.

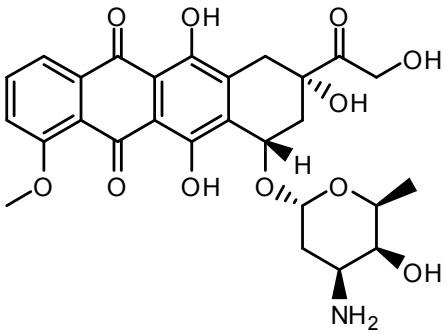

Figure 1.15 Doxorubicin

DOXIL places the chemical doxorubicin inside a liposome, which is then coated in methoxypolyethylene glycol to give the pegylated liposome (Figure 1.16). One of the advantages of DOXIL is that it shows reduced cardiotoxicity in comparison to the non-liposomal form of the drug.[42]

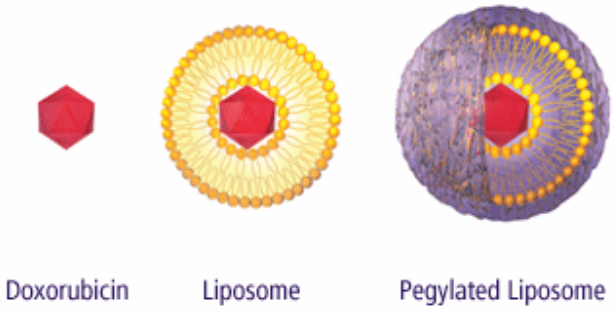

Figure 1.16 Schematic representation of DOXIL[43]

1.6. Hypoxia Selective Cobalt(III) Cytotoxins

In order to develop new hypoxia selective cancer treatments, Denny and his group have conducted work relating to prodrugs activated by a reductive mechanism.[44, 45, 46, 47, 48] While much of the work dealt with the development of organic drugs that were activated in a manner similar to that of tirapazamine, they also conducted work using cobalt(III) complexes.

The d^6 low-spin electronic configuration of octahedral cobalt(III) complexes renders them kinetically inert. For example, the aquation of $[Co(NH_3)_6]^{3+}$ has a rate constant of $5.8x10^{-12}$ s^{-1}, which corresponds to a half-life of ~3800 years.[49] This is in stark contrast to cobalt(II), a labile metal ion where the rate constant for the aquation of the first ethane-1,2-diamine from $[Co(en)_3]^{2+}$ is $6.8x10^{2}$ s^{-1}, a half-life of ~0.001 s.[50]

Since the cobalt(III)-cobalt(II) reduction potential can fall within the range of cellular reductants, it is reasonable to expect that the one-electron reduction needed to facilitate this massive change in behaviour can occur *in vivo*. Hypoxia selectivity is achieved through reoxidation of the labile cobalt(II) species to the inert cobalt(III) species, by molecular oxygen before ligand release occurs.

Binding a nitrogen mustard such as *N*,*N*-bis(2-chloroethyl)ethane-1,2-diamine to an inert cobalt(III) metal centre effectively renders it much less active, as the lone pair on the nitrogen atom needed to form the highly reactive aziridinium is involved in binding to the metal. Following reduction of the metal centre in the hypoxic region of the cell, the mustard may be released. The lone pair of the nitrogen is now no longer involved in binding and the drug is active (Figure 1.17).

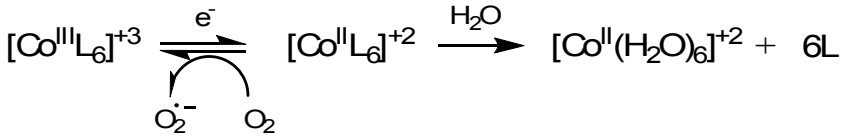

Figure 1.17 Reductive activation of cobalt(III) complexes as hypoxia selective cytotoxins

The activity of these complexes was tested *in vitro* against both the AA8 and UV4 cell lines. The UV 4 cell line is hypersensitive to alkylating agents and is used to confirm that the cytotoxicity is due to alkylation and not some other process. The degree of hypoxia selectivity was also assessed using the UV4 cell line. The concentration multiplied by the time taken to reduce cell survival to 10% (CT_{10}) was measured under both aerobic and hypoxic conditions.

Table 1.1 Cytotoxic data for alkylating ligands and their cobalt(III) complexes[45]

Compound	IC_{50} (air) AA8	HF (air) AA8/UV4	Aerobic CT_{10}/hypoxic CT_{10}
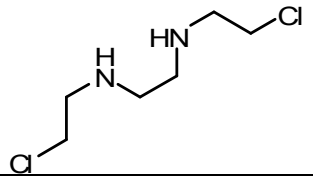	30 μM	29	
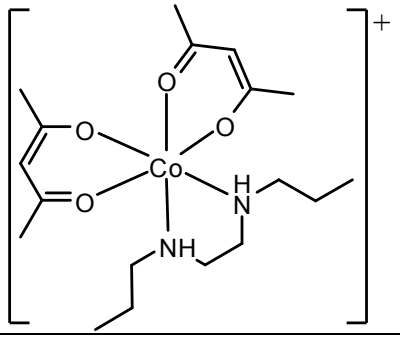	5000 μM	ND	
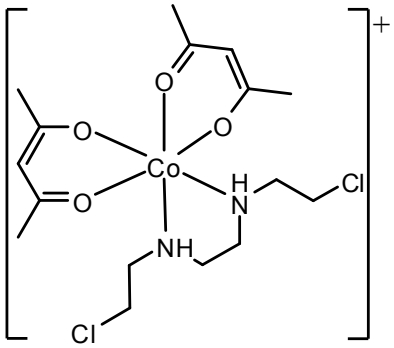	890 μM	14	1.6

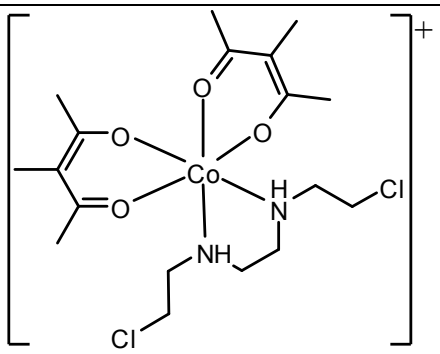	650 μM	2.7	>1
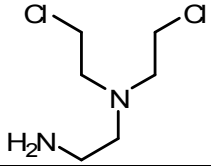	1.5 μM	53	2.0
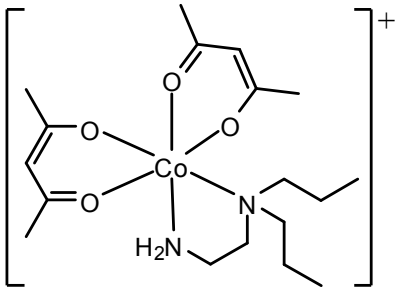	34 μM	0.9	
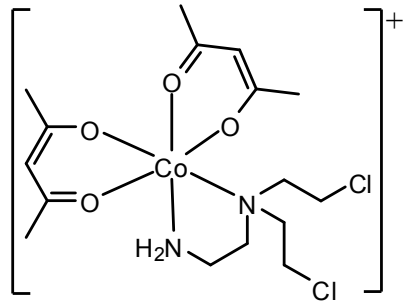	3.1 μM	64	1.9
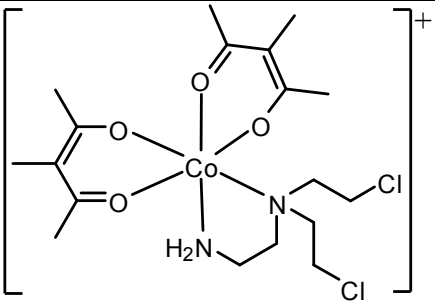	4.6 μM	48	20

Although the study showed that the cobalt(III) was being reduced to cobalt(II) and releasing the bound mustards, the small variation in the CT_{10} values under aerobic and hypoxic conditions means that the complexes exhibit only modest hypoxia selectivity *in vitro*.

Additional *in vivo* studies showed little activity against hypoxic cells and the series has not been developed further.[37]

1.7. Photodynamic Therapy

Photodynamic therapy is a cancer treatment where light and a photosensitizer interact to destroy tumour tissue. Patients are injected with a light-activated photosensitizer that makes their body sensitive to light. The drug is more readily retained by cancerous cells than normal tissue, so that following exposure to light the photosensitizer produces a toxic reaction that selectively destroys the tumour.[10]

The use of visible or near-IR light to trigger cytotoxicity presents both advantages and disadvantages in cancer therapy. The main advantage is the ability to localise the toxicity to a selected site, reducing the damage done to normal cells. One of the disadvantages is the limited depth of effect due to problems associated with penetration of the light into tissues. Another disadvantage is the inability to treat widespread metastases.[51]

Photodynamic reactions were first studied in 1900 when Raab used acridine and light to facilitate the killing of paramecium. The first photosensitizer used in humans was hematoporphyrin derivative (Hpd), which is a series of hematoporphyrin (Hp) oligomers, joined by a mixture of ether and ester linkages, ranging up to six units long. Hpd was first prepared by acetylating Hp and then dissolving the mixture in an aqueous alkali solution.[51] Hpd is now sold under the trade name of Photofrin and is used to treat obstructing endobroncial non-small lung carcinoma and obstructing oesophageal cancer.

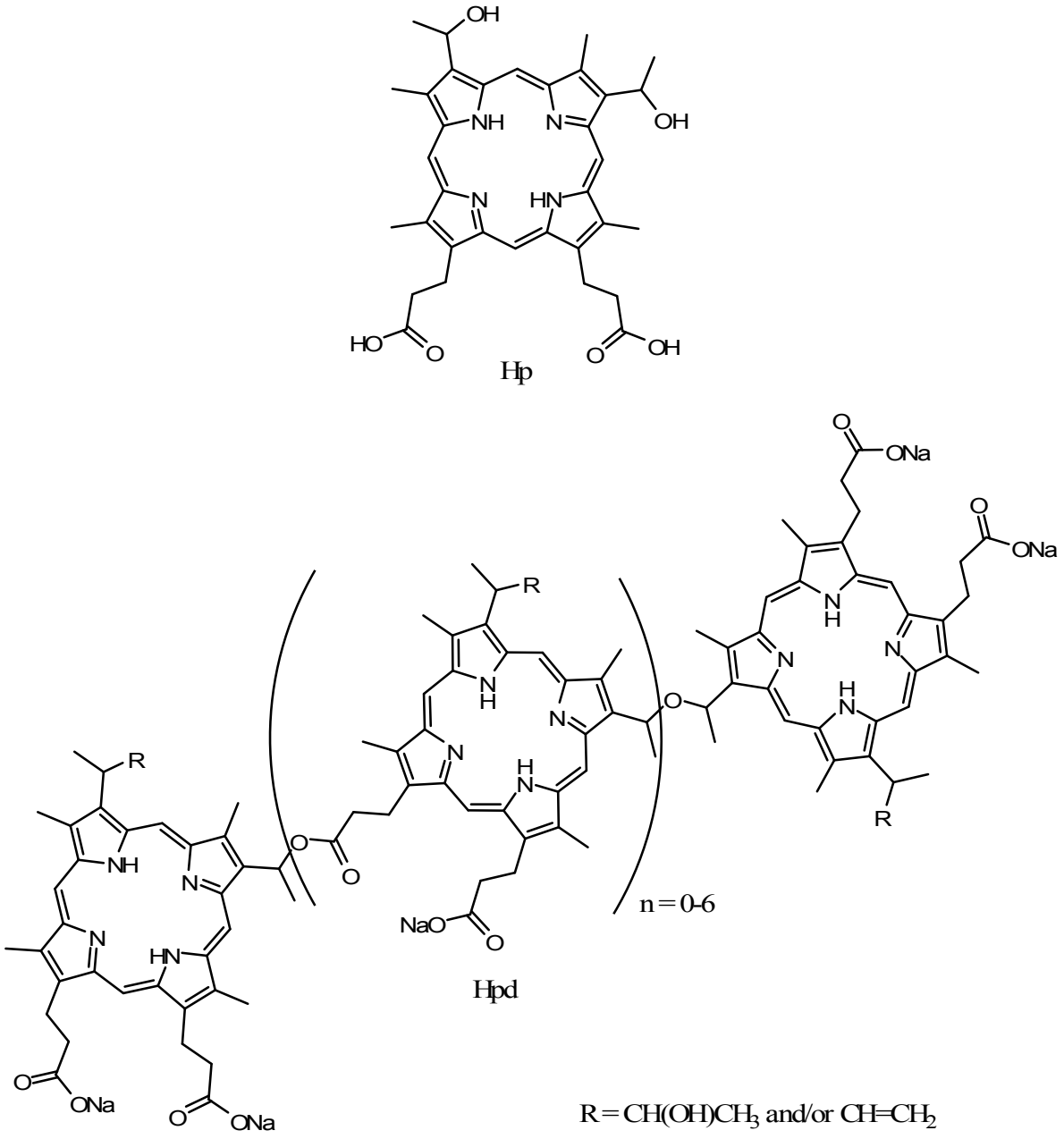

Figure 1.18 Hematoporphyrin and the oligomer hematoporphyrin derivative (Photofrin)

The mechanism by which a photosensitizer operates is believed to involve the sensitizer first absorbing a photon and going to an excited singlet state, from this singlet state intersystem crossing gives rise to an excited triplet state. The excited triplet state is able to interact with molecular oxygen, which results in the photosensitizer relaxing back to the

ground state and the formation of singlet oxygen (Figure 1.19). Singlet oxygen is highly reactive and the damage it causes to DNA can result in cell death.[51]

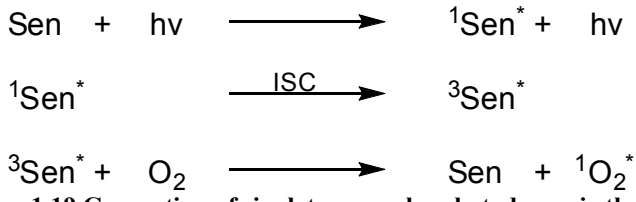

Figure 1.19 Generation of singlet oxygen by photodynamic therapy

1.8. Photo-activated Cytotoxins

The purpose of this project was to synthesise a system in which heteronuclear metal centres are connected by a bridging ligand. When light strikes one of the metal centres, it excites an electron through the bridging ligand onto the other metal, which causes it to be reduced to a labile state. In this labile state it will swap its current ligands for water. By choosing to have a cytotoxic molecule as one of the ligands a photo-activated release is achieved (Figure 1.20). Provided the cytotoxin is relatively inactive while bound to the metal centre, the light induced release will serve as the trigger for enhanced anti-cancer activity.

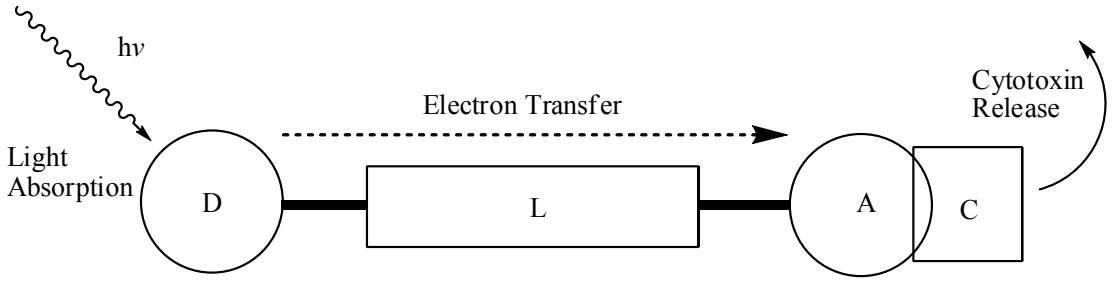

Figure 1.20 Schematic of a photo-activated cytotoxin: Photo-induced electron transfer from the donor (D) to the acceptor (A) through the bridging ligand (L) results in release of the cytotoxin (C)

Several aspects were considered when selecting a donor site. Firstly, the chosen donor must be able to undergo photo-oxidation, for example by a metal-to-ligand-charge-transfer process, as well as being relatively stable in both oxidation states. Ruthenium polypyridyl

complexes are an example of a class of compounds which could be used for this purpose. Another option is to use zinc porphyrin complexes, where the excitation would involve a π to π^* transition instead of a MLCT. Ruthenium polypyridyl complexes have often been used in studies involving intramolecular electron transfer between two metal sites,[52] and are the main focus of this study.

The acceptor site must be able to accept the electron generated by the donor and in doing so change from an inert to labile state. Metal ions such as cobalt(III) and chromium(III) are capable of doing this. The fact that most cobalt(III) complexes are diamagnetic makes them a great deal more convenient to study than the related paramagnetic chromium(III) species, principally because diamagnetic compounds are more readily studied by NMR techniques.

As soon as more than one kind of metal ion binding site is present in an unsymmetrical bridging ligand, a synthetic problem arises, in that the binding of the first metal to the ligand could, in principle, occur at either site. There are two ways that selective binding can be achieved: either the ligand can be synthesised on one of the metal centres, or synthetic strategies designed to introduce exploitable differences between the binding sites can be used.

Synthetic differentiation between the sites can be achieved by controlling the binding geometries of the sites, as well as the number of donor atoms at each binding domain. For example, a tridentate ligand can bind either meridionally or facially. If a metal atom is already bound by a tridentate ligand, in either manner, then this will restrict the coordination geometry of a second tridentate ligand, since a meridional ligand prohibits the binding of a facial ligand and vice versa. It is therefore possible, through the use of tridentate ligands with appropriate geometry, to control the end to which the donor and acceptor metals will bind.

The bridging ligand used must allow for the transfer of the electron from the donor to the acceptor site. This is best achieved by transmission of the electron through the bridging ligand. Bridging ligands with conjugated π-bonds are better suited to allowing this electron transfer to occur. Since the bridging ligand also heavily influences the structure of the final system, especially the distances between the donor and accepter sites, rigidity is desirable. Spacers with aromatic ring systems satisfy both of these criteria and were the focus of this project.[53]

1.9. Ruthenium

The element ruthenium was discovered in 1844 by Karl Klaus, who was examining the residues being produced by the St. Petersburg platinum refinery. These residues were the insoluble parts of the mineral which remained after treatment with aqua regia. Klaus treated the residue with a variety of reagents and examined the resulting compounds by smell, taste, and appearance under a microscope. Eventually, from the 8 kg of crude residue originally given to him, Klaus was able to isolate 6 g of pure ruthenium metal. Klaus sent the samples of his ruthenium compounds to Jöns Berzelius who initially proclaimed them to be dirty iridium salts. Klaus responded by sending additional salts as well as his most recent publications to Berzelius who finally accepted it as being a new element.[54, 55]

The name ruthenium is taken from *Ruthenia*, the Latin name for an historical area of Europe comprised of Western Russia, Ukraine, Belarus, and small regions of Poland and Slovakia. The name ruthenium had first been proposed by Gottfried Osann in 1827 when he believed he had discovered three new metals in platinum residues, this claim was rejected by Berzelius causing Osann to withdraw his claim. Klaus chose to reuse the name ruthenium as an acknowledgment to Osann as well as to honour his native land of Russia.

Ruthenium is observed in a number of oxidation states, with +2, +3 and +4 being the most common (Table 1.2). The raw metal is not oxidised by cold air but will readily form RuO_2 on heating. The metal is not soluble in either hot or cold acids; it was this insolubility that led to its discovery. However, if potassium perchlorate is added to an acid in contact with ruthenium metal the resulting oxidation is explosive.

Table 1.2 Ruthenium complexes of various oxidation states[55]

Complex	Oxidation State
$[RuO_4]$	8
$[RuO_4]^-$	7
$[RuO_2Cl_4]^{2-}$	6
$[RuF_6]^-$	5
$[Ru(bpy)Cl_4]$	4
$[RuO_2]$	4
$[Ru(NH_3)_6]^{3+}$	3
$[Ru(bpy)_3]^{2+}$	2
$[Ru(C_6H_6)_2]^{2+}$	2
$[Ru(CO)_5]$	0

Ruthenium is in group 8 of the periodic table and has an atomic electron configuration of $[Kr](4d)^7(5s)^1$. As a second row transition metal, the ligand field is substantially larger than that encountered in first row metals. Because of this, higher temperatures are needed to facilitate ligand exchange and the obtained compounds are very stable. This stability extends to the reaction conditions normally utilised in synthetic organic chemistry. The ligands on a ruthenium metal centre can be exchanged in a systematic manner. In addition, after binding to a ruthenium metal centre, the properties of a ligand do not differ greatly from its uncoordinated form. These characteristics of ruthenium compounds mean that they can be tailored to form designer compounds.[56]

The two oxidation states of ruthenium that are of interest to us in our study are ruthenium(II) and ruthenium(III). Ruthenium(II) is a low spin d^6 metal centre which usually

forms monomeric, six-coordinate octahedral complexes. Ruthenium(III) is a low spin d^5 metal centre and like ruthenium(II) will usually form six-coordinate monomers. Because both oxidation states of ruthenium are usually low spin they are kinetically inert,[57] which has the advantage that complexes of these metals are usually quite stable under laboratory conditions. With no unpaired electrons, ruthenium(II) is diamagnetic, meaning that complexes of this metal centre can easily be studied by NMR techniques.

1.9.1. Ruthenium (III)

The quantity of ruthenium(III) complexes makes an exhaustive discussion of this class of compounds and their properties unfeasible in this introduction. Ruthenium(III) forms many stable cationic, neutral and anionic complexes. The compound $RuCl_3.xH_2O$ is the most common starting material in ruthenium chemistry. However, this material is actually a mixture of monomeric and polymeric ruthenium complexes in various oxidation states coordinated with various ligands, and despite being commonly referred to as ruthenium(III) the average oxidation state is actually closer to four than three.[55] $RuCl_3.xH_2O$ is usually prepared by evaporation of a solution of RuO_4 in HCl, while true ruthenium(III) chloride is prepared by heating ruthenium metal in an atmosphere of chlorine and carbon monoxide.[58]

$RuCl_3.xH_2O$ is used as a starting material in the synthesis of most ruthenium(II) polypyridyl complexes. This is because when $RuCl_3.xH_2O$ is reacted with polypyridyl ligands, the resulting ruthenium(III) polypyridyl complexes are usually unstable and readily reduce to the corresponding ruthenium(II) complexes.

1.9.2. Ruthenium(II)

The field of ruthenium(II) complexes is even more extensive than that of ruthenium(III) complexes. I shall restrict the discussion to polypyridyl complexes, since these have the most relevance to this project. The electrochemical and photophysical properties of these compounds, combined with their chemical stability, make them an ideal subject for study. In fact $[Ru(bpy)_3]^{2+}$ and its derivatives have been the subject of more attention than any other class of ruthenium compound.[55]

These polypyridyl complexes have many applications: In dye-sensitised solar cells, ruthenium complexes are used to facilitate the generation of electricity at longer wavelengths.[59, 60, 61] Ruthenium(II) complexes have shown potential for use in the splitting of water into hydrogen and oxygen.[62, 63] Because their photophysical properties can be altered by their surroundings complexes such as $[Ru(bpy)_2(dppz)]^2$ have been used as luminescent DNA probes.[64, 65] Ruthenium complexes are also used in organic light emitting diodes.[66]

1.9.2.1. Photochemistry of Ruthenium(II) Complexes

Ruthenium polypyridyl complexes are the most studied class of transition metals from a photochemical viewpoint. In addition to being good absorbers of visible light, they exhibit long-lived excited states, luminescence, and can undergo reversible redox processes in both their ground and excited states.[67]

The highly coloured nature of these complexes is due to their ability to absorb energy in the visible region, often through a metal-to-ligand-charge-transfer transition (MLCT). The MLCT gives rise to a singlet excited state, which quickly undergoes intersystem crossing to a triplet excited state. For most ruthenium(II) polypyridyl complexes, this ^{3}MLCT is the lowest

excited state, and relaxation back to the ground state is usually accompanied by an intense luminescent emission that often falls in the visible region (Figure 1.21).[68, 69]

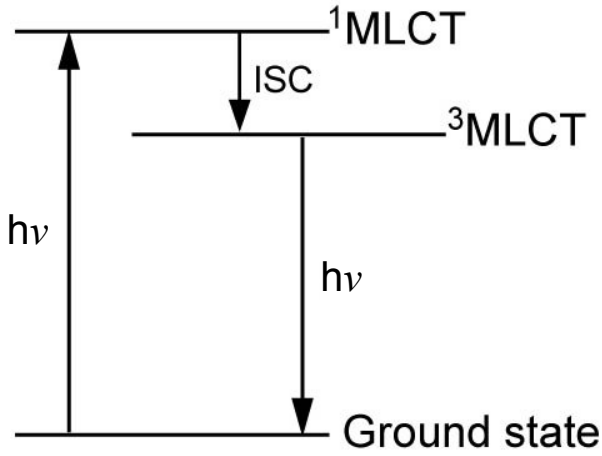

Figure 1.21 Energy diagram showing the emissive pathway for ruthenium(II) complexes

The MLCT involves an electron from the π_M metal orbital being excited to the antibonding π_L^* orbital, which is more or less delocalised about the aromatic rings of the ligand. The intense colour is due to the large transition dipole associated with this transfer. The lifetime of the excited state can be extended if the electron can be delocalised over several aromatic rings, and such species can participate in photochemical redox reactions.[70]

In addition to the MLCT excited states, both metal-centred (MC) and ligand-centred (LC) excited states can be obtained. These involve promotion of an electron from the π_M to σ_M^* and π_L to π_L^* respectively (Figure 1.22). These excited states may have singlet or triplet multiplicity. However, spin-orbit coupling can cause large singlet-triplet mixing, especially in the MC and MLCT excited states.[71, 72]

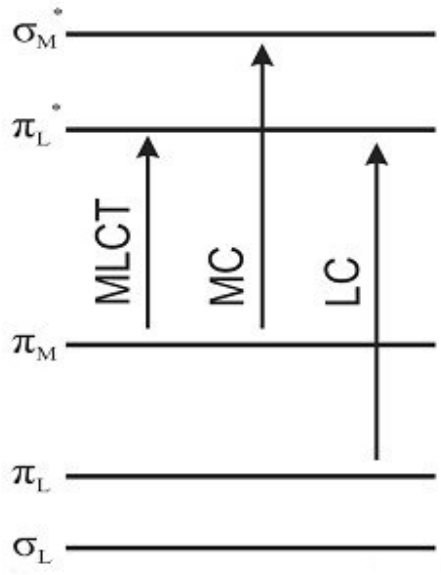

Figure 1.22 Simplified molecular orbital diagram showing the three low energy electronic transitions in ruthenium(II) polypyridine complexes[67]

The lifetime of the ^{3}MLCT is heavily influenced by the energy level of the metal-centred triplet state (^{3}MC). This is because ^{3}MC excited states of d^6 metal centres are strongly displaced with respect to the ground state geometry along metal-ligand vibrational coordinates and relaxation to the ground state is both fast and radiationless.[73] One of the mechanisms for non-radiative decay from the ^{3}MLCT is through this thermally accessible ^{3}MC. A rough rule of thumb is that the lifetime of the ^{3}MLCT state in ruthenium(II) polypyridyl complexes is determined by the thermal accessibility of the ^{3}MC state. This is why the lifetime for $[Ru(tpy)_2]^{2+}$ is much shorter than $[Ru(bpy)_3]^{2+}$, the 2,2′:6′,2″-terpyridine (tpy) ligands cause a greater distortion from the ideal octahedral geometry and as a result the ligand field strength is weaker, lowering the ^{3}MC energy level (Figure 1.23).[68, 69]

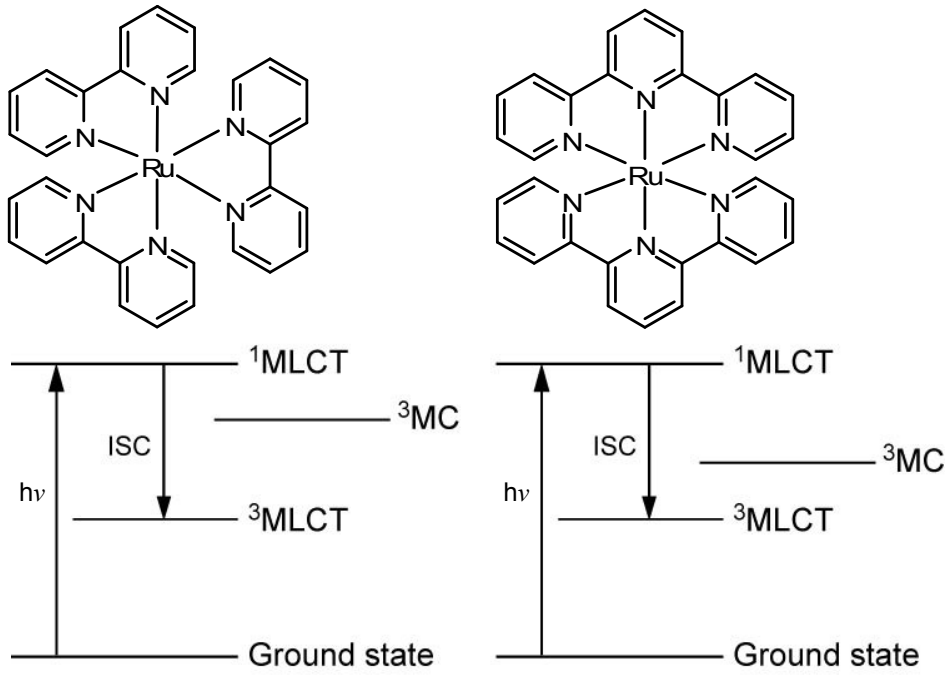

Figure 1.23 Effect of ligands on the ^{3}MC energy level. In the case of $[Ru(bpy)_3]^{2+}$ (left) there is a larger gap between the ^{3}MC and ^{3}MLCT energy levels than in the $[Ru(tpy)_2]^{2+}$ case (right).[68]

In the absence of deactivation *via* the ^{3}MC, the lowest ^{3}MLCT excited state often lives long enough to encounter other solute molecules and, in doing so, can act as an energy donor, electron donor or electron acceptor. For example, the energy available to $^*[Ru(bpy)_3]^{2+}$ for energy transfer processes is 2.21 eV and its reduction and oxidation potentials are +0.84 and -0.84 V. This means that through interactions with other species the excited state can be quenched (Figure 1.24).[67]

$$^*[Ru(bpy)_3]^{2+} + Q \rightarrow [Ru(bpy)_3]^{2+} + {}^*Q$$
$$^*[Ru(bpy)_3]^{2+} + Q \rightarrow [Ru(bpy)_3]^{3+} + Q^-$$
$$^*[Ru(bpy)_3]^{2+} + Q \rightarrow [Ru(bpy)_3]^{+} + Q^+$$

Figure 1.24 Mechanisms for the quenching of $^*[Ru(bpy)_3]^{2+}$

Usually the redox products of such interactions rapidly decay, either through back electron transfer into the starting materials or through secondary reactions.

1.10. Cobalt

Cobalt containing pigments have been used since ancient times; it is present in Egyptian pottery dated from around 2600 BCE and in Iranian glass beads of 2250 BCE. However, it was not until 1735 that cobalt metal was first prepared by Georg Brandt. The name comes from the German word *kobold*, meaning goblin. Miners had used the name *kobold* ore long before the metal was discovered. The reason for this name is that miners found that smelting these ores would not only fail to give the expected metal, but also produce highly toxic fumes, this phenomenon was blamed on goblins.[74, 75]

Cobalt is in Group 9 of the periodic table, and has an atomic electron configuration of [Ar]$3d^7 4s^2$. The most common oxidation states for cobalt complexes are 2+ and 3+, although compounds with 1+ and 4+ oxidation states are also known. The reduction potential of the cobalt(III)-cobalt(II) couple is highly sensitive to the nature of the coordinated ligands (Table 1.3). The complex $[Co(H_2O)_6]^{3+}$ is highly oxidising, capable of oxidising water, and for this reason few simple cobalt(III) salt hydrates are able to be isolated.

Table 1.3 Selected Co(III)/Co(II) reduction potentials[75]

Couple	E/V
$[Co(H_2O)_6]^{3+} + e^- \rightleftharpoons [Co((H_2O)_6]^{2+}$	1.83
$[Co(C_2O_4)_3]^{3-} + e^- \rightleftharpoons [Co(C_2O_4)_3]^{4-}$	0.57
$[Co(EDTA)]^- + e^- \rightleftharpoons [Co(EDTA)]^{2-}$	0.37
$[Co(bpy)_3]^{3+} + e^- \rightleftharpoons [Co(bpy)_2]^{2+}$	0.31
$[Co(en)_3]^{3+} + e^- \rightleftharpoons [Co(en)_3]^{2+}$	0.18
$[Co(NH_3)_6]^{3+} + e^- \rightleftharpoons [Co(NH_3)_6]^{2+}$	0.108
$[Co(CN)_6]^{3-} + e^- \rightleftharpoons [Co(CN)_5(H_2O)]^{3-} + CN^-$	-0.8

1.10.1. Cobalt(III)

The d^6 cobalt(III) oxidation state is able to form a wide range complexes, particularly with nitrogen donor ligands. Complexes of cobalt(III) are almost exclusively octahedral, low

spin and kinetically inert.[76] The kinetic inertness of these complexes is primarily due to the low spin nature of these complexes resulting in a high crystal field splitting energy associated with the $(t_{2g})^6$ electronic configuration.

Because cobalt(III) complexes are so kinetically inert, they are usually prepared by indirect methods. The most common method involves adding the ligand to an aqueous solution on the appropriate cobalt(II) salt; the resulting complex is oxidised into the cobalt(III) state. It is quite common for molecular oxygen to be used as the oxidant. This is often achieved by simply drawing a stream of air through the solution. The low-spin diamagnetic nature of cobalt(III) complexes means that they can easily be characterised by NMR techniques.

1.10.2. Cobalt(II)

Cobalt(II) complexes have seven d electrons and are much more labile than cobalt(III) complexes.[76] However, despite being less numerous, cobalt(II) complexes show a greater diversity of types than cobalt(III) complexes. Cobalt(II) complexes are usually high-spin octahedral, although certain complexes, such as $[Co(tpy)_2]X_2.nH_2O$, exhibit an equilibrium between the high-spin and low-spin states.[77] Both high-spin and low-spin states of a cobalt(II) complex are paramagnetic and as such cannot be easily analysed by NMR techniques.

Because of the potential for cobalt(II) to oxidise to cobalt(III), the possibility of oxidation must always be considered when synthesising a cobalt(II) complex. However, as long as the solution is not alkaline and the ligands not too high on the electrochemical series, a wide range of complexes can be isolated without the need for special precautions.[75]

The main feature of cobalt(II) complexes that we intend to utilise in our study is their highly labile nature. This can be exploited to facilitate ligand release following reduction of an inert cobalt(III) complex into the labile cobalt(II) complex.

1.11. Metal-to-Metal-Charge-Transfer

A metal-to-metal-charge-transfer (MMCT) is 'an electronic transition of a bi- or poly-nuclear metal complex that corresponds to excitation populating an electronic state in which considerable electron transfer between two metal centres has occurred.'[78] A subset of this is intervalence charge transfer where the two metal sites differ only in oxidation states. Often this transfer results in the two metal centres swapping oxidation states.

Mixed valence ruthenium complexes provide an insight into the barriers relating to intramolecular charge transfers. The first reported mixed valence complex was the Creutz-Taube ion $[(\mu\text{-pyz})\{Ru(NH_3)_5\}_2]^{5+}$ (Figure 1.25), where, despite having an odd charge and neutral ligands, spectroscopic studies showed the two ruthenium centres to be equivalent. This equivalence is not what would be expected for a complex containing a ruthenium(II) and ruthenium(III) metal centre.[79, 80, 81]

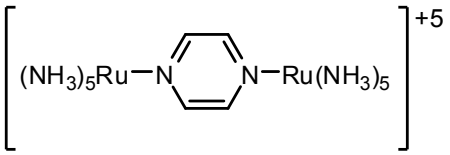

Figure 1.25 Creutz-Taube ion

The equivalence of the two ruthenium metal centres shows the ease with which the electron is transferred between the two metals. The extent of the electronic coupling is measured by the comproportionation constant K_c. Comproportionation is the unification of the oxidation numbers of two atoms of the same element with different oxidation numbers. The comproportionation constant is a reflection of the stability of the mixed-valence state as

opposed to the isovalent state. In the absence of any coupling the two metal centres will undergo reduction or oxidation at the same potential. The value of K_c, and hence the degree of communication, can be easily calculated experimentally through the use of electrochemistry. By measuring the values of E_f associated with each step of the reduction:

$$\text{Ru(III), Ru(III)} \xrightarrow{E_1^0} \text{Ru(III), Ru(II)} \xrightarrow{E_2^0} \text{Ru(II), Ru(II)}$$

K_c can then be calculated by the equation: $K_c=\exp((E_1^0-E_2^0)F/RT)$

The bridging ligand in such a system controls the distance and orientation of the two metal centres. There are a large number of studies which investigate the effect of the bridging ligand on K_c. In addition to this, there are studies showing the effect of the non-bridging ligands as well as solvent and environmental effects on the value of K_c. While this does not relate directly to the work that we conducted, such studies could, in principle, be used to gain an insight into how well a particular bridging ligand might perform in a photo-activated cytotoxin.

1.12. Ruthenium(II)-Cobalt(III) Systems

During his research on inner sphere electron transfer reactions, Taube examined ruthenium(II)-cobalt(III) bridged systems.[82, 83, 84, 85] In these experiments dinuclear complexes of ruthenium(III) and cobalt(III) were bridged by functionalised pyridyl and polypyridyl ligands (Figure 1.26). The ruthenium(III) was then reduced to ruthenium(II), either by addition of $[Ru(NH_3)_6]^{2+}$ or ascorbate, and the rate of the electron transfer between the two metal centres was measured in each case.

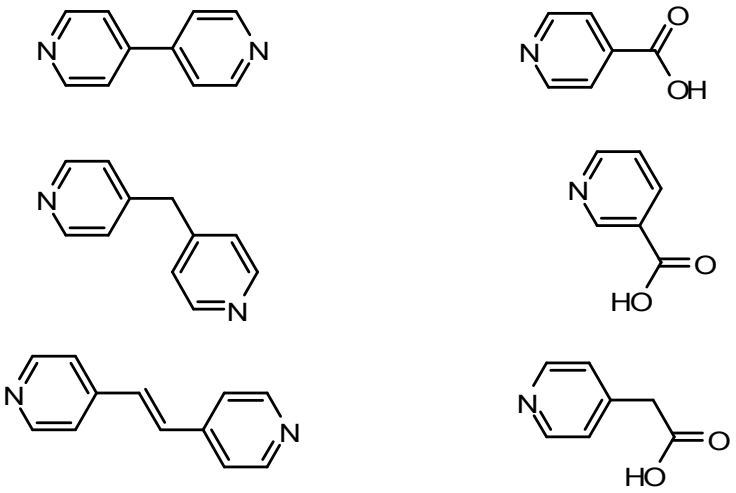

Figure 1.26 Examples of bridging ligands used by Taube

During these studies Taube was able to examine the effects of distance, type of bridging ligand, solvent and orientation on the rate of electron transfer. Taube observed that after the formation of the ruthenium(II) species, the cobalt(III) metal centre would be reduced to the cobalt(II) state. There are two possible explanations for this observation, either the transfer is intermolecular, occurring through an outer sphere interaction, or alternatively the reaction could be intramolecular (Figure 1.27).

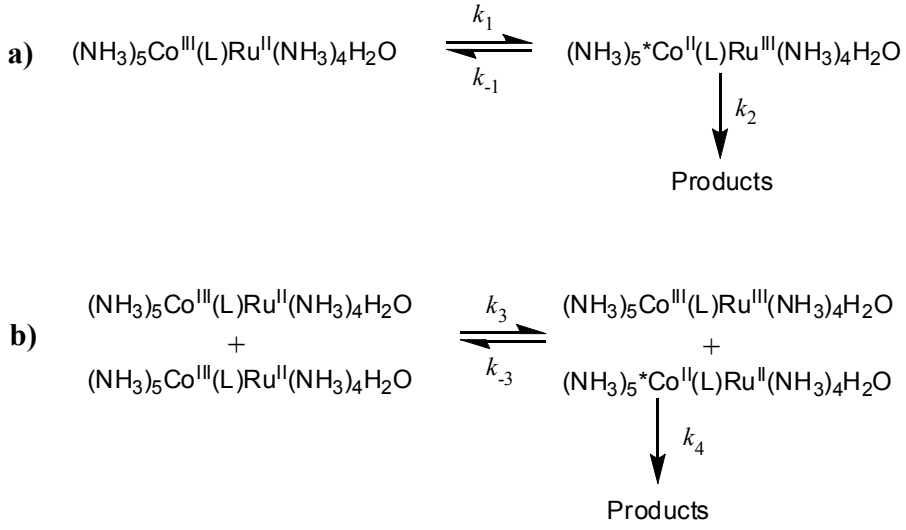

Figure 1.27 General reaction scheme for a) the intramolecular reaction and b) the intermolecular reaction[83]

By a consideration of the rate and its lack of dependence on the concentration of the products Taube was able to deduce that the transfer was intramolecular. However, this did not determine if the measured rate is k_1 or K_1k_2 (K_1 is the equilibrium constant for the intramolecular electron transfer). If the reaction establishes an equilibrium between the ruthenium(II)-cobalt(III) and ruthenium(III)-cobalt(II) states, with the latter slowly going to form the final products, then the measured rate corresponds to K_1k_2. The alternative is that the formation of the final products (k_2) is fast, in which case the rate is determined by k_1. At the time of first publication Taube was not able to conclusively say which was the case, although the evidence favoured k_1 being the rate determining step.

In addition to this Taube also noted a relationship between the rate of electron transfer in the heterodinuclear complexes and the intensity of the intervalence band measured for the corresponding ruthenium(II)-ruthenium(III) mixed-valence complexes. Since these measurements were first made, the reaction has shown to be dependent on k_1, and a correlation has been observed between the electronic factors (κ_{e1}) for ruthenium(II)-cobalt(III) reactions and κ_{e1} for diruthenium complexes; this suggests a common mechanism for the electronic coupling.[86]

1.13. Prior Work on Photo-activated Cytotoxins

This thesis carries on from the work conducted by Ramin Zibaseresht for his PhD, titled "Approaches to Photo-activated Cytotoxins".[87] Zibaseresht synthesised and examined the coordination of eleven bridging ligands based on the tridentate terpyridyl system. The two metal ion binding sites in these ligands were differentiated by the number of atoms in each site, the configuration of the binding domain or the types of donor atoms present.

Zibaseresht synthesised many ruthenium(II) complexes where the ruthenium ion was bound to the terpyridyl sites of the ligands. These mono-ruthenium complexes were reacted with a range of other metal ions, which enabled the complexes to be classified into three main types: ruthenium(II) complexes which can react with cobalt(III) ions; ruthenium(II) complexes which react only with silver (I) ions; and ruthenium(II) complexes that have no detectable ability to coordinate other common metal ions.[88, 89, 90, 91, 92, 93]

These studies provided us with a starting point for our research and more details on the ruthenium(II)-cobalt(III) heterodinuclear systems synthesised by Zibaseresht are given in 2.1.3.

1.14. Thesis Overview

The purpose of this thesis is to outline challenges and strategies associated the synthesis of several photo-activated cytotoxins. These photo-activated cytotoxins utilise a ruthenium(II) metal centre as the electron donor and a cobalt(III) metal centre as the electron acceptor. Selectivity with respect to the coordination of different metal centres to different binding domains was achieved through the use of different steric arrangements of the binding domains, pre-binding the ruthenium(II) metal centre before completing the synthesis of the bridging ligand and in the case of symmetrical bridging ligands an excess of ligand was used to minimise the formation of the homodinuclear complex.

Chapter 2 describes our initial work with terpyridine-based ligands, carrying on from that of Zibaseresht. The primary target system that this chapter is concerned with involved a bridging ligand with one terpyridine-based binding domain and one cyclam-based binding domain.

Chapter 3 introduces bridging ligands in which there is either no or limited steric differentiation between the two binding domains, and outlines how the mono-ruthenium(II) complexes of these ligands can be synthesised. In addition to this, the binding of a second metal centre is explored through the use of silver(I), zinc(II) and copper(I) metal salts.

Chapter 4 relates to the synthesis of ruthenium(II)-cobalt(III) heterodinuclear systems, with non-cytotoxic ligands coordinated to the cobalt(III) metal centre. This chapter also describes the photo-activated ligand release of the cobalt bound ligands, showing that such systems could potentially be used as photo-activated cytotoxins.

Chapter 5 takes the heterodinuclear systems described in chapter 4 and attempts to replace the non-cytotoxic ligands on the cobalt(III) metal centre with cytotoxic ones. Finally this chapter details the results of the cytotoxicity tests we conducted during our study.

Chapter 6 outlines the prospects for future study in this field. In some cases we have already conducted preliminary experiments towards these studies, the details of which are also given in this chapter.

Chapter 2: Terpyridine-Based Systems

2.1. Introduction

The key component in the design and synthesis of our photo-activated cytotoxin system is the bridging ligand. It is the bridging ligand which must be able to bind both metal centres as well as facilitate the transition of an electron between these two metals. We began our study by continuing from the previous experiments of Zibaseresht, who was working towards synthesising a bridging ligand, based on functionalised terpyridines, for use as a photo-activated cytotoxin.[87, 88]

In this chapter the synthetic strategies involved in the synthesis of functionalised terpyridines will be outlined. This will be followed by an explanation of the results achieved by Zibaseresht that served as a starting point for our research. Finally the results of our work with cyclam functionalised ttp and its possible use as a bridging ligand will be discussed.

2.1.1. Methods for Synthesis of 4'-*p*-Tolylterpyridine Ligands

When synthesising an aryl-terpyridine, such as ttp (**2.2**), the key step is the condensation of two equivalents of 2-acetylpyridine with the appropriate aryl aldehyde (in this case 4-methylbenzaldehyde), followed by ring closure with an ammonia source at high temperatures. Various strategies for the synthesis of ttp have been described in the literature.[94, 95, 96, 97, 98, 99, 100] A brief review of the synthetic strategies we explored during our research is given below.

2.1.1.1. The Kröhnke Methodology

The synthetic strategy employed in the Kröhnke methodology[95] assembles a substituted terpyridine over multiple steps. In the synthesis of ttp, the first step is the formation

of the enone **2.1** by an aldol condensation between 2-acetylpyridine and 4-methylbenzaldehyde (Figure 2.1).

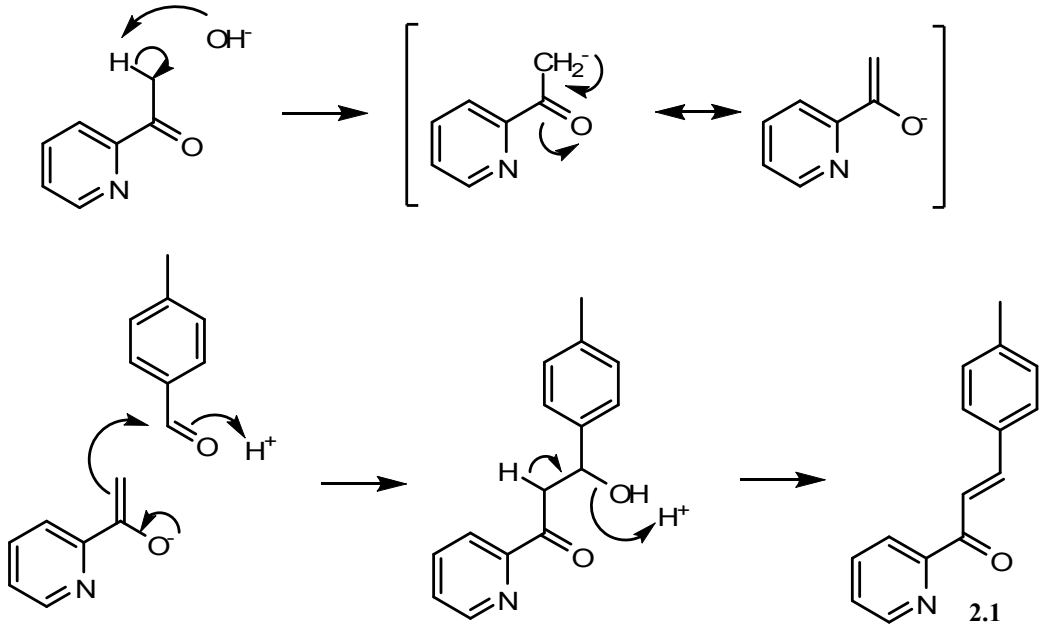

Figure 2.1 Mechanism for the formation of (*E*)-1-(pyridin-2-yl)-3-*p*-tolylprop-2-en-1-one

2.1 is isolated and then reacted with (2-pyridacyl)pyridinium iodide (synthesised by reacting 2-acetylpyridine with iodine in pyridine)[101] which results in the formation of a 1,5-diketone *via* a Michael addition. Finally, ring closure is achieved by the addition of ammonium acetate, and the resulting dihydropyridine is oxidised by O_2 to give ttp (**2.2**) (Figure 2.2).

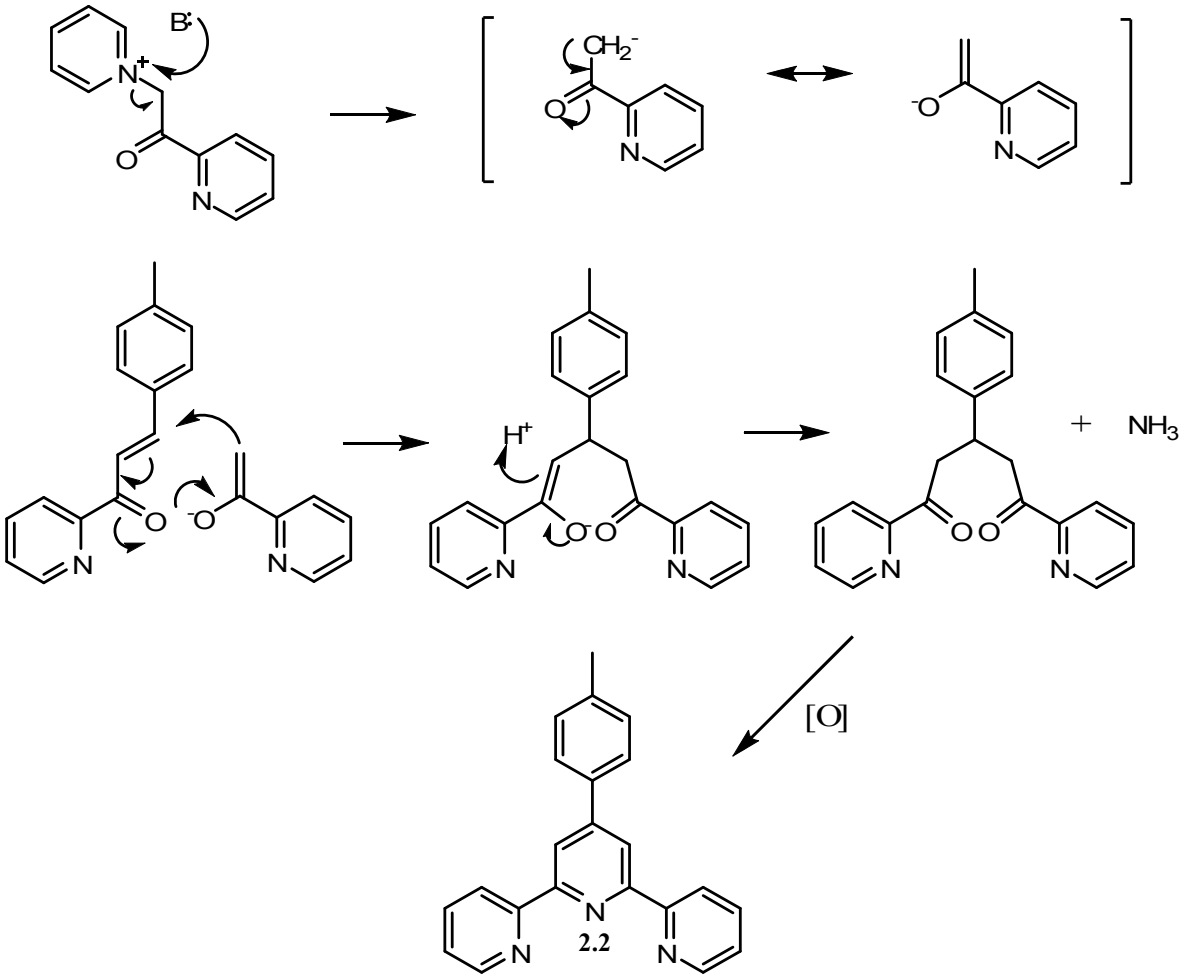

Figure 2.2 Mechanism for the formation of ttp by the Kröhnke Methodology

The advantage of the Kröhnke methodology is that it can be adapted to generate a wide variety of terpyridines. This is achieved by using appropriately substituted 2-acetylpyridines and aromatic aldehydes in the synthesis of the enone, which can then be reacted with a range of pyridinium ions.[102] This means that the Kröhnke methodology can be used to tune and adjust the terpyridines to suit their application. The major disadvantage is that synthesising a ligand where the non central pyridine rings of the terpyridine are identical, such as ttp, is more time consuming because of the multiple steps involved. Additionally, the overall yield is lower than that of other methods.

2.1.1.2. Collin-Balzani-Sauvage Methodology

The symmetrical nature of ttp means that the stepwise Kröhnke methodology is not required for its synthesis, and one-pot reactions can be used instead. The one-pot scheme initially selected for use was that of Collin-Balzani-Sauvage.[99] Two equivalents of 2-acetylpyridine were reacted with 4-methylbenzaldehyde in the presence of acetamide and ammonium acetate. After basification and cooling to room temperature, the crude products were precipitated out.

Even after recrystallisation the product is a mixture of two isomers with ttp (**2.2**) as the major isomer and 6′-*p*-tolyl-2,2′:4′,2″-terpyridine (**2.3**) as the minor isomer. The major isomer is formed by a 1,4-Michael addition and follows the same general mechanism as described in Figure 2.2. However, a 1,2-aldol reaction results in the formation of the minor isomer as detailed in Figure 2.3.

The two isomers are separated by exploiting the difference in their binding domains. Ttp has a tridentate binding domain, while the sterically hindered minor isomer **2.3** has only a bidentate binding domain. The addition of iron(II) results in the preferential binding of ttp to form the highly stable $[Fe(ttp)_2](PF_6)_2$ complex as a purple precipitate, which is isolated by vacuum filtration. The minor isomer can then be recovered by extraction of the filtrate with toluene. The complexed ttp is then liberated from the iron by the addition of hydrogen peroxide under alkali conditions. The peroxide oxidizes the iron from iron(II) to iron(III), forming a precipitate of iron oxides; this brown precipitate is then removed by filtration to leave pure ttp.[103]

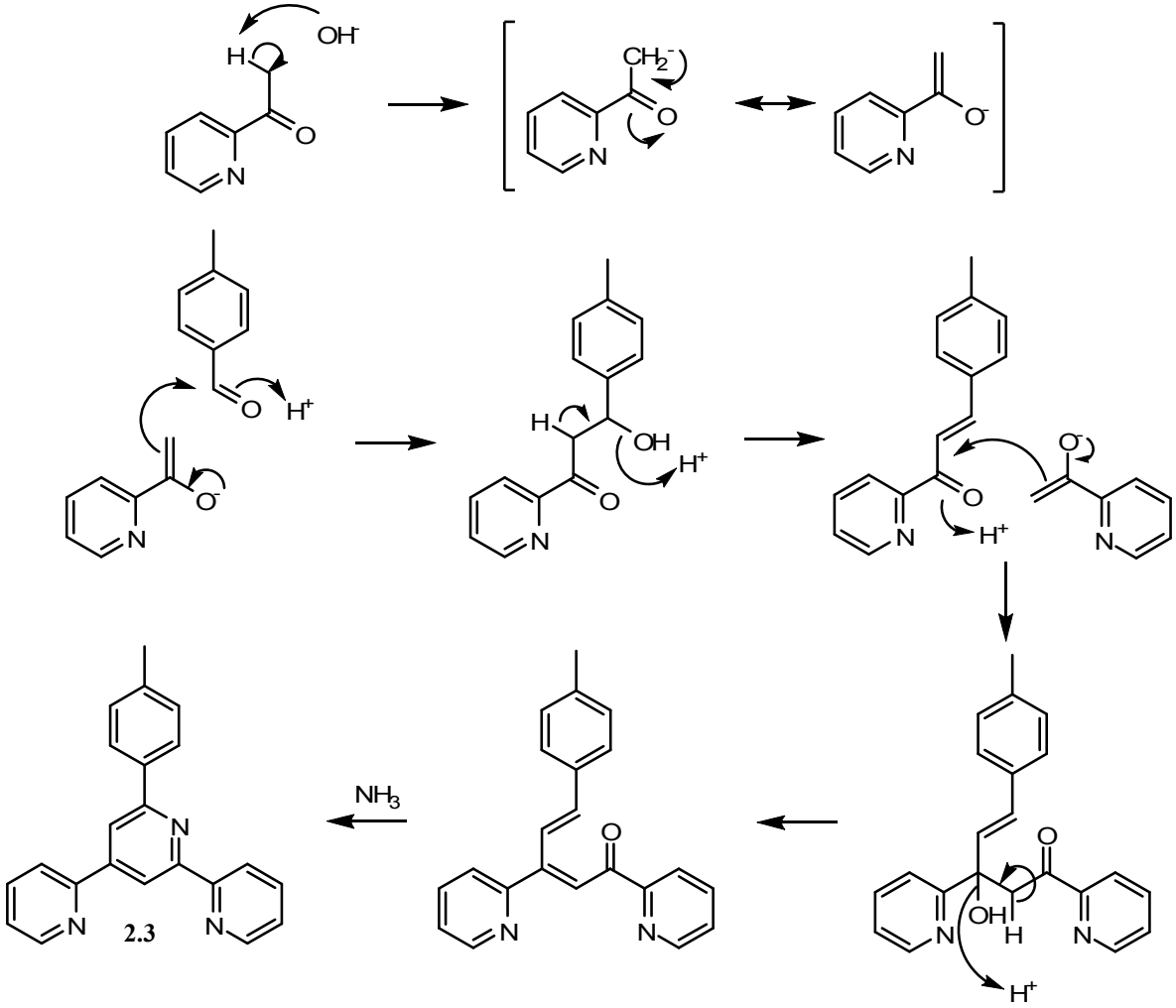

Figure 2.3 Mechanism for the formation of 6′-*p*-tolyl-2,2′:4′,2″-terpyridine

The advantage of using this method is that it can be carried out in a single reaction vessel and can be easily scaled up; the disadvantage is that it forms the minor isomer **2.3**, which has to be separated from the desired product.

2.1.1.3. Hanan Methodology

A revised one-pot synthesis was developed and optimised by Hanan in order to easily obtain large amounts of pure 4′-aryl substituted terpyridines, such as ttp.[100] This synthesis involves the addition of an aryl aldehyde to two equivalents of 2-acetylpyridine in ethanol with potassium hydroxide and aqueous ammonia. When 4-methoxybenzaldehyde is used as

the aryl aldehyde ttp is produced in a 49% yield after only two hours of reaction time, with no other isomers present.

2.1.2. Functionalisation of 4'-*p*-Tolylterpyridine Ligands

Ttp needs to be further functionalised in order to introduce the second binding domain necessary for it to act as the bridging ligand in our final system. This could be achieved either by using various funtionalised aryl aldehydes during ligand synthesis, or by introducing functionality after the ligand is synthesised.

One of the most versatile methods of introducing functionality to an unfunctionalised centre is through radical bromination. In the case of ttp, the methyl group can be brominated by reacting ttp with *N*-bromosuccinimide in either carbon tetrachloride or benzene, with a catalytic amount of dibenzoyl peroxide under an inert atmosphere. Although the bromination is successful in both solvents, we found that a slightly higher yield was achieved when using carbon tetrachloride.

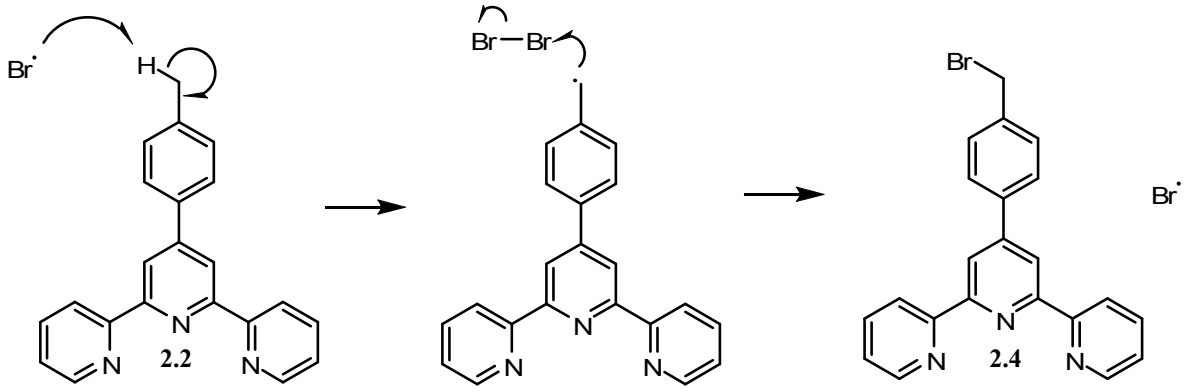

Figure 2.4 Propagation steps of the radical bromination of ttp

The high reactivity of the bromomethyl group towards nucleophiles means that it can be reacted with a variety of nitrogen or oxygen containing molecules in basic solution (Figure 2.5).[104, 105, 106, 107] This provides an easy route to synthesise various ligands with multiple

binding domains. It was this synthetic strategy of bromination, followed by substitution to introduce functionality, that Zibaseresht used in his research.

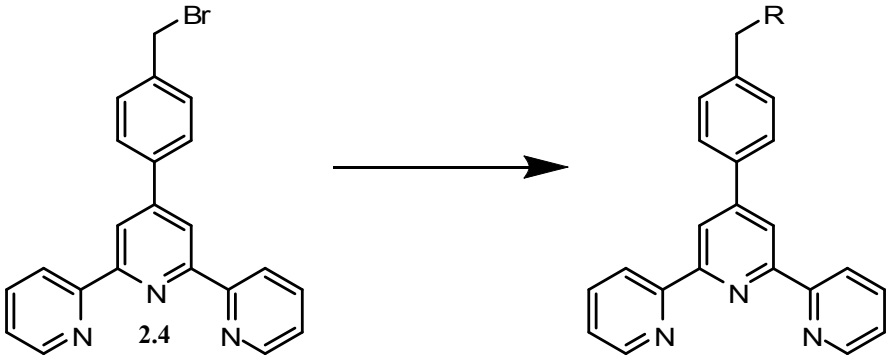

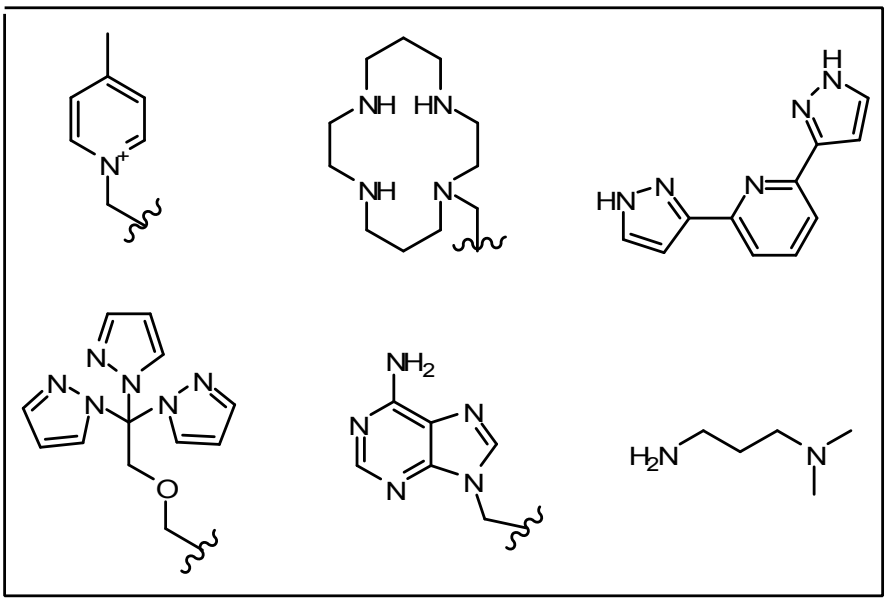

Figure 2.5 Examples of functionalised 4′-*p*-tolylterpyridine ligands

2.1.3. Some Ligand Systems and Coordination Compounds Synthesised by Zibaseresht

Using the method described above, Zibaseresht synthesised a variety of functionalised ttp ligands (Figure 2.6) and examined their binding to different metal ions. His intentions were to gain an understanding of how these ligands bind to different metals, as well as produce a

heterodinuclear ruthenium-cobalt species which could then be evaluated for use as a photo-activated cytotoxin.

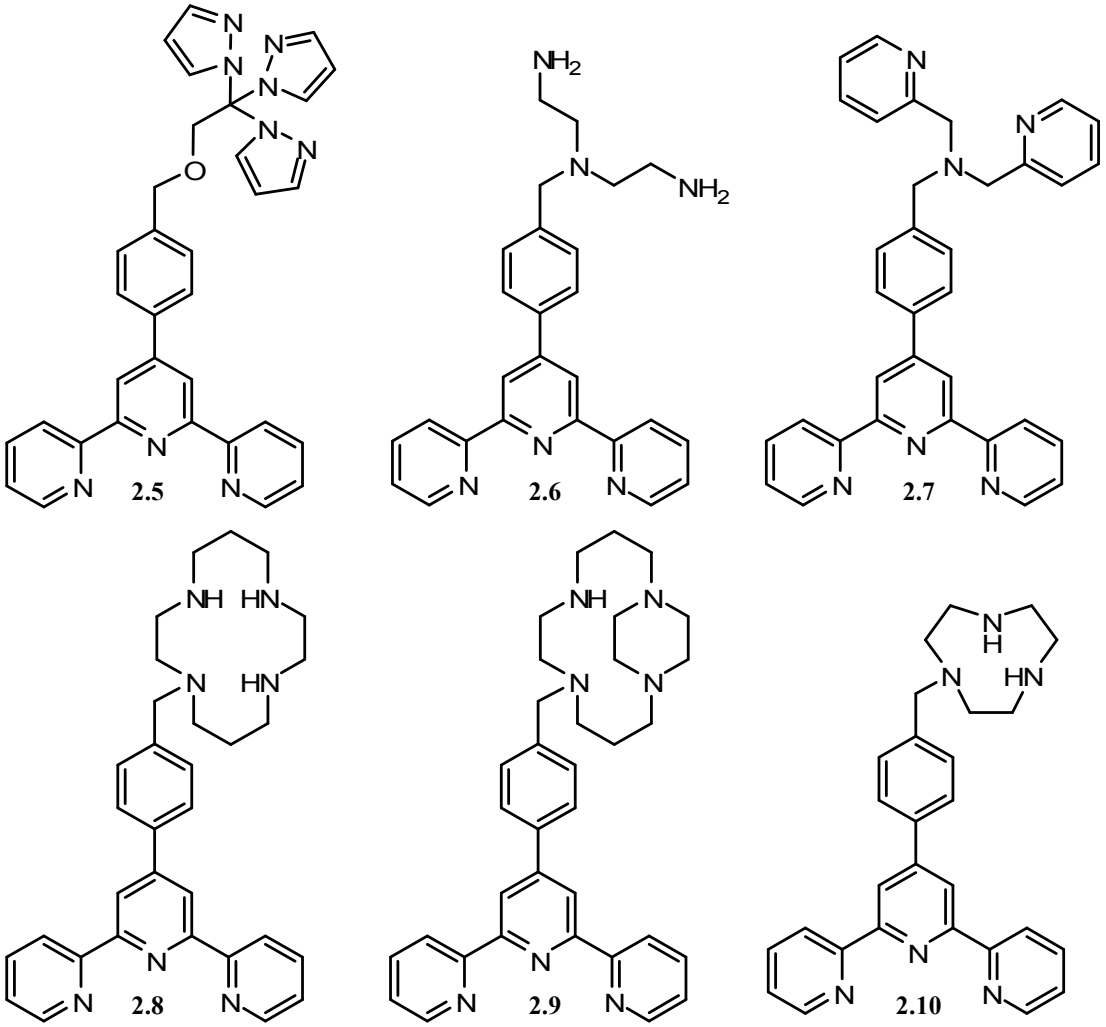

Figure 2.6 Bridging ligands synthesised by Zibaseresht

Zibaseresht reacted the ligand **2.5** with ruthenium(II), iron(II), copper(II), zinc(II) and silver(I) ions. By forming these homonuclear complexes, Zibaseresht was able to examine the affinity of each of the binding domains towards various metals. However, with the exception of the silver(I) ions, the only observed binding in the products was through the terpyridine end of the molecule. In the silver(I) case, the silver ion was bound in a planar tridentate fashion to the terpyridine site of one ligand and to a single pyrazole donor group from a second ligand,

forming a [2 + 2] complex. This demonstrated that the terpyridine portion of the molecule is a better binding domain than the pyrazole, but that it still might be possible to form heterodinuclear complexes.

Attempts were then made to produce heterodinuclear metal complexes. This was done by taking the previously synthesised mononuclear iron and ruthenium complexes of **2.5** and reacting them with various metal salts. The resulting products were examined with ^{1}H NMR and ESI-MS. Of all the metal ions trialled, only silver(I) ions showed evidence of binding to the pyrazole donors. This means that **2.5** is not an appropriate bridging ligand because it cannot bind to both cobalt(III) and ruthenium(II) ions at the same time.

However, Zibaseresht was able to generate heterodinuclear ruthenium(II)-cobalt(III) complexes by using the ligand **2.8**. First **2.8** was reacted with Ru(ttp)Cl_3 in ethanol to form the ruthenium(II) complex **2.11**. The cobalt(III) ion was then coordinated by reaction of **2.11** with $Na_3[Co(NO_2)_6]$ and the complex **2.12** was isolated as its PF_6^- salt. The dinitrito complex **2.12** could then be converted into the dichlorido complex **2.13** by treatment with 6 M HCl. (Figure 2.7)

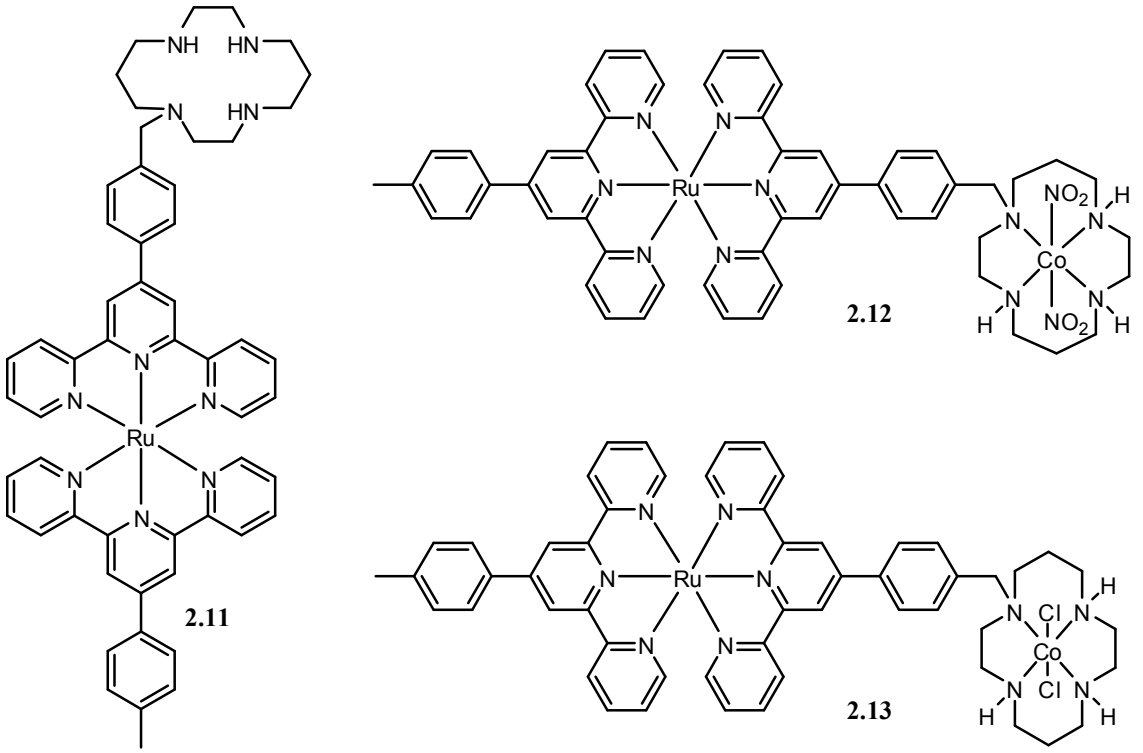

Figure 2.7

Finally Zibaseresht exposed the system to the cytotoxin analogue ethane-1,2-diamine (en). Reaction of the dichlorido complex **2.13** with an excess of en resulted in removal of the cobalt ion from the macrocycle and re-isolation of the parent complex **2.11**. This was a disappointing result because the en complex would have been very useful in monitoring any light induced ligand release. This result was also unusual because cyclam complexes are generally considered to be quite stable. Use of less en and milder reaction conditions resulted in the majority of the sample undergoing no reaction. However, a small amount of cobalt(III) was still lost from the macrocycle and a trace amount of the protonated ruthenium-cobalt complex with en bound was detected by mass spectrometry.

One possible explanation for the poor binding of en is the binding geometry of the cobalt(III) metal centre, which could prohibit the coordination of a bidentate ligand. Cyclam is able to bind to an octahedral metal, such as cobalt(III), in such a way that the two remaining

coordination sites are either in a *cis* or *trans* arrangement, giving rise to two different possible isomers (Figure 2.8).

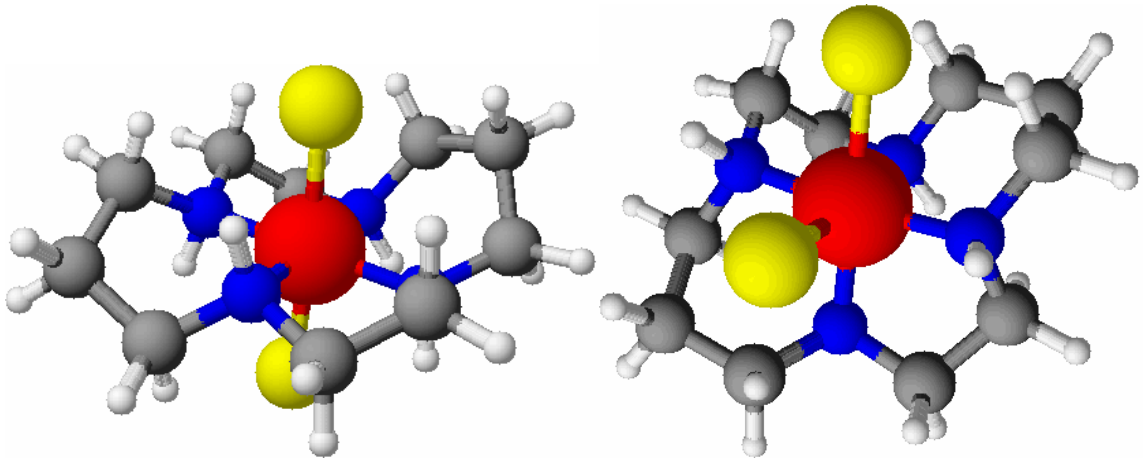

Figure 2.8 Cyclam bound to an octahedral metal centre in a *trans* (left) and *cis* (right) fashion. The yellow balls identify the remaining free coordination sites

When acting as a bidentate ligand for an octahedral metal centre, en binds to two *cis* related positions. A *trans* arrangement of the complex could be counterproductive as it would require isomerisation to occur before binding. However, attempts by Zibaseresht to definitively identify which isomers of the dinitrito and dichlorido complexes had been formed proved unsuccessful. Cobalt complexes show well-established changes in the d-d transitions of their UV-visible spectra when in different binding geometries. However, the UV-visible spectra of **2.11**, **2.12** and **2.13** were all very similar in appearance, with the dominant peak at 490 nm being the MLCT transition characteristic of the ruthenium(II)polypyridyl systems. The presence of these large MLCT bands obscured the cobalt(III) d-d bands. The shape and location of the d-d bands could not, therefore, be used to determine which of the *cis* or *trans* isomers were formed.

Poon and Tobe suggest that *trans* isomers of cobalt(III) complexes of cyclam and two monodentate ligands, such as in **2.12** and **2.13**, are the dominant products in aqueous solution.[108, 109] They have also reported that *cis* complexes with monodentate ligands

eventually isomerise to a *trans* configuration in aqueous solution.[110] The similarities between the cobalt bound cyclam end of the systems **2.12**, **2.13** and the systems of Poon and Tobe lead us to conclude that the product complexes are most likely *trans* isomers.

2.1.4. Synthesis of Strapped Cyclams

Since Zibaseresht's inability to bind en to the heterodinuclear ruthenium-cobalt complex **2.13** in more than trace amounts was potentially due to the cobalt being bound to the cyclam with the vacant sites in a *trans* arrangement, we began our research by looking for an established way to force the vacant sites into a *cis* geometry. Such a restriction can be achieved by strapping the cyclam molecule with an ethyl bridge between two of the nitrogen atoms. Depending on which nitrogen atoms are connected to the strap, different coordination geometries can be realised.[111, 112]

The synthetic route for a strapped cyclam with the vacant sites in a *cis* relationship is reported by Weisman and Wong.[111] First the cyclam is reacted with aqueous glyoxal in acetonitrile to give the tetra cyclic bis aminal product **2.15**. **2.15** is then dialkylated in a single step before reduction with sodium borohydride (Figure 2.9).

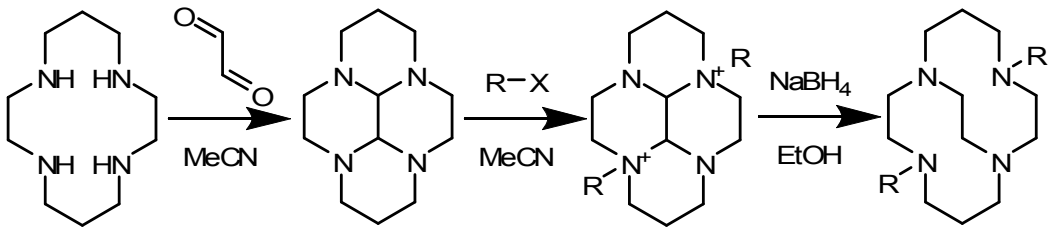

2.14 **2.15** **2.16** **2.17**

Figure 2.9 Synthesis of cross strapped cyclam

Weisman and Wong also report that particular R groups can be removed by hydrogenation using gaseous hydrogen and 10% palladium on carbon. This means that it is

possible to synthesise an unsubstituted cross strapped cyclam. This unsubstituted cross strapped cyclam can then be reacted with alkyl halides to give a wide range of products.

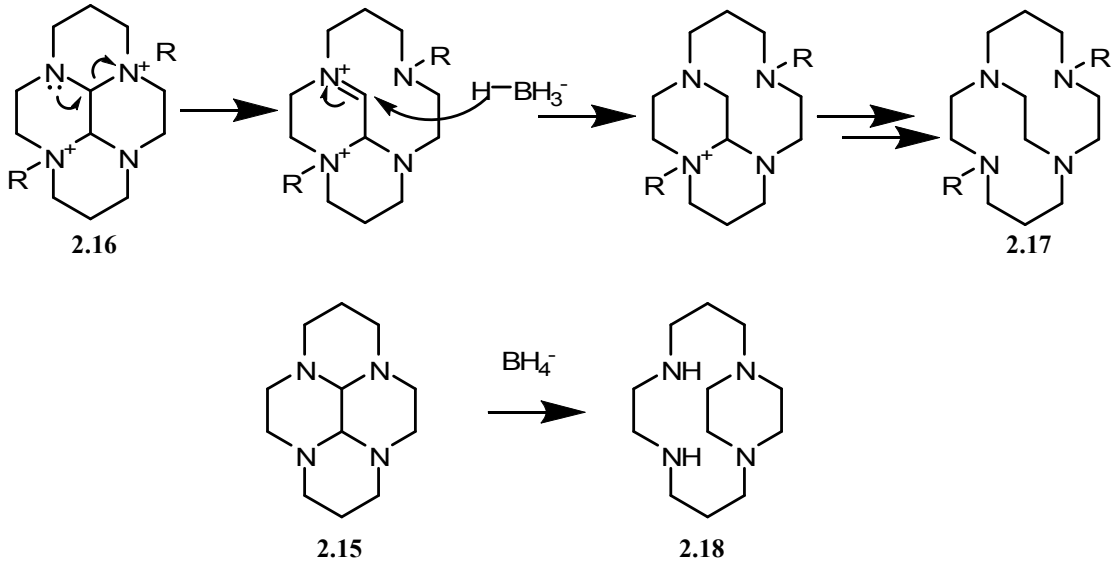

Figure 2.10 Reduction of cyclam based tetracycles

The dialkylation is important because it ensures that the double reductive ring expansion gives the cross strapped product and not the piperazine **2.18**, which is the observed product from the reduction of either the mono or unalkylated tetracycle (Figure 2.10). The piperazine **2.18** can also be directly synthesised by reaction of cyclam with 1,2-dibromoethane. If the reaction is carried out with a large excess of 1,2-dibromoethane, the doubly bridged species **2.19** is formed (Figure 2.11). These bridges provide a steric barrier which should be sufficient to prohibit the ligand binding in such a way that the other coordination sites are *cis* to each other.[112]

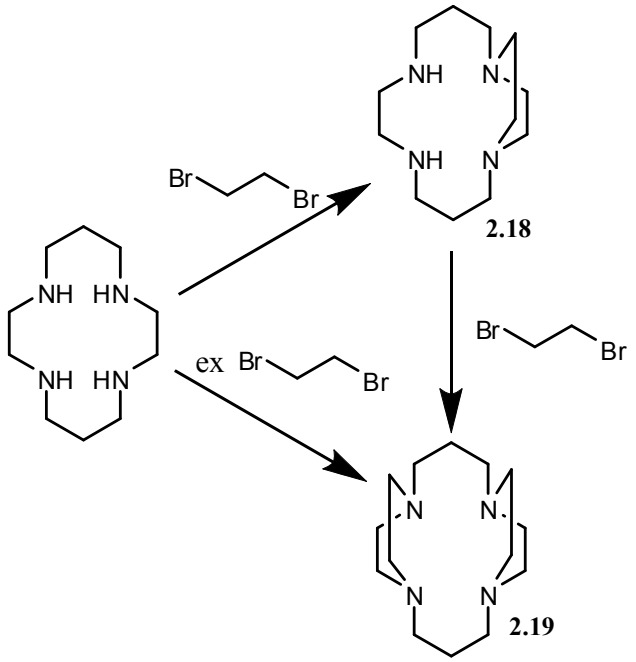

Figure 2.11 Reactions of 1,2-dibromoethane with cyclam

Therefore, by using the synthetic strategies outlined above, it is possible to synthesise ligands based on the cyclam macrocycle which can only exhibit specific binding geometries.

2.2. Results and Discussion

2.2.1. Synthesis of Strapped Cyclam with a 4'-*p*-Tolylterpyridine Substituent

We began our experimental work with the intention of synthesising a ligand similar to **2.8**, with the difference being that the cyclam end would be strapped in such a way so as to force *cis* binding. Such a synthesis would involve the formation of a dialkylated tetracycle, as outlined in Figure 2.9 and Figure 2.10, where at least one of the alkyl arms is ttp. The tetracycle could then be reduced to give the final ligand.

2.2.1.1. Formation of the Dialkylated Tetracyclic Intermediate

The first step was to alkylate the tetracycle with ttp. This was done by reacting **2.15** with **2.4** in THF and resulted in the formation of an off white solid. ^{1}H NMR in D_2O was then used to identify the product as the monoalkylated product **2.20**. Although the experimental method reported by Weisman and Wong[111] exclusively resulted in double alkylation of the tetracycle, **2.15**, only the monoalkylated product could be observed. However, it should be noted that the method reported by Weisman and Wong only used benzyl bromide and iodomethane as alkylating agents.

Since, as detailed in **2.1.4**, reduction of a monoalkylated tetracycle results in the formation of a piperazine, the product needs to be alkylated a second time. However, the mono substituted product had a poor solubility profile and a satisfactory reaction scheme for direct alkylation with iodomethane to give the dialkylated product **2.21** could not be found. We propose that it was this poor solubility which prevented the formation of any dialkylated product in the initial reaction, as the monoalkylated form is no longer soluble in THF.

In order to improve the solubility profile of **2.20** we decided to coordinate the monoalkylated ligand to ruthenium. To do this **2.20** was heated at reflux with [Ru(ttp)Cl_3] in dry methanol for 4 hours, after which the solution was cooled to room temperature, water was added and the complex **2.22** was precipitated out as the PF_6^- salt (Figure 2.12). The newly synthesised complex was soluble in acetonitrile and therefore reaction with iodomethane was now possible.

The complex **2.23**, bearing a dialkylated macrocycle, was synthesised by methylating **2.22** with an excess of iodomethane in acetonitrile. The product **2.23** was identified through

the appearance of a new singlet at approximately 3.5ppm in the ^{1}H NMR spectrum, assigned to the new methyl group.

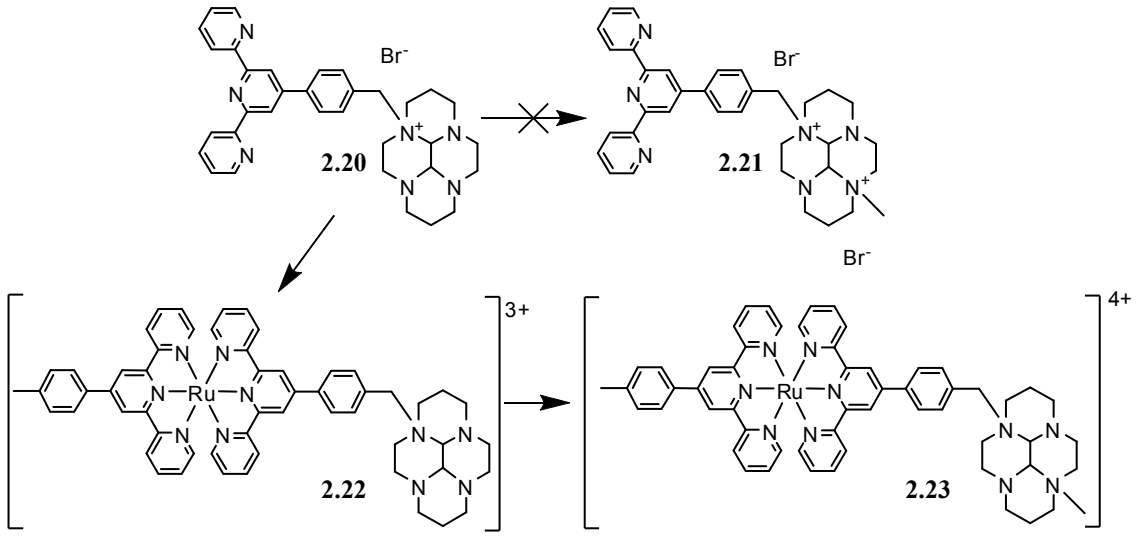

Figure 2.12

2.2.1.2. Reduction of the Tetracyclic Intermediate

After completing the synthesis of **2.23**, the next step in our proposed synthetic route was to reduce the macrocycle and produce the cross strapped ligand **2.24**. In order to achieve this, we carried out a reduction reaction using sodium borohydride. The ^{1}H NMR spectrum of the reduced product showed fewer peaks than expected in the aromatic region and only one in the aliphatic region, which was a singlet. This indicated that the cyclam group had been removed. The ^{1}H NMR spectrum of the reduced product was then compared to that of $[Ru(ttp)_2](PF_6)_2$, and appeared to be identical. From this result we concluded that the product of the reduction reaction was the complex $[Ru(ttp)_2]^{2+}$, **2.25**, instead of the desired product, **2.24** (Figure 2.13). There are two possible explanations for how **2.25** was formed: either the sodium borohydride was breaking the carbon nitrogen bond between the ttp and the cyclam, or the ligands on the ruthenium were exchanging and we were only seeing one of several products. Since the latter of these two explanations both fails to explain what was happening

to the other ligands and does not conform to the classification of ruthenium as an inert metal, we suspect that it was the sodium borohydride breaking the carbon nitrogen bond that was responsible for the formation of **2.25**.

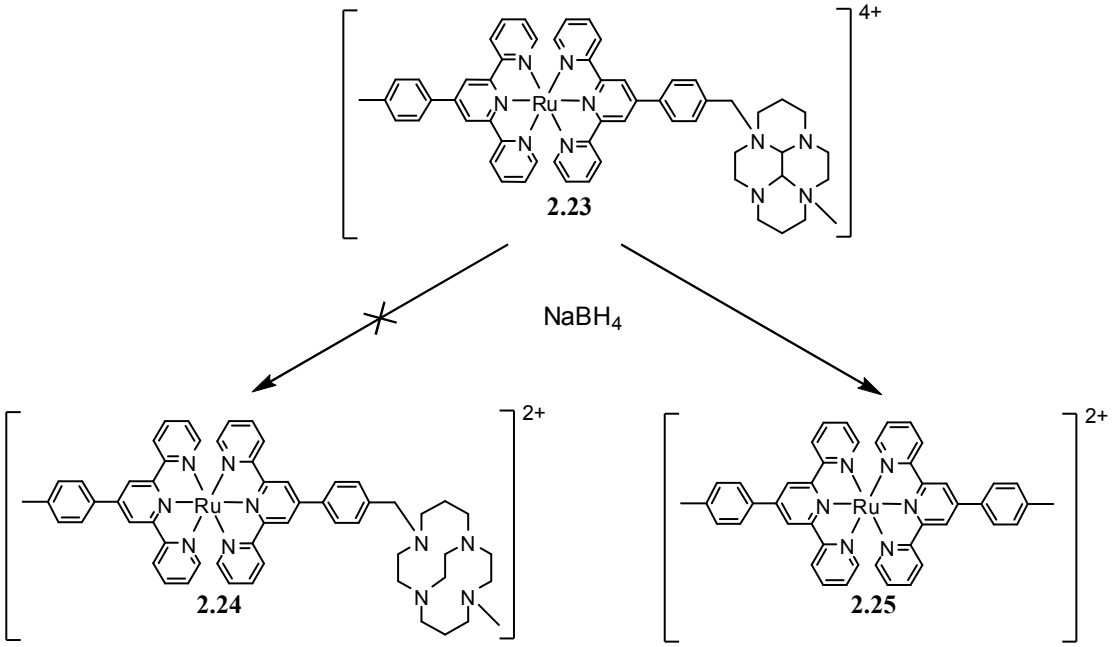

Figure 2.13

In order to assess whether the final product, **2.25**, was being directly formed by the reduction of **2.23** or was formed by a further reduction of the desired product **2.24**, the reaction was monitored by TLC. This revealed that two products were initially formed; however, after 5 minutes only one product was left, presumably $[Ru(ttp)_2]^{2+}$. From this we hypothesise that although some of the borohydride was reducing the macrocycle to give the desired product, this species was short lived because the ttp-cyclam bond was also easily broken by the borohydride.

2.2.2. Reduction of a Related Ruthenium Complex

Because the observed product from the reduction of **2.23** could potentially be formed by ligand exchange, an additional experiment with the ruthenium complex **2.26** was carried

out. In **2.26** there is a carbon oxygen bond analogous to the carbon nitrogen bond in **2.23**. If this carbon oxygen bond was broken by reaction with sodium borohydride, the product, **2.27**, could be definitively identified as being formed by this method as the two ligands on the ruthenium(II) metal centre would not be identical (Figure 2.14).

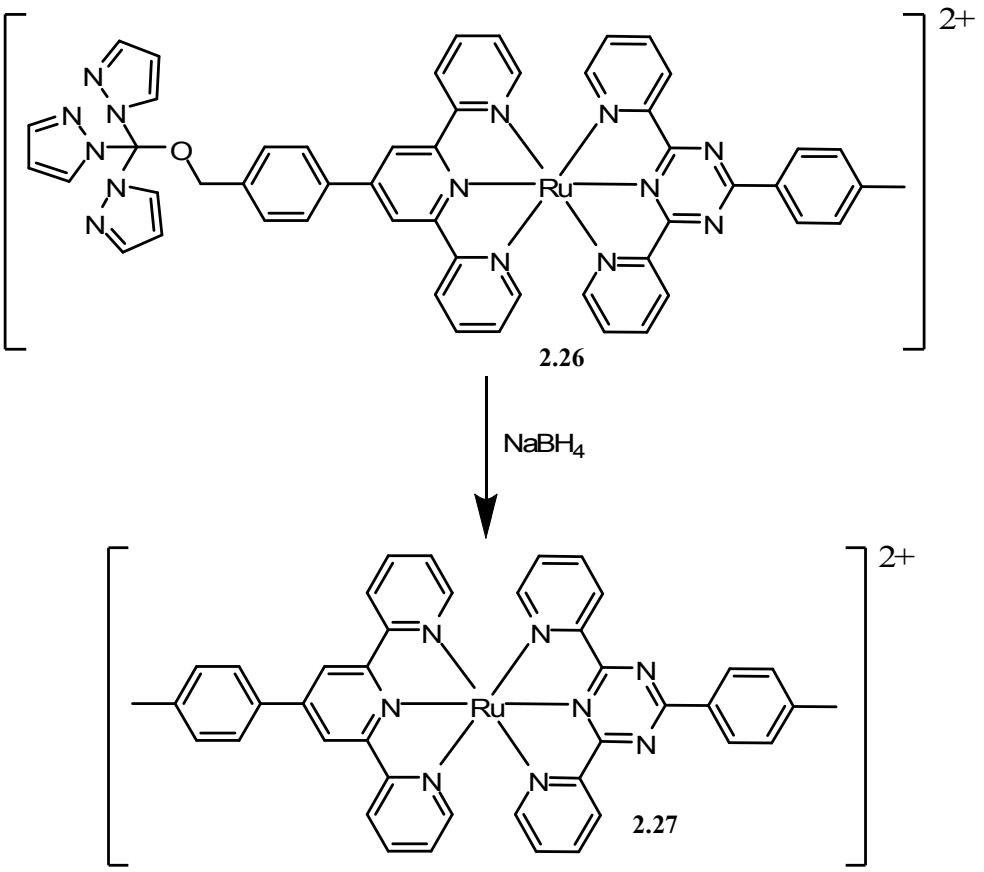

Figure 2.14

The complex **2.26** was subjected to the same reaction conditions as **2.23** and the ^{1}H NMR and mass spectra were recorded. ^{1}H NMR spectroscopy was not as definitive in this case as it was for **2.25**, due to the complex having two different ligands and less internal symmetry, which made the change less obvious. Mass spectrometry showed a major peak with m/z of 375. Both this mass and the observed isotope pattern around it agree with what would be predicted for **2.27** and led us to conclude that the same type of reaction was occurring (Figure 2.15).

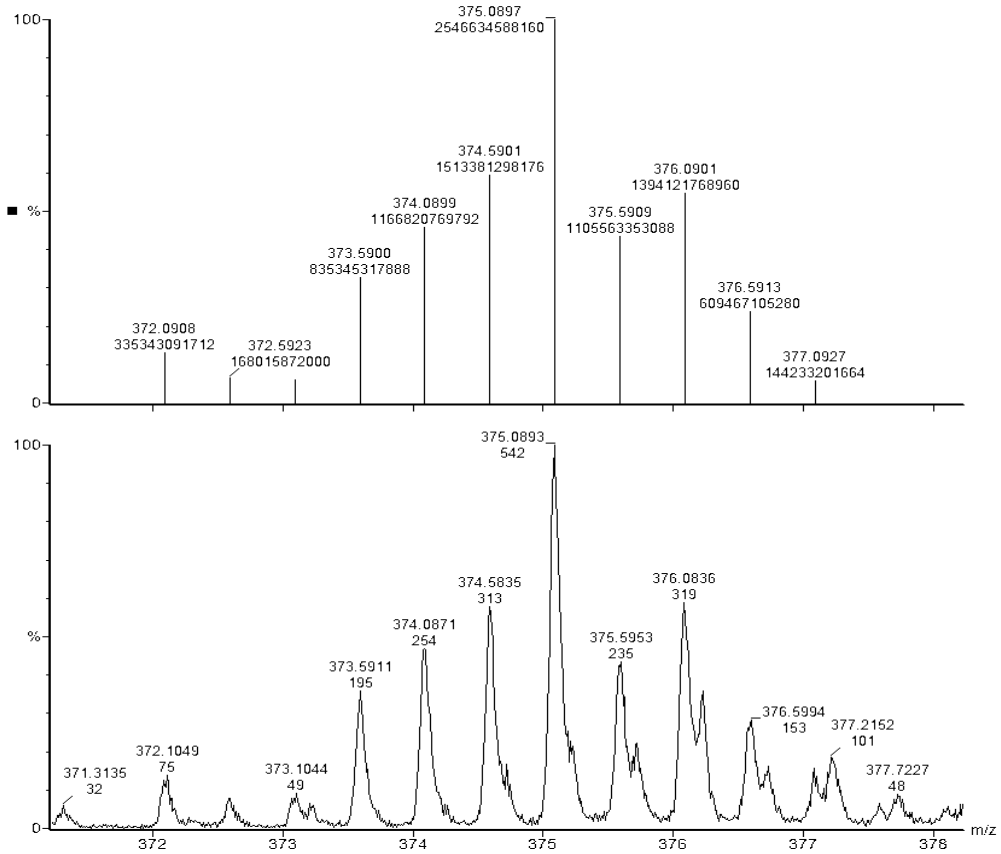

Figure 2.15 Predicted and experimental isotope pattern for 2.27

Because the two ligands are not the same, this result, unlike the previous one, could only have resulted from the breaking of the bond between the carbon atom and the uncharged oxygen atom. From this we concluded that a sodium borohydride reduction of a ruthenium complex containing a carbon-hetero atom single bond can result in the breaking of the bond.

One possible way to circumvent this problem would be to cross strap the cyclam molecule before reaction with ttp, as this would remove the need for treatment with sodium borohydride. Unsubstituted cross strapped cyclam can be synthesised in three steps from **2.16**. The first step involves the double alkylation of **2.16** with benzyl bromide; this is then followed by reduction with sodium borohydride before the benzyl groups are removed by hydrogenation (Figure 2.16). This unsubstituted cross strapped cyclam could then be reacted

with **2.4** to give a ligand with potential application in our study. However, we decided to explore other methods for synthesising potential bridging ligands rather than pursue this further.

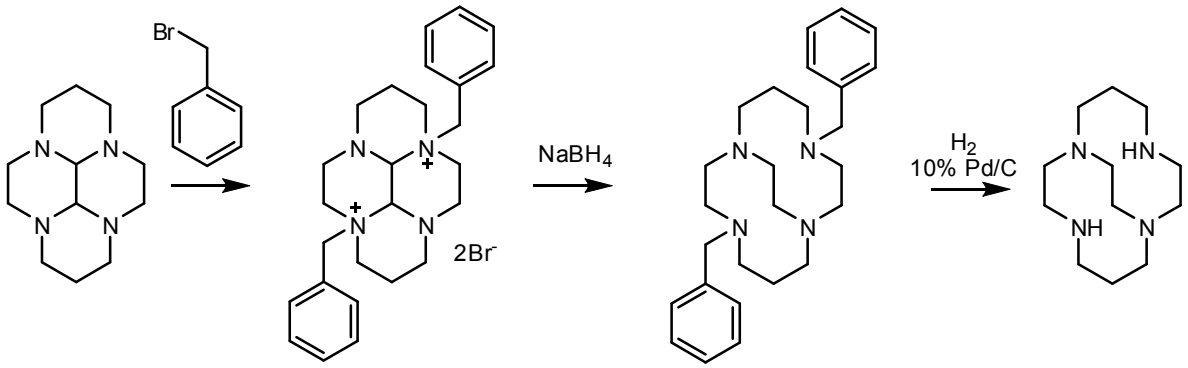

Figure 2.16 Synthesis of unsubstituted cross strapped cyclam

2.2.3. Binding of 6'-*p*-tolyl-2,2':4',2''-terpyridine to Ruthenium(II)

When ttp is synthesised using the Collin-Balzani-Sauvage method, the side product **2.3** can also be isolated.[99] Although ttp has been featured in 109 peer reviewed journal articles, the minor product has only been featured in 7. We therefore took the opportunity to look into the binding properties of a relatively ignored ligand.

In order to further study the binding of the minor isomer, **2.3** was heated at reflux with $RuCl_3.xH_2O$ in ethanol for 3 hours. Slowly cooling the reaction mixture to room temperature caused a deep red crystalline solid to form, from which a crystal was selected and examined by X-ray diffraction (Figure 2.17).

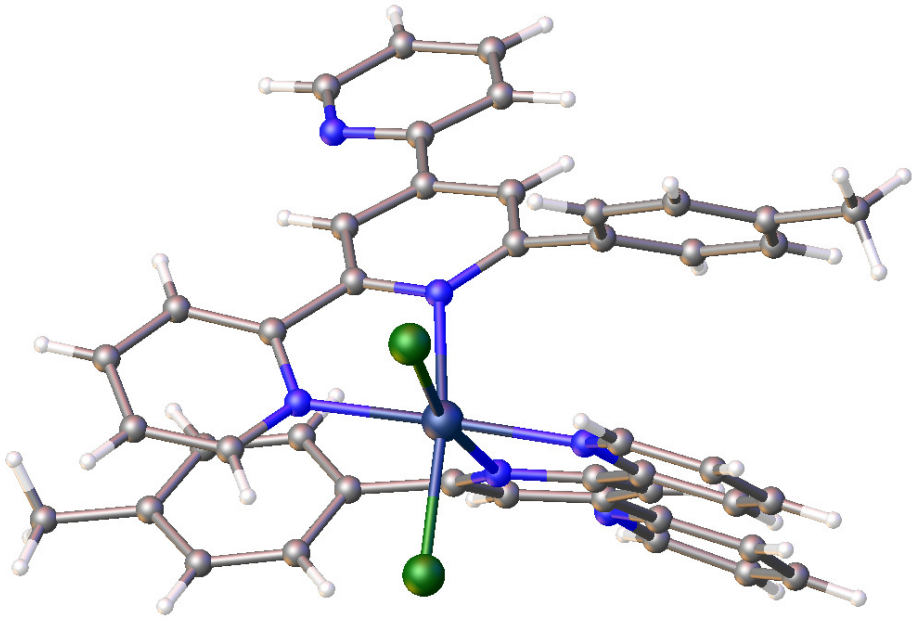

Figure 2.17 X-ray crystal structure of [Ru(6′-*p*-tolyl-2,2′:4′,2″-terpyridine)$_2$Cl$_2$]; solvent molecules have been omitted for clarity

In the obtained structure the ruthenium(II) atom is bound to two ligands of **2.3** as well as two chloride ligands. **2.3** is bound in a bidentate manner through the nitrogen atoms of the central and 2′ pyridine rings. The structure shows intramolecular π-π stacking between the bound singly substituted pyridine ring and the tolyl ring of the other ligand, as well as intermolecular π-π stacking between the unbound and central pyridine rings. Unfortunately additional electron density, which can be attributed to solvent channels existing in the crystal lattice, meant that the ethanol solvent molecules could not be satisfactorily modelled. However, since we obtained this crystal structure, Bray has reported an X-ray crystal structure with copper bound to 6′-*p*-tolyl-2,2′:4′,2″-terpyridine instead of ruthenium, which shows the same binding motif.[113]

Since **2.3** has similar binding to bpy and can be functionalised in the same manner as outlined for ttp in section 2.1.2, there are many potential applications for this ligand and its derivatives which could be studied in the future.

2.3. Conclusion

The synthesis of the ruthenium bound potential bridging ligand **2.24**, consisting of ttp with an appended strapped cyclam molecule, was attempted. The synthesis of the precursor **2.20** was achieved by reacting the tetracycle **2.15** with the brominated form of ttp (**2.4**). However, due to the poor solubility of **2.20**, it could not be methylated directly. To circumvent this problem, **2.20** was complexed to $[Ru(ttp)Cl_3]$ to give **2.22**, and then this was methylated to give **2.23**. Unfortunately, sodium borohydride reduction of **2.23** resulted in the breaking of the bond between the nitrogen atom of the cyclam and methyl carbon of the ttp, resulting in the formation of $[Ru(ttp)_2]^{2+}$ instead of the desired product **2.24**.

Although the problem associated with the reductive step could, in principle, be circumvented by synthesis of the strapped cyclam molecule prior to it being appended to the ttp ligand, we decided that it would be more productive to pursue new bridging ligands rather than adding additional steps to this synthetic route.

Chapter 3: Two Bridging Ligand Series and Their Ruthenium Complexes

3.1. Introduction

The bridging ligand of a photo-activated cytotoxin would ideally be able to selectively bind two different metal centres, as well as permitting electron transfer between these two metals. In Chapter 2 we examined ligands with different coordination numbers and binding geometries at each of the binding domains. In this chapter we will demonstrate that ligands with little or no variation between the binding geometry of their domains can also be used as potential bridging ligands.

First we will outline the process for the synthesis of two series of bridging ligands. We will then discuss how to form ruthenium(II) complexes of these ligands with one vacant binding domain. Finally the coordination and interactions of these ruthenium(II) complexes with various metals, excluding cobalt(III), will be discussed. The formation and reactivity of ruthenium-cobalt heterodinuclear complexes of these ligands is discussed in Chapter 4.

3.1.1. Jurgen Sauer's 'LEGO' System

In 1998 Jurgen Sauer first published details of his 'LEGO' system.[114, 115, 116, 117, 118] This system provides a synthetic strategy for the formation of a wide range of oligopyridines over two steps (Figure 3.1).

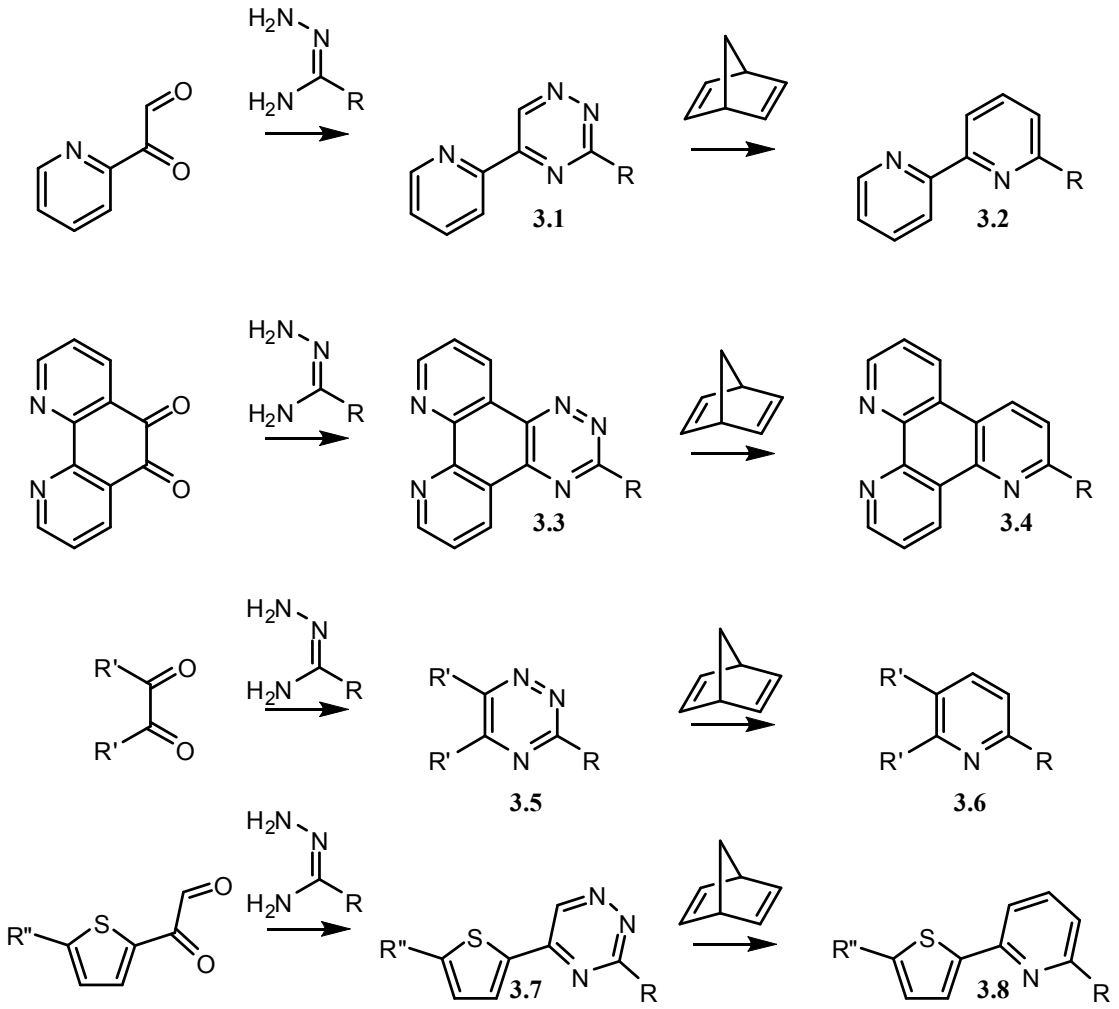

Figure 3.1 Examples of ligands produced by the 'LEGO' system

Step one is a condensation reaction between a hydrazonamide and a 1,2-dicarbonyl compound. After the product from the condensation reaction is isolated, it undergoes an inverse-type Diels-Alder reaction (Figure 3.2) to give the final product.

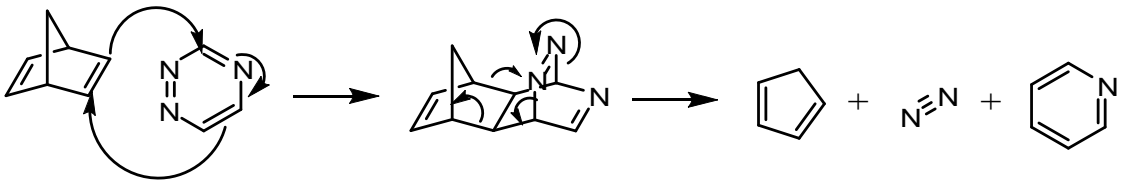

Figure 3.2 Mechanism for an inverse-type Diels-Alder reaction

The paper which was of particular interest to us related to the synthesis of 6-oligopyridyl-1,5,12-triazatriphenylenes (**3.4**).[114] However, it was not the final product that we

intended to use in our research, but rather the triazine intermediate **3.3**. In addition to the 1,10-phenanthroline binding domain in **3.3**, a second binding domain can be formed by having an appropriate R group, such as 2-pyridine (Figure 3.3).

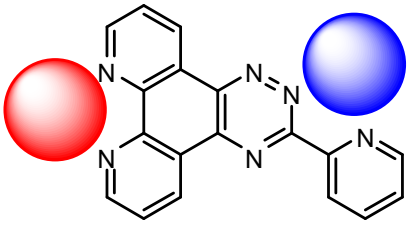

Figure 3.3 3-(pyridin-2-yl)-[1,2,4]triazino[5,6-f][1,10]phenanthroline (pytp) and its potential binding domains

One way to achieve selective binding of a ruthenium metal centre to a ligand such as pytp is to synthesise the ligand on the metal centre. Such a synthesis involves coordinating the phendione to a ruthenium(II) metal centre before reaction with the hydrazonamide.[119]

3.1.2. 3,6-Disubstituted-1,2,4,5-Tetrazines

The carboxamidrazones used in the 'LEGO' system are prepared by the reaction of hydrazine with an aryl nitrile (**3.9**). However, while these reactions result in the formation of a hydrazonamide under mild conditions, more vigorous reaction conditions result in the formation of a dihydrotetrazine (**3.10**). Oxidation of this generates a 1,2,4,5-tetrazine (**3.10**).[120, 121, 122, 123, 124]

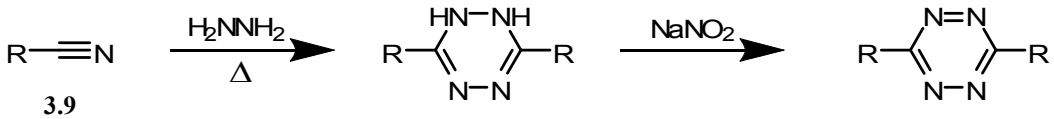

3.9 **3.10** **3.11**

Figure 3.4 Formation of disubstituted-1,2,4,5-tetrazines

These tetrazines are of interest to the wider academic community because they can undergo inverse-type Diels-Alder reactions to generate a variety of complexes. However, our interest in these ligands relates to the possibility of generating bidentate binding domains. This

can be achieved through the incorporation of a nitrogen containing substituent, such as pyridine, to the tetrazine core (Figure 3.5).

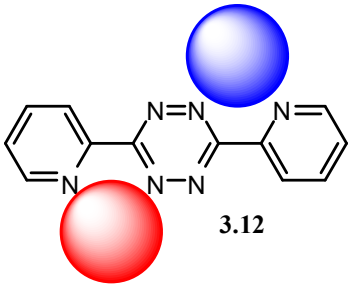

3.12

Figure 3.5 3,6-di(pyridin-2-yl)-1,2,4,5-tetrazine (pytz) and its potential binding domains

Ligands such as pytz (**3.12**) are of interest to us because the low-lying π^* orbitals of the ligand enable longer wavelength MLCT absorption events to occur. Diruthenium complexes of pytz have previously been reported to have an unusually long wavelength MLCT band at 685 nm.[124] Since longer wavelengths of light are not as readily absorbed by the body, if the MLCT band for a ruthenium-cobalt heterodinuclear complex of pytz is at a similar wavelength to that of the diruthenium complex, this could add additional benefit to our photo-activated cytotoxin.

3.2. Results and Discussion

The ligands we selected for further investigation were based on the 1,2,4,8,9-pentaazatriphenylene intermediates (**3.3**). The first of these triazine intermediates was 3-(1,10-phenanthrolin-2-yl)-[1,2,4]triazino[6,5-f][1,10]phenanthroline (phtp) (**3.13**). This ligand has two potential binding domains: one is tridentate, utilising the appended phenanthroline group and a single nitrogen from the triazine; the other is bidentate and arises from the fused 1,10-phenathroline. (Figure 3.6) It was this tridentate vs bidentate nature of the two domains that we intended to use to achieve selective binding during the formation of metal complexes. The

intention was to bind ruthenium to the tridentate domain, leaving the bidentate domain free to coordinate to another metal.

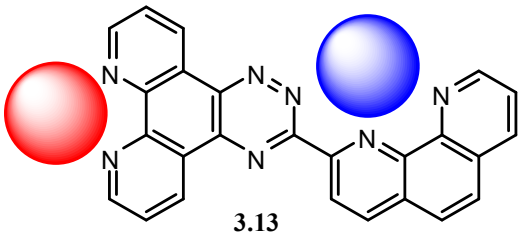

3.13

Figure 3.6The ligand phtp and its potential binding domains

The other series that we selected for study was based around a substituted 1,2,4,5-tetrazine core. However, because these substituted tetrazines have identical binding domains, we could not use coordination geometry to prevent a metal centre from binding to both domains.

3.2.1. 3-(1,10-Phenanthrolin-2-yl)-[1,2,4]triazino[6,5-f][1,10]phenanthroline

The first step in the synthesis of phtp (**3.13**) was to generate 2-cyano-1,10-phenanthroline (**3.16**); this was synthesised by first forming the *N*-oxide (**3.15**) of 1,10-phenanthroline (**3.14**) and then treating this with potassium cyanide (Figure 3.7).[125]

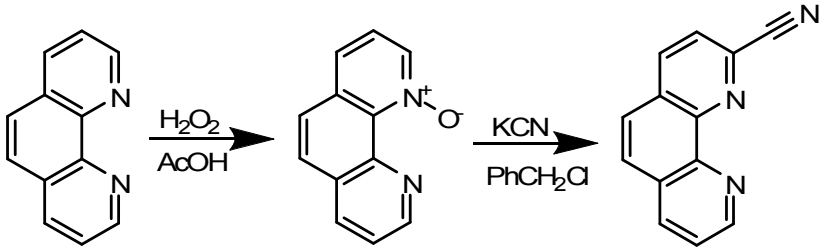

3.14 **3.15** **3.16**

Figure 3.7 Synthesis of 2-cyano-1,10-phenanthroline

3.16 was then reacted with hydrazine to give the carboxamidrazone **3.17**.[126] Using the synthetic strategy outlined by Sauer, the carboxamidrazone is reacted with 1,10-phenanthroline-5,6-dione to yield the yellow ligand phtp. (Figure 3.8)

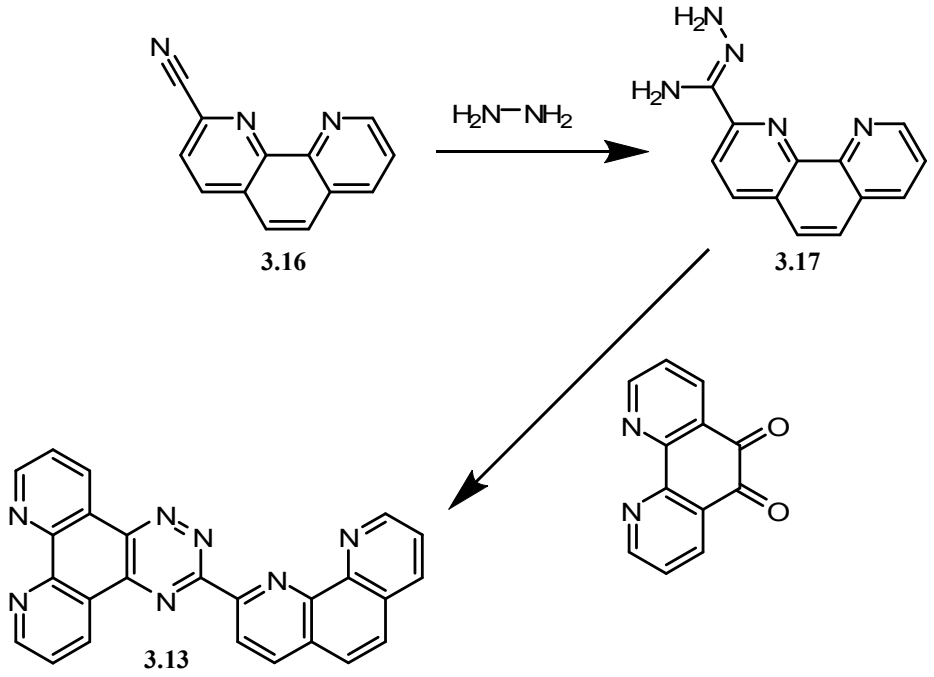

Figure 3.8 Synthesis of phtp

3.2.2. 3-(Pyridin-2-yl)-[1,2,4]triazino[6,5-f][1,10]phenanthroline and 3-(Pyrazin-2-yl)-[1,2,4]triazino[6,5-f][1,10]phenanthroline

The synthesis of the ligands 3-(pyridin-2-yl)-[1,2,4]triazino[5,6-f][1,10]phenanthroline (pytp) (**3.18**) and 3-(pyrazin-2-yl)-[1,2,4]triazino[5,6-f][1,10]phenanthroline (pztp) (**3.19**) (Figure 3.9) followed the same synthetic pathway as the synthesis of phtp (**3.13**). However, since both 2-cyanopyridine and 2-cyanopyrazine are readily available, they did not need to be synthesised prior to the reaction with hydrazine.

Figure 3.9 The ligands pytp (3.18) and pztp (3.19)

3.2.2.1. Crystal Structure of Pytp

Dissolving pytp in a dilute solution of hydrochloric acid and then allowing slow evaporation to occur yielded large yellow needles suitable for use in X-ray crystallography. The X-ray structure showed the pytp to be in a doubly-protonated form with two chloride ions present to balance the charge. The protons are bound to a phenanthroline nitrogen atom and a pyridyl nitrogen atom and highlight the intended metal binding domains of the ligand. The ligand is planar, with the pyridine ring in the plane of the molecule.

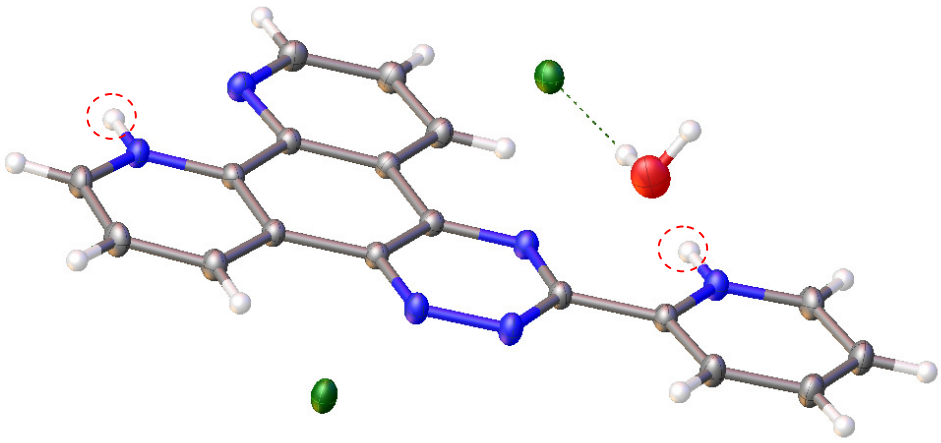

Figure 3.10 X-ray crystal structure of pytp.2HCl. The nitrogen bound H atoms are circled

There is an average distance of 3.255 Å between the planes of the molecules, which is close enough for π-π interactions to occur. However, there is poor overlap between the ligands. The main intermolecular interaction is a hydrogen bonding network between the protonated nitrogen atoms, chloride ions and water molecule (Figure 3.11).

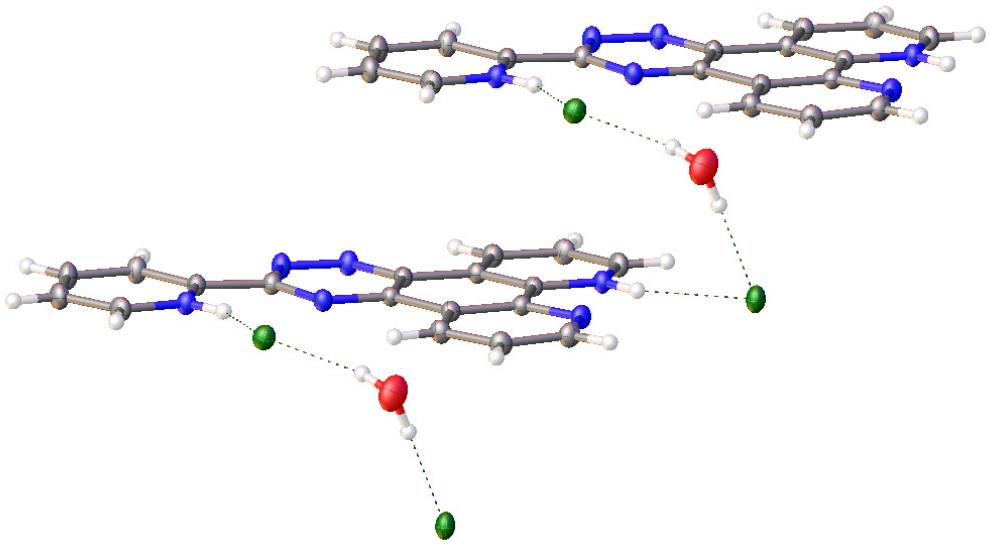

Figure 3.11 Hydrogen bonding network in the X-ray crystal structure of pytp.2HCl

3.2.3. 3,6-di(pyridin-2-yl)-1,2,4,5-tetrazine and 3,6-di(pyrazin-2-yl)-1,2,4,5-tetrazine

The next ligands we synthesised were not from the 'LEGO' system but were the substituted tetrazines pytz (**3.12**) and pztz (**3.22**). These ligands were synthesised in two steps from 2-cyanopyridine and 2-cyanopyrazine respectively. The first step was reaction with hydrazine to generate the dihydrotetrazines **3.20** and **3.21**. This was followed by oxidation with $NaNO_2$ in acetic acid to give pytz and pztz. (Figure 3.12)

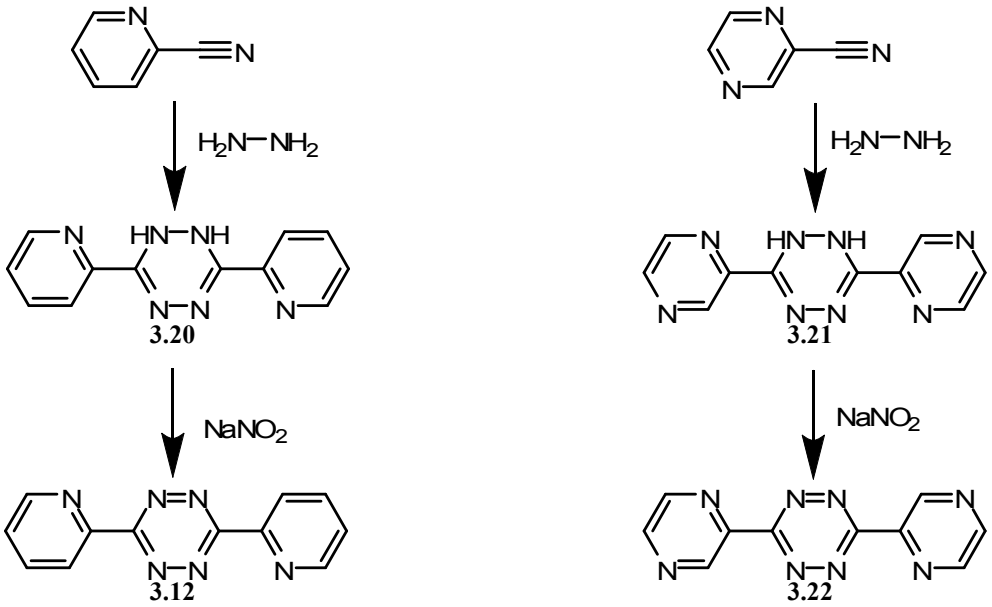

Figure 3.12 Syntheses of pytz (left) and pztz (right)

In the literature relating to the synthesis of the ligands pytz and pztz, three different reaction conditions for the synthesis of the dihydro intermediate are reported. The first of these involved heating a mixture of the appropriate nitrile, an excess of hydrazine, and sulfur in ethanol at reflux for three hours.[120] The next was simply to heat the nitrile and hydrazine together at reflux for 5 hours, with a minimal amount of ethanol added to aid dissolution of the nitrile.[122] The final method we evaluated was to heat a solution of the nitrile and hydrazine at reflux in THF with a small amount of HCl for five hours.[121]

All three of these methods gave an orange solid as the product. These orange solids were analysed by ^{1}H NMR spectroscopy. In all cases the desired dihydrotetrazine product was present. However, the reaction involving sulfur showed a large number of impurities. Of the other two, the reaction in THF gave a slightly lower yield but was easier to conduct because it lacked the solubility problems associated with the neat nitrile-hydrazine reaction.

The final step in the synthesis of pytz and pztz was using $NaNO_2$ to oxidise the dihydrotetrazine to the final product, which had the added benefit of removing any impurities. This was true even in the case of the sulfur reaction, although the overall yield was lower.

Unlike the 'LEGO' system ligands, these substituted tetrazines have identical binding domains. This could prove problematic during the coordination of a metal centre to these ligands as they could easily generate a dinuclear complex.

3.2.4. Formation of Triazine Based Ligands on Ruthenium

One way to ensure selective binding of ruthenium to the ligands phtp, pytp and pztp, is the synthetic strategy of pre-binding ruthenium to the 1,10-phenanthroline-5,6-dione before synthesising the ligands.[119] To achieve this an ethanolic solution of the carboxamidrazone was added to a solution of $[(bpy)_2Ru_2(phendione)](PF_6)_2$ in acetonitrile; after heating at reflux for 1 hour, the solution was cooled to room temperature and the solvent removed under vacuum to give the crude product. The final product was isolated by column chromatography on silica. (Figure 3.13)

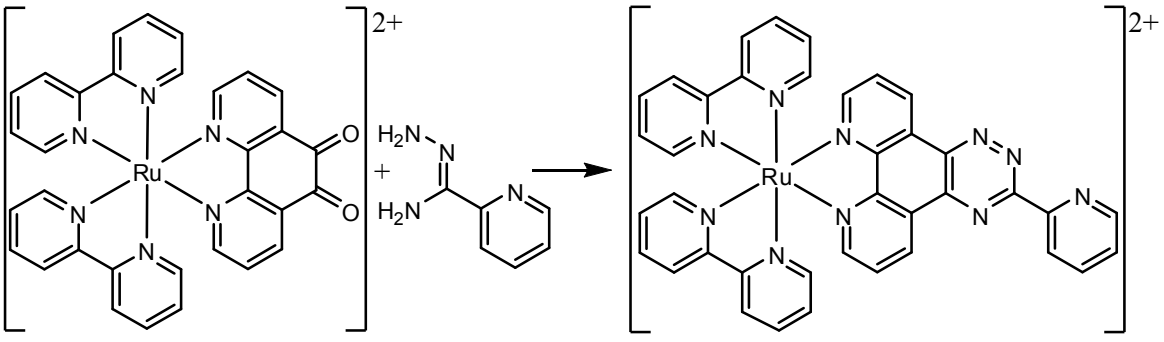

Figure 3.13 Synthesis of the ligand pytp on a ruthenium(II) metal centre

Characterisation of these complexes was achieved through the use of ESI-MS and NMR spectroscopy. gCOSY NMR techniques were employed to identify the various ring systems (Figure 3.14), and the assigned spectra are illustrated for $[(bpy)_2Ru(pytp)](PF_6)_2$

(Figure 3.15). The assignment of the ^{1}H NMR peaks proved invaluable during the later coordination studies, as detailed in Section 3.2.8.

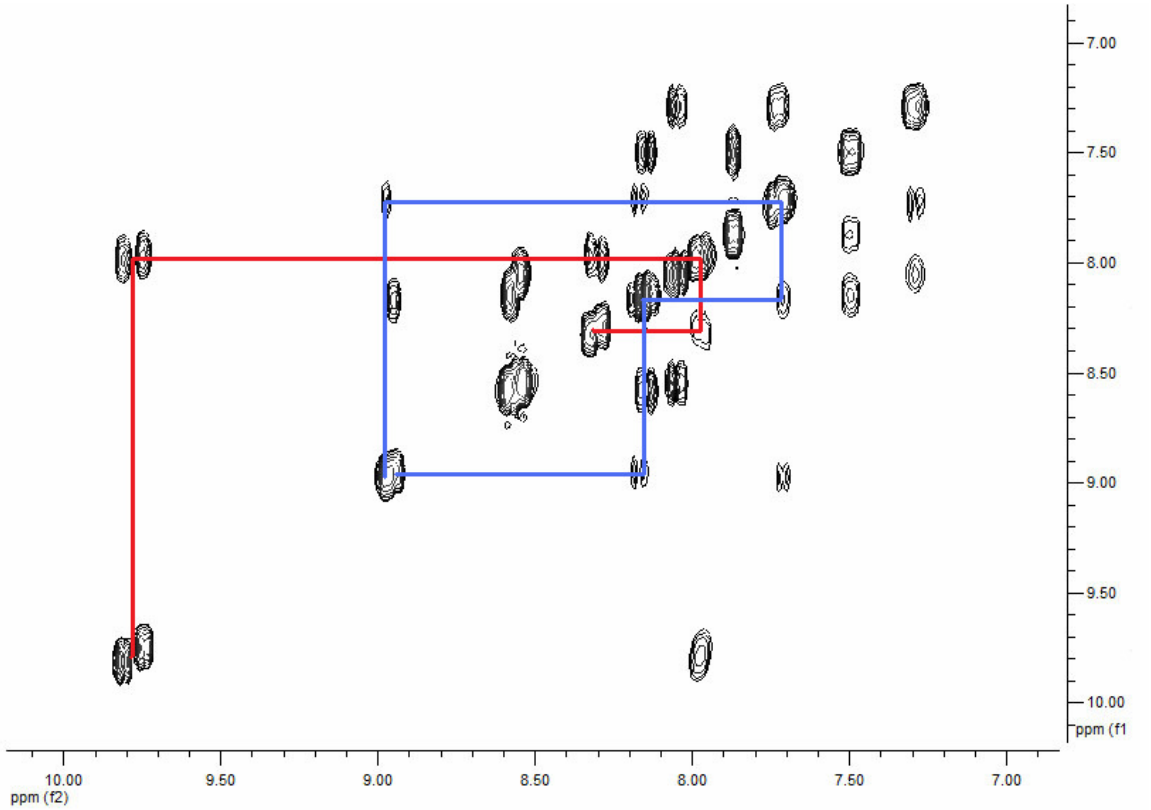

Figure 3.14 gCOSY NMR spectrum of $[(bpy)_2Ru(pytp)]^{2+}$ with the non-bpy spin systems highlighted

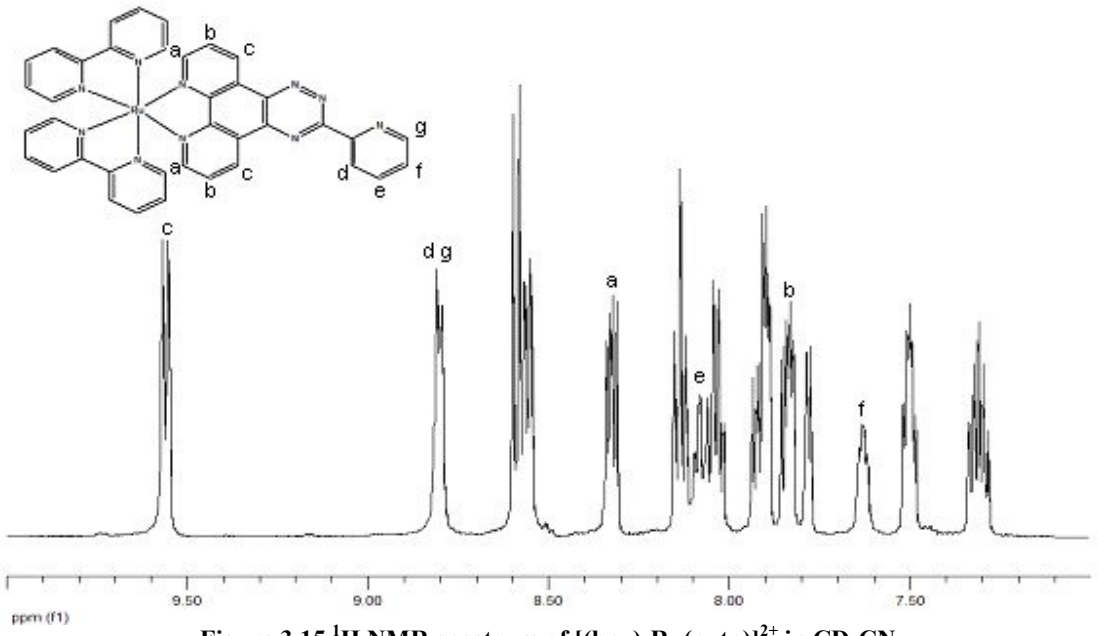

Figure 3.15 ^{1}H NMR spectrum of $[(bpy)_2Ru(pytp)]^{2+}$ in CD_3CN

The visible absorption spectrum was also recorded and showed a maximum absorption at 440 nm (Figure 3.16).

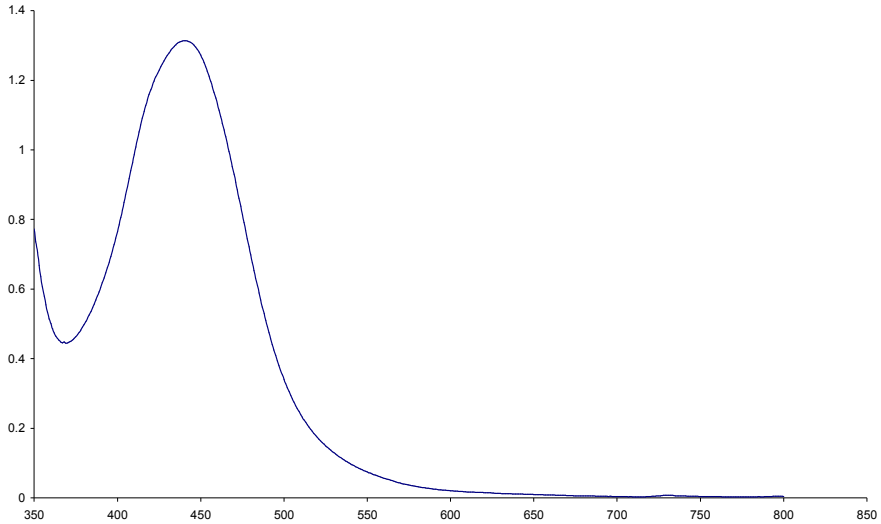

Figure 3.16 UV-vis absorption spectrum of $[(bpy)_2Ru(pytp)]^{2+}$ in CH_3CN

3.2.4.1. Crystal Structure of $[(bpy)_2Ru(pztp)](PF_6)_2$

Vapour diffusion of ether into a solution of $[(bpy)_2Ru(pztp)](PF_6)_2$ in acetonitrile produced red crystalline plates that were suitable for use in X-ray crystallography (Figure 3.17). The crystal structure confirmed that the ruthenium is bound to the phenanthroline end of the bridging ligand in an octahedral geometry. It is also worth noting the position of the pyrazine ring. This ring, which can freely rotate about its bond, is in a planar arrangement with respect to the rest of the ligand. This alignment, with the pyrazine-triazine rings forming a potential bidentate domain, is the desired configuration for binding a second metal centre.

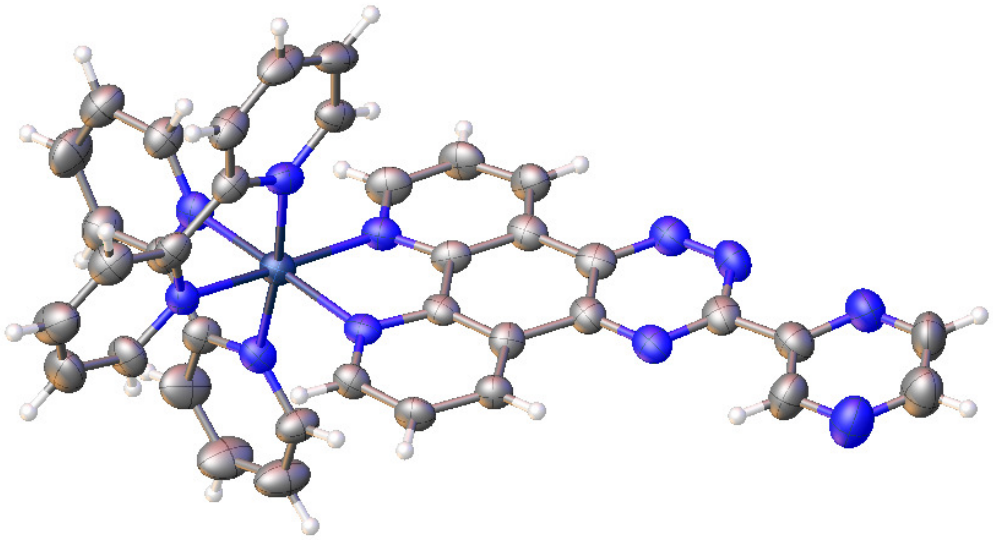

Figure 3.17 X-ray crystal structure of $[(bpy)_2Ru(pztp)](PF_6)_2$; counter ions and solvent molecules have been omitted for clarity

3.2.4.2. Glycolation of $[(bpy)_2Ru(phendione)](PF_6)_2$

The formation of the complex $[(bpy)_2Ru(phendione)](PF_6)_2$, which involves the reaction of $[Ru(bpy)_2Cl_2]$ with phendione in ethanol, was initially conducted using ethylene glycol and water as the solvent, as we believed that conducting the reaction at a higher temperature would result in a better yield. The change to ethanol was necessitated by the discovery of an impurity in the product. This impurity was the result of the ethylene glycol reacting with the phendione to form **3.23** (Figure 3.18). The non-nitrogen containing analogue of the free ligand of **3.23** was first reported in 1971 by Erenz *et al* as part of a series of complexes formed by the condensation of cyclic 1,2-diketones with ethylene glycol in the presence of an acid catalyst.[127]

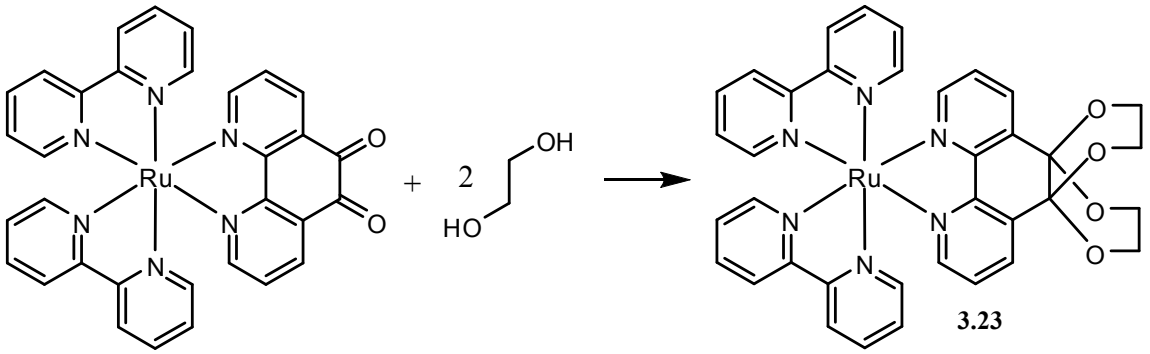

Figure 3.18 Glycolation of $[(bpy)_2Ru(phendione)](PF_6)_2$

3.23 was only a minor product in the formation of $[(bpy)_2Ru(phendione)](PF_6)_2$, presumably because the water can react with **3.23** to regenerate the phendione, and any **3.23** still present was almost always removed during column chromatography. However, we discovered that this was not always the case. When attempting to grow crystals of $[(bpy)_2Ru(pytp)Co(en)_2](PF_6)_5$, by diffusion of ether into acetonitrile, the majority of the solid formed was an orange-brown precipitate. In addition to this precipitate, there were about half a dozen red crystals present, which were examined by X-ray crystal diffraction. The data collected from these crystals was very poor, but nevertheless the structure of **3.23** could be resolved (Figure 3.19).

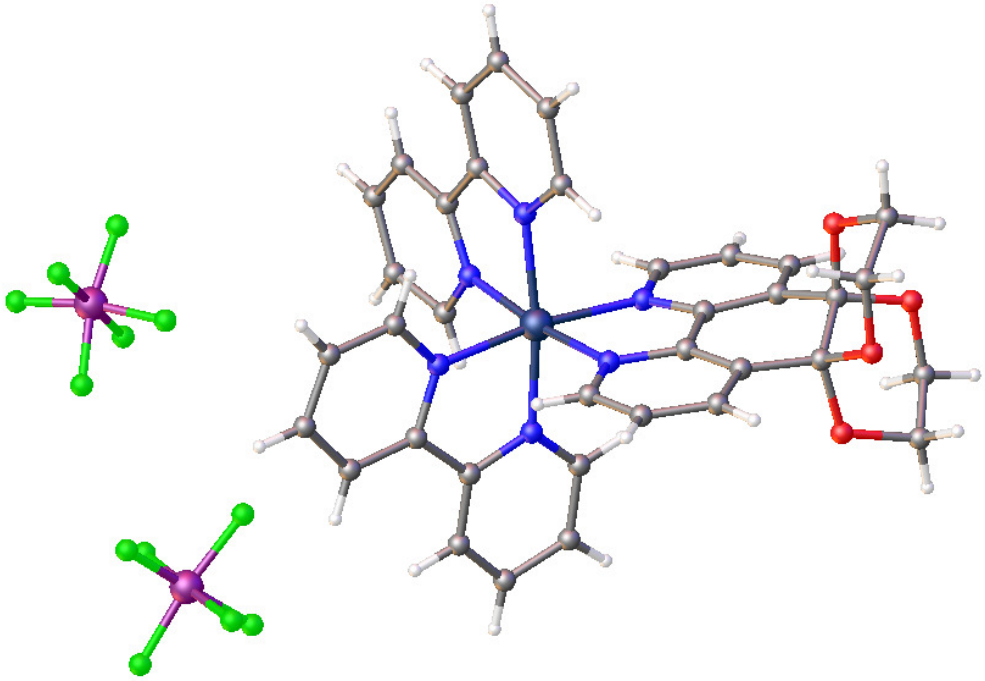

Figure 3.19 X-ray crystal structure of 3.23

In order to assess if the glycolation was occurring before or after coordination of the phendione to the ruthenium metal centre, or both, two additional experiments were conducted. The first of these simply involved heating phendione in ethylene glycol at reflux for three hours. The product of this reaction was not analysed by ^{1}H NMR spectroscopy due to a poor solubility profile. Instead, it was reacted with $[Ru(bpy)_2Cl_2]$ and the product of this reaction examined by ^{1}H NMR spectroscopy. The other experiment was to heat a sample of $[(bpy)_2Ru(phendione)](PF_6)_2$, prepared from ethanol, at reflux in ethylene glycol. In both cases the product was substantially different from the pure $[(bpy)_2Ru(phendione)](PF_6)_2$, with the sample prepared by heating phendione in ethylene glycol being the least different. This demonstrates that the glycolation is not hindered by the presence of the ruthenium(II) metal centre, and may even be promoted by it.

3.2.5. Ruthenium Complexes of Pytp and Pztp

In addition to synthesising the ligands pytp and pztp on ruthenium, the complexation of the preformed ligands with $[Ru(bpy)_2Cl_2]$ was carried out. The ^1H NMR spectrum of the crude complex resulting from the reaction (Figure 3.20) had more peaks above 8.5ppm than the ruthenium synthesised complex (Figure 3.15). Since these peaks are assigned to the protons on pytp, this suggests that the ruthenium is coordinated through the pyridyl-triazine end of the molecule.

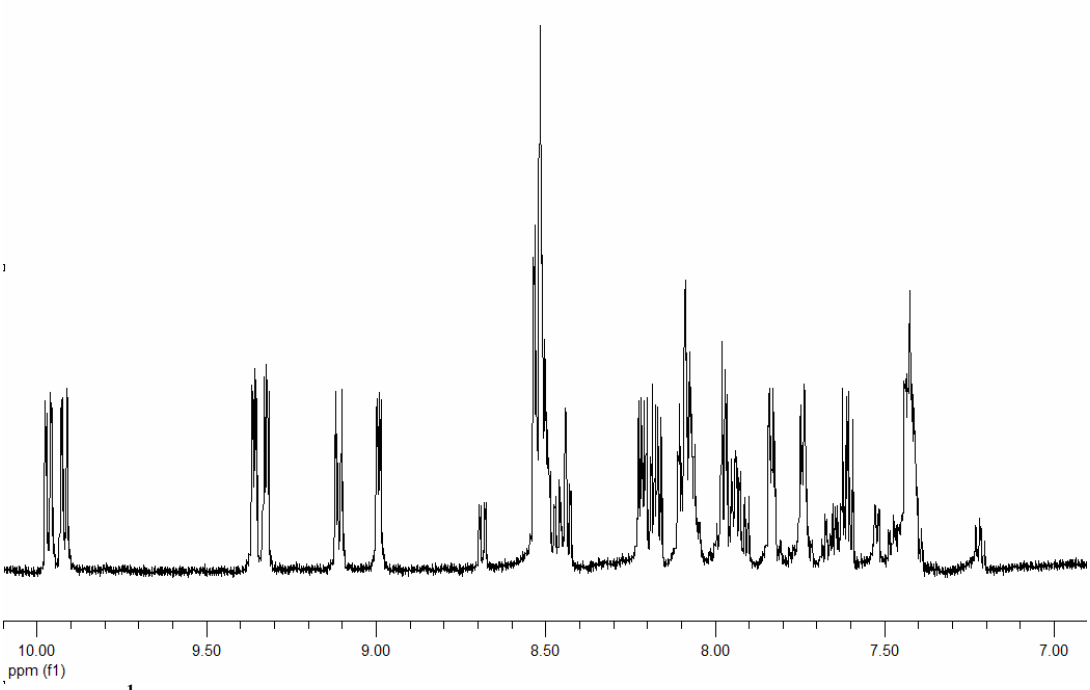

Figure 3.20 ^1H NMR spectrum of the crude product from the reaction of $[Ru(bpy)_2Cl_2]$ with pytp in CD_3CN

The crude product from the reaction with pztp was examined by ^1H NMR spectroscopy. The large number of peaks in the aromatic region of the ^1H NMR spectrum was assessed as being due to a mixture of products (Figure 3.21). We were able to assign some of these peaks to the complex with the ruthenium(II) ion bound to the phenanthroline end of the

ligand. The remaining peaks were most probably related to the complex with the ruthenium(II) ion bound to the pyrazine end of the ligand.

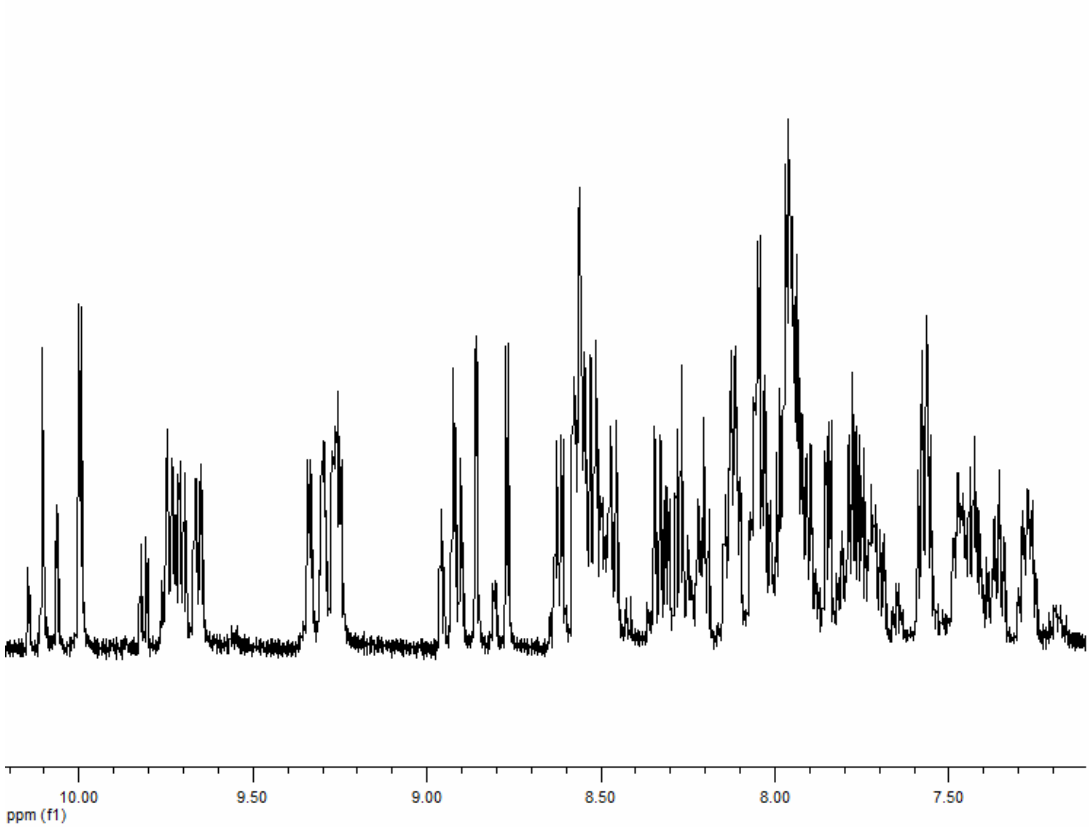

Figure 3.21 ^{1}H NMR spectrum of the crude product from the reaction of $[Ru(bpy)_2Cl_2]$ with pztp in CD_3CN

Purification of the crude material by column chromatography on silica gel resulted in the isolation of one major band. The ^{1}H NMR spectrum of this band still contained the peaks that had previously been assigned to the complex with the ruthenium(II) ion bound to the phenanthroline end of the ligand (Figure 3.22). However, while the number of peaks in this spectrum was fewer than in the spectrum of the crude material, the product still was not pure.

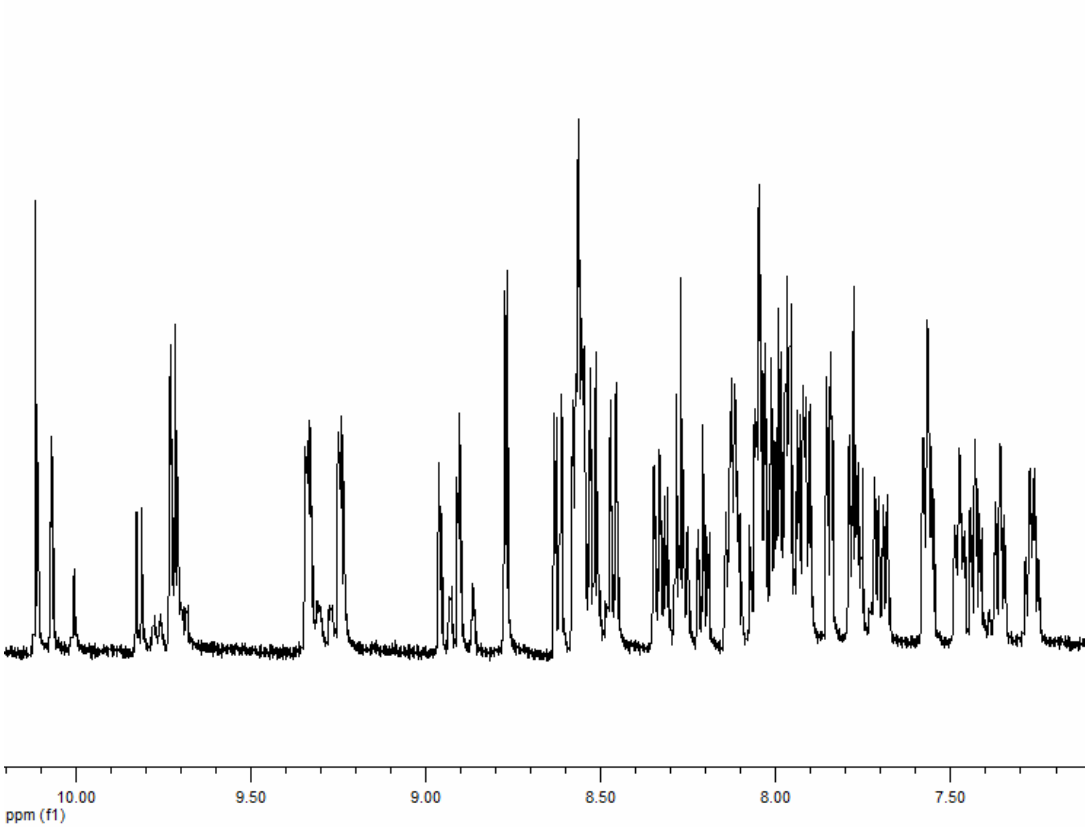

Figure 3.22 ^{1}H NMR spectrum of the major band from the purification of the reaction of $[Ru(bpy)_2Cl_2]$ with pztp in CD_3CN

3.2.6. Ruthenium Complexes of Pytz and Pztz

The synthetic pathway for the synthesis of the tetrazine ligands, pytz and pztz, prohibits the use of selective binding as a strategy to generate the monoruthenium(II) complex. Our intention was to simply carry out the reaction between $[Ru(bpy)_2Cl_2]$ and the ligand in a one to one ratio and remove any diruthenium complexes after the reaction was completed. Carrying out the one to one reaction by heating the reactant at reflux in ethylene glycol for 3 hours gave a blue solution, from which a blue solid could be precipitated by addition of a saturated methanolic solution of NH_4PF_6. Recording the UV-vis spectrum of the product in acetonitrile and comparing the recorded spectrum with that reported in the literature for the

compound $[(bpy)_2Ru(pytz)Ru(bpy)_2](PF_6)_4$ showed that we had formed the diruthenium complex (Figure 3.23).[128]

Ernst and Kaim describe the ready formation of the diruthenium complex as being due to charge transfer assisted polynucleation.[124] Back donation from the first bound ruthenium ion increases the electron density of the other binding domain and makes it a better ligand than the unbound species.

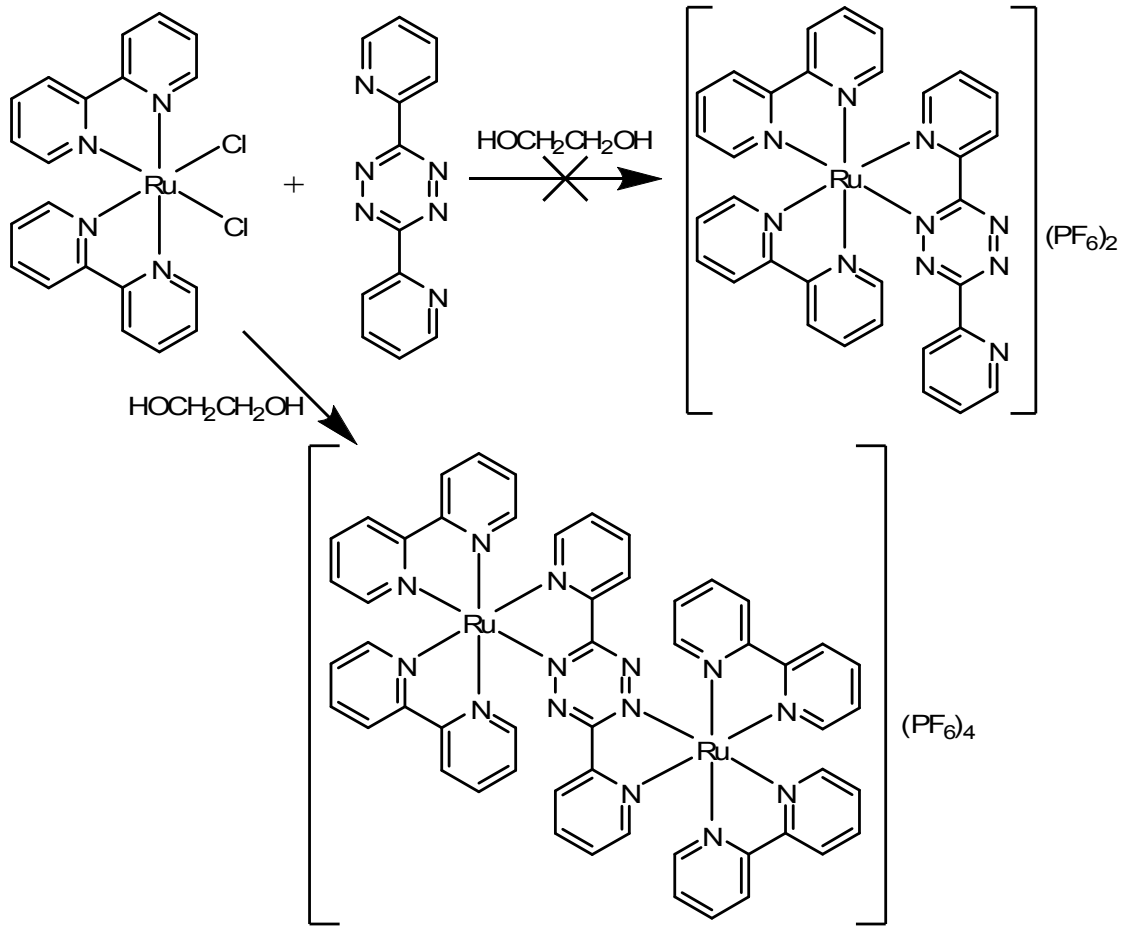

Figure 3.23 Attempted synthesis of $[(bpy)_2Ru(pytz)](PF_6)_2$ instead resulting in the formation of $[(bpy)_2Ru(pytz)Ru(bpy)_2](PF_6)_4$

The blue colour is due to a maximum absorption of visible light at just under 700 nm (Figure 3.24). Usually ruthenium polypyridyl complexes have a maximum absorption in the range of 400-500 nm; for example $[Ru(bpy)_3]^{2+}$ has λ_{max}=451 nm.[129] This bathochromic shift

is due to the complex having an extremely low energy LUMO (π^*) associated with the bridging ligand.[124, 128, 130]

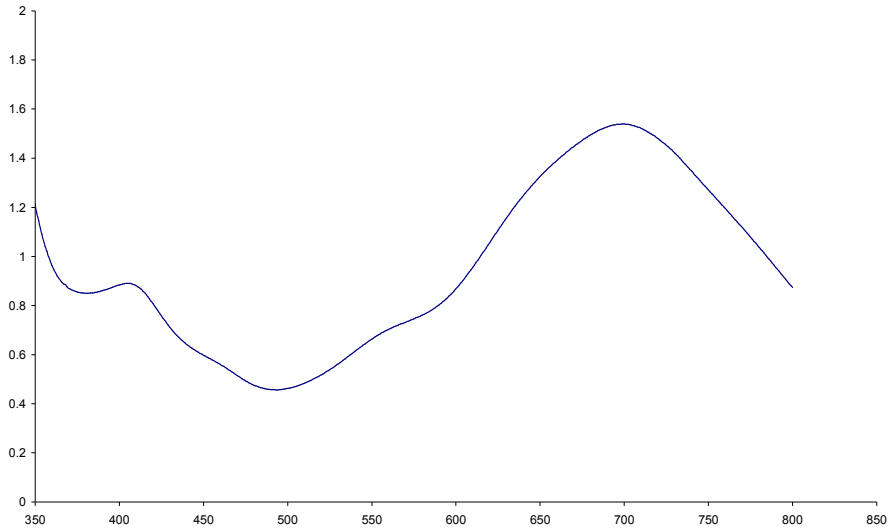

Figure 3.24 UV-vis absorption spectrum of $[(bpy)_2Ru(pytz)Ru(bpy)_2]^{4+}$ in CH_3CN

In order to obtain the monoruthenium complex, a revised synthetic procedure based on that used for the coordination of ruthenium(II) to 2,5-dipyridylpyrazine was used.[131] An excess of either pytz or pztz was heated to reflux in methanol; to this a stirred suspension of $[Ru(bpy)_2Cl_2]$ in methanol was slowly added. After being cooled to room temperature, the mono-ruthenium complex was isolated through column chromatography on silica gel (Figure 3.25). The reason that this method produced the monoruthenium complex while the previous method produced the diruthenium complex is because it uses kinetic control instead of thermodynamic.

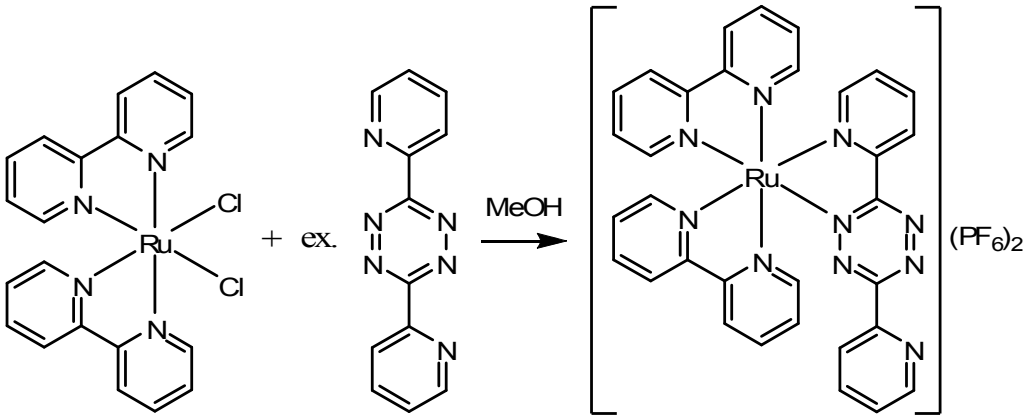

Figure 3.25 Formation of $[Ru(bpy)_2(pytz)](PF_6)_2$

The absorption of the mono-ruthenium complex $[(bpy)_2Ru(pytz)]^{2+}$ in acetonitrile was recorded with a λ_{max} of 510 nm (Figure 3.26).

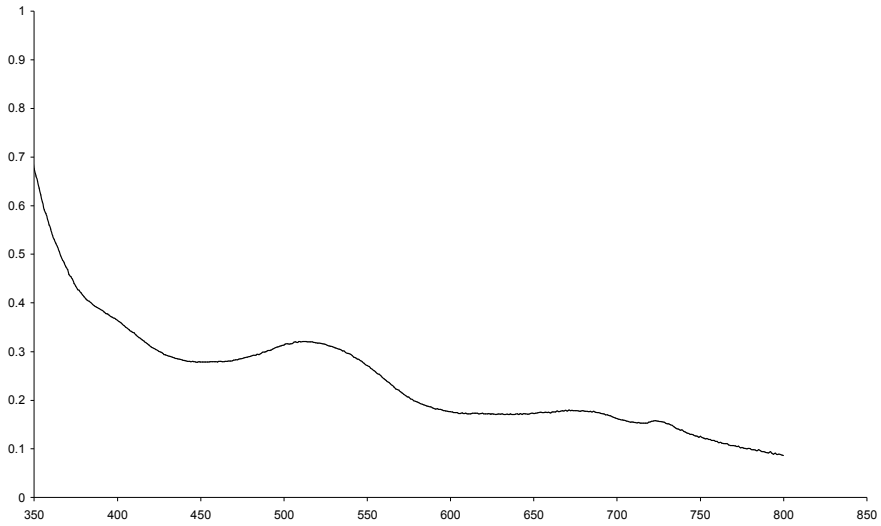

Figure 3.26 Absorption spectrum of $[(bpy)_2Ru(pytz)]^{2+}$ in CH_3CN

3.2.7. Formation of Diruthenium Complexes

We have already shown that the ligand pytz readily forms diruthenium complexes and in addition to our own evidence, there is also a literature example of ruthenium binding to the pyridyl end of pytp.[132] In order to further investigate the coordination ability of the second binding domain of pytp, we decided to synthesise the diruthenium pytp complex. Heating a mixture of $[Ru(bpy)_2Cl_2]$ and $[(bpy)_2Ru(pytp)](PF_6)_2$ at reflux in methanol for two weeks gave

a red precipitate as the product (Figure 3.27). Because no attempt was made to control the configuration of the ruthenium(II) metal centres this product should be a mixture of both the *meso* and *rac* stereoisomers.

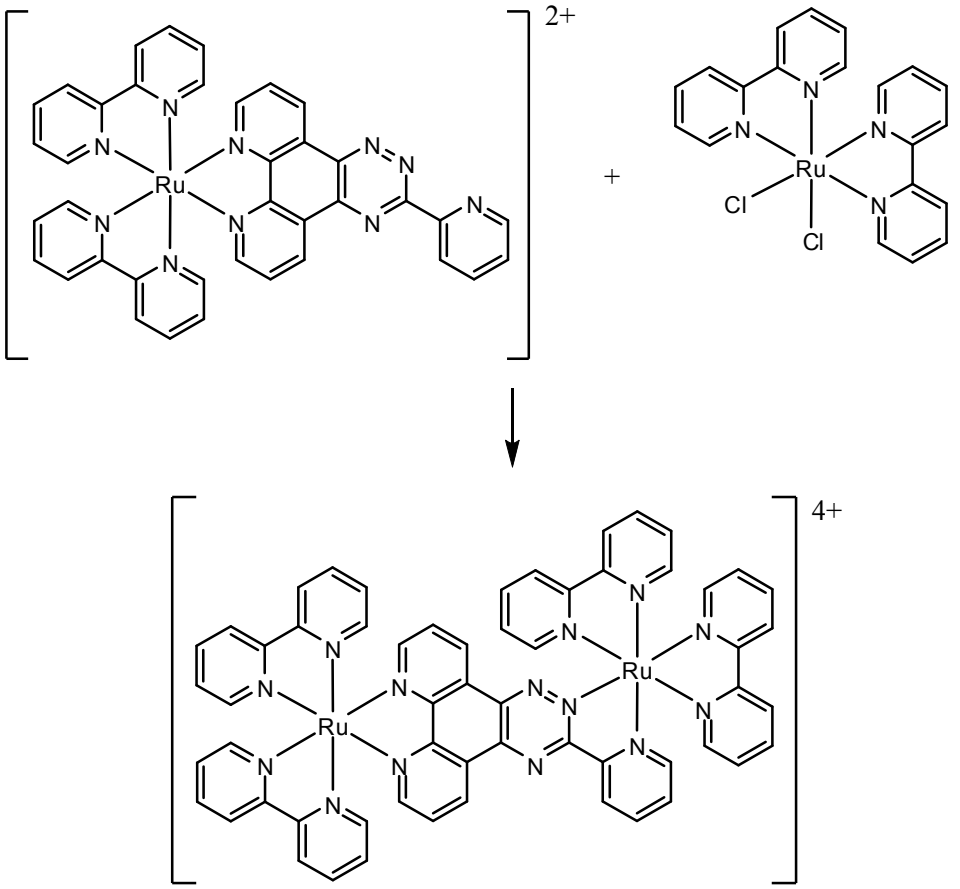

Figure 3.27 Formation of $[(bpy)_2Ru(pytp)Ru(bpy)_2](PF_6)_4$

The ^{1}H NMR spectrum of the resulting product was recorded and shows that the peaks relating to the pytp ligand are shifted by up to about 1ppm from the mononuclear complex (Figure 3.28). However, full assignment and characterisation of the products from this reaction was not achieved.

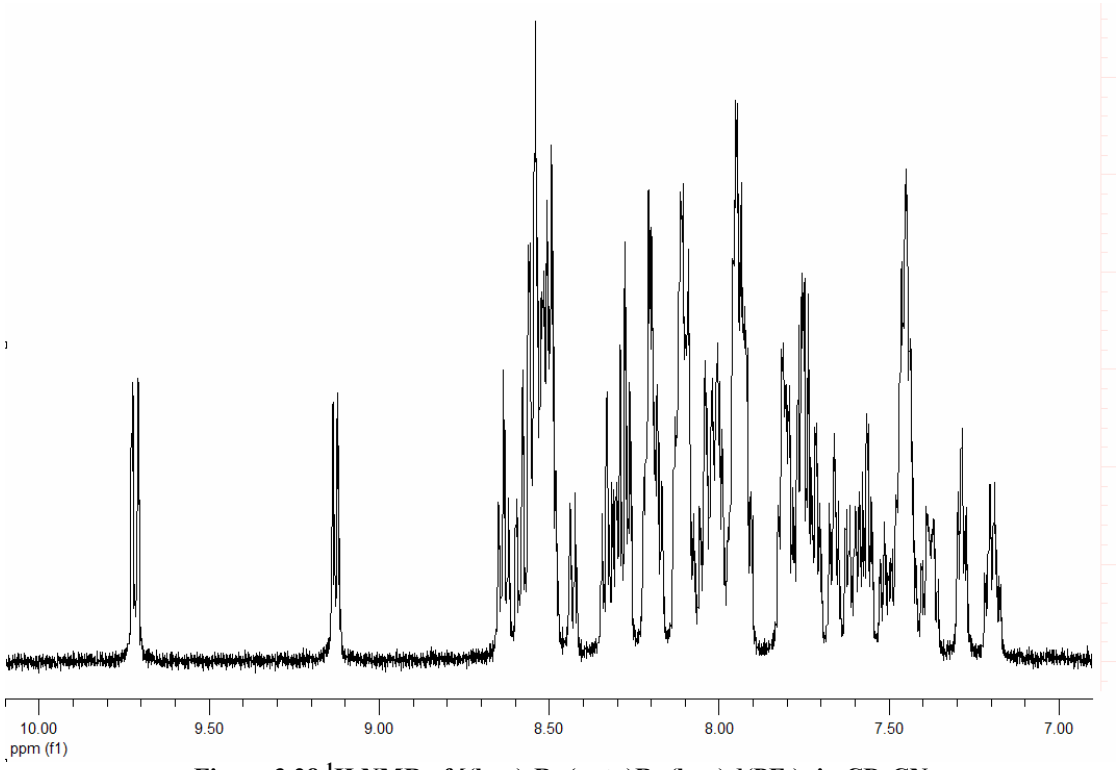

Figure 3.28 ^{1}H NMR of $[(bpy)_2Ru(pytp)Ru(bpy)_2](PF_6)_2$ in CD_3CN

3.2.8. Heterodinuclear Complexes of $[(bpy)_2Ru(pytp)](PF_6)_2$

$[(bpy)_2Ru(pytp)](PF_6)_2$ was dissolved in acetonitrile-d_3 and its interactions with silver(I) were monitored by ^{1}H NMR. An increasing amount of $Ag(ClO_4)$ was slowly added with the observed result being a gradual shift of the pytp peaks until the ruthenium:silver ratio was one to one (Figure 3.29). Further addition of silver had a minimal affect on the position of the pytp peaks. This is consistent with one to one binding of silver ions and a fast equilibrium between the bound and unbound state. If the silver was irreversibly bound or the rate of exchange slow on the NMR timescale, then we would expect to see a new set of peaks growing in with the addition of $Ag(ClO_4)$.

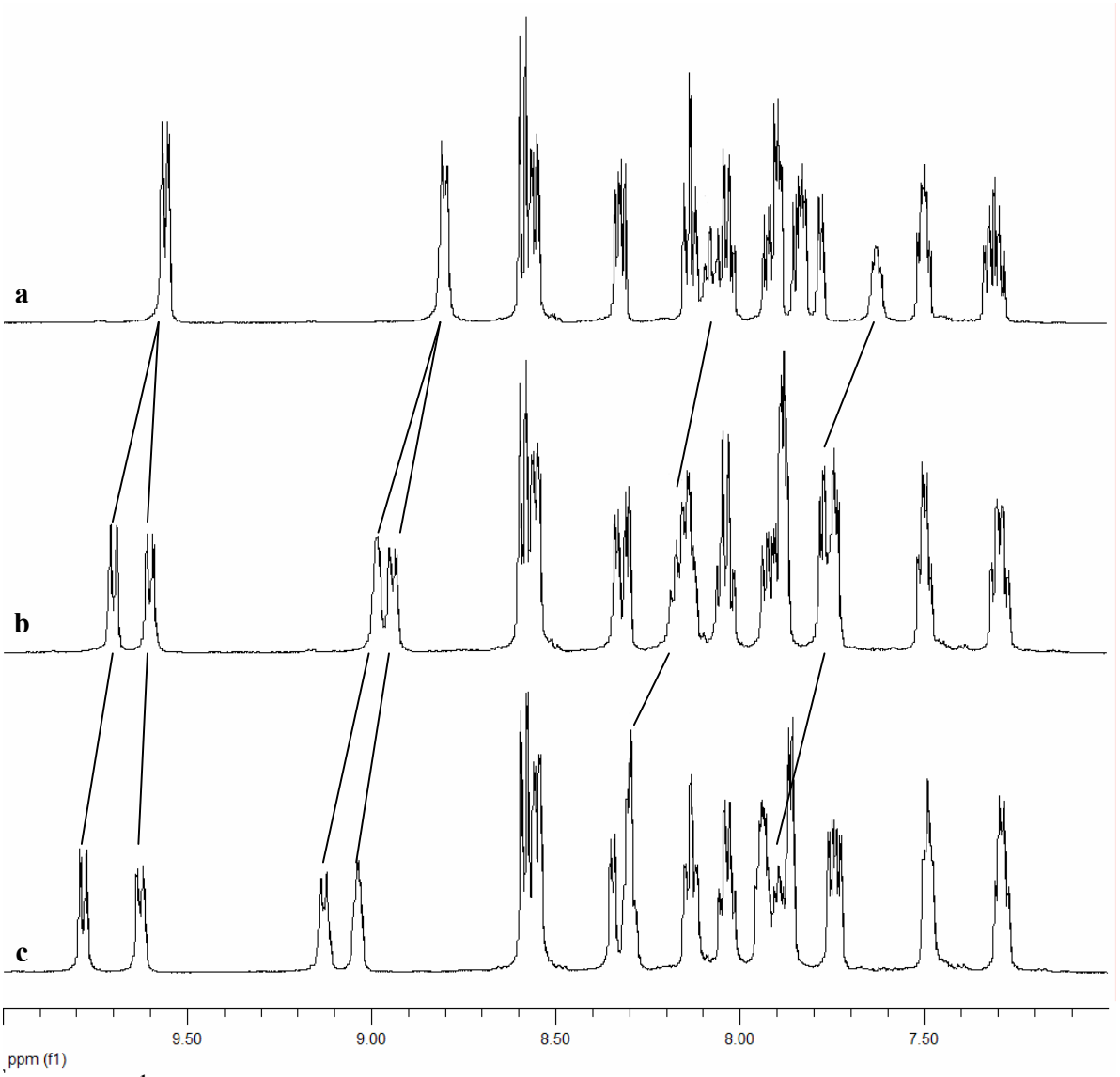

Figure 3.29 ^{1}H NMR spectra of $[(bpy)_2Ru(pytp)](PF_6)_2$ in CD_3CN with: (a) 0 equivalents of $Ag(ClO_4)$; (b) 0.3 equivalents of $Ag(ClO_4)$; (c) 1 equivalent of $Ag(ClO_4)$

At the conclusion of the silver titration, a small amount of the solution was used to prepare a sample suitable for analysis by mass spectrometry. The mass spectrometry showed three major isotope patterns that were of interest. These were at m/z ratios of 362, 466, and 823 corresponding to $[(bpy)_2Ru(pytp)]^{2+}$, $[(bpy)_2Ru(pytp)Ag](ClO_4)^{2+}$ and $[(bpy)_2Ru(pytp)](ClO_4)^{+}$ respectively (Figure 3.30). This was consistent with the ^{1}H NMR result in indicating that silver was binding to the vacant site.

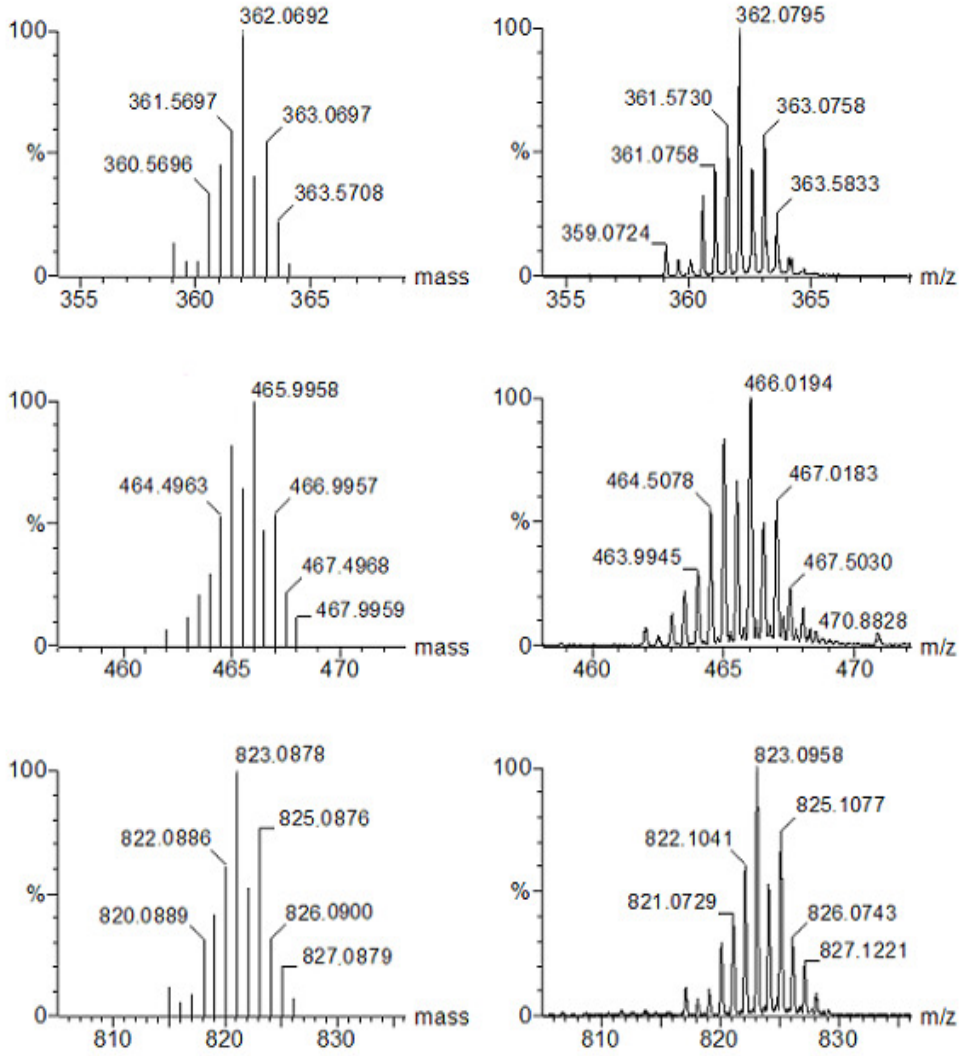

Figure 3.30 Modelled and experimental isotope patterns for $[(bpy)_2Ru(pytp)]^{2+}$, $[(bpy)_2Ru(pytp)Ag](ClO_4)^{2+}$ and $[(bpy)_2Ru(pytp)](ClO_4)$+

In addition to the ^{1}H NMR study carried out with $Ag(ClO_4)$, additional studies were conducted using CuSCN and $Zn(NO_3)_2$. The addition of $Zn(NO_3)_2$ resulted in a similar change in the ^{1}H NMR peak positions as was observed for the addition of $Ag(ClO_4)$.

CuSCN was initially observed to behave like silver(I); however, as the experiment continued, the pytp peaks broadened as well as shifted. This was potentially due to oxidation of the copper(I) to the paramagnetic copper(II). To confirm that it was paramagnetic

broadening causing the suppression of the pytp peaks, another experiment was carried out, this time with the paramagnetic copper(II) salt copper acetate. The addition of copper(II) resulted in the pytp peaks quickly broadening to the point that they could no longer be observed. Since both the ^{1}H NMR spectra of the copper(I) and copper(II) experiments show peak broadening, we conclude that it was oxidation of the copper(I) metal ions to copper(II) metal ions that caused the original result. Oxidation of the copper(I) could have potentially arisen through aerial oxidation.

In order to ensure that it was the transition metal ions that were responsible for the observed changes, the non-transition metal-containing salts $NaClO_4$, NH_4PF_6 and LiCl were also tested. In each case they had little or no effect on the recorded ^{1}H NMR spectrum. We infer from this that these metal ions are not associating with the pytp ligand, and that the observed changes were due to the coordination of the transition metal to the vacant binding domain of the pytp ligand.

3.2.9. Heterodinuclear Complexes of $[(bpy)_2Ru(pytz)](PF_6)_2$

The complex $[(bpy)_2Ru(pytz)](PF_6)_2$ was also dissolved in acetonitrile and the ability to coordinate a second metal centre assessed by use of a silver titration. Again the result was a gradual shifting of the ^{1}H NMR peaks consistent with the silver being in equilibrium between a bound and unbound state.

3.3. Conclusion

From our studies we have been able to produce two series of ligands and synthesise their ruthenium complexes. In addition, we have been able to show that by prebinding a

ruthenium metal centre prior to ligand synthesis, selectivity towards only a single domain can be achieved.

Furthermore, we have shown that all of these complexes are capable of binding a second metal centre and that the coordination of the second metal centre can be monitored by ^{1}H NMR spectroscopy. This promising result meant that each of these complexes was a suitable candidate for coordination to a cobalt metal centre, a process which will be detailed further in Chapter 4.

Chapter 4: Heterodinuclear Ruthenium(II)-Cobalt(III) Complexes

4.1. Introduction

We have shown that the free binding domains of the ligand systems described in Chapter 3 are able to coordinate a second metal centre. These ligands are therefore potential bridging ligands for ruthenium(II)-cobalt(III) heterodinuclear complexes. Ideally an electron transfer between the two metal centres would enable these complexes to be further developed into photo-activated cytotoxins.

4.1.1. Applications of Ruthenium(II) Heterodinuclear Complexes

In many cases the synthesis and study of heterodinuclear complexes containing ruthenium(II) is motivated by the need for a particular photochemical or electrochemical property in a possible application. For example ruthenium(II)-platinum(II) complexes have been investigated as possible photosensitisers to enhance the photochemical reduction of water to molecular hydrogen by the disodium salt of ethylenediaminetetraacetic acid.[133] Both ruthenium(II)-rhenium(I) and ruthenium(II)-rhodium(III) complexes are being investigated for use as charge separating sensitisers in dye-sensitised solar cells.[60]

Recently the first example of photochemical reduction of nitrite into nitrogen monoxide by a ruthenium(II)-copper(II) complex was reported (Figure 4.1).[134]

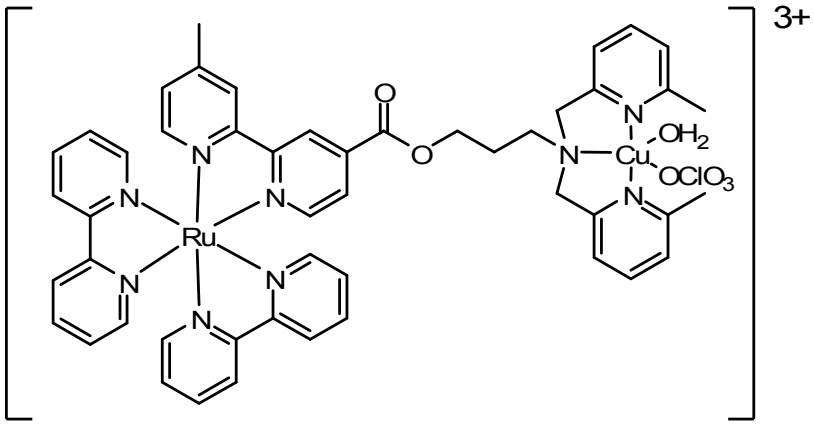

Figure 4.1 Ruthenium(II)-copper(II) heterodinuclear species capable of the photochemical reduction of NO_2^-

Replacing the copper(II) centre with zinc(II) resulted in the NO_2^- no longer being reduced to NO. From this, it was therefore concluded that the copper(II) centre is the site for the reduction. The proposed mechanism for this photo-reduction is:

$$Ru^{2+}\text{-}Cu^{2+} + h\nu \rightarrow Ru^{2+*}\text{-}Cu^{2+}$$

$$Ru^{2+*}\text{-}Cu^{2+} \rightarrow Ru^{3+}\text{-}Cu^{+}$$

$$Ru^{3+}\text{-}Cu^{+} + NO_2^- + 2H^+ \rightarrow Ru^{3+}\text{-}Cu^{2+} + NO + H_2O$$

$$Ru^{3+}\text{-}Cu^{2+} + X(e.g.\ CH_2Cl_2) \rightarrow Ru^{2+}\text{-}Cu^{2+} + X^{\bullet}(e.g.\ Cl^{\bullet})$$

The first step involves a photo-induced intramolecular electron transfer from the ruthenium(II) centre to the copper(II) centre which results in the formation of a ruthenium(III)-copper(I) species. The copper(I) metal centre then reduces the nitrite ion into nitrogen monoxide, being oxidised back to copper(II) in the process. The final regenerative step is the reduction of the ruthenium(III) metal centre back to ruthenium(II); this step is proposed to involve the oxidation of a solvent molecule, such as CH_2Cl_2. The rationale behind the regenerative step is that the photo-reduction continued without the need for a sacrificial reductant, and the UV-visible absorption spectrum of the solution at the end of the experiment

was very similar to that before. This is consistent with the ruthenium metal centre still being in the 2+ oxidation state.

4.1.2. Heterodinuclear Ruthenium(II)-Cobalt(III) Complexes

The majority of ruthenium(II)-cobalt(III) complexes in the literature were synthesised for the purpose of electron transfer studies. The complexes used by Taube in his experiments were synthesised first by forming the ruthenium(III)-cobalt(III) complex (Figure 4.2) and then reducing it to the ruthenium(II)-cobalt(III) complex with either $[Ru(NH_3)_6]^{2+}$ or ascorbate. [82, 83, 84, 85]

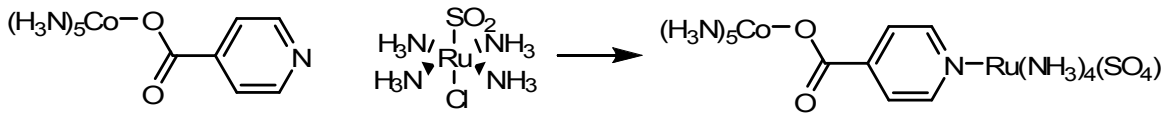

Figure 4.2 Taube synthesis of a ruthenium(III)-cobalt(III) complex

Toreida *et al.* synthesised ruthenium(II)-cobalt(III) complexes by heating the ruthenium(II) complex with either $[Co(tpy)Cl_3]$ or $[Co(tpy)(CF_3SO_3)_3]$ (Figure 4.3).[135, 136]

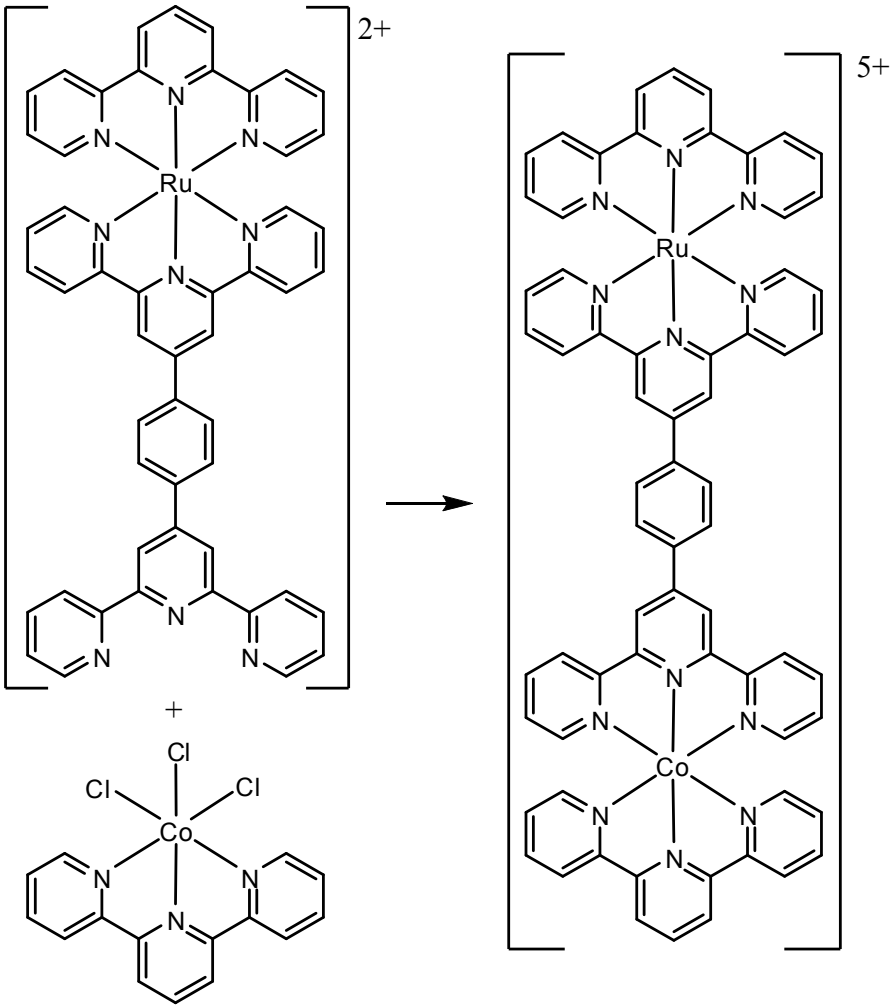

Figure 4.3 Synthesis of a ruthenium(II)-cobalt(III) heterodinuclear complex

4.2. Results and Discussion

4.2.1. Synthetic Strategy

For our purposes, a modification of the method proposed by Toreida seemed the most useful. However, the products which resulted from heating our ruthenium(II) complexes at reflux with $[Co(en)_2Cl_2]Cl$ were unable to be assigned due to paramagnetic contamination. This paramagnetism could be due to the ruthenium(II) being oxidised to ruthenium(III) and/or the reduction of the cobalt(III) to cobalt(II).

By using the triflate salts of selected cobalt(III) complexes (for example $[Co(tren)(OTf)_2](OTF)$ and $[Co(en)_2(OTf)_2](OTf)$) it should be possible to successfully synthesise a variety of heterodinuclear complexes simply by stirring equimolar amounts of the ruthenium(II) and cobalt(III) complexes in acetonitrile at room temperature (Figure 4.4). The reason for using the triflate complex is that in addition to being soluble in acetonitrile, the triflate ligands in cobalt(III) triflato complexes are weakly coordinating. For example, the rates of aquation for $[Co(NH_3)_5L]^{2+}$ are for L= triflate 2.7×10^{-2} s^{-1}, chloride 1.7×10^{-6} s^{-1} and nitrite 1.2×10^{-8} s^{-1}.[49] Since the use of triflate ligands will mitigate the problem of cobalt(III) being inert, it is possible that the heterodinuclear complexes will be successfully formed at room temperature.

During the formation of the ruthenium(II)-cobalt(III) heterodinuclear complexes, it is important to minimise exposure to light. Failing to reduce the amount of light to which the complex is exposed could result in photo-induced electron transfer from the ruthenium(II) metal centre to the cobalt(III) metal centre.

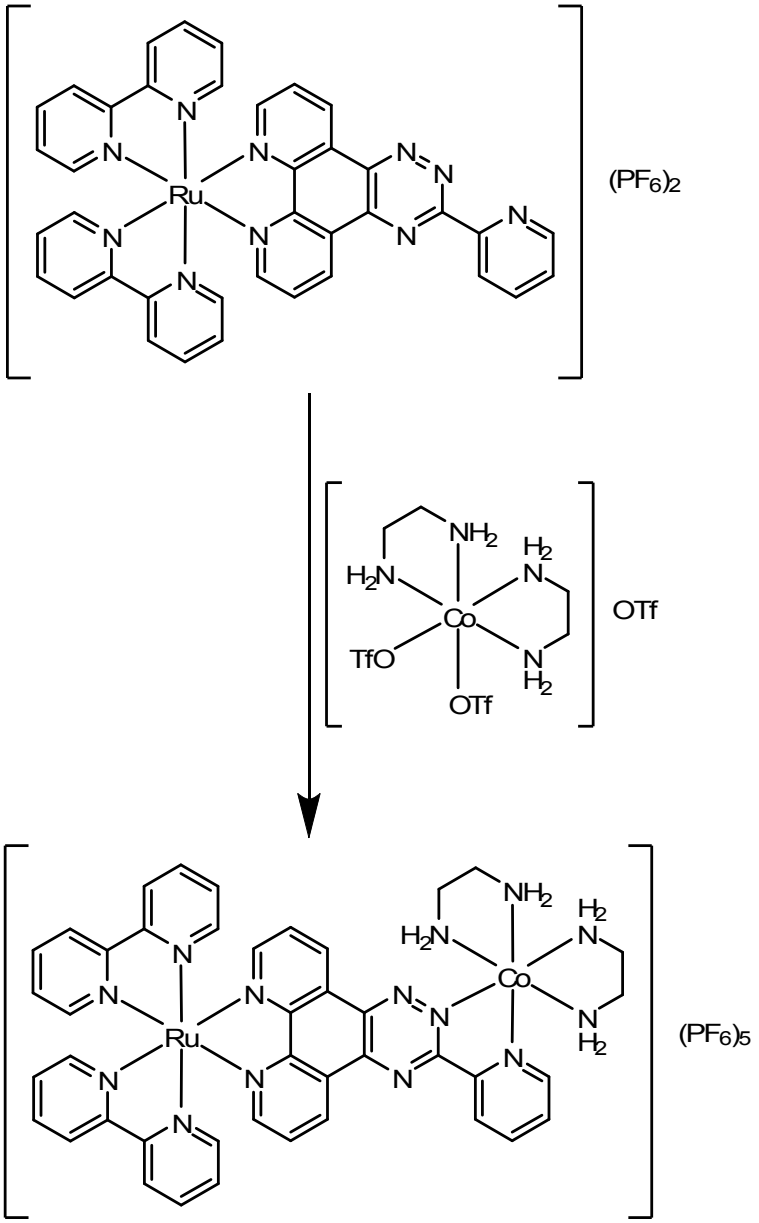

Figure 4.4 Proposed synthesis of $[(bpy)_2Ru(pytp)Co(en)_2](PF_6)_5$

4.2.2. Complexes Utilising a Pytp Bridging Ligand

The ruthenium(II) complex $[(bpy)_2Ru(pytp)](PF_6)_2$ was used in the formation of ruthenium(II)-cobalt(III) heterodinuclear complexes. This was achieved by stirring the ruthenium complex with either $[Co(en)_2(OTf)_2]OTf$ or $[Co(tren)(OTf)_2]OTf$ in acetonitrile, in the dark. The final heterodinuclear complexes were then isolated as the PF_6 salts. ^1H NMR

spectra showed the products to be relatively free from contamination, even though no attempt was made to purify them after isolation because of their potential instability. Additional experiments were conducted on the NMR scale so that the formation of the product could be monitored. Monitoring the reaction in this manner showed the ^{1}H NMR peaks which corresponded to the starting material decreasing, while the ^{1}H NMR peaks associated with the product grew (Figure 4.5).

The rationale for synthesising these complexes was that ethane-1,2-diamine has a similar binding domain to the bidentate nitrogen mustards N,N′-bis(2-chloroethyl)ethane-1,2-diamine and N,N-bis(2-chloroethyl)ethane-1,2-diamine, while tris(aminoethyl)amine, being tetradentate, should be more stable towards substitution. In both cases the product will be a mixture of isomers. Firstly, this is due to the complex $[(bpy)_2Ru(pytp)](PF_6)_2$ being a mixture of the Λ and Δ forms. Secondly, the cobalt complexes can bind in either of two configurations. For the en complex these will be the Λ and Δ forms, while for the tren complex the tertiary amine can be in either a *cis* or *trans* arrangement with the pyridyl nitrogen.

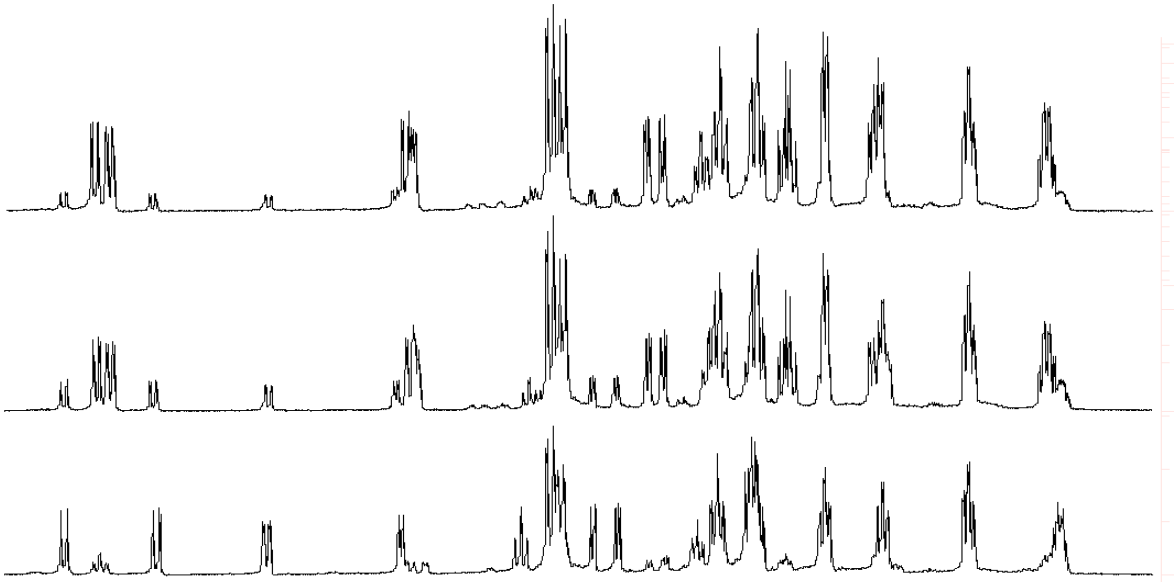

Figure 4.5 Aromatic regions of the ^{1}H NMR spectra taken during the reaction between $[(bpy)_2Ru(pytp)]^{2+}$ and $[Co(tren)(OTf)_2]^{+}$ in CD_3CN; the top spectrum is primarily unreacted $[(bpy)_2Ru(pytp)]^{2+}$ while the bottom is primarily the heterodinuclear complex.

The complex $[(bpy)_2Ru(pytp)Co(tren)](PF_6)_5$ was characterised by ^{1}H, ^{13}C, gCOSY, and HSQCad NMR techniques. In addition to the peaks we assigned to the two bpy ligands, the aromatic region of the gCOSY shows three discrete spin systems. These systems correspond to the four protons on the cobalt bound pyridine ring and the two sets of three protons on each side of the phenanthroline portion of the pytp ligand (Figure 4.6).

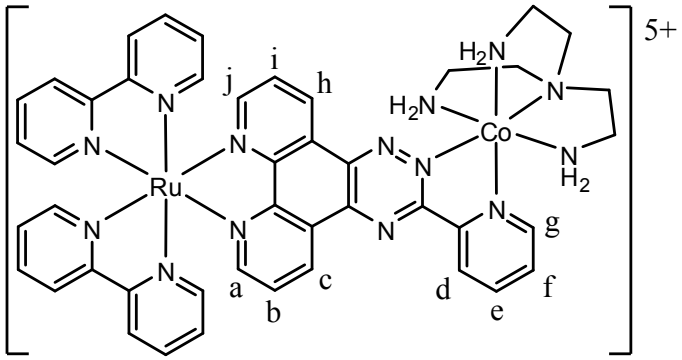

Figure 4.6 $[(bpy)_2Ru(pytp)Co(tren)]^{5+}$

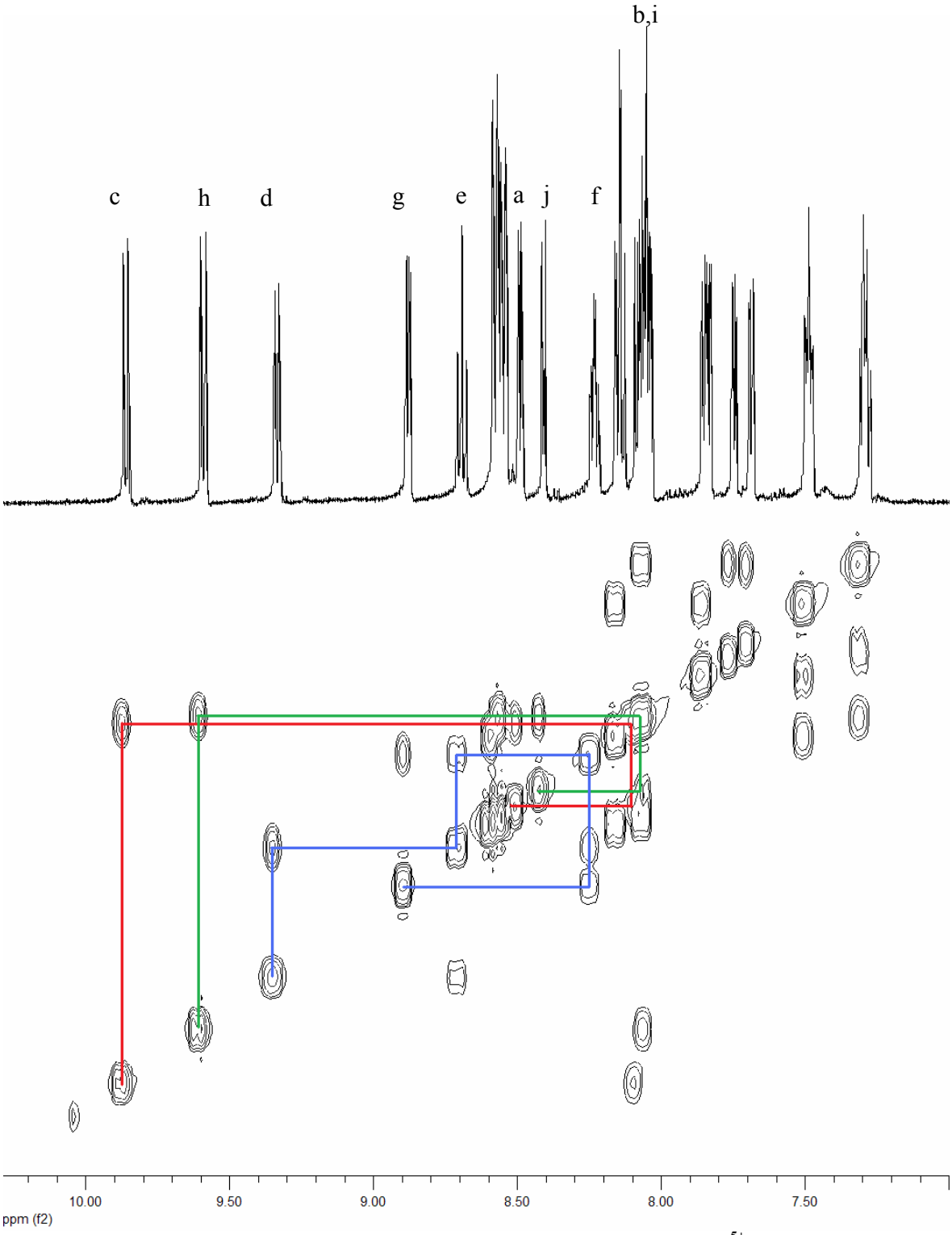

Figure 4.7 Aromatic region of the gCOSY spectrum of $[(bpy)_2Ru(pytp)Co(tren)]^{5+}$ with the spin systems not corresponding to the bpy ligands highlighted

Assignment of the ^{1}H NMR peaks associated with the two sides of the phenanthroline ring system was achieved by utilising the NOE experiment. Irradiation of the positions of the ^{1}H NMR peaks corresponding to the tren ligand results in the amplification of the signal peaks relating to nearby protons. A correlation between the tren peak at 4.6 ppm and the pytp peak at 9.6 ppm means that the ring system corresponding to 9.6, 8.0 and 8.4 ppm are on the same side of the pytp molecule as the cobalt bound tren. The peak at 4.6 ppm was assigned to a single CH_2 group next to an NH_2 group. This means that the NOE experiment result can also be used to assign the orientation of the tren molecule as having the tertiary amine opposite the coordinated nitrogen of the triazine (Figure 4.8).

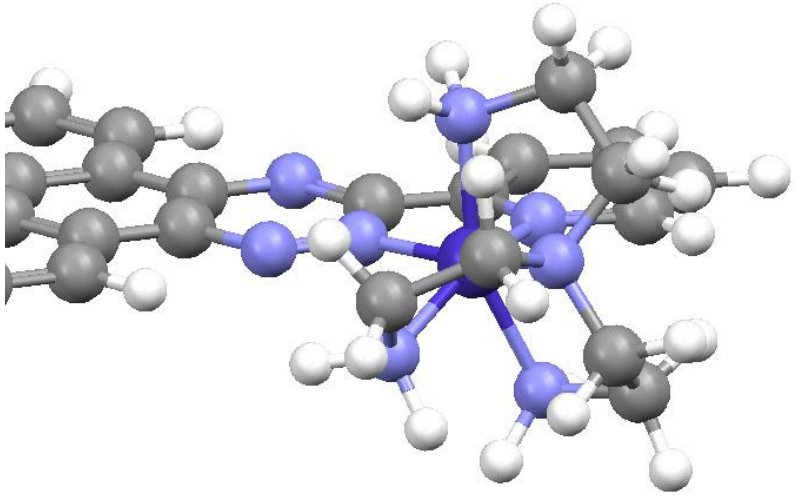

Figure 4.8 3D representation of the coordination of Co(tren)$^{3+}$ to pytp

Having fully assigned the proton peaks correlating to the pytp ligand, HSQC was used to assign the ^{13}C spectra.

Table 4.1 Selected ^{1}H and ^{13}C NMR peak assignments for $[(bpy)_2Ru(pytp)Co(tren)](PF_6)_5$

Peak Position (ppm)	phen	pyridyl	phen
9.85, 136.4	c		
9.59, 135.0			h
9.33, 130.4		d	
8.88, 155.5		g	
8.69, 144.7		e	
8.49, 159.8	a		
8.41, 157.8			j
8.23, 133.0		f	
8.08, 129.6	b		
8.04, 129.6			i

The formation of the bis(en) complex (Figure 4.9) proceeded under the same reaction conditions as the tren complex and an orange-brown precipitate was isolated.

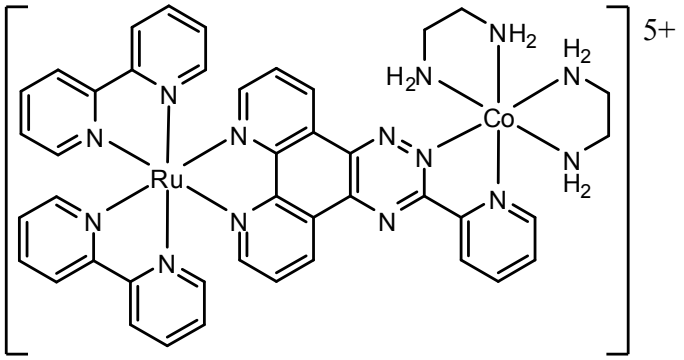

Figure 4.9 $[(bpy)_2Ru(pytp)Co(en)_2]^{5+}$

The ^{1}H NMR spectrum of the complex revealed significant changes in position of the pytp peaks, in comparison to that of $[(bpy)_2Ru(pytp)]^{2+}$, as well as additional peaks in the alkyl region (Figure 4.10). As no efforts were made to control the configuration of the two metal centres, we would expect the product to be a mixture of up to four isomers (ΛΛ, ΛΔ, ΔΛ and ΔΔ). However, the ^{1}H NMR spectrum does not show multiple sets of peaks. This suggests that there is either little difference in the electronic environment of each isomer or the product is selective for one of the pairs of enantiomers. Constructing models of the different isomers showed that there is a substantial distance between the two metal centres. This large

distance makes it unlikely that stereoselective binding is occurring and that there is actually a mixtures of isomers present.

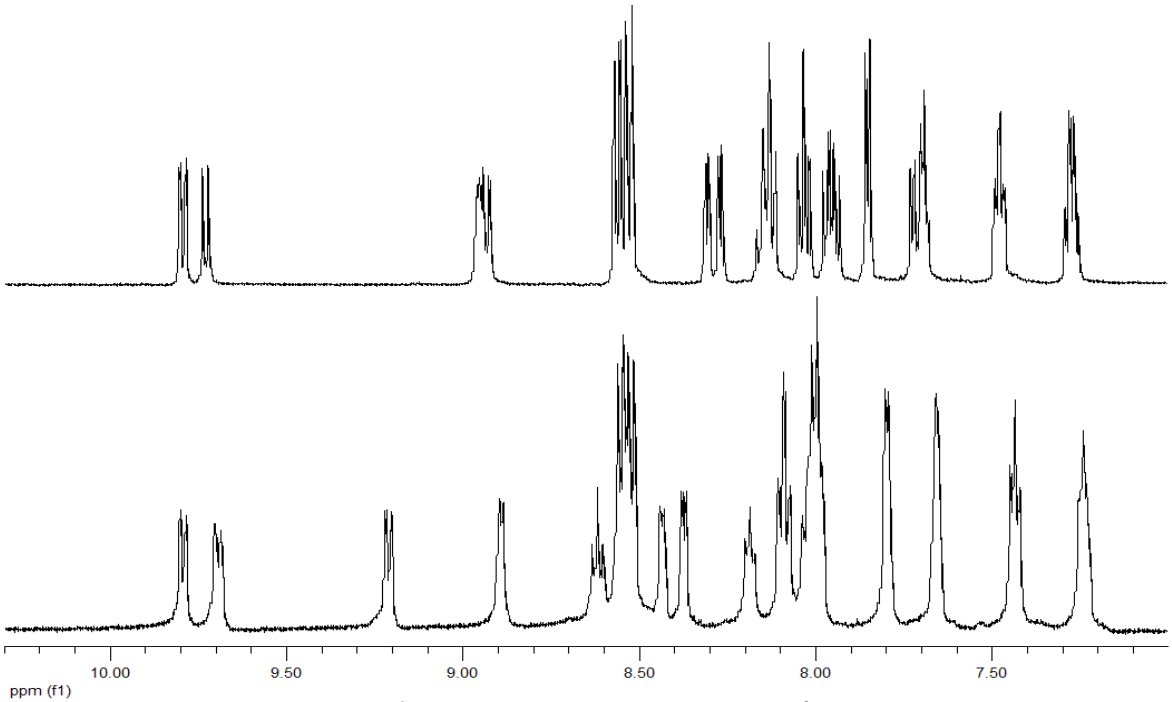

Figure 4.10 Aromatic regions of the ^{1}H NMR spectra of $[(bpy)_2Ru(pytp)]^{2+}$ before (top) and after (bottom) coordination of a $Co(en)_2^{3+}$ fragment in CD_3CN

In both cases coordination of the cobalt complex resulted in a change of the UV-vis spectra. The value associated with λ_{max} was slightly red shifted, while the absorbance below 400 nm increased. In order to determine if these changes were due to the coordination of the cobalt(III) centre or just due to the overlapping of the peaks associated with the ruthenium centre and those of the cobalt centre, the UV-vis spectrum of a freshly prepared acetonitrile solution containing both $[(bpy)_2Ru(pytp)](PF_6)_2$ and $[Co(tren)(OTf)_2](OTf)$ was recorded. In this case the spectrum was identical to that of the ruthenium(II) complex. The solution was then placed in the dark for twenty four hours and the spectrum was recorded again; this time the spectrum was identical to that of the ruthenium(II)-cobalt(III) complex. This is consistent

with the idea that it is the coordination of the cobalt metal centre that is responsible for the observed changes in the UV-vis spectra.

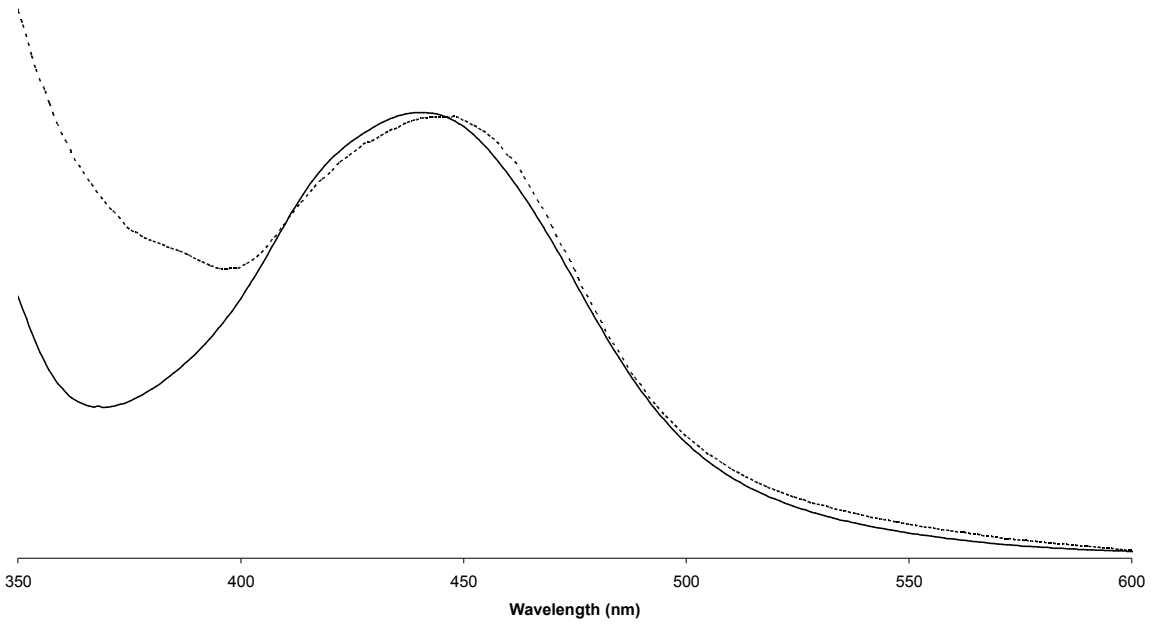

Figure 4.11 UV-visible spectra of $[(bpy)_2Ru(pytp)]^{2+}$ before (solid line) and after (dotted line) coordination of cobalt(III) in CH_3CN

4.2.2.1. Luminescence

Many ruthenium(II) polypyridyl complexes have been observed to luminesce in the visible region.[129, 137] The generally accepted rationale is that luminescence such as this arises after a MLCT from the ground state to a singlet excited state (^{1}MLCT). The excited state then crosses to a triplet state (^{3}MLCT) *via* an intersystem crossing (ISC), and it is the relaxation of this triplet state back to the ground state that occurs with luminescence.

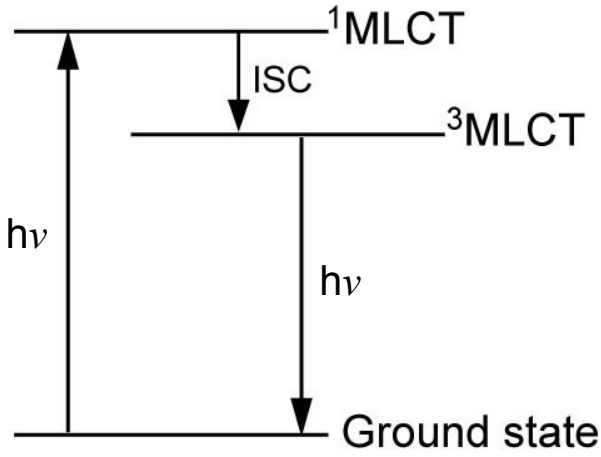

Figure 4.12 Fluorescent pathway for ruthenium(II) polypyridyl complexes

The emission spectra of the complexes, both before and after coordination of the cobalt, were recorded (Figure 4.13). The complex with cobalt bound was observed to emit less light than the complex without.

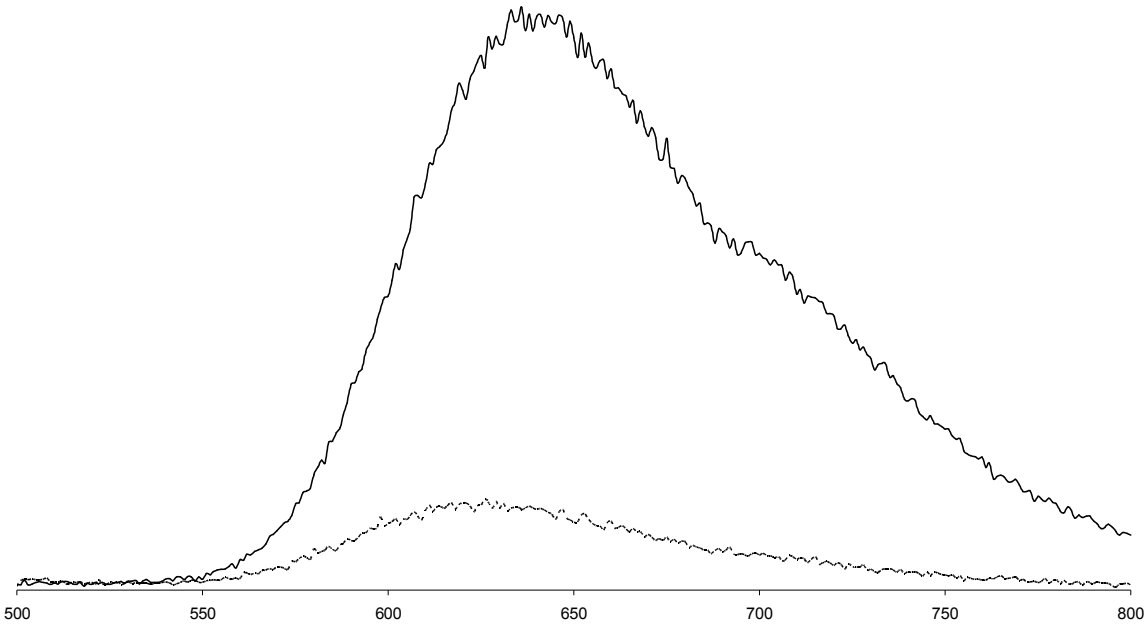

Figure 4.13 Comparison of the emission spectra of $[(bpy)_2Ru(pytp)]^{2+}$ (upper, solid line) and $[(bpy)_2Ru(pytp)Co(tren)]^{5+}$ (lower, dashed line) in CH_3CN

4.2.2.2. Lifetime study

The mononuclear and heterodinuclear pytp complexes were sent to Dr Evan Moore at the University of Melbourne, for measurement of the excited state lifetimes. The samples were placed in dry aerated acetonitrile and exposed to an excitation wavelength of 440 nm; the emission at 625 nm was then monitored.

The mononuclear complex was found to have a lifetime of 212 ns; while the heterodinuclear complex was found to have a lifetime of 72 ns. These values were calculated by fitting an exponential curve to the observed emission data (Figure 4.14).

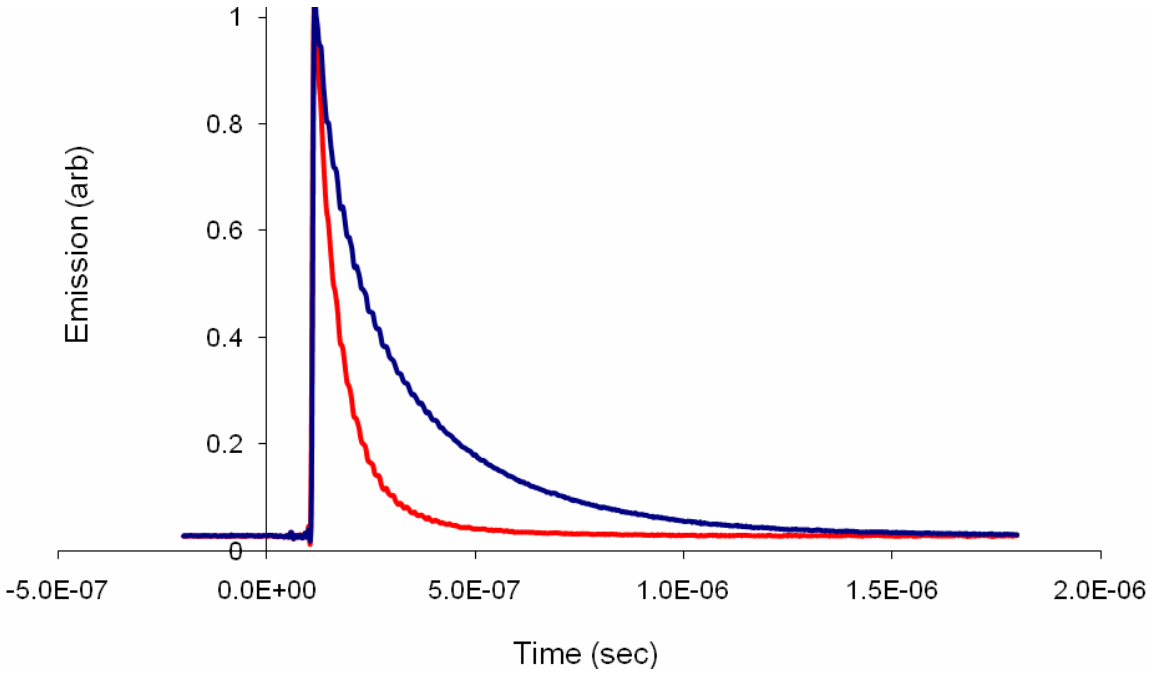

Figure 4.14 Lifetime measurements for $[(bpy)_2Ru(pytp)]^{2+}$ (blue) and $[(bpy)_2Ru(pytp)Co(tren)]^{5+}$ (red)

In addition to the lifetime measurements, the quantum yields were calculated by using $[Ru(bpy)_3]Cl_2$ as a standard with a known quantum yield of 4.2 %.[138] This involved measuring the relationship between the absorption at 440 nm and the integrated emission, and comparing this to the $[Ru(bpy)_3]Cl_2$ standard. From these measurements the mononuclear

complex was found to have a quantum yield of 1.11 % and the heterodinuclear complex a quantum yield of 0.21 %.

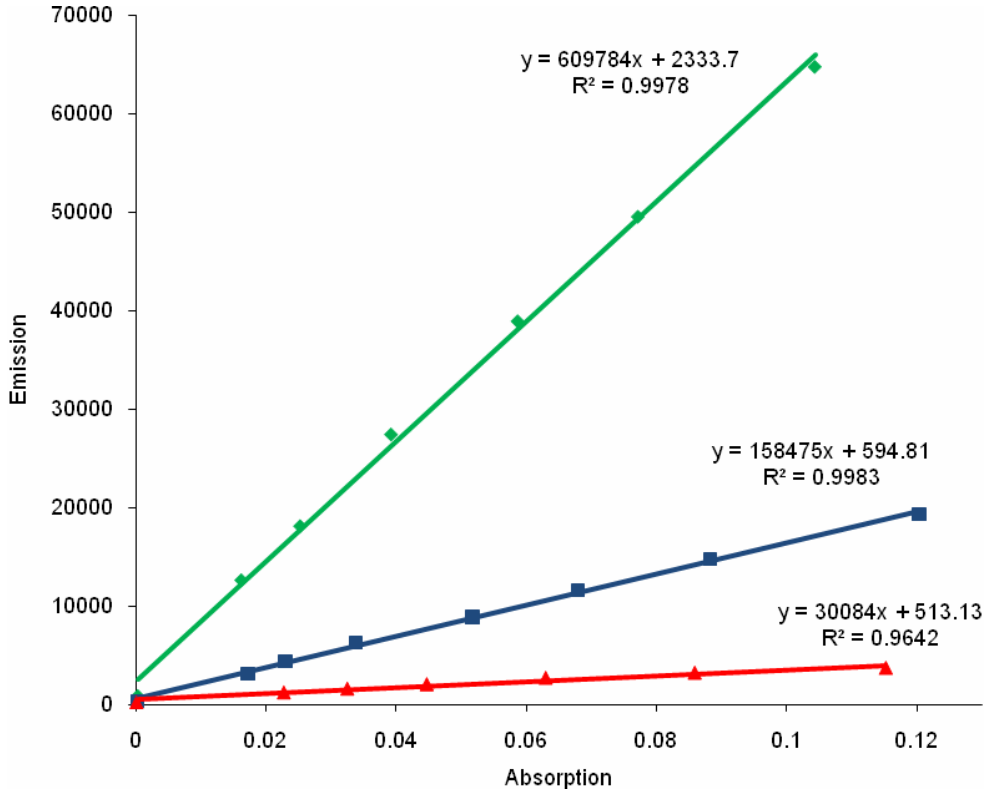

Figure 4.15 Emission-absorption relationship for $[Ru(bpy)_3]^{2+}$ (green), $[(bpy)_2Ru(pytp)]^{2+}$ (blue) and $[(bpy)_2Ru(pytp)Co(tren)]^{5+}$ (red)

All of these measurement are consistent with the coordination of the cobalt(III) metal centre resulting in a quenching of the luminescence. Furthermore, if we assume that the radiative and non-radiative decay paths are the same for each complex then the rate of electron transfer can be approximated from the formula $k_{obs} = k_{rad} + k_{et}$. If we assume that k_{rad} is equal to k_{obs} in the mononuclear complex, then in the heterodinuclear complex $k_{et} = k_{obs} - k_{rad}$. This calculation gives a k_{et} value of 9.6×10^6 s^{-1}.

4.2.2.3. Photo-activated Ligand Release

The purpose of synthesising these ruthenium(II)-cobalt(III) heterodinuclear complexes is to use them as an analogue for a photo-activated cytotoxin. Therefore the ability of the complex to release the ligands coordinated to the cobalt(III) metal centre must be assessed. In order to examine the photo-activated ligand release, the complex $[(bpy)_2Ru(pytp)Co(en)_2](PF_6)_5$ was dissolved in a 5 mm NMR tube with 50:50 mixture of deuterated acetonitrile and D_2O. The sample was then placed in a water bath in front of a 200 W incandescent lamp, and ^1H NMR spectra recorded at regular intervals.

Monitoring the changes between the ^1H NMR spectra showed a new singlet peak at 3.21 ppm growing in over time (Figure 4.16). We assigned this peak to the two CH_2 groups on the free en ligand. This process was shown to be light dependent as placing the samples in the dark overnight did not result in any change being detected by ^1H NMR methods. This supports the proposal that photo-activated electron transfer from the ruthenium(II) metal centre results in the reduction of cobalt(III) to cobalt(II) and triggers ligand release.

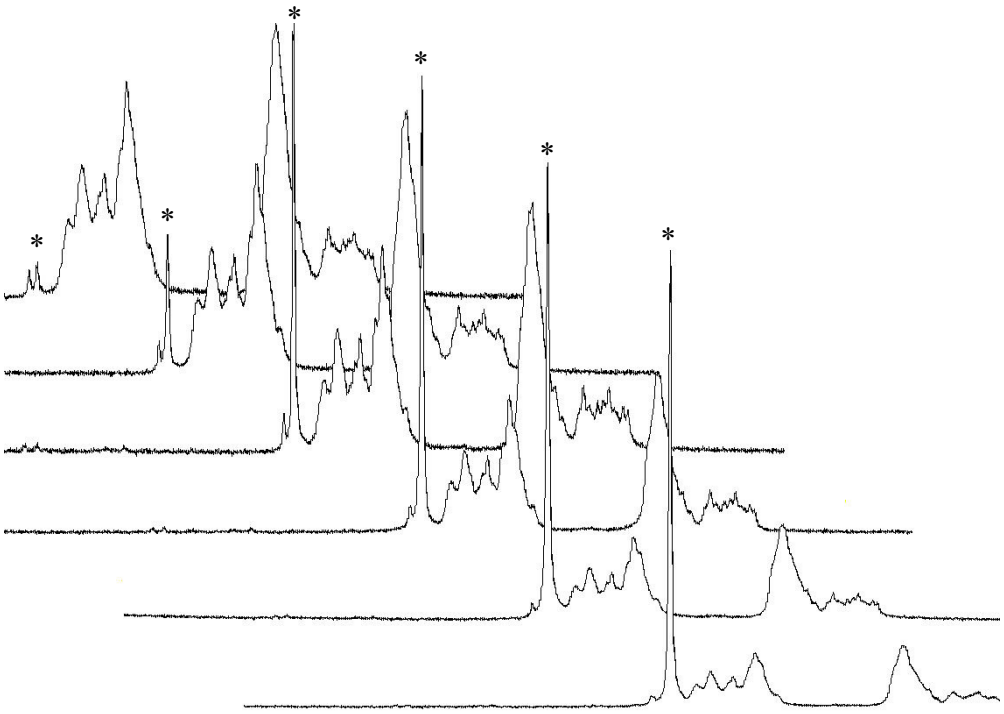

Figure 4.16 Photo-activated release of en from $[(bpy)_2Ru(pytp)Co(en)_2]^{5+}$; the peak associated with the free en molecule is marked with an asterisk

A similar experiment was performed with the $[(bpy)_2Ru(pytp)Co(tren)](PF_6)_5$ complex under the same reaction conditions. In this case two new triplets were observed to form at 2.99 and 2.73 ppm in the ^1H NMR spectra. The integration of these signals increased with time (Figure 4.17). The multiplicity and chemical shifts are entirely consistent with release of the tren ligand from the cobalt centre. The independent experiments with the tren and en systems together demonstrate that photo-induced ligand release can be achieved.

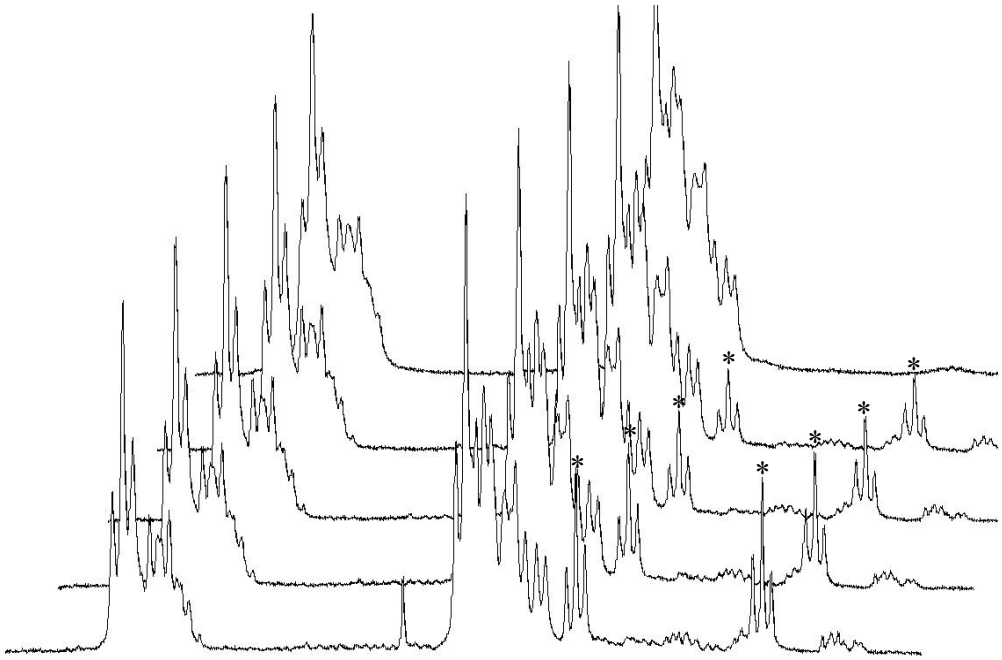

Figure 4.17 Photo-activated release of tren from $[(bpy)_2Ru(pytp)Co(tren)]^{5+}$; the peaks associated with the free tren molecule are marked with an asterisk

Further experiments were undertaken to examine whether the rate of ligand release depended on the O_2 concentration. O_2 dependent ligand release may provide a route to selective treatment of hypoxic cells like those found in poorly vascularised solid tumours.

In these experiments, three ^1H NMR samples were prepared in different manners. The first sample was prepared in exactly the same manner as above, the second had N_2 bubbled through it for one minute in order to remove some of the O_2, and the third was put through several freeze-pump-thaw cycles, the NMR tube was back filled with nitrogen before thawing so as to prevent excessive evaporation of acetonitrile from the solution. The three samples were then irradiated and the amount of en released was estimated by comparing the integral of the en singlet with the integral of the peak at 9.21 ppm corresponding to pytp bridging ligand of the unreacted starting material. Plotting these values revealed that the freeze-pump-thaw

sample released its ligands fastest, with the nitrogen bubbled samples being the second quickest (Figure 4.18). This suggests that the rate of ligand release may be oxygen dependent.

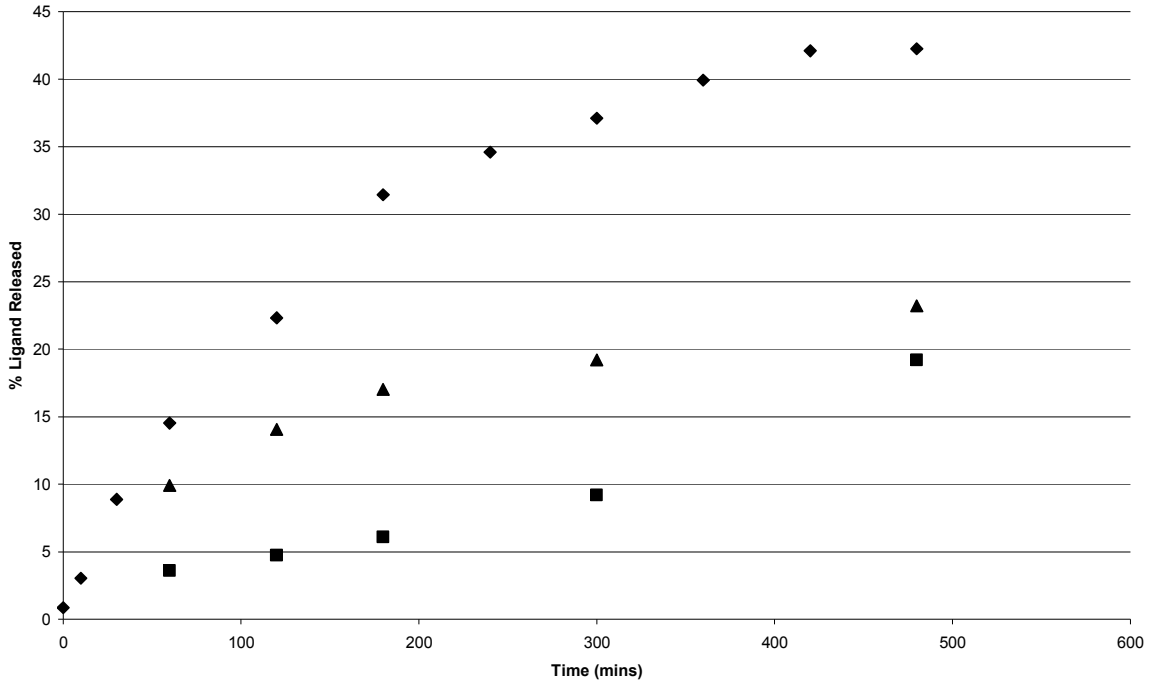

Figure 4.18 Difference in rate of ligand release between freeze-pump-thaw (♦), N_2 bubbled (▲) and air (■)

4.2.3. Complex Utilising a Pztp Bridging Ligand

The complex $[(bpy)_2Ru(pztp)](PF_6)_2$ was reacted with $[Co(en)_2(OTf)_2](OTf)$ in a similar manner to above. The reaction was much slower than the one with pytp as the bridging ligand. After three hours most of the starting material was still unreacted. We did not want to heat the reaction as a means to increase the reaction rate, because when we had heated similar reaction mixtures previously, the resulting solutions contained paramagnetic material. Instead, the formation of $[(bpy)_2Ru(pztp)Co(en)_2](PF_6)_5$ was achieved by stirring equimolar quantities of the reactants at room temperature in the dark for three days.

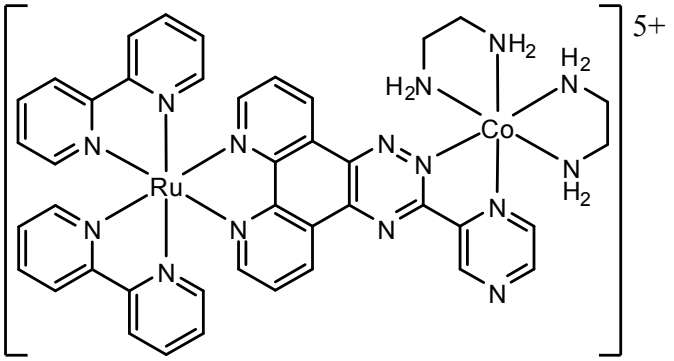

Figure 4.19 $[(bpy)_2Ru(pztp)Co(en)_2]^{5+}$

In comparison to the ^{1}H NMR spectrum the starting material, the spectrum for the resulting complex shows major changes in the positions of the peaks associated with the pyrazine ring. The singlet at 9.99 ppm, assigned to the CH group in the 3 position, shifted downfield to 10.33 ppm, and the two doublets at 8.90 and 8.86 ppm also shifted downfield to 9.41 and 9.01 ppm. The rest of the pztp protons were also shifted as a result of the cobalt coordination, while the bpy peaks only showed small changes.

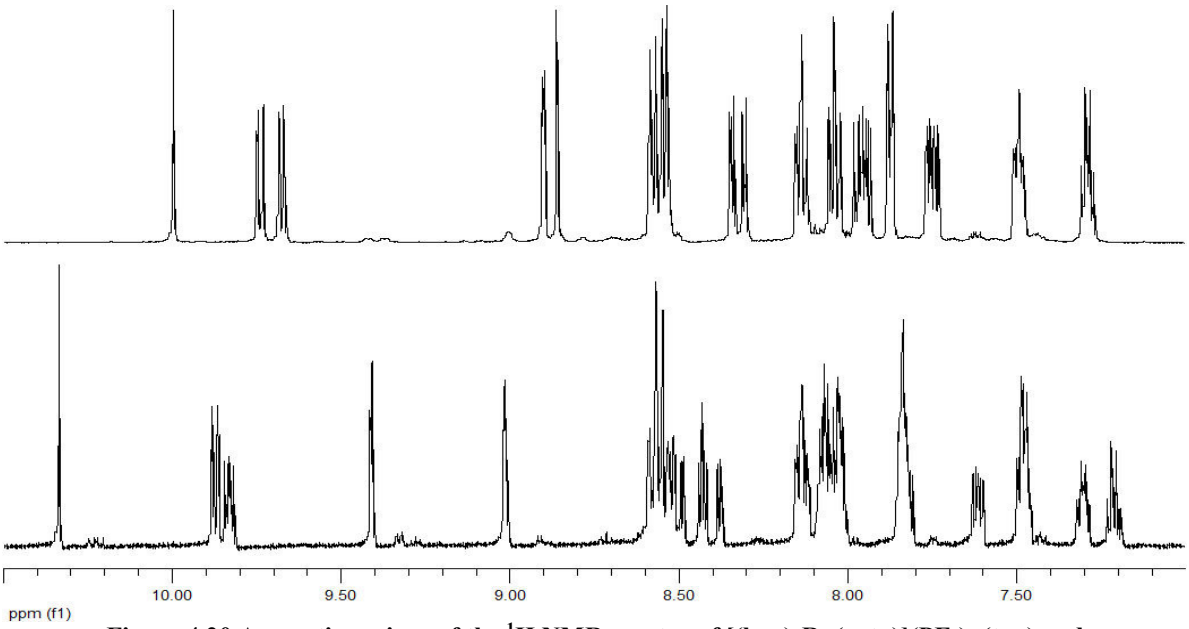

Figure 4.20 Aromatic regions of the ^{1}H NMR spectra of $[(bpy)_2Ru(pztp)](PF_6)_2$ (top) and $[(bpy)_2Ru(pztp)Co(en)_2](PF_6)_5$ (bottom) in CD_3CN

As with the pytp complexes, the coordination of the cobalt(III) centre resulted in a slight red-shift of λ_{max} and an increase in the absorbance in the near UV region.

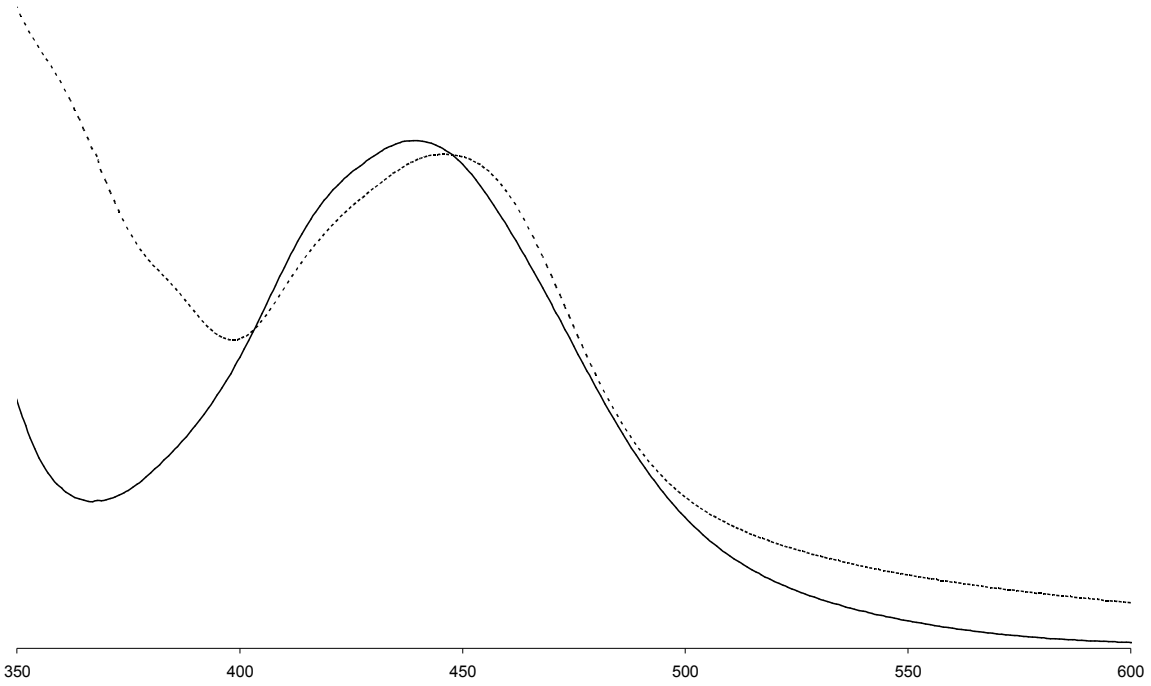

Figure 4.21 UV-visible spectra of $[(bpy)_2Ru(pztp)]^{2+}$ before (solid line) and after (dotted line) coordination of the $Co(en)_2^{3+}$ fragment in CH_3CN

4.2.3.1. Photo-activated Ligand Release

The examination of the photo-activated ligand release from the complex $[(bpy)_2Ru(pztp)Co(en)_2](PF_6)_5$ was conducted in the same manner as for $[(bpy)_2Ru(pytp)Co(en)_2](PF_6)_5$. Two samples were prepared; one with 5 iterations of freeze-pump-thaw, back filling with argon before thawing, and the other with no effort made to remove oxygen from the system. In both cases a singlet corresponding to the CH_2 groups on the free en appeared at 3.05 ppm. The generation of this singlet was quicker in the freeze-pump-thaw sample, which is consistent with the oxygen dependence observed for the pytp complex. In addition to the appearance of the en singlet following irradiation, the recorded ^1H

NMR spectra for both samples showed the reappearance of the peaks corresponding to $[(bpy)_2Ru(pztp)]^{2+}$ (Figure 4.22).

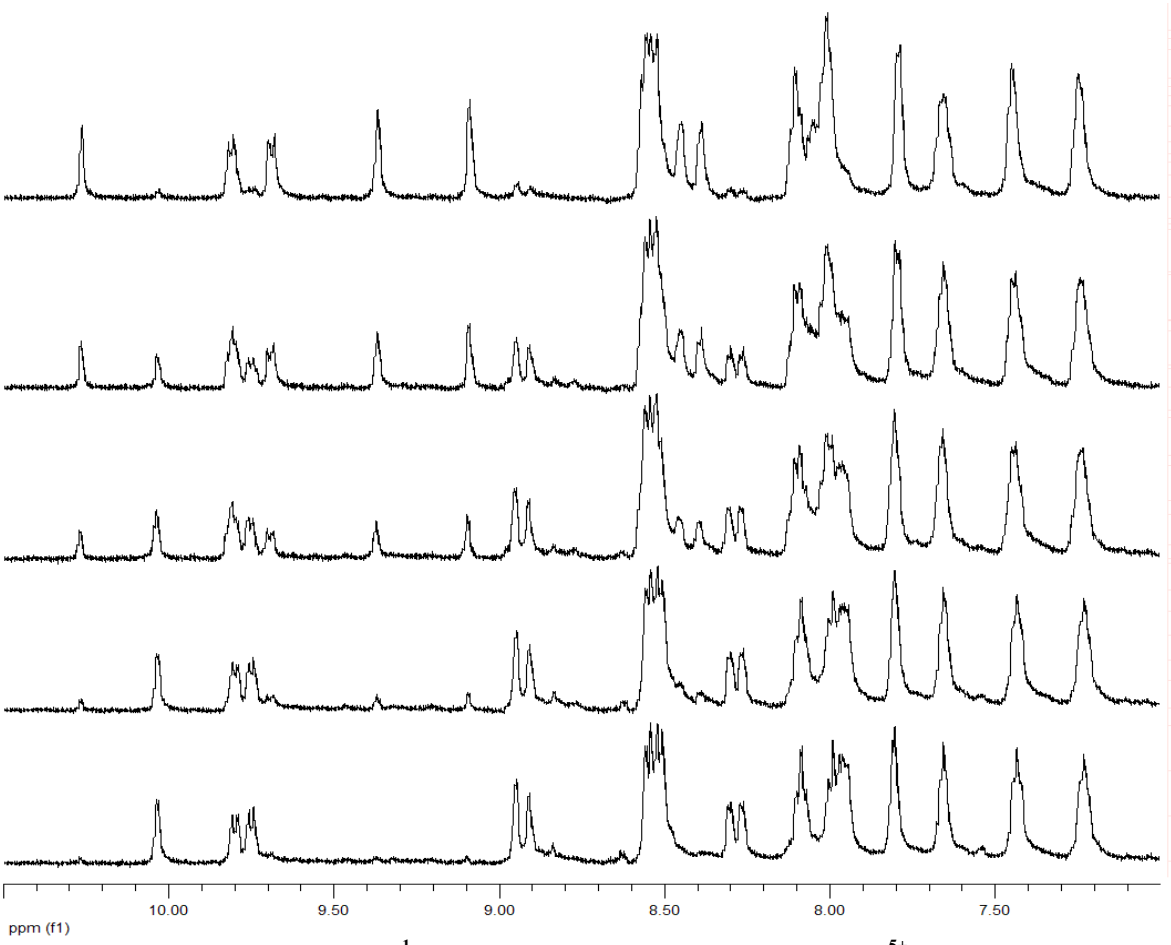

Figure 4.22 Aromatic regions of the ^{1}H NMR spectra of $[(bpy)_2Ru(pztp)Co(en)_2]^{5+}$ during irradiation in a 50:50 D_2O/CD_3CN mixture, recorded from time = 0 (top) to time = 3 hours (bottom)

The regeneration of the original ^{1}H NMR spectrum was not seen in any of the pytp experiments. This could be due to either the ruthenium(III) complex being reduced back to ruthenium(II) after release of the cobalt metal centre and the cobalt(II) metal not recoordinating to the vacant binding domain, or the ligand release is occurring by some other process. In order to examine whether the reformation of $[(bpy)_2Ru(pztp)]^{2+}$ was related to the irradiation, a sample of $[(bpy)_2Ru(pztp)Co(en)_2](PF_6)_5$ was placed in a 50:50 mix of acetonitrile and water and left in the dark for 17 hours. After this time the ^{1}H NMR spectrum

of the sample was recorded. The recorded ^{1}H NMR spectrum showed peaks consistent with a mixture of $[(bpy)_2Ru(pztp)Co(en)_2]^{5+}$ and $[(bpy)_2Ru(pztp)]^{2+}$ being in solution (Figure 4.23). While the ^{1}H NMR spectrum for the 17 hour sample showed an approximately equal amount of cobalt coordinated and uncoordinated species in solution, the irradiated sample with oxygen removed had no cobalt coordinated species in solution by 3 hours, and the irradiated sample with oxygen present had only a small amount of the cobalt coordinated species left after 3 hours. This suggests that the electron transfer and subsequent ligand release is potentially thermally accessible. The potential thermal accessibility of the electron transfer could explain why we observed paramagnetic contamination in the products of the reactions involving heating the ruthenium(II) complexes with $[Co(en)_2Cl_2]Cl$.

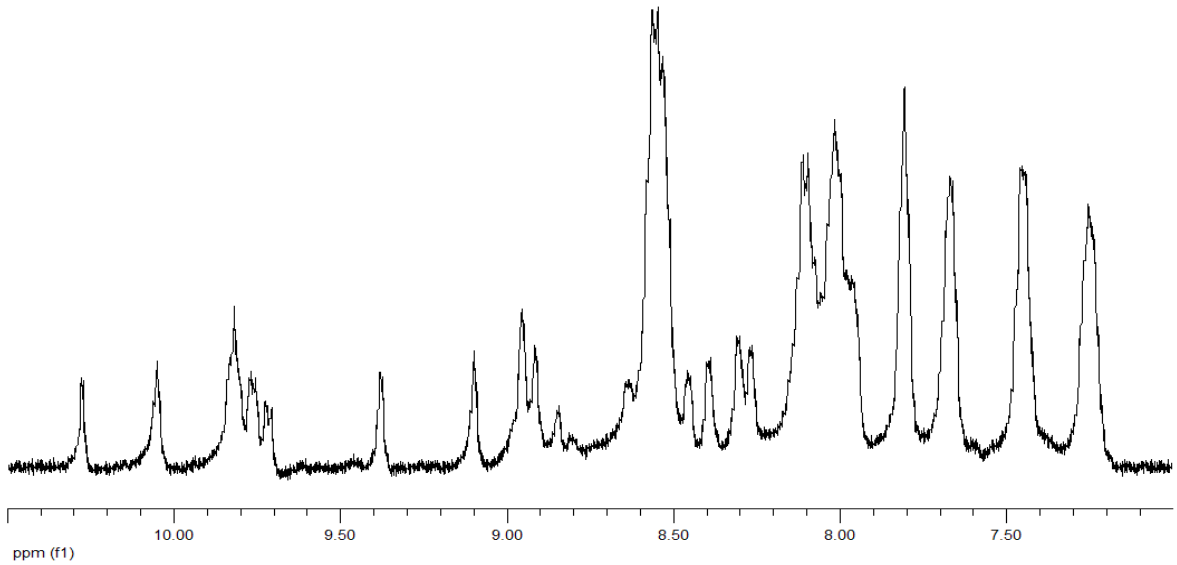

Figure 4.23 Aromatic region of the ^{1}H NMR spectrum of $[(bpy)_2Ru(pztp)Co(en)_2]^{5+}$ after 17 hrs in the dark in a 50:50 D_2O/CD_3CN mixture

4.2.4. Complexes Utilising a Pytz Bridging Ligand

The other bridging ligand used in our study was pytz. Unlike pytp and pztp, pytz has two identical binding domains and had to be synthesised before being coordinated to a

ruthenium(II) metal centre. The complex $[(bpy)_2Ru(pytz)Co(tren)](PF_6)_5$ was formed in the same manner as the heterodinuclear pytp complex (Figure 4.24).

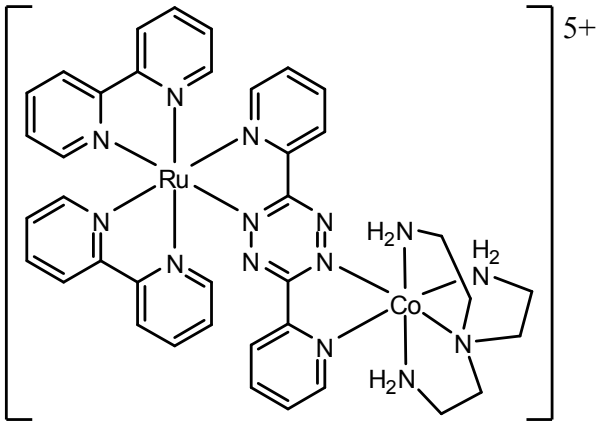

Figure 4.24 $[(bpy)_2Ru(pytz)Co(tren)]^{5+}$

The product from the reaction was an intense blue colour and comparison of the ^1H NMR spectra showed a changed aromatic region (Figure 4.25), as well as additional peaks in the alkyl region.

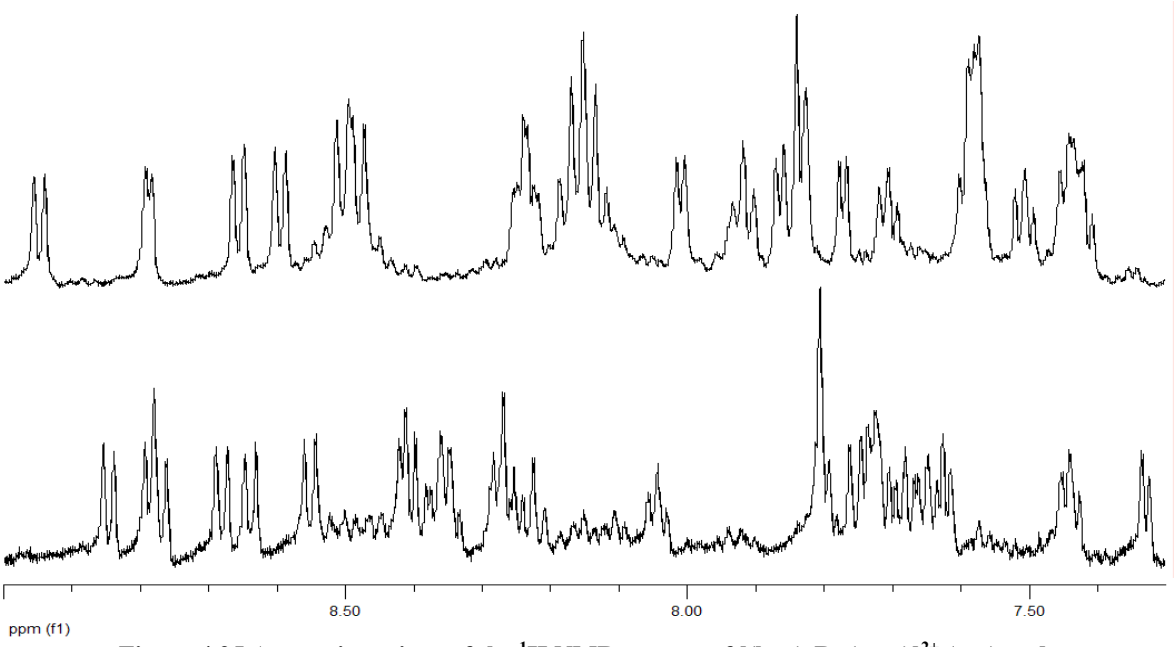

Figure 4.25 Aromatic regions of the ^1H NMR spectra of $[(bpy)_2Ru(pytz)]^{2+}$ (top) and $[(bpy)_2Ru(pytz)Co(tren)]^{5+}$ (bottom) in CD_3CN

The coordination of the cobalt(III) metal centre resulted in a major change in the UV-visible spectrum. The λ_{max} in the visible region shifted from 514 nm to 570 nm. This red shift is similar to that observed with the diruthenium complex where λ_{max} is shifted to 700 nm following coordination of the second ruthenium centre.

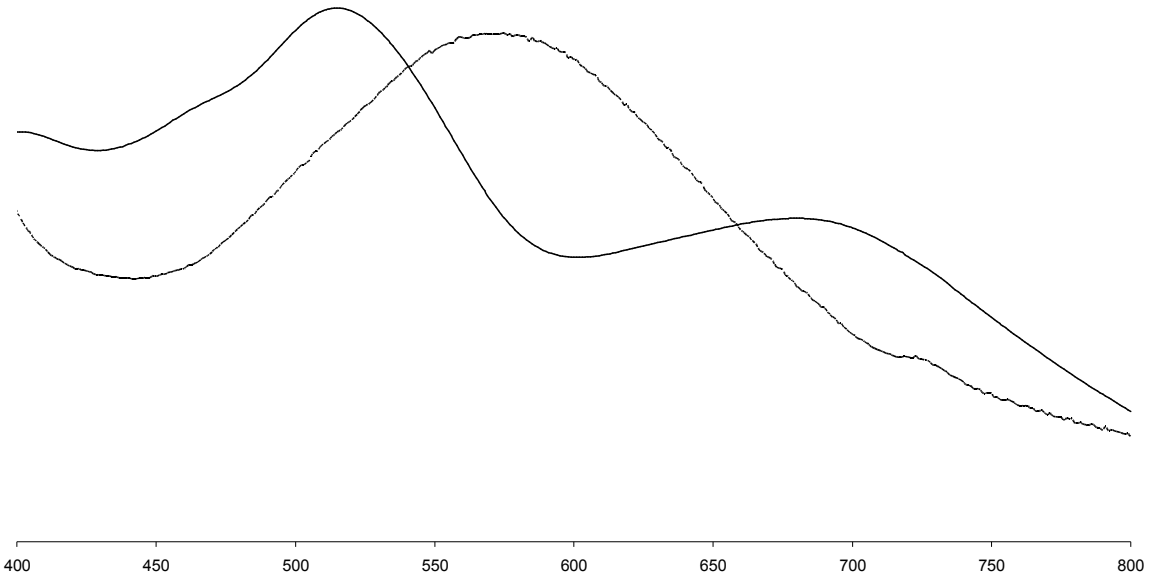

Figure 4.26 UV-visible spectra of $[(bpy)_2Ru(pytz)]^{2+}$ before (solid line) and after (dotted line) coordination of the $Co(tren)^{3+}$ fragment in CH_3CN

4.2.4.1. Photo-activated Ligand Release

Addition of water to a solution of $[(bpy)_2Ru(pytz)Co(tren)](PF_6)_5$ resulted in an immediate colour change to a much less intense orange solution. On standing this solution gradually changed colour to green (Figure 4.27).

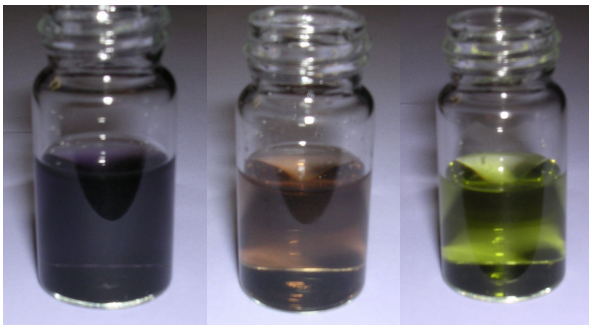

Figure 4.27 Change in colour of $[(bpy)_2Ru(pytz)Co(tren)](PF_6)_5$ in acetonitrile following addition of water

The aromatic region of the ^1H NMR spectrum of the complex shortly after the addition of water is similar to that of the $[(bpy)_2Ru(pytz)]^{2+}$ species. However, there are large broad peaks in both the aromatic and alkyl regions, which suggest the presence of paramagnetic species. The ^1H NMR spectrum of the green solution still shows a broadened aromatic region similar to that of the orange solution. However, there are now two triplet peaks in the alkyl region, which we assign as being the free tren ligand.

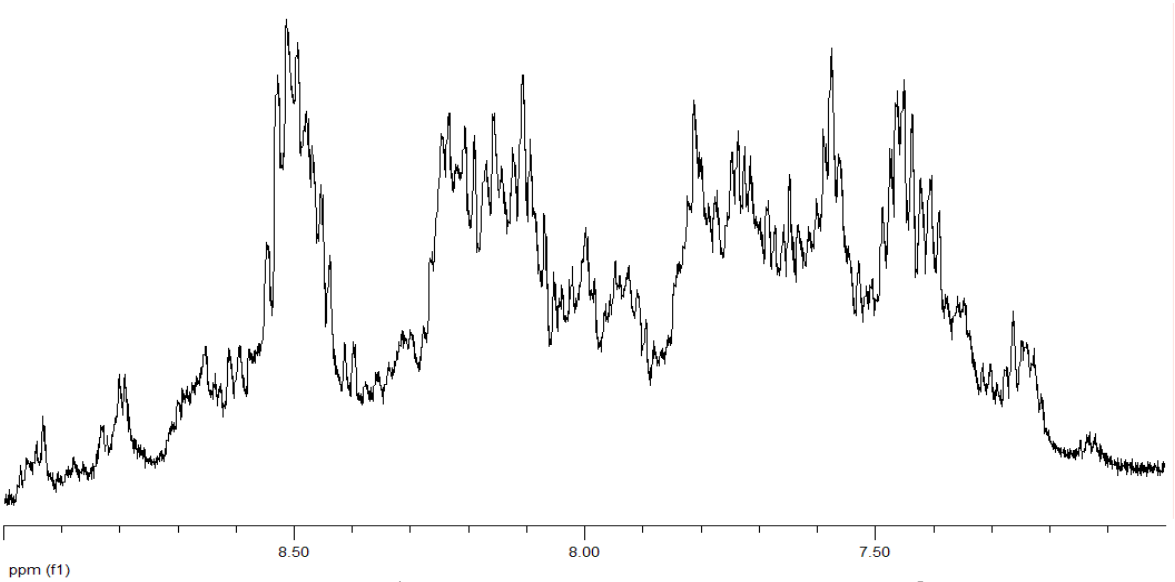

Figure 4.28 Aromatic region of the ^1H NMR spectrum of $[(bpy)_2Ru(pytz)Co(tren)]^{5+}$ in CD_3CN following addition of D_2O (orange solution)

Attempts to show photo-activation of the colour change were unsuccessful as addition of water resulted in the formation of the orange solution regardless of light levels. By comparison the diruthenium complex showed no change when exposed to the same

conditions. This indicates that the electron transfer between the two metal centres is easily realised and that, since cobalt(III) is needed as the second metal centre for ligand release to occur, the process still involves the formation of a cobalt(II) centre. The ease with which the ligand release occurs in this system makes it unsuitable for development as a photo-activated cytotoxin. However, the rapid ligand release could prove useful in cytotoxicity studies to assess the effect of coordinating a cytotoxic ligand to the cobalt(III) metal centre.

4.3. Conclusion

Through the use of cobalt(III) triflate compounds we have been able to synthesise several ruthenium(II)-cobalt(III) heterodinuclear complexes capable of undergoing ligand release. These complexes are all synthesised by reaction of the mono-ruthenium(II) complex with the appropriate cobalt(III) triflate complex. The coordination of the cobalt(III) metal centre results in a red shift of the UV-visible spectra, when compared to the mono-ruthenium complex, with the pytz complex showing the largest shift of 56 nm (Table 4.2).

Table 4.2 λ_{max} for mononuclear and heterodinuclear complexes

	λ_{max} (Ru)	λ_{max} (Ru-Co)
pytp	440	445
pztp	439	445
pytz	514	570

All of the ruthenium(II)-cobalt(III) heterodinuclear complexes synthesised show evidence of ligand release under various conditions. The pytp systems were observed to be the slowest ligand releasing complexes and showed evidence of re-coordinating to the cobalt(II) species generated following ligand release. In both the pytp and pztp systems, oxygen was seen to retard the rate of ligand release.

While the pytp system required light in order for the ligand release to proceed, both the pztp and pytz systems showed the ability to undergo ligand release without light, although the

pztp system was greatly accelerated by it. This suggests that the electron transfer between the two metal centres may be thermally accessible. Further theoretical and physical studies will be required before this can be established.

It needs to be mentioned that we conducted our studies using the PF_6^- salts because it made characterisation and subsequent investigation of the photo-activated ligand release easier. Other counter ions can also easily be obtained; for example the addition of tetrabutyl ammonium bromide to the complexes dissolved in acetonitrile results in the precipitation of the bromide salt.

The ruthenium(II)-cobalt(III) heterodinuclear complexes described in this chapter have all been observed to exhibit ligand release from the cobalt metal centre. This means that complexes such as these are possible candidates for development as photo-activated cytotoxins. The synthetic strategies relating to the incorporation of cytotoxic ligands into these complexes are given in Chapter 5.

Chapter 5: Synthesis of Cobalt(III) Complexes and Cytotoxicity Studies

5.1. Introduction

Having been able to demonstrate the photo-activated ligand release of both en and tren from a ruthenium(II)-cobalt(III) heterodinuclear complex, the next step is to look towards the coordination of cytotoxic ligands. This could be achieved either by the coordination of further non-cytotoxic analogues, such as *N*,*N*′-diethyl(ethane-1,2-diamine) which may better model the size and coordination geometry of a nitrogen mustard, or by forming nitrogen mustard complexes on the cobalt(III) metal centre (Figure 5.1).

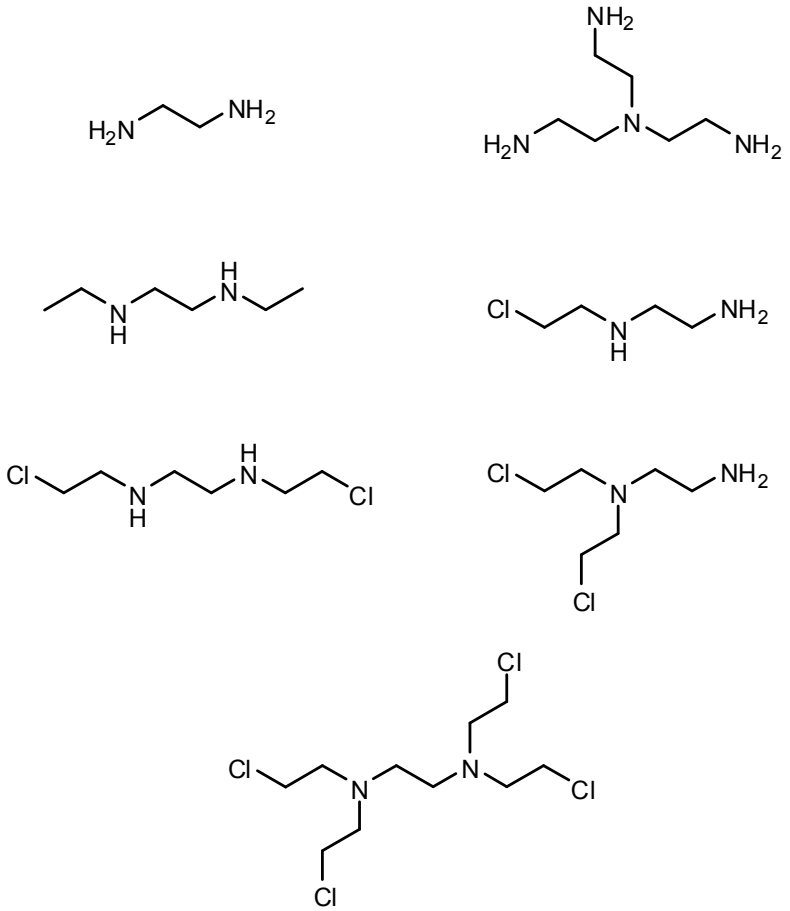

Figure 5.1 Examples of ligands which could be bound to a cobalt(III) metal centre in the study of photo-activated ligand release

Nitrogen mustards of this general kind can be synthesised by the reaction of an appropriate hydroxyethylamine with thionyl chloride (Figure 5.2).[45] However, doing this before coordination does have the potential to be problematic because the lone pair on the nitrogen can displace the chlorine atom to give a highly reactive aziridinium, as detailed in section 1.4.1. Thus decomposition of the mustard may compete with coordination. Furthermore, the later the reactive group is introduced into the molecule, the better.

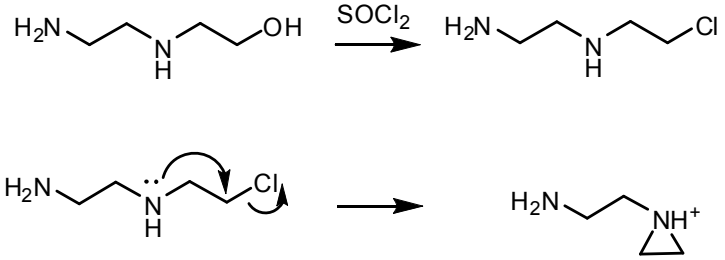

Figure 5.2 Synthesis of a nitrogen mustard and subsequent formation of the reactive aziridinium ion

In order to prevent the formation of the aziridinium ion, we used a synthetic strategy of coordinating the appropriate mustard precursors to the cobalt(III) metal centre, followed by reacting this complex with thionyl chloride.

This strategy of coordinating hydroxyethyl amine to a cobalt(III) metal centre and then converting to the nitrogen mustard has its own potential problems, the most obvious of which is the possibility for the oxygen atom to also coordinate to the metal centre. Cobalt(III) complexes with coordinated alcohols have been previously observed to form.[139, 140, 141] One alcohol containing ligand which we were interested in using had been coordinated to a cobalt(III) metal centre. This ligand was *N*-(2-hydroxyethyl)ethane-1,2-diamine (heen), and it was concluded that depending on the reaction conditions the ligand could be either bidentate, binding through just the amine groups, or tridentate, binding through the amine and hydroxyl groups.[142, 143]

The coordination of the ligand *N*,*N*′-bis-(2-hydroxyethyl)ethane-1,2-diamine (bheen) to a cobalt(III) metal centre has not previously been reported. However, there are several examples of bheen coordinating to different metal centres.

The X-ray crystal structure for the complexation of bheen with zinc(II) and cadmium(II) metal ions has previously been reported.[144] In the case of zinc(II) metal ions the complex formed was a discrete M_1L_2 complex with coordination through the amines in a distorted tetrahedral geometry (Figure 5.3). The four oxygen atoms of the hydroxyethyl arms are not deprotonated and are positioned around the metal centre at an average distance of 3.00 Å.

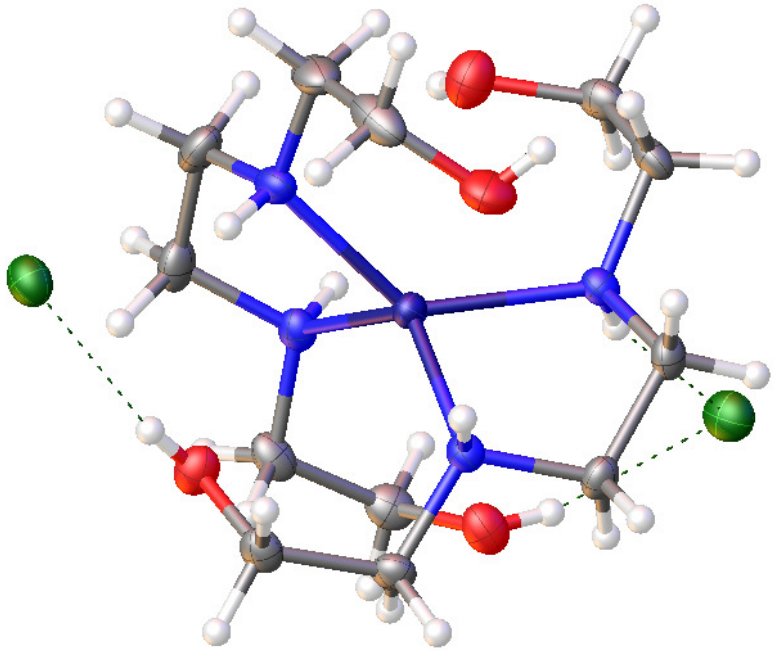

Figure 5.3 X-ray crystal structure of $[Zn(bheen)_2]Cl_2$[144]

The crystal structure of the cadmium(II) complex showed a M_2L_2 dimer, with the two cadmium metal centres being bridged by two chloride ions (Figure 5.4). The bheen ligand coordinated in a tridentate fashion with coordination occurring through the two amines and

one of the hydroxyethyl oxygen atoms. However, ESI-MS data indicated that this dimer is not the predominant species in solution and is instead produced during the crystallisation process.

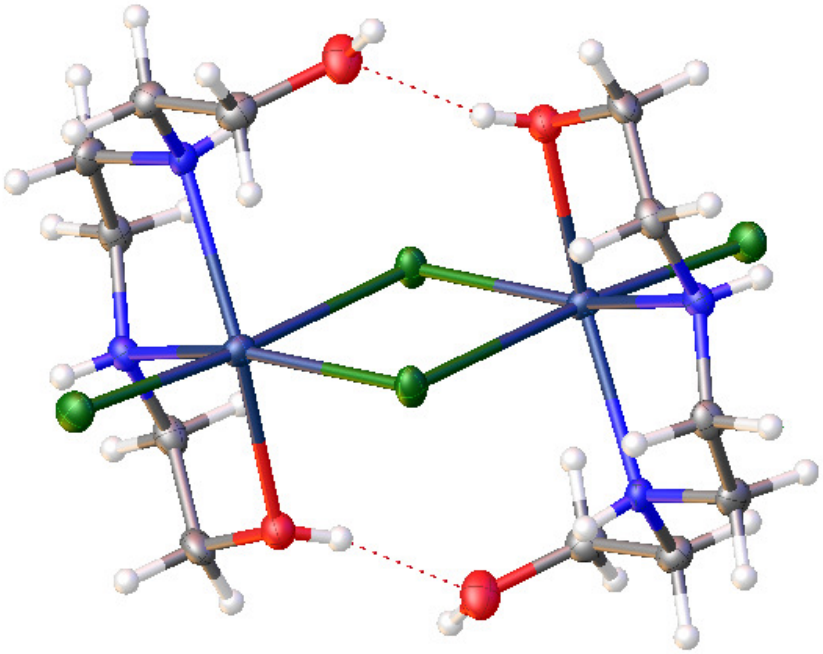

Figure 5.4 X-ray crystal structure of $[(\mu\text{-Cl})_2(\text{Cd(bheen)Cl})_2]$[144]

Oligomeric crystal structures containing bheen have also previously been prepared, Christou *et al* synthesised two such structures using iron(III) as the metal ion, one with 6 iron atoms and the other with 18.[145] In the complex with 6 iron atoms 3 of the 4 bheen molecules had both alcohol groups deprotonated and the fourth had one deprotonated alcohol. In the 18 iron atom complex all the bheen alcohols were deprotonated (Figure 5.5). In both complexes the iron molecules formed a chain with the iron atoms being bridged by the deprotonated hydroxyl groups.

These complexes show that bheen is versatile in respect to its number of binding atoms, charge and binding geometry and we therefore considered it likely that this ligand would show coordination to a cobalt(III) metal centre through the alcohol groups.

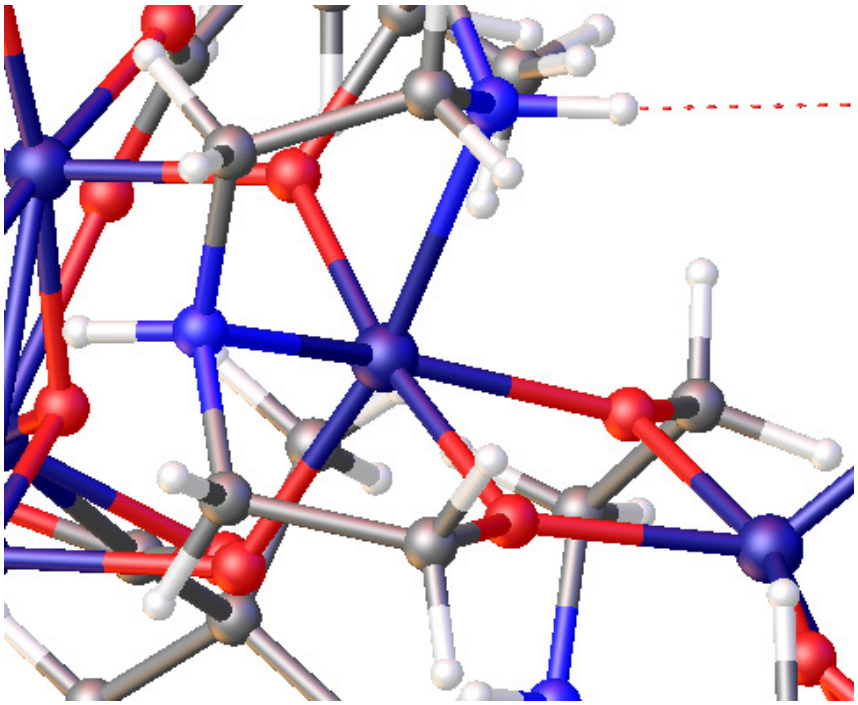

Figure 5.5 Part of the X-ray structure of an $Fe(III)_{18}$ complex with bheen, showing the bridging of the iron atoms by the hydroxyl group on the ligand[145]

In this chapter we will detail the synthesis of several ligands which could prove useful in the study of photo-activated cytotoxins. We will then describe the complexation of two of these ligands to a cobalt(III) metal centre. Of the two complexes formed one was found to be suitable for conversion to the cobalt(III) mustard complex, which was then converted to the triflate compound and used to produce a potential photo-activated cytotoxin. Finally the results of our cytotoxicity studies will be discussed.

5.2. Results and Discussion

5.2.1. Ligand Synthesis

5.2.1.1. *N,N′*-diethyl(ethane-1,2-diamine)

The ligand *N*,*N*′-diethyl(ethane-1,2-diamine) is a closer structural analogue for the final mustard ligands because the ethyl arms will approximate the steric bulk associated with the chloroethyl arms on the mustards. The ligand is synthesised from en in two steps. The first reaction is an acetylation, with the water produced by the reaction removed by distillation.[146] The second step is to reduce the amides to amines with lithium aluminium hydride, under an inert atmosphere, in dry ether (Figure 5.6).[147]

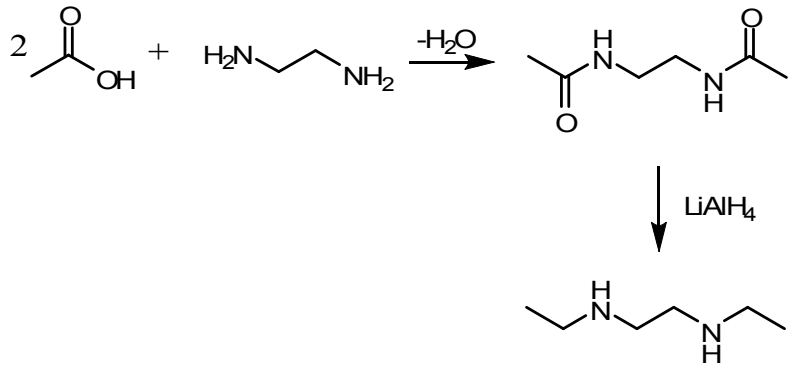

Figure 5.6 Synthesis of *N,N′*-diethyl(ethane-1,2-diamine)

5.2.1.2. *N,N*′-bis(2-hydroxyethyl)ethane-1,2-diamine

Although the ligand *N*,*N*′-bis(2-hydroxyethyl)ethane-1,2-diamine is commercially available, it can be easily and cheaply synthesised in a single step.[148] The ligand is synthesised by reacting 2-chloroethanol with *N*-(2-hydroxyethyl)ethan-1,2-diamine in the presence of sodium carbonate, with the product being purified by trituration in THF (Figure 5.7).

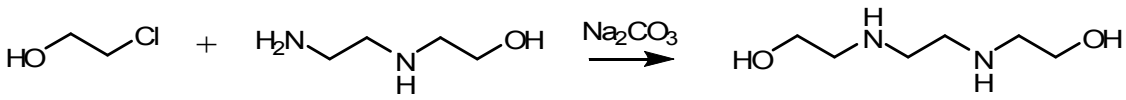

Figure 5.7 Synthesis of *N,N′*-bis(2-hydroxyethyl)ethane-1,2-diamine

5.2.1.3. *N,N*-bis(2-hydroxyethyl)ethane-1,2-diamine

N,N-bis(2-hydroxyethyl)ethane-1,2-diamine, like *N,N′*-bis(2-hydroxyethyl)ethane-1,2-diamine, is commercially available. However, its expense led us to look for an established synthetic route to produce it.

The literature method we followed[149] involved a two step synthesis. The first step was the reaction of *N*-(2-bromoethyl)phthalimide with a nine fold excess of diethanolamine. The product then had to be separated from the excess diethanolamine by a silica gel column. The second step involved treating the product obtained from the first reaction with hydrazine to remove the phthalimide group and give the final product of *N,N*-bis(2-hydroxyethyl)ethane-1,2-diamine (Figure 5.8).

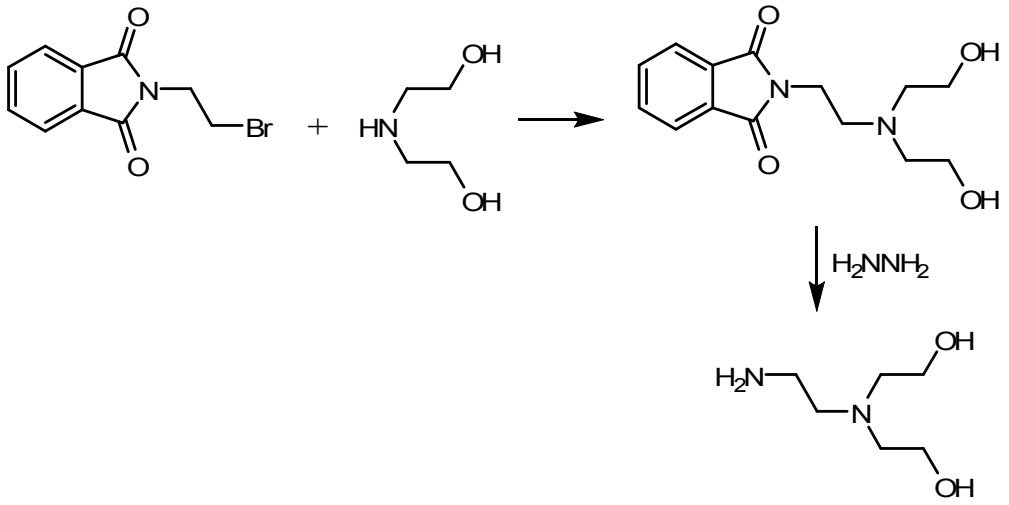

Figure 5.8 Synthesis of *N,N*-bis(2-hydroxyethyl)ethane-1,2-diamine

The main problem we found with this procedure was that, as written, it only produced about 0.25 g of *N,N*-bis(2-hydroxyethyl)ethane-1,2-diamine, and we wanted to work on the 10 g scale. Directly scaling up the reaction forty times was not practical as this would involve 1

litre of diethanolamine, the vast majority of which would need to be removed after the first step. We explored several alternatives such as using less diethanolamine or carrying out the reaction with equimolar amounts of reactants, using ethanol as the solvent. However, conditions suitable to the synthesis of large quantities of *N,N*-bis(2-hydroxyethyl)ethane-1,2-diamine could not be found, and further experiments with this ligand were abandoned.

5.2.1.4. *N,N,N',N'*-tetra(2-hydroxyethyl)ethane-1,2-diamine

The nitrogen mustard *N,N*-bis(2-chloroethyl)ethane-1,2-diamine is observed to be more cytotoxic than the *N,N'*-bis(2-chloroethyl)ethane-1,2-diamine mustard (IC_{50} against AA8 cell line being 1.5 μM and 30 μM respectively).[45] It is reasonable to assume that having four reactive arms would result in the production of an even more cytotoxic mustard as the potential for crosslinking DNA would be increased. Therefore, the synthesis of *N,N,N',N'*-tetra(2-hydroxyethyl)ethane-1,2-diamine was also investigated.

The reaction involved reacting 1,2-dibromoethane with diethanolamine in the presence of a base.[150] The literature method on which we based our method used potassium carbonate as the base. However, we found that this resulted in only partial formation of the final product. By changing the base to triethylamine we found that the reaction proceeded in a higher yield and generated purer products. Unfortunately, attempts to complex this ligand with a cobalt metal centre gave a red solution and we were unable to characterise the products formed. This was likely due to the coordination of the alcohol arms to the cobalt metal. This, amplified by the number of arms, could result in a wide range of products being formed.

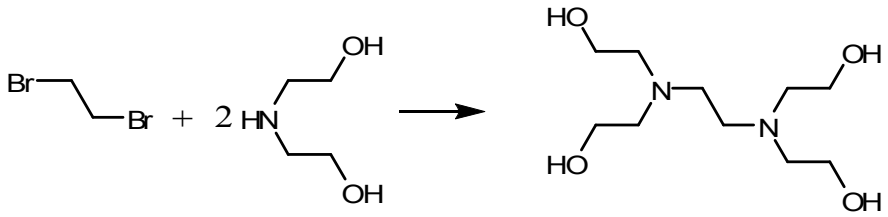

Figure 5.9 Synthesis of *N,N,N′,N′*-tetra(2-hydroxyethyl)ethane-1,2-diamine

5.2.2. Cobalt Complexes

5.2.2.1. Cobalt(III) Complex of *N*-(2-hydroxyethyl)ethane-1,2-diamine

We require the ligand *N*-(2-hydroxyethyl)ethane-1,2-diamine (heen) to bind to the cobalt(III) metal centre in a bidentate fashion. While the binding of alcohol groups to a cobalt(III) metal centre has been observed several times in prior studies,[139, 140, 141] we were able to find one example where heen was coordinated to the cobalt(III) metal centre in a bidentate fashion. However, this report had limited characterisation of the final product (only elemental analysis and molar conductance measurements).[143] Ultimately, because we were already familiar with the experimental procedure for the synthesis of *trans*-$[Co(en)_2(NO_2)_2]NO_3$, we decided to attempt the formation of $[Co(heen)_2(NO_2)_2](NO_3)$ using a modification of this experimental procedure first (Figure 5.10).

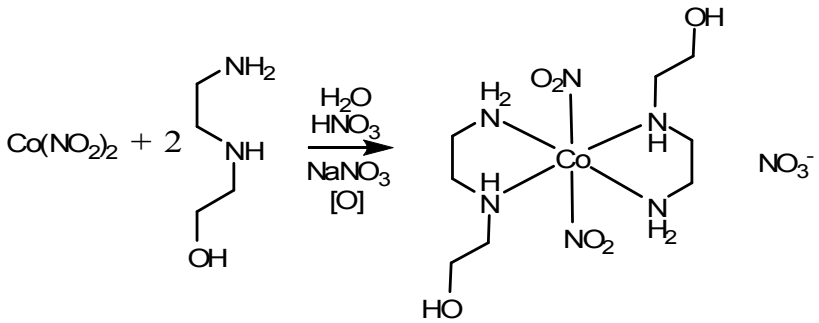

Figure 5.10 Synthesis of $[Co(heen)_2(NO_2)_2](NO_3)$

The reaction yielded orange crystals, some of which were suitable for characterisation by X-ray crystal diffraction (Figure 5.11). The structure showed that two heen ligands were

coordinated to the cobalt(III) centre through the amines, in a bidentate manner. The other two binding domains, *trans* to each other, were occupied by N-bound nitrite ligands. The two nitrite ligands were each involved in two hydrogen bonding interactions. One ligand bridges the secondary amines and the other bridges the primary amines; these interactions are shown as dotted lines in Figure 5.11.

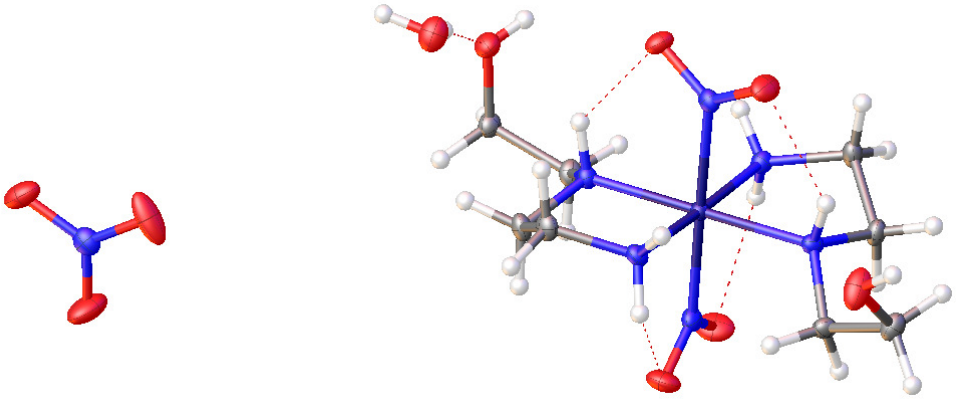

Figure 5.11 X-ray crystal structure of $[Co(heen)_2(NO_2)_2]NO_3.H_2O$

There is no direct hydrogen bonding between the cobalt complexes in the crystal lattice. However, a hydrogen bonding network exists with the cobalt complexes being bridged by solvent water molecules and nitrate counter ions (Figure 5.12).

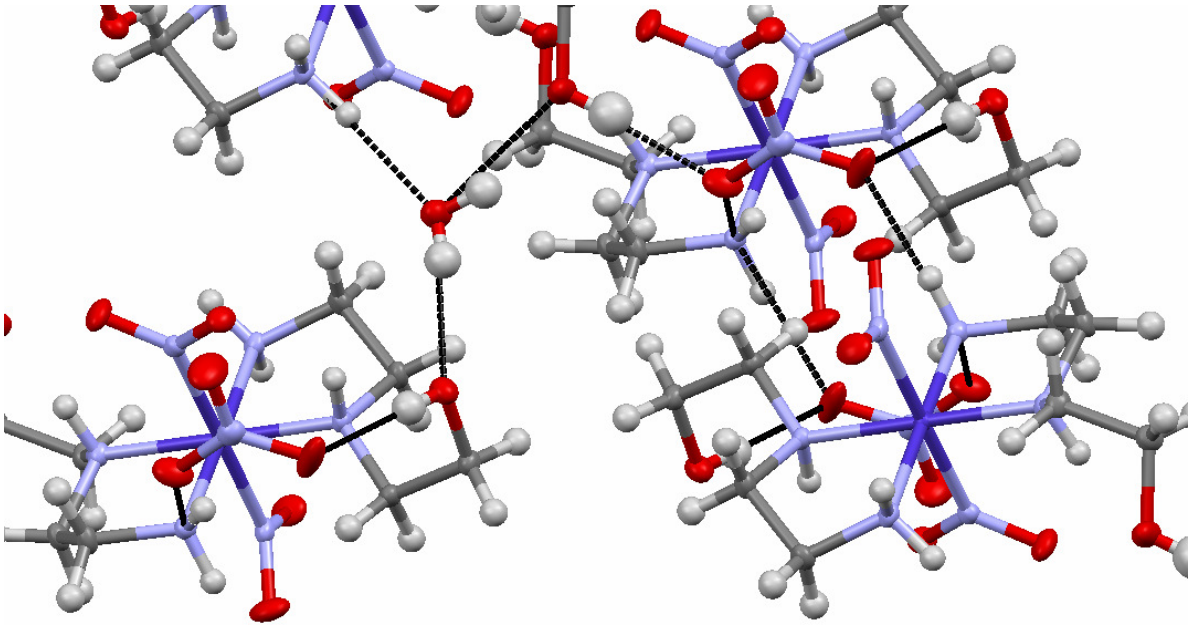

Figure 5.12 Hydrogen bonding network in the X-ray crystal structure of $[Co(heen)_2(NO_2)_2]NO_3.H_2O$ shown by dashed lines

Since a single crystal is not always representative of the bulk product, additional analysis of the bulk product was conducted using ^{1}H, ^{13}C, gCOSY and HSQCad NMR techniques, as well as mass spectrometry and elemental analysis. The NMR spectra were able to be almost fully assigned (differentiation between two protons on the same carbon but in different electronic environments was not achieved) and showed that, as in the X-ray crystal structure, the two heen ligands were in equivalent electronic environments (Figure 5.13). Elemental analysis confirmed that the single water of crystallisation observed in the X-ray crystal structure was also present in the bulk sample.

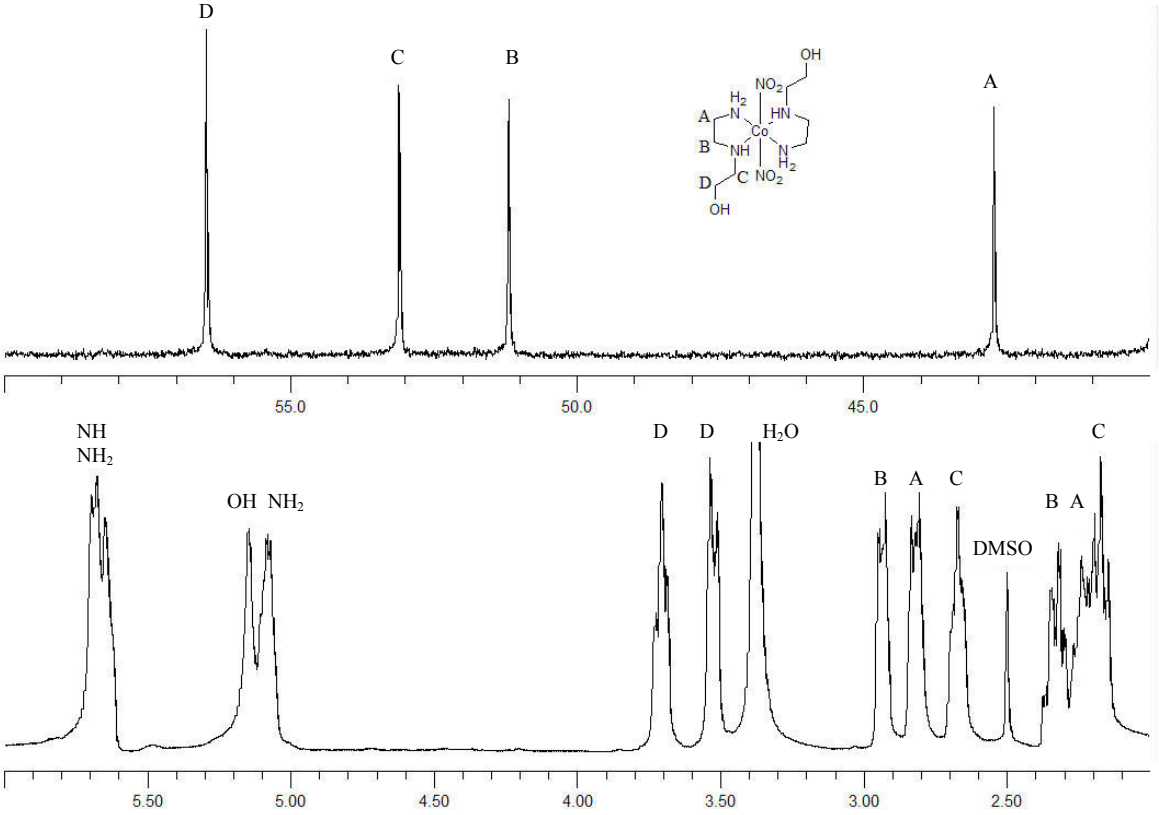

Figure 5.13 ^{13}C and ^{1}H NMR spectra of $[Co(heen)_2(NO_2)_2]^+$ in DMSO

Attempts to replace the nitrite ligands with either chloride or triflate ligands by treatment with the appropriate acid were not successful. For example, following the attempted chloride replacement, the ^{1}H and ^{13}C NMR of the product showed a large increase in the number of peaks. Although this increase in complexity is not totally unexpected, given that the secondary amine is a stereogenic centre, the signals in these spectra could not be assigned. Mass spectrometry was able to identify two main ions. One had a mass charge ratio consistent with replacing a single nitrite ligand with a chloride ligand, and the other was consistent with the expected mass for the alcohol deprotonating and the adoption of a tridentate binding motif (Figure 5.14).

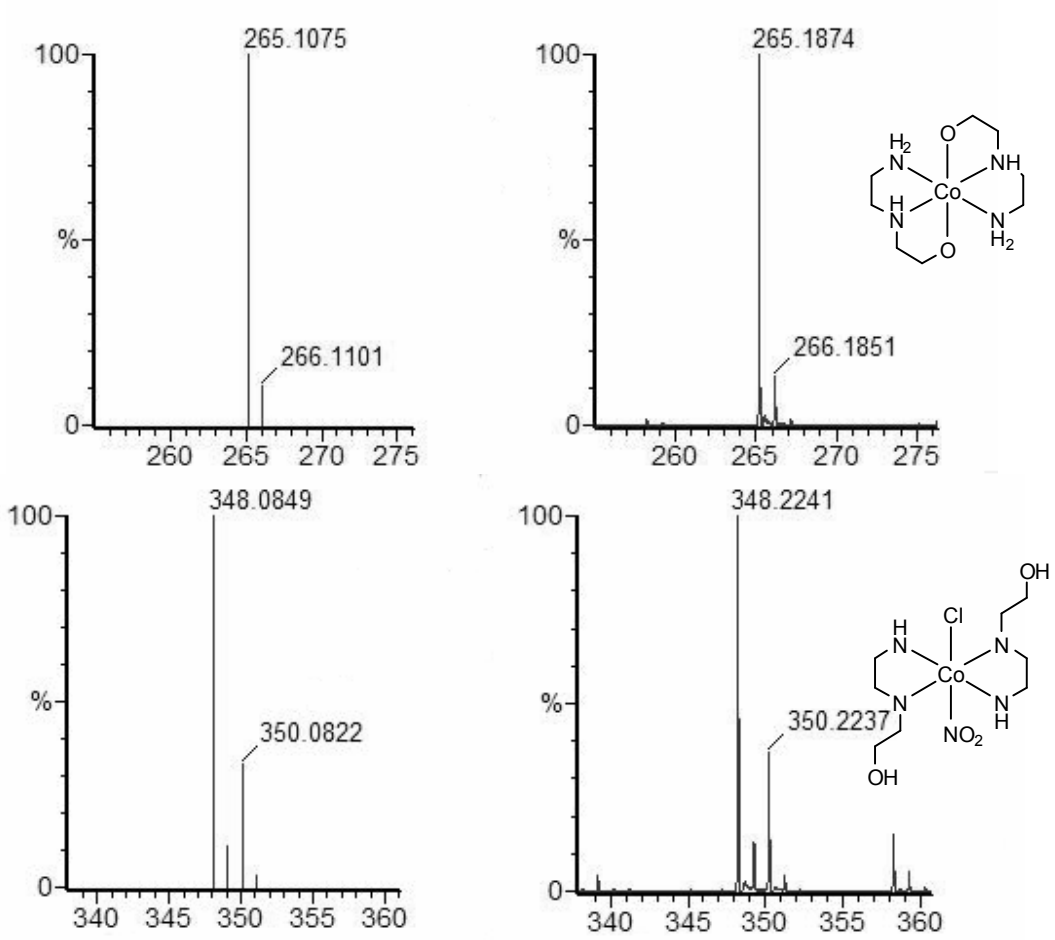

Figure 5.14 ESI-MS spectrum of the major peaks from the reaction of $[Co(heen)_2(NO_2)_2](NO_3)$ and HCl

On the basis of the ESI-MS result we concluded that coordination of the alcohol to the cobalt metal centre was occurring and that the alcohol would need to be converted to the alkyl chloride before the formation of the triflate salt.

5.2.2.2. Cobalt(III) complex of *N*,*N*′-bis(2-hydroxyethyl)ethane-1,2-diamine

Cobalt(II) nitrate was reacted with *N*,*N*′-bis(2-hydroxyethyl)ethane-1,2-diamine under the same reaction conditions used in the formation of $[Co(heen)(NO_2)_2](NO_3)$, with the intention of forming a similar complex (Figure 5.15). This resulted in the formation of an

orange-red precipitate, in contrast to the yellow product of the $[Co(heen)(NO_2)_2](NO_3)$ complex.

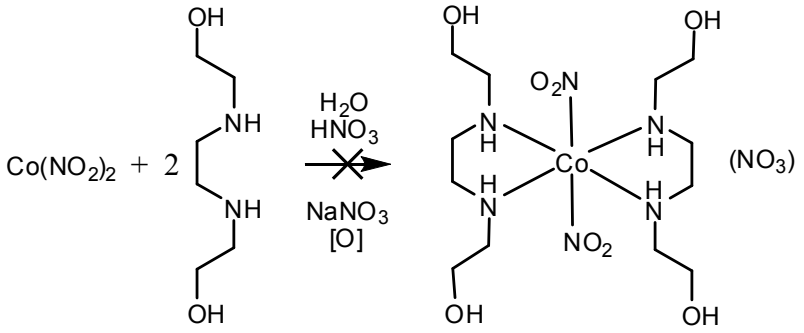

Figure 5.15 Proposed synthesis of $[Co(bheen)_2(NO_2)_2](NO_3)$

Unlike $[Co(heen)_2(NO_2)_2](NO_3)$, the orange-red precipitate which formed was insoluble in both DMSO and water. However, the addition of a small amount of acid to a suspension of the product in water would readily dissolve the precipitate, resulting in an orange solution which slowly changed to pink on standing. Dissolving the precipitate in concentrated HCl resulted in a green solution, which is indicative of two chlorides binding (*trans*-$[Co(NH_2)_4Cl_2]^+$ is green).[75]

The initially formed orange solution was analysed by ^1H and ^{13}C NMR techniques and mass spectrometry. The ^{13}C NMR spectrum showed six unique carbon environments associated with the initial orange solution, and if left running overnight an additional six smaller peaks associated with the slowly formed pink solution. The ^1H NMR spectrum associated with the orange solution was relatively simple, having only eight peaks. However, the spectrum associated with the solution after standing was much more complex and could not be assigned; this was in part due to the conversion being incomplete.

The mass spectrum of the sample in water with a small amount of formic acid was recorded. The most prominent peak recorded had a mass-charge ratio of 299.07. In addition to this there was another prominent peak present with a mass-charge ratio of 597.16, almost

twice that of the major peak. A mass charge ratio of 299.07 is what would be expected for a cobalt(III) complex with one bheen ligand and two nitrites. The presence of the heavier peak could mean that the complex is a mixture of oligomeric products, with the 299.07 mass charge ratio species being the monomeric unit.

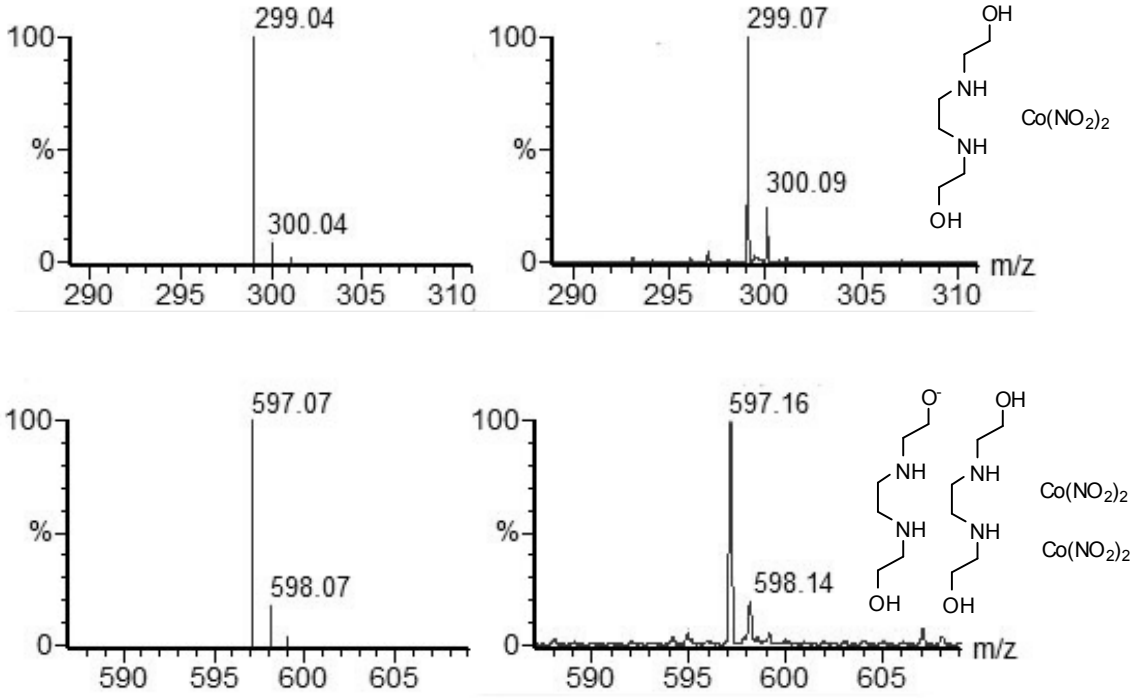

Figure 5.16 ESI-MS spectrum of the product for the reaction between bheen and Co(II)$(NO_2)_2$

Examination of the spectrum at higher mass-charge ratios revealed small peaks at 895.23 and 1193.26. These compare well with the expected values for a singly charged trimer (895.11) and tetramer (1193.14), adding support to the proposal that oligomers were being formed. Unfortunately, because the complex was not stable in solution, crystals suitable for use in structure determination by X-ray crystallography could not be produced.

5.2.2.3. Synthesis of Cobalt(III) Bound Mustards

The conversion of the hydroxyethyl group into a chloroethyl group was achieved through the use of thionyl chloride. The complex $[Co(heen)_2(NO_2)_2](NO_3)$ was stirred in a solution of thionyl chloride, to which a small amount of DMF was added (the complex $[Co(heen)_2(NO_2)_2](NO_3)$ is otherwise insoluble in thionyl chloride at room temperature). The reaction mixture was then stirred at room temperature for 30 minutes and the excess solvent removed (Figure 5.17). These reaction conditions are similar to those that have previously been reported by Broomhead in an analogous system.[151]

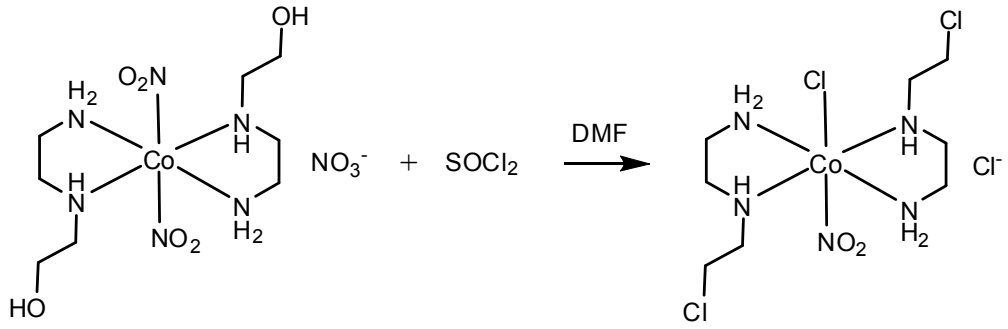

Figure 5.17 Reaction of $[Co(heen)_2(NO_2)_2](NO_3)$ with thionyl chloride

The ^1H and ^{13}C NMR spectra showed more peaks than expected, which we interpreted to mean that the product was not pure. ESI-MS results were consistent with the formation of several products. The major components of the mass spectrum were consistent with the complexes $[Co(ceen)_2(NO_2)(Cl)]^+$, $[Co(ceen)_2(NO_2)_2]^+$, and $[Co(ceen)(heen)(NO_2)_2]^+$ being present. The varying amount of chlorine atoms in these complexes results in distinctive isotope patterns being associated with each species, which gives us additional confidence in the assignment. Recrystallisation of the crude product from water and ethanol gave pure $[Co(ceen)_2(NO_2)(Cl)]Cl$ as the final product.

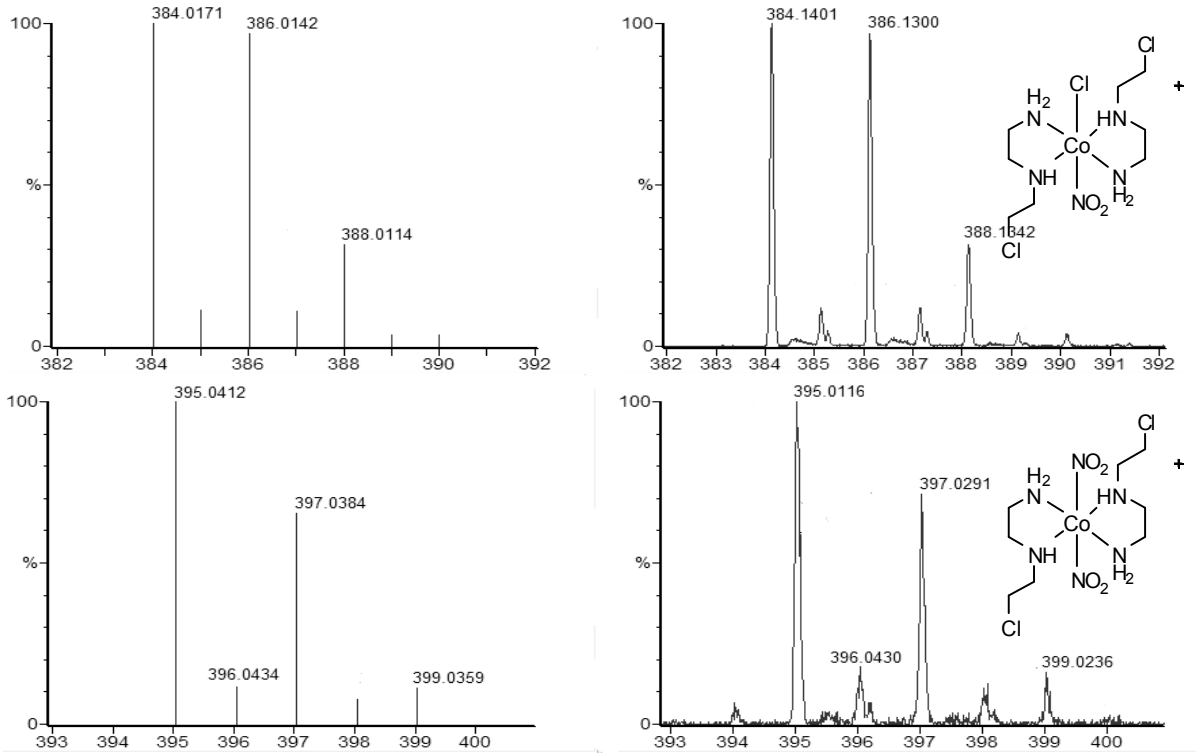

Figure 5.18 Predicted and measured ESI-MS spectra for the possible products from the reaction of thionyl chloride with $[Co(heen)_2(NO_2)_2](NO_3)$

The ratio between the different products was found to be dependent on the age of the thionyl chloride used. Older thionyl chloride proved to be much less reactive and the reaction could be conducted by heating at reflux overnight. Using newer thionyl chloride resulted in the complex decomposing if heated.

The attempted conversion of the $[Co(bheen\text{-}H)(NO_2)_2]_n$ to the corresponding mustard was carried out following the same procedure as used in the formation of $[Co(ceen)(NO_2)(Cl)]Cl$. The reaction following from the addition of the DMF to the thionyl chloride suspension was much more vigorous than for the reaction with $[Co(heen)_2(NO_2)_2](NO_3)$ and resulted in a deep green solution. The remaining thionyl chloride was then removed to give a thick green slurry. Attempting to recrystallise this slurry from ethanol resulted in a deep blue solution with a pale green precipitate. The blue solution would

turn pink upon the addition of water, which is the same colour change seen for the conversion of the tetrahedral complex $[CoCl_4]^{2-}$ into the octahedral complex $[Co(H_2O)_6]^{2+}$ (Figure 5.19).[75]

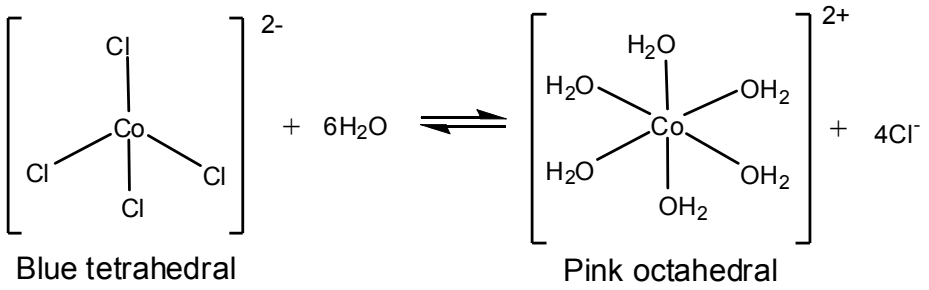

Figure 5.19 Interconversion of blue $[CoCl_4]^{2-}$ and pink $[Co(H_2O)_6]^{2+}$

The ^{1}H NMR spectrum of the pale green precipitate showed three major peaks: two triplets and a singlet. This is the same ^{1}H NMR pattern as would be expected for the free ligand. We therefore concluded that the ligand was dissociating from the cobalt(III) metal centre, and that the free metal was reduced from the +3 oxidation state to the +2 oxidation state, presumably oxidising water in the process.

The ^{1}H NMR spectrum of the precipitate obtained after heating $[Co(bheen\text{-}H)(NO_2)_2]_n$ at reflux overnight in thionyl chloride, without DMF, is identical to that of the original starting material. This lack of reactivity is most probably due to the complex being insoluble in thionyl chloride.

5.2.2.4. Synthesis of Cobalt(III) Triflate Compounds

In order to use the synthetic route we have developed for the preparation of ruthenium(II)-cobalt(III) heterodinuclear complexes, the mustard containing complex needs to be made soluble in acetonitrile. This solubility is achieved through the formation of the corresponding triflate salt. The conversion of cobalt(III) complexes into their triflate salts has

been well studied.[152, 153, 154, 155] This process generally involves either the nitrito or chlorido complex being treated with triflic acid under vacuum at a temperature of between 60 and 100 °C.

While this experimental procedure was successfully employed with both the en and tren cobalt complexes, this could not be realised for the nitrogen mustard complex $[Co(ceen)_2(NO_2)(Cl)]Cl$. We found that if the reaction was heated, either through an external heat source or by the exothermic nature of the reaction itself, the ligands would dissociate from the cobalt metal centre and the isolated product would be the triflate salt of the doubly protonated ligand (Figure 5.20).

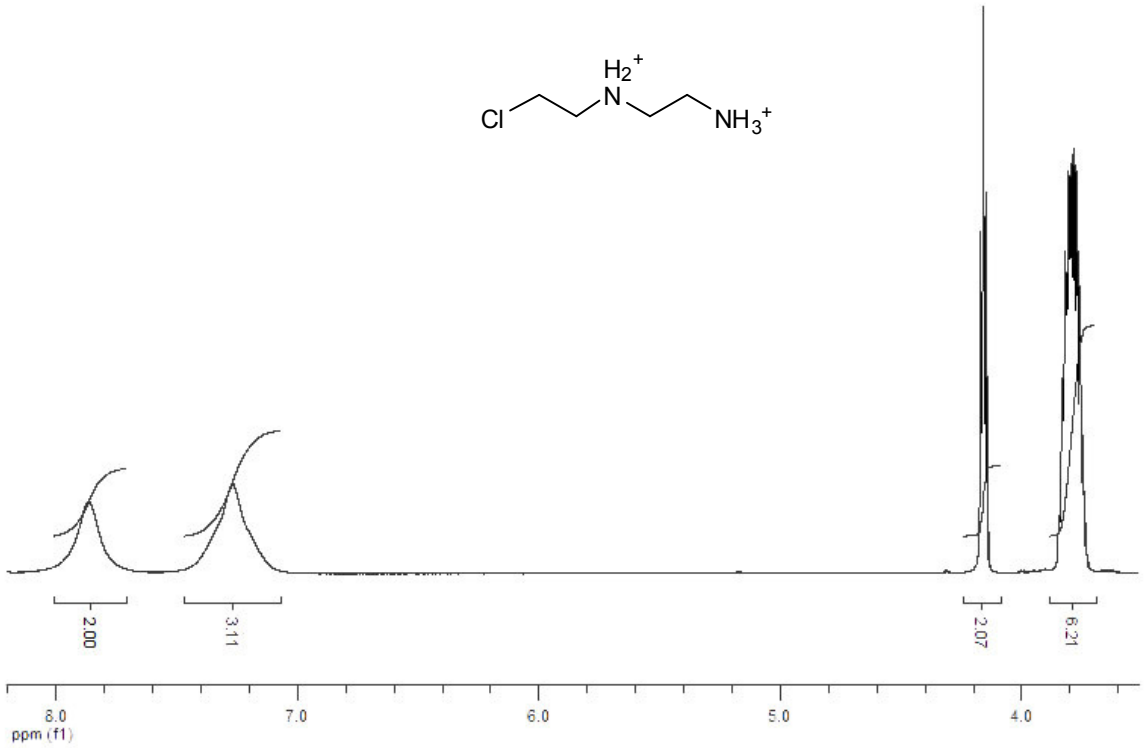

Figure 5.20 ^{1}H NMR spectrum of the protonated mustard *N*-(2-chloroethyl)ethane-1,2-diamine in CD_3CN

In order to get around this problem, the reactions were conducted in a ice-salt bath. By keeping the temperature of the reaction low we were able to prevent the decomposition of the

complex. The product isolated from this reaction was green in colour, which is consistent with having both a chloride and triflate bound to the metal centre (*trans*-$[Co(en)_2(OTf)Cl](OTf)$, which is obtained by controlled solvolysis of $[Co(en)_2(Cl)_2]^+$ in triflic acid, is also green).[155]

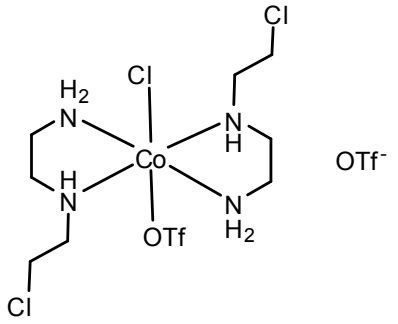

Figure 5.21 $[Co(ceen)_2(OTf)(Cl)](OTf)$

If the reaction is conducted at room temperature instead of in a salt-ice bath then the purple triflato complex $[Co(ceen)_2(OTf)_2](OTf)$ is formed. However, this complex is heavily contaminated with cobalt(II) and not suitable for further use.

Another method that might have permitted us to both avoid the decomposition of the complex and not have a chloride ion on the final complex, was through the formation of the complex $[Co(ceen)_2(H_2O)_2](OTf)_3$. This reaction was conducted by heating aqueous triflic acid and the complex in a water bath.[154] This caused the mixture to effervesce quite noticeably, with the final isolated product being a very pale pink colour. The ^1H NMR spectrum of the product was examined and assigned as being that of the free ligand.

5.2.3. Synthesis of Photo-activated Cytotoxins

The rate of exchange for a cobalt(III) bound chloride is much slower than for a similarly bound triflate (rate of aquation for $[Co(NH_3)_5X]^{2+}$ 1.7×10^{-6} and 2.7×10^{-2} s^{-1} respectively).[49] While this decreased rate has the potential to significantly slow the formation of a ruthenium(II)-cobalt(III) heterodinuclear complex, the bidentate nature of the incoming

ligand may facilitate replacement of the chloride ligand. If the reaction were too slow then silver(I) could be added to aid in the removal of the chloride. Ultimately, silver(I) was not needed as the reaction was able to progress without it.

Mixing $[Co(ceen)_2(OTf)Cl](OTf)$ with $[(bpy)_2Ru(pytp)](PF_6)_2$ on the NMR scale and monitoring the changes in the ^1H NMR spectrum showed that the mustard containing complex was coordinating to the ruthenium complex. However, the observed ^1H NMR was not as clean as for either the en or tren complex. This increase in complexity could be due to the asymmetry of the ligand resulting in a greater difference in the electronic environments of the various isomers, as well as there being a larger number of isomers possible.

$[(bpy)_2Ru(pytz)](PF_6)_2$ was mixed with $[Co(ceen)_2(OTf)Cl](OTf)$ in a minimal amount of acetonitrile in the dark for three hours. The blue product was precipitated out by drop wise addition of the reaction mixture to an aqueous solution of NH_4PF_6. Unfortunately the complex was not able to be characterised by ^1H NMR techniques as there was too much noise in the aromatic region. However, the colour changes associated with this complex are the same as those for the coordination of the $[Co(tren)]^{3+}$ fragment, suggesting that a heterodinuclear complex may have been produced.

5.2.4. Cytotoxicity Studies

In order to assess whether or not complexes similar to those formed in this study could potentially be used as photo-activated cytotoxins, cytotoxicity studies were carried out with the murine leukaemia cell line P388. These studies involved determination of the IC_{50} (concentration at which cell growth is inhibited by 50%) by way of a twofold dilution series incubated for 72 hours. The inhibition of cell growth was assessed by using the yellow dye 3-

(4,5-dimethylthiazol-2-yl)-2,5-diphenyltetrazolium bromide which is reduced to the purple 3-(4,5-dimethylthiazol-2-yl)-2,5-diphenylformazan by a healthy cell (Figure 5.22).

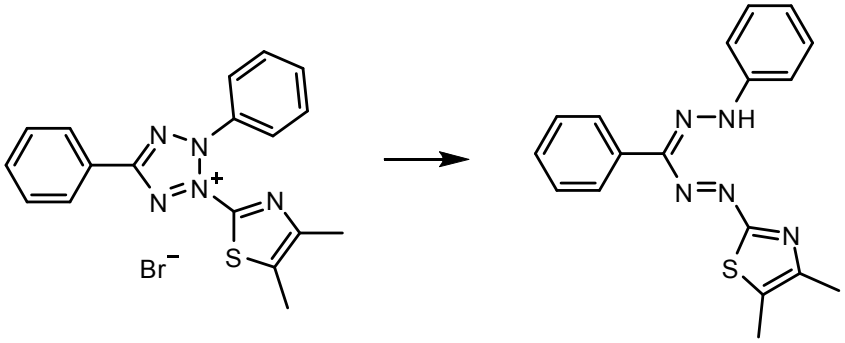

Figure 5.22 Reduction of the dye 3-(4,5-dimethylthiazol-2-yl)-2,5-diphenyltetrazolium bromide

Before exposing the cell line to the mustard containing species, the mononuclear ruthenium and non-mustard containing heterodinuclear complexes were assayed. The various complexes showed a range of cytotoxicity; for example, while all complexes based on the 'LEGO system' were active with IC_{50} values in the range of 30-50 μmol/L, the tetrazine complexes were much less cytotoxic with IC_{50} values of ~500 μmol/L. The IC_{50} value for the complex $[(bpy)_2Ru(pytp)Co(tren)]^{5+}$ should be treated as an indication of the minimum value, as some of the complex could have been converted into the more active $[(bpy)_2Ru(pytp)]^{2+}$ complex as a result of exposure to light. The cytotoxicity associated with the 'LEGO system' ligands was not unexpected as similar results had previously been reported by Liu *et al* against different cell lines.[156]

The low cytotoxicity of the pytz and pztz complexes coupled with their rapid ligand release made them ideal candidates for examining any increased cytotoxicity associated with having nitrogen mustards as the ligands on the cobalt(III) metal centre. For this reason the heterodinuclear complexes $[(bpy)_2Ru(pytz)Co(tren)]^{5+}$ and $[(bpy)_2Ru(pytz)Co(ceen)_2]^{5+}$ were also assayed. The complex containing the tren molecule did not show any cytotoxicity at the maximum tested concentration of 641 μmol/L. However, the complex containing the ceen

ligands had an IC_{50} value of 181 μmol/L. This value is approximately three times smaller than the non-cobalt containing complex.

The complexes $[Co(en)_2(OTf)_2](OTf)$ and $[Co(ceen)_2(OTf)Cl](OTf)$ were also assayed and found to have similar IC_{50} values of ~300 μmol/L. The lack of increased activity for the complex with ceen coordinated is presumably due to the ligands remaining bound to the cobalt metal centre, which would prevent the lone pair on the nitrogen atom from displacing the chlorine and forming a highly reactive and potentially cytotoxic aziridinium ion.

Table 5.1 Cytotoxicity data for non-mustard containing complexes

Complex	IC_{50} (μmol/L)	
	P388	HL-60[156]
$[(bpy)_2Ru(pytp)]^{2+}$	47	65.4
$[(bpy)_2Ru(pytp)Co(tren)]^{5+}$	195	
$[(bpy)_2Ru(pztp)]^{2+}$	66	6.7
$[(tbpy)_2Ru(pytp)]^{2+}$	166	
$[(phen)_2Ru(pytp)]^{2+}$	38	98.6
$[(bpy)_2Ru(pytz)]^{2+}$	472	
$[(bpy)_2Ru(pztz)]^{2+}$	547	
$[(bpy)_2Ru(pytz)Co(tren)]^{5+}$	>641	
$[(bpy)_2Ru(pytz)Co(ceen)_2]^{5+}$	181	
$[(bpy)_2Ru(pytz)Ru(bpy)_2]^{5+}$	660	
$[Co(en)_2(OTf)_2](OTf)$	303	
$[Co(ceen)_2(OTf)Cl](OTf)$	349	

From these results we conclude that the incorporation of a nitrogen mustard in a ruthenium(II)-cobalt(III) heterodinuclear complex can result in a marked increase in cytotoxicity. This increased cytotoxicity is most likely due to an electron transfer between the two metal centres resulting in the formation of a labile cobalt(II) metal centre and the subsequent release and activation of the nitrogen mustard.

5.3. Conclusion

In order to synthesise complexes that could potentially act as photo-activated cytotoxins, several ligands closely related to the nitrogen mustards, *N,N*-bis(2-

chloroethyl)ethane-1,2-diamine and *N,N′*-bis(2-chloroethyl)ethane-1,2-diamine, were synthesised and their coordination to a cobalt(III) metal centre investigated.

The most promising ligand investigated was *N*-(2-hydroxyethyl)ethane-1,2-diamine, which readily forms the complex *trans*-$[Co(heen)_2(NO_2)_2](NO_3)$ under the same reaction conditions as for the formation of *trans*-$[Co(en)_2(NO_2)_2](NO_3)$. The hydroxyl groups on this complex can then be converted into the alkyl chloride by treatment with thionyl chloride and DMF. Following conversion to $[Co(ceen)_2(Cl)(OTf)](OTf)$, the complex can then be coordinated to a ruthenium(II) complex with a vacant bidentate binding domain. However, the complex $[Co(ceen)_2(Cl)(OTf)](OTf)$ is not stable and should be used as soon after being synthesised as possible.

Cytotoxicity studies showed that by coordinating the ligand ceen to the cobalt centre of a ruthenium(II)-cobalt(III) heterodinuclear complex, utilising pytz as the bridging ligand, a marked increase in cytotoxicity is achieved. This result shows the promise of systems such as these as potential chemotherapeutic agents.

Chapter 6: Future Work

6.1. Introduction

At the conclusion of our study, there are a number of avenues for future experiments which could still be pursued. In this chapter we present an overview of some of these potential studies. In some cases we have already done some preliminary experiments towards this research and details of these will be given where appropriate.

6.2. Altering the Ruthenium Bound Ancillary Ligands

Many dye sensitised solar cells use a ruthenium(II) metal complex which absorbs light and, through a MLCT, injects electrons into the semiconductor conduction band.[59] In order to tune the efficiency and wavelength at which this occurs, the energy levels associated with the electron transfer need to be altered. One way to achieve this is through varying the non-bridging ligands bound to the ruthenium metal. Altering these ligands results in changes in the electron transfer associated with the bridging ligand and can greatly improve the performance of the solar cell by permitting it to operate at longer wavelengths and with a higher efficiency.

It has also been observed that the degree of metal-metal communication in bridged diruthenium complexes is influenced by the non-bridging ligands. For example the ΔΛ form of the azobis(2-pyridine) diruthenium complex has a log K_c value of 8.28 when the non-bridging ligands are bpy, and 8.79 when the non-bridging ligands are 4,4′-dimethyl-2,2′-bipyridine (K_c is the comproportionation constant and represents the degree of metal-metal communication).[157] The large bathochromic shift associated with the coordination of the second ruthenium metal centre is also increased by approximately 11 nm when Mebpy is used as the non-bridging ligand.

6.2.1. 4,4'-dicarboxy-2,2'-bipyridine (dcbpy)

The ligand dcbpy is often used in dye sensitised solar cells to help tune the energy levels of the electron transfer. In a photo-activated cytotoxin, the carboxylic acid groups on the dcbpy ligand could be deprontonated, which would decrease the charge on the complex. This change in charge could also have an effect on the interaction of the molecule with biological systems or the mode of entry into cells.

Dcbpy is an ideal ligand for future study and one that we were interested in using in our own work. However, the high cost associated with this ligand prohibited its use until we were made aware of an as of yet unpublished method for its synthesis by Paul Kruger.[158]

The first step proceeds as per the standard literature method, with 4-picoline being coupled by Pd/C to give 4.4′-dimethyl-2,2′-dipyridine. The traditional literature method for the oxidation of 4.4′-dimethyl-2,2′-dipyridine to dcbpy involves the use of chromium, and care needs to be taken to ensure the product is free from contamination and to appropriately dispose of the chromium. Kruger's method is to use nitric acid at 180 °C in a sealed bomb. This reaction proceeds in about a fifty percent yield and the pure product is isolated by filtration (Figure 6.1).

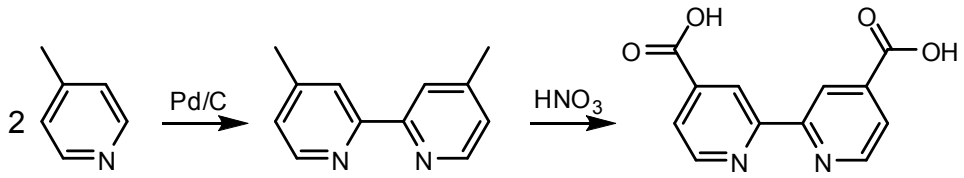

Figure 6.1 Synthesis of dcbpy

We were successfully able to use the dcbpy synthesised by this method to form $[Ru(dcbpy)_2(Cl)_2]$. However, reacting this with phendione and then subsequently using the product of that reaction to form $[(dcbpy)_2Ru(pytp)](PF_6)_2$ (Figure 6.2) gave a product which was highly contaminated. While column chromatography on silica gel was able to remove

some of these impurities, a pure sample could not be obtained. We feel that this could have been remedied through the use of additional purification steps; however, the scale on which we were working did not make this feasible.

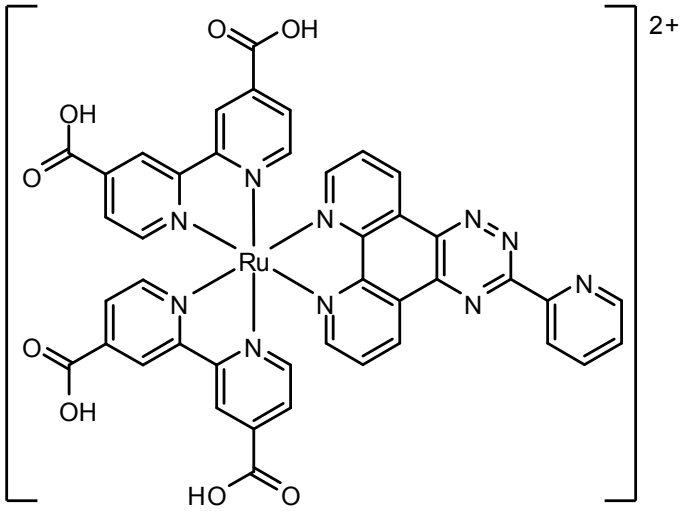

Figure 6.2 $[(dcbpy)_2Ru(pytp)]^{2+}$

6.2.2. 1,10-phenanthroline

While the differences between the ligands bpy and phen are generally considered to be slight, they are not identical, and we decided to synthesise the complex $[(phen)_2Ru(pytp)]^{2+}$ (Figure 6.3).

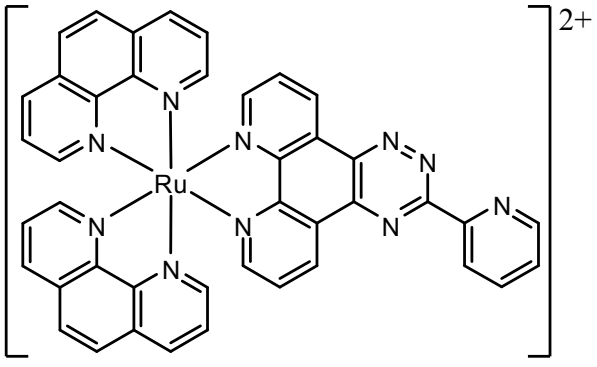

Figure 6.3 $[(phen)_2Ru(pytp)]^{2+}$

The complex $[(phen)_2Ru(pytp)]^{2+}$ was synthesised in the same manner as the bpy analogue and the UV-vis spectrum was recorded. The result was a slight blue shift, with

λ_{max}=435 nm. A more detailed analysis of this complex was not carried out as it was decided that this would be better left to a more thorough study concentrating solely on the effects of changing the auxiliary ligands.

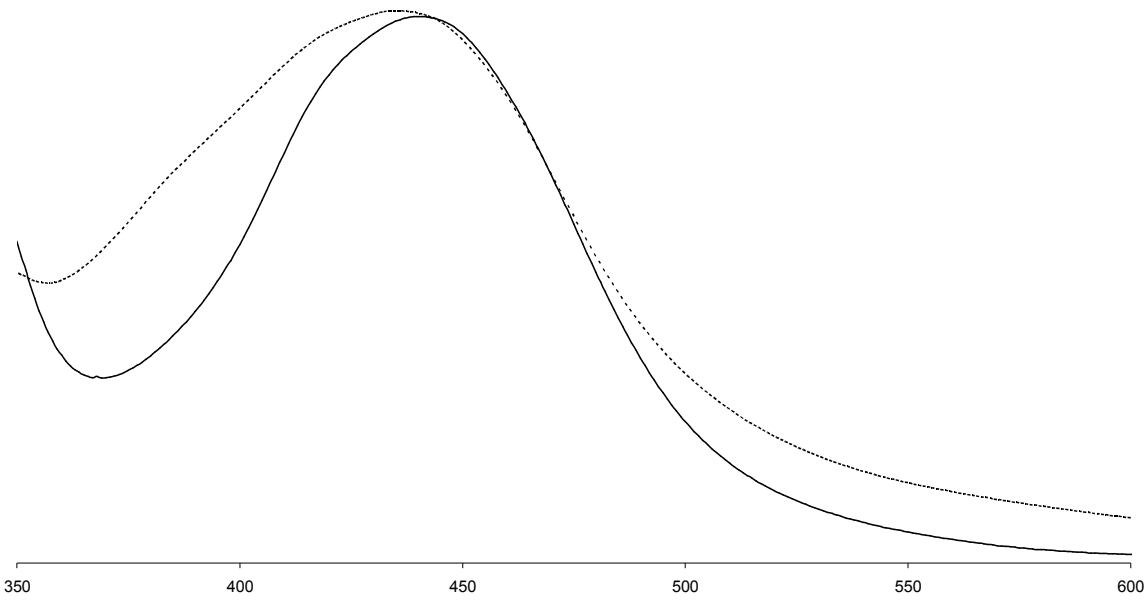

Figure 6.4 UV-vis spectra for $[(bpy)_2Ru(pytp)]^{2+}$ (solid line) and $[(phen)_2Ru(pytp)]^{2+}$ (dashed line) in CH_3CN

In addition to any photophysical changes, the cytotoxicity of the phen complexes could vary greatly from that of the bpy complexes. This is potentially due to the ruthenium(II) bound phen complex, $[Ru(phen)_3]^{2+}$, being capable of weakly intercalating with DNA whereas the analogous bpy complex, $[Ru(bpy)_3]^{2+}$, is not.[159]

It should also be mentioned that attempting to make the ruthenium(II) phen complexes of either pytz or pztz was not successful. This is probably due to the phen ligand either preventing or decomposing the desired complex. It should be mentioned that although the complex $[(bpy)_2Ru(pytz)Ru(bpy)_2]^{4+}$ was first reported in 1985,[128] the complex $[(phen)_2Ru(pytz)Ru(phen)_2]^{4+}$ has never been reported.

6.3. Changing the Bridging Ligand

One of the most obvious avenues for future study involves altering the bridging ligand between the two metal centres. A wide range of bridging ligands which have been successfully used in the formation and study of diruthenium complexes are described in the literature (Figure 6.5). By utilising these ligands in the formation of ruthenium(II)-cobalt(III) complexes, we would be able to compare the observed behaviour of the heterodinuclear complex with that of the corresponding homodinuclear complex.

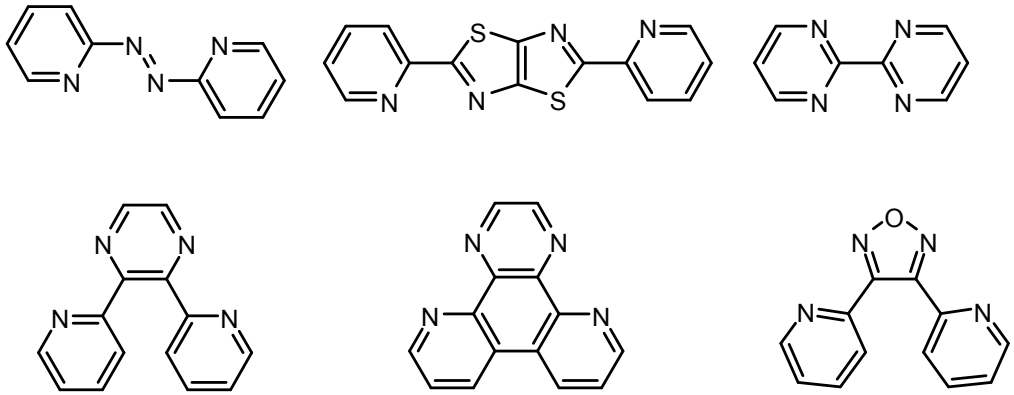

Figure 6.5 Potential future bridging ligands

A new systematic MSc study, utilising ligands known to form dinuclear ruthenium(II) complexes with various degrees of metal-metal communication, has recently commenced. The goal of this study is to establish if there is a relationship between the degree of metal-metal communication in the diruthenium complex and the ease with which electron transfer occurs in the heterodinuclear complex.

As a result of previous studies involving ruthenium(II) polypyridyl complexes, there were several potential bridging ligands already available in the department and we conducted tests with two of these on the NMR scale, as detailed below.

6.3.1. Tetrapyrido[3,2-a:2',3'-c:3",2"-h:2"',3"'-j]phenazine (tpphz)

The complex $[(tbbpy)_2Ru(tpphz)](PF_6)_2$ was synthesised in a similar manner as the pytp and pztp complexes used in our study, by reaction of $[Ru(tbbpy)_2(phendione)]^{2+}$ with 1,10-phenanthroline-5,6-diamine. This complex was then mixed with $[Co(tren)(OTf)_2](OTf)$ in a 3 mm NMR tube. The heterodinuclear ruthenium(II)-cobalt(III) complex was then observed to form and addition of water to the solution resulted in the gradual release of the cobalt bound ligands.

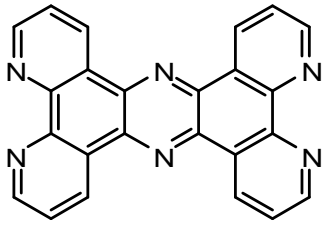

Figure 6.6 Tetrapyrido[3,2-a:2′,3′-c:3″,2″-h:2‴,3‴-j]phenazine (tpphz)

6.3.2. 2,3-di(pyridin-2,yl)quinoxaline (dpq)

The complex $[(tbbpy)_2Ru(dpq)](PF_6)_2$ was reacted in an 3 mm NMR tube with $[Co(en)_2(OTf)_2](OTf)$. The reaction mixture was observed for several days and during that time there was no evidence of binding cobalt(III) to the vacant domain. However, despite the lack of evidence for the formation of a heterodinuclear complex, free en was observed to build up in solution.

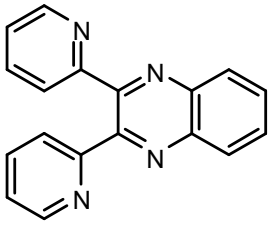

Figure 6.7 2,3-di(pyridin-2-yl)quinoxaline

The accumulation of en suggests several possibilities. Firstly, that the complex $[Co(en)_2(OTf)_2](OTf)$ is not stable in acetonitrile over several days. Alternatively, the cobalt(III) metal centre is being reduced by the ruthenium complex to the labile cobalt(II) state and subsequently releasing its ligands. This reduction could occur either by slow coordination to the ruthenium(II) complex followed by comparatively rapid electron transfer, or by intervalent charge transfer from the ruthenium.

The formation of the complex $[(bpy)_2Ru(pztp)Co(en)_2](PF_6)_5$ was achieved by reacting the ruthenium complex with $[Co(en)_2(OTf)_2](OTf)$ over a period of three days, and during this time no free en was observed. This suggests that the most likely of these explanations is that the cobalt complex is slowly coordinating to the ruthenium and then being reduced, resulting in ligand release. As long as the rate for the reduction step is faster than the rate for coordination, the heterodinuclear complex will not be observed by ^1H NMR as there will not be an appreciable amount in solution.

This observation is interesting, as it is the only time that ligand release was observed to occur without the addition of water. The K_c values of the diruthenium complex $[(bpy)_2Ru(dpq)Ru(bpy)_2]$ are 1800 for the *meso* compound and 1120 for the *rac* compound.[160] For comparison, the K_c value for the $[(bpy)_2Ru(pytz)Ru(bpy)_2]$ complex is 3×10^8 (this measurement was made using a mixture of the *meso* and *rac* isomers).[53] These K_c values can be interpreted to suggest that the ease of electron transfer in ruthenium(II)-cobalt(III) heterodinuclear pytz complex is greater than in the dpq complex. However, the complex $[(bpy)_2Ru(pytz)Co(tren)](PF_6)_5$ is stable in acetonitrile at room temperature. Further study of the dpq system as well as related systems is desirable as it could provide insight into this result.

6.4. Controlling the Configuration of Complexes

During our study we made no attempt to control the configration of the complexes we formed. Additional studies attempting this could prove useful, as the degree of communication between two bridged ruthenium(II) metal centres has been shown to vary depending on the orientation of the ligands around the metal centres.[80, 157, 161] For example ΛΔ-$[(bpy)_2Ru(azobis(2\text{-}pyridine))Ru(bpy)_2]^{4+}$ has an observed log K_c of 8.28 while the ΛΛ and ΔΔ forms have a log K_c of 8.45 (Figure 6.8). An approximately 6 nm difference in the λ_{max} of the MLCT transfer absorption was also observed.[157]

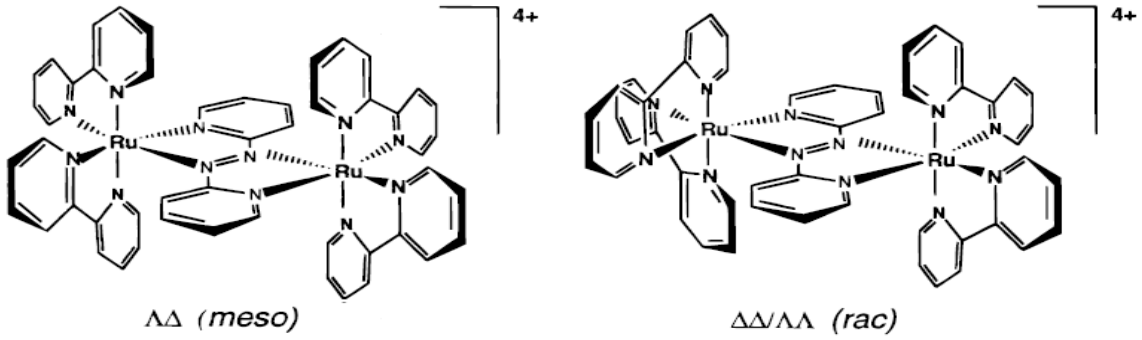

Figure 6.8 *meso* and *rac* forms of $[(bpy)_2Ru(azobis(2\text{-}pyridine))Ru(bpy)_2]^{4+}$

The separation of the *meso* and *rac* isomers from each other in these studies was achieved through the use of column chromatography on Sephadex with bulky anions. Because of the stereochemical arrangement around the ruthenium(II) metal centres there is a difference in the gap between the *meso* and *rac* forms; the *meso* form has a 'v' shaped groove while the *rac* form has the bpy ligands parallel to each other (Figure 6.9). This difference in the size and shape of the gap means that the ability of the anion to associate with these molecules is also different. This means that after a sufficient elution time the complexes can be separated.

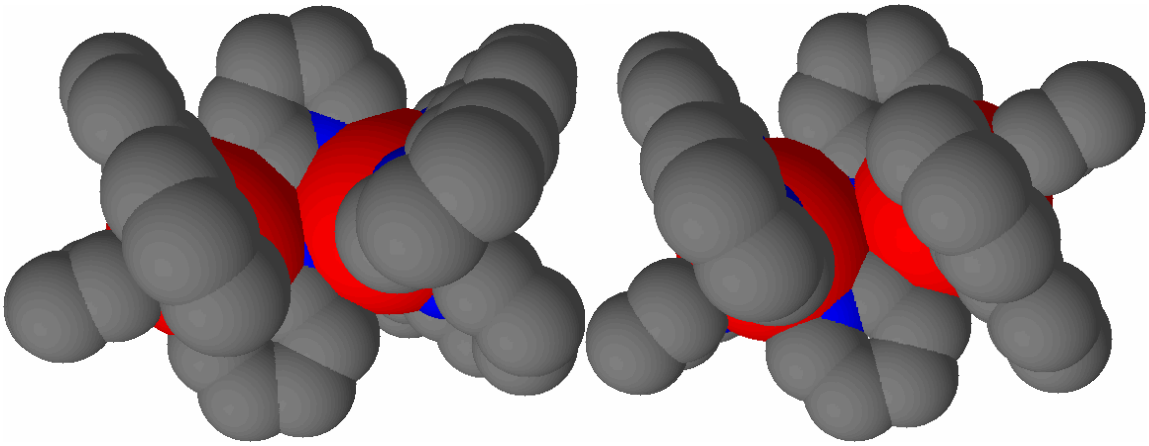

Figure 6.9 Representation of the differences in groove shape between the *meso* (left) and *rac* (right) forms of $[(bpy)_2Ru(azobis(2\text{-}pyridine))Ru(bpy)_2]^{4+}$

While a similar strategy might be feasible for our heterodinuclear complexes, there are several foreseeable complications. Firstly, because the two metal centres are non-equivalent, the number of unique isomers is greater than the heterodinuclear case. The second complication relates to the stability of the heterodinuclear complex. Since the Sephadex columns are done under aqueous conditions, the possibility of the complexes decomposing cannot be ignored. As was previously shown, the nature of the bridging ligand greatly affects the stability of the final complexes and their rate of ligand release. This means that the column would have to be conducted with minimal light exposure and even then only with select complexes.

However, despite these potential problems it is possible to easily introduce some degree of stereo control through the use of enantiomeric ruthenium(II) complexes such as $[Ru(bpy)_2(Py)_2](L)_2$. The Λ and Δ forms of these complexes can be separated by precipitation with a chiral salt, such as disodium (+)-*O*,*O*′-dibenzoyl-D-tartrate (Figure 6.10). This means that by using resolved ruthenium(II) complexes, the final complex will be restricted to only two possible orientations depending on the how the cobalt(III) complex coordinates.

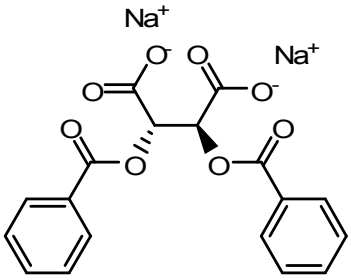

Figure 6.10 disodium (+)-*O*,*O*′-dibenzoyl-D-tartrate

Further control of the overall stereochemistry is potentially possible by treating the cobalt(III) complexes in a similar manner; $[Co(en)_3]^{3+}$ can be resolved through the use of *d*-tartrate.[162, 163] The major problem with a strategy such as this is that there is no guarantee that the configuration of the product will be retained during the formation of the triflate salt. For example treatment of *trans*-$[Co(en)_2(Cl)_2]Cl$ with triflic acid results in the formation of the *cis* product,[152, 153] meaning that any attempt to control the binding geometry of the cobalt end of the molecule, by a process of resolving the complex before coordination to the bridging ligand, may not actually result in any additional stereochemical control for the final complex.

Even if no changes in the stability and rate of activation are observed between the various isomers of these complexes, it is still worthwhile to pursue ways of controlling the orientation of the ruthenium(II) centre. This is because, following activation and subsequent loss of the cobalt complex, the remaining ruthenium fragment is capable of interacting with DNA. It has previously been shown that these interactions are dependent on the configuration of the ruthenium metal centre.[164, 165]

6.5. Synthesis of the Bridging Ligands on Cobalt

The synthetic strategy utilised during our study involved the formation of a ruthenium(II) bound bridging ligand to which a cobalt(III) complex was then coordinated. This approach was problematic in that appropriate conditions for the formation of the final

heterodinuclear complex were not immediately obvious. One way to circumvent this problem involves forming the bridging ligand on the cobalt(III) metal centre and then coordinating the ruthenium fragment.

The complex $[Co(en)_2(phendione)](ClO_4)_3$ is well known and easily synthesised from $[Co(en)_2(phen)]Br_3$. There are numerous examples of $[Co(en)_2(phendione)](ClO_4)_3$ being used as a reactant in the synthesis of additional complexes, such as $[Co(en)_2(dppz)](ClO_4)_3$.[166, 167] However, when we attempted to synthesise $[Co(en)_2(phtp)](ClO_4)_3$ by a similar process the resulting ^1H NMR spectrum had too many peaks in the aromatic region, and no peaks that could be assigned to the en ligands. The ESI-MS spectrum of the sample had only one peak that we were able to assign, which we ascribed to the free phtp ligand.

From this we concluded that although the formation of phtp did seem to occur, the final product was not what we desired and we abandoned this line of study. However, further study in the formation of complexes such as these could prove useful as similar cobalt(III) complexes have been shown to exhibit cytotoxic activity.[156, 166] Unfortunately, such complexes could probably not be used in the synthesis of photo-activated cytotoxins, as the attachment of the ruthenium would most likely involve heating the reaction mixture; something that we found to be detrimental to the formation of ruthenium(II)-cobalt(III) heterodinuclear complexes.

6.6. Development of New Cytotoxins

One of the major problems we encountered in synthesising a potential photo-activated cytotoxin, related to the formation of the cobalt(III) bound nitrogen mustard triflate compound. The standard literature procedures call for heating either the nitrito or chlorido complex in neat triflic acid. [152, 153, 154, 155] However, we found that this resulted in

decomplexation of the ligand from the cobalt metal centre and resulted in the isolation of the doubly protonated ligand.

While we did develop a new experimental procedure for the formation of the triflate compound, this reaction was very sensitive. Insufficient cooling at almost any point during the reaction results in some of the ligand dissociating from the cobalt metal centre, causing the final product to be contaminated with both the free ligand and cobalt(II) ions. One way that it might be possible to prevent the dissociation of the ligand is to develop new cytotoxins that coordinate more strongly to the cobalt(III) metal centre. This additional coordination strength could be achieved through the development of either tri or tetradentate cytotoxic ligands. The coordination of ligands such as *N*-(2-aminoethyl)ethane-1,2-diamine (dien), *N*,*N*′-(ethane-1,2-diyl)dipropane-1,3-diamine (3,2,3-tet), and tren (Figure 6.11) to a cobalt(III) metal centre has been well studied.[168, 169, 170] The introduction of a nitrogen mustard moiety onto ligands such as these could enable the formation of more stable cytotoxin containing cobalt(III) triflate compounds.

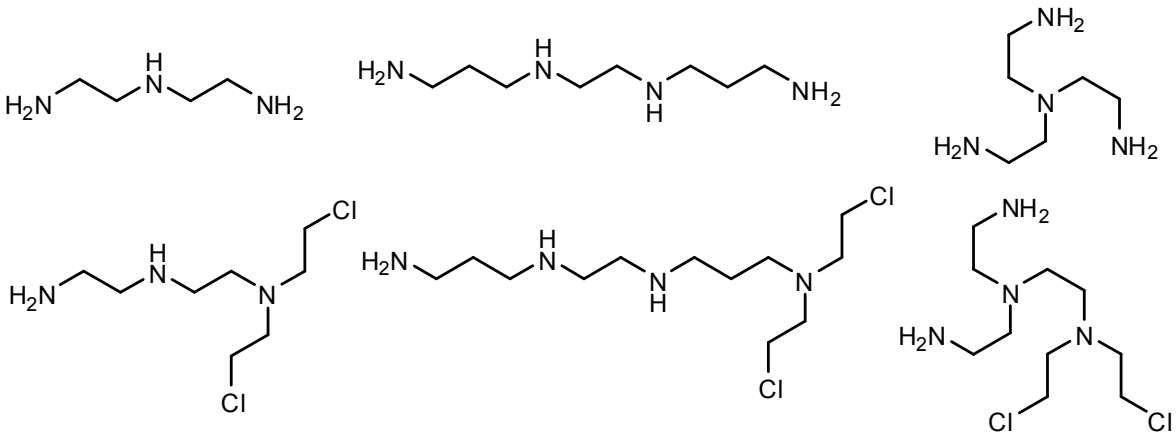

Figure 6.11 The ligands dien (left), 3,2,3-tet (centre) and tren (right) and their potential nitrogen mustard analogues

6.7. Electrochemical Studies

Several of the mononuclear cobalt(III) and ruthenium(III) complexes that have been synthesised for use as chemotherapeutic agents are activated *in vitro*, by a reductive pathway. As mentioned in section 1.6, Denny *et al* synthesised a series of cobalt(III) complexes, such as $[Co(acac)_2(bceen)]$ (Figure 6.12), which relied on natural biological processes for activation. It is also believed that the mechanism by which the ruthenium(III) complexes NAMI-A and KP1019 are activated involves reduction to the ruthenium(II) complex.

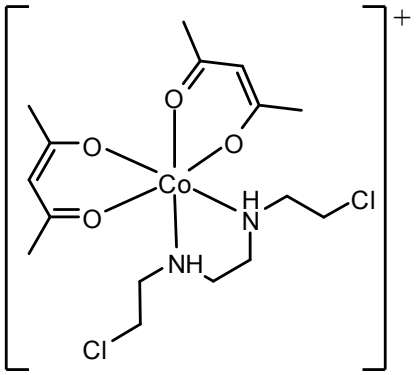

Figure 6.12 $[Co(acac)(bceen)]^+$

The oxidation and reduction potentials for the multiple metal centres in our photo-activated cytotoxin could be determined through electrochemical studies. Such information would give an indication as to whether or not the complexes could be prematurely reduced to an active state by biological systems. Studies on the degree of metal-metal communication in diruthenium complexes use the measured oxidation potentials of the complexes to evaluate K_c. In a complex with a good degree of metal-metal communication, the oxidation potentials of the two ruthenium(II) metal centres have been shown to be non-equivalent (Figure 6.13); this is due to the metal centre that is oxidised first being able to 'communicate' this oxidation to the other metal centre. The difference between these two oxidation potentials correlates to the degree of interaction between the two metal centres ($K_c=\exp((E_1^0-E_2^0)F/RT)$).

Figure 6.13 Representation of the cyclic voltammograms of a diruthenium(II) complex with no metal-metal communication (left) and a diruthenium(II) complex with metal-metal communication (right)

In a similar way electrochemistry could provide valuable insights into the nature of the ruthenium(II)-cobalt(III) heterodinuclear complexes, and possibly help describe the ease with which the two metal centres can interact.

6.8. Photochemical and Theoretical Studies

The lifetime measurements taken for the complexes $[(bpy)_2Ru(pytp)]^{2+}$ and $[(bpy)_2Ru(pytp)Co(tren)]^{5+}$ provide a valuable insight into the mechanism by which the intravalent charge transfer occurs and any future study should, where possible, include similar measurements as part of the complex characterisation. These studies could also be expanded to include the measurement of excited state adsorption spectra.

In order to gain a better understanding of the electron transfer pathways involved in the observed photo-activated ligand release, theoretical and computational studies should also be undertaken. Such studies would provide a valuable insight into the energy levels associated with the various complexes reported in this thesis, and ideally would give rise to an explanation for the various observed results, such as the rate at which ligand release occurs.

Chapter 7: Conclusion

The primary goal of our study was the production of a ruthenium(II)-cobalt(III) heterodinuclear complex with a potential application as a photo-activated cytotoxin. Ideally, the final complex would involve a ruthenium(II) metal centre bound to a bridging ligand, with the other binding domain coordinated to a cobalt(III) metal centre with potentially cytotoxic ligands coordinated. Irradiation of the complex would then result in an electron being transferred from the ruthenium metal through the bridging ligand to the cobalt metal, oxidising the ruthenium to ruthenium(III) and reducing the cobalt to cobalt(II). Because cobalt(II) is a labile metal, the cytotoxic ligands could then be rapidly displaced by water (Figure 7.1).

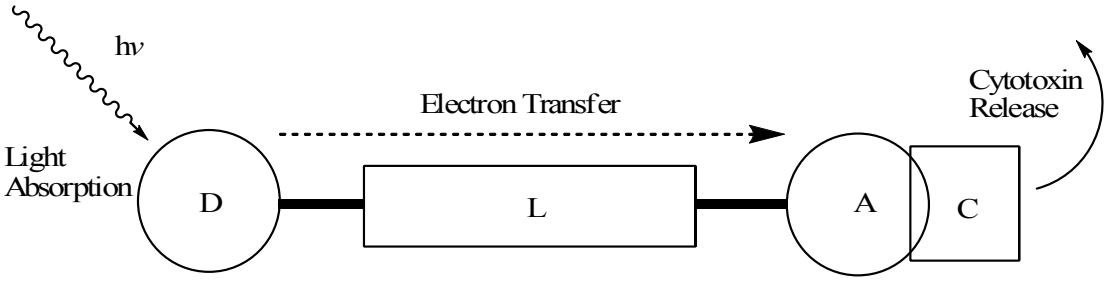

Figure 7.1 Schematic of a photo-activated cytotoxin: Following irradiation the donor metal (D) transfers an electron through the bridging ligand (L) into the acceptor metal (A) which triggers release of the bound cytotoxins

In order to achieve this, several synthetic challenges needed to be overcome. The first was the selective binding of the metal centres to the appropriate end of the bridging ligand. The initial synthetic strategy pursued is described in Chapter 2 and involved varying the geometry and coordination number of the binding domains (Figure 7.2). The research into these bridging ligands followed on from the work conducted by Zibaseresht[87] and was based on using functionalised terpyridines as the bridging ligand. Unfortunately, this line of research had to be abandoned due to a range of synthetic problems.

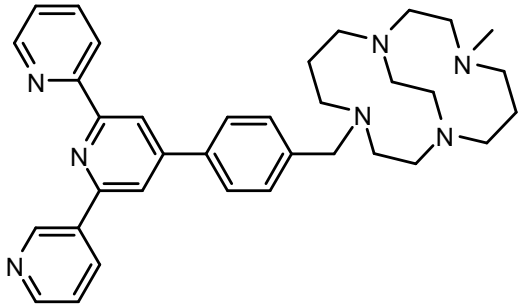

Figure 7.2 Example of a terpyridine based bridging ligand with a different coordination geometry and a different number of donor atoms at each binding domain

The next series of bridging ligands, as detailed in Chapter 3, did not have a vastly different binding domain for each metal centre, but instead achieved selectivity through synthesising the ligand on the ruthenium(II) metal centre. These ligands were intermediates in the formation of Jurgen Sauer's 'Lego' system[114] and were synthesised by the condensation reaction between a hydrazonamide and a 1,2-dicarbonyl compound (Figure 7.3).

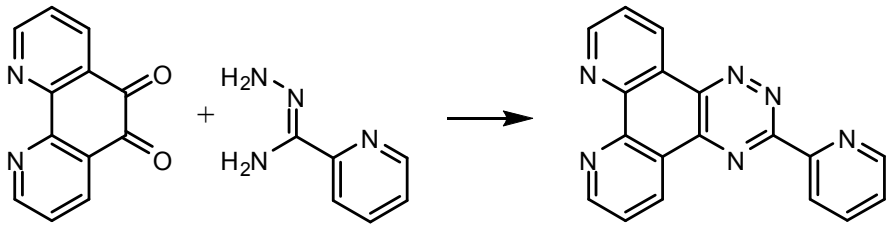

Figure 7.3 Synthesis of pytp

Binding the phendione to a ruthenium(II) metal centre before carrying out the condensation reaction did not prevent the reaction from occurring. This gave an easy route for forming ruthenium(II) complexes with a vacant binding domain. Additionally, it should be noted that attempting to bind a ruthenium(II) metal centre to the free ligand results in a mixture of products as the metal is capable of binding to either of the two binding domains.

The final series of bridging ligands we investigated in Chapter 3 were symmetrical, with no difference between the two binding domains. These ligands required care when

binding the ruthenium(II) metal centre, so as to minimise the formation of the undesired diruthenium complex.

The coordination of the ruthenium(II) complexes synthesised in Chapter 3 to non-cobalt metal centres was also investigated and we were able to demonstrate binding to copper(I), copper(II), silver(I) and zinc(II), through the use of ^{1}H NMR and ESI-MS techniques.

In Chapter 4 the synthesis of ruthenium(II)-cobalt(III) heterodinuclear complexes, with the non-cytotoxic ligands en and tren coordinated to the cobalt metal centre, was described. These complexes had to be formed using the triflate salts of the cobalt complexes; making both reactants soluble in acetonitrile at room temperature. This solubility at room temperature was important since all attempts to synthesise these complexes at higher temperatures failed.

By exposing these heterodinuclear complexes to light in the presence of water, we were able to demonstrate photo-activated ligand release. This ligand release was monitored by ^{1}H NMR spectroscopy. Following irradiation of the complexes, peaks in the recorded ^{1}H NMR spectra attributed to the non-bound ligand could be observed to increase in size. The different bridging ligands were associated with different rates of ligand release. Of the bridging ligands trialled, pytp based systems released their ligands the slowest, over a period of days, while pytz took only minutes to achieve complete ligand release. The rate of ligand release was also retarded by atmospheric oxygen; this decrease in the rate of ligand release was observed in both pytp and pztp bridged systems (the effect of oxygen on pytz was not investigated because of the rapid ligand release associated with such systems). This oxygen dependent decrease in the rate of ligand release is a very promising result as cancerous growths tend to have hypoxic regions; this would increase the selectivity of a photo-activated cytotoxin based on these complexes for these regions.

In Chapter 5 we discussed how it might be possible to move from the non-cytotoxic analogues (en and tren) used in Chapter 4 to a cytotoxin containing system. The cytotoxins we selected for use were nitrogen mustards. The reason for using nitrogen mustards is that they are less cytotoxic when bound to a metal centre than as the free ligand. Our strategy for the synthesis of the cobalt(III) bound mustards began with the coordination of the alcohol precursor to the cobalt(III) metal centre. The resulting complex was then treated with thionyl chloride to convert the alcohols into alkyl chlorides. The final step, before complexation with a ruthenium complex, was to react the complex with triflic acid to form the triflate compound (Figure 7.4).

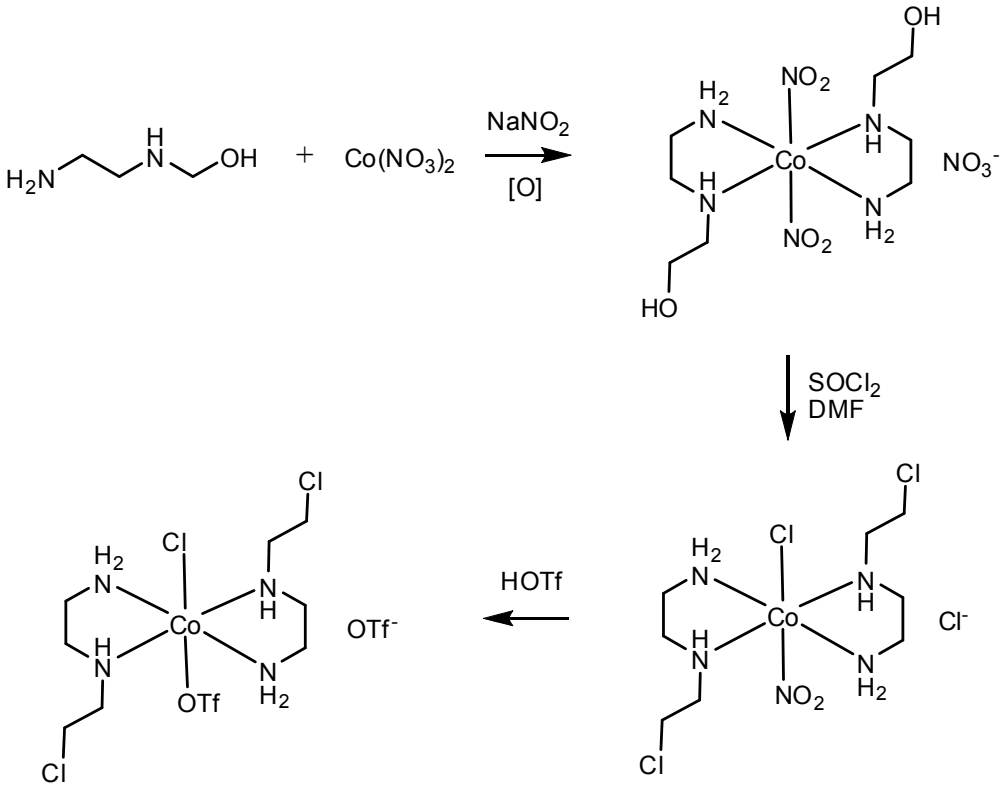

Figure 7.4 Formation of a cobalt(III) bound cytotoxin

The problems we discovered with this approach were that sometimes the alcohol group would also coordinate to the metal centre and that even in complexes where this did not occur, the mustard containing complex was not as stable as its non-cytotoxic analogue and was prone

to dissociation during the treatment with triflic acid. The first of these problems could potentially be solved by the use of a protecting group, such as a silyl ether, which would prevent the alcohol from being able to coordinate to the metal centre. The second problem was alleviated, to some extent, by carrying out the reaction with triflic acid in a salt-ice bath. However, this resulted in the final complex having a chloride still bound to the metal centre and the stability was still lower than the non-cytotoxic analogue. The product from the reaction of this complex with the complexes $[(bpy)_2Ru(pytp)]^{2+}$ and $[(bpy)_2Ru(pytz)]^{2+}$ showed evidence of binding, although the product was not able to be fully characterised. A cytotoxicity assay against the murine leukaemia cell line P388, showed that the complex we believe to be $[(bpy)_2Ru(pytz)Co(ceen)](PF_6)_5$ was about three times more cytotoxic than the $[(bpy)_2Ru(pytz)Co(tren)](PF_6)_5$ complex.

Ultimately this thesis provides a synthetic strategy which, with minor modification, can be used for the synthesis and study of photo-activated cytotoxins. Unfortunately, we were not able to produce a fully characterised photo-activated cytotoxin, but the ^1H NMR experiments which demonstrate photo-activated ligand release from a ruthenium(II)-cobalt(III) heterodinuclear system provide a proof of concept.

Chapter 8: Experimental

^{1}H NMR spectra were recorded on either a Varian INOVA 500 spectrometer at 23°C, operating at 500 MHz or a Varian UNITY 300 NMR spectrometer at 23°C operating at 300 MHz. gCOSY, HSQCAD and gHMBC experiments were all performed on a Varian INOVA 500 spectrometer at 23°C, operating at 500 MHz. ^{13}C NMR spectra were recorded on either a Varian INOVA 500 spectrometer at 23°C operating at 125 MHz or a Varian UNITY 300 NMR spectrometer at 23°C operating at 75 MHz. The INOVA was equipped with a variable temperature and inverse-detection 5 mm probe or a triple-resonance indirect detection PFG probe. The UNITY was equipped with a variable temperature direct broadband 5 mm probe. Chemical shifts are expressed in parts per million (ppm) on the δ scale and were referenced to the appropriate solvent peaks, TMS or TMPS. DMSO-d_6 referenced to $CD_3(C\mathbf{H}D_2)SO$ at δ_H 2.50 (^{1}H) and $(\mathbf{C}D_3)_2SO$ at δ_C 39.43 (^{13}C). Acetonitrile-d_3 referenced to $C\mathbf{H}D_2CN$ at δ_H 1.94 (^{1}H) and $\mathbf{C}D_3CN$ at δ_C 1.24 (^{13}C). Methanol-d_4 referenced to $C\mathbf{H}D_2OD$ at δ_H 3.31 (^{1}H) and $\mathbf{C}D_3OD$ at δ_C 49.05 (^{13}C). TMS and TMPS were both referenced to δ_H 0 (^{1}H) and δ_C 0 (^{13}C).

Infrared spectra were obtained using a Shimadzu 8201PC Series FTIR using diffuse reflectance method in solid KBr.

High Resolution Electrospray Ionisation Mass Spectra were recorded on a Micromass LCT spectrometer using a probe voltage of 3200 V, an operating temperature of 150°C and a source temperature of 80°C. The carrier solvent was 1:1 CH_3CN/H_2O at 20 μL min^{-1}. Typically, 10 μL of a 10 μL mL^{-1} solution was injected. Leucine enkephalin was used as the lock mass internal standard.

UV-visible spectra were recorded on a Varian CARY Probe 50 UV-vis spectrophotometer or a Varian CARY 100 UV-vis spectrophotomer.

X-Ray crystal data was collected on a Bruker-Nonius APEX II system using graphite monochromatised Mo Ka (l = 0.71073 A) radiation at the temperature indicated in the tables

that may be found in Appendix 1. The data collection, cell determination and data reduction were all performed with the APEX software.[171] All structures had intensities corrected for Lorentz and polarisation effects and for absorption using SAINT. All structures were solved by direct methods using SHELXS and refined on F^2 using all data by full-matrix least squares procedures using SHELXL-97. Unless otherwise stated, all non-hydrogen atoms were refined with anisotropic displacement parameters 1.2 and 1.5 times the isotropic equivalent of their carrier carbon atoms. Some of the refinements reported may change a little upon preparation for final publication. The crystal structure pictures were generated using Olex^2.[172]

Steady state absorption measurements were performed using an absorption spectrometer (Cary Bio50, Varian). Steady state emission spectra were acquired with an emission spectrometer (Cary Eclipse, Varian). Quantum yield measurements were performed using the optically dilute method, using $[Ru(bpy)_3]Cl_2$ in aqueous solution as a standard (Φref = 4.2%). Time resolved emission lifetime experiments were performed using a nanosecond laser setup. The 355 nm tripled output of a Q-switched Nd:YAG (Continuum NY-61-10, Coherent) was used to drive an OPO system (Casix BBO, Shanghai Uniwave Technologies) which was tuned to 440 nm, and this output was focused on the sample using all quartz optics. Emission was collected perpendicular to the excitation, collimated then refocused onto the entrance port of a 0.3 m triple grating monochromator (SpectraPro 300i, Acton Instruments) for spectral selection at 630 nm. The detector was a PMT tube (R928P, Hamamatsu), the output of which was sampled directly using a 500 MHz digital oscilloscope (TDS520, Tektronix). The instrument response function (IRF) for this setup was measured using scattered excitation to be *ca*. 8 ns at FWHM. Each resulting trace contained at least 1000 data points, and was averaged over 1000 shots. Data analysis was performed using a commercially

available software package (Igor, Version 6.1.2.1, Wavemetrics). The quality of the fit was assessed using the reduced chi-squared χ^2 function and by an inspection of the weighted residuals.

Elemental analyses were performed by the Campbell Microanalytical Laboratory at the University of Otago.

8.1. Chapter 2

4′-p-tolyl-2,2′-6′,2″-terpyridine (ttp)

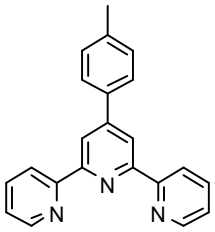

i)[99] A mixture of 183 g acetamide, 118g ammonium acetate, 12.4g p-tolylaldehyde and 25 g 2-acetylpyridine was heated at reflux for 2 hours. After this time the mixture was cooled to 120 °C and a solution of 90g NaOH dissolved in water was added. The mixture was kept at 120 °C without stirring for a further 2 hours before being cooled to room temperature. A brown solid 'glass' was separated from the rest of the reaction mixture, washed with water and dissolved in 60 ml of acetic acid. The hydrobromide salt was then precipitated out with 60 ml 47% HBr, filtered off and dissolved in 200 ml water. KOH was added until the pH of the solution was 10. The resulting suspension was extracted with 3 portions of 200 ml CH_2Cl_2. Following evaporation of the solvent the residue was recrystallised from 400 ml ethanol to give 7.46g of white needles. These needles were a mixture of the desired 4′-p-tolyl-2,2′:6′2″-terpyridine and 6′-p-tolyl-2,2′:4′,2″-terpyridine.

The mixture of these two product was dissolved in 380 ml of EtOH:CH_2Cl_2 (1:1), to which a solution of 4.5 g $(NH_4)_2Fe(SO_4)_2 \cdot 6H_2O$ in 76 ml H_2O was added. The mixture was left to stand for 5 hours at room temperature before the CH_2Cl_2 was removed under reduced pressure. A solution of 4.27 g KPF_6 in 38 ml H_2O was then added to form a purple precipitate. This precipitate was filtered off and washed with 3 portions of 100 ml toluene. The precipitate was then dissolved in 100 ml CH_3CN and 100 ml H_2O. KOH is added until the aqueous layer is pH > 12. H_2O_2 was then added drop wise until there was only one layer with a heavy orange precipitate and a flocculent pale lavender precipitate, which could not be removed with more H_2O_2. The solution was then filtered and the lavender layer scrapped off. The remaining

precipitate was then boiled with charcoal in 50 ml chloroform, before being refiltered. The filtrate was then taken to dryness giving 4.98g of 4′-p-tolyl-2,2′:6′2″-terpyridine as a bright white powder. Yield 4.98 g (15%)

ii)[100] 4.84 g of 2-acetylpyridine was dissolved in 100 ml ethanol, to which 2.4 g of p-tolylaldehyde was added. To this reaction mixture was then added 3.08 g KOH and 58 ml of aq. NH_3. The solution was stirred at room temperature for 4 hours, after which it was filtered and the precipitate washed three times with 10 ml cold ethanol. The product was further purified by recrystallisation from ethanol. Yield 1.223 g (19%)

^{1}H NMR (500 MHz; solvent $CDCl_3$): δ 8.742 (s, 2 H), 8.732 (m, 2 H), 8.675 (d, 2 H), 7.884 (m, 2 H), 7.831 (d, 2 H), 7.356 (m, 2 H), 7.318 (d, 2 H), 2.430 (s, 3 H).

4′-(*p*-bromomethylphenyl)-2,2′:6′,2″-terpyridine (Br-ttp)

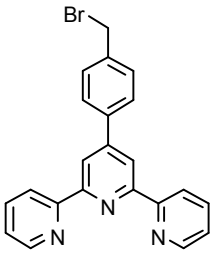

The *N*-bromosuccinamide and benzoylperoxide were both purified before being used in this reaction.[173]

0.84 g of ttp, 0.46 g of *N*-bromosuccinimide and a catalytic amount of dibenzoyl peroxide were heated at reflux in 50 ml dry benzene under an argon atmosphere for 4 hours. The solution was then cooled to room temperature and the crude product obtained by vacuum filtration. The product was then purified by recyrstallisation from an ethanol:acetone mix (2:1). Yield 0.86 g (83%). ^{1}H NMR (300 MHz; solvent $CDCl_3$): δ 8.735 (s, 2 H), 8.7272 (m, 2 H), 8.674 (d, 2 H), 7.901 (m, 4 H), 7.541 (d, 2 H), 7.367 (m, 2 H), 4.570 (s, 2 H).

1,4,8,11-tetraazacyclotetradecane (cyclam)[174]

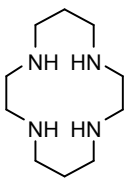

54.7 g of nickel(II) perchlorate was dissolved in 400 ml water. With

adequate stirring 26 g of 1,5,8,12-tetraazadodecane was added to the solution, which was then cooled to 5 ºC in an ice bath. 30 ml of 30% glyoxal was then added to the cooled solution, which was left to stand at room temperature for 4 hours. The solution was then returned to the ice bath and 11 g of $NaBH_4$ slowly added over a 1 hour period. The mixture was then heated to 90 ºC for 15-20 minutes and then quickly filtered through a large medium glass frit. The filtrate was then transferred to a single necked flask with 29 g of NaCN, which was heated at reflux for 2 hours before being cooled to room temperature. 15 g of NaOH was then added and the solution concentrated on a rotary evaporator until a semi-solid remains. 100 ml of $CHCl_3$ was added and the mixture filtered through a large glass frit. The precipitate was washed twice with 100 ml of $CHCl_3$. The organic layer was separated from the aqueous and dried over Na_2SO_4, before being taken to dryness under vacuum. The yellow solid was recrystallised from 800 ml of chlorobenzene. The white product was obtained by filtration and washed with 50 ml ether before being air dried. Yield 12.31 g (41%). ^{1}H NMR (300 MHz; solvent $CDCl_3$): δ 2.757 (m, 8 H), 2.688 (s, 8 H), 2.402 (br s, 4 H), 1.727 (m, 4 H).

(10bα,10cα)-decahydro-1*H*,6*H*-3a,5a,8a,10a-tetraazapyrene (bisaminal-cyclam)[111]

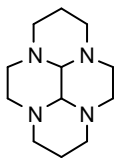

4 g of cyclam and 3.3 g of glyoxal were dissolved in 300 ml of CH_3CN. The solution was stirred at room temperature for 1 hour after which the temperature was increased to 50-60 ºC and stirring continued for a further 2 hours. The solution was then cooled to room temperature and the solvent removed under vacuum. The residue was dissolved in $CHCl_3$, dried over Na_2SO_4 and filtered. Evaporation of the filtrate gave the product as a yellow oil, which can be solidified by trituration with ether. Yield 3.5 g (78%). ^{1}H

NMR (300 MHz; solvent $CDCl_3$): δ 3.532 (t, 2 H), 3.080 (s, 2 H), 2.948 (m, 6 H), 2.735 (d, 2 H), 2.344 – 2.072 (m, 8 H), 1.224 (m, 2 H).

4′-[p-{(10bα,10cα)-decahydro-1H,6H-3a,5a,8a,10a-tetraazapyrenium-3a-methyl}phenyl]-2,2′:6′,2″-terpyridine bromide

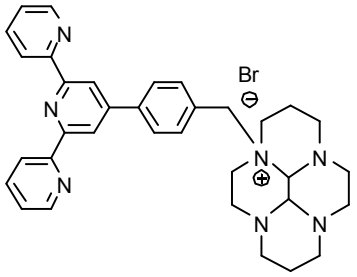

A solution of 0.12 g bisaminal-cyclam in 10 ml THF was added to another solution of 0.25 g Br-ttp in 10 ml THF. The combined solution was stirred at room temperature until the solvent had fully evaporated. The resulting white precipitate was washed with THF, and the insoluble white solid filtered off. Yield 0.26 g (70%). ^{1}H NMR (500 MHz; solvent D_2O): δ 7.87 (d, 2 H, H_6, $H_{6''}$), 7.28 (d, 2 H, H_3, $H_{3''}$), 7.25-7.22 (m, 2 H, H_4, $H_{4''}$), 7.00 (s, 2 H, $H_{3'}$, $H_{5'}$), 6.94-6.92 (m, 2 H, H_5, $H_{5''}$), 6.87 (d, 2 H, $H_{3'''}$, $H_{5'''}$), 6.79 (d, 2 H, $H_{2'''}$, $H_{6'''}$), 4.69-4.66 and 4.19-4.16 (AB, 2H, H_{7A}, H_{7B}), 4.05 (br s, 1 H, H_{015}), 3.88-3.67 (1 H, $H_{02(ax)}$), 3.50 (br s, 1 H, H_{016}), 3.36-3.34 (1 H), 3.23 (1 H, $H_{014(ax)}$), 2.94-2.88 (6 H, including $H_{03(eq)}$, $H_{05(ax)}$, $H_{012(eq)}$), 2.76-2.74 (2 H, including $H_{014(eq)}$), 2.53-2.50 (2 H, $H_{02(eq)}$, $H_{03(ax)}$), 2.37-2.35 (2 H, including $H_{05(eq)}$), 2.15-2.13 (2 H, $H_{012(ax)}$, $H_{06(eq)}$), 1.95-1.93 (1 H, $H_{013(eq)}$), 1.60-1.58 (1 H, $H_{013(ax)}$), 1.37-1.35 (1 H, $H_{06(ax)}$). ^{13}C NMR (75 MHz; solvent D_2O): δ 153.71, 153.30, 147.90 (2 C, C_6, $C_{6''}$), 146.26, 137.79, 137.54, 133.21 (2 C, $C_{3'''}$, $C_{5'''}$), 126.47, 125.93 (2 C, $C_{2'''}$, $C_{6'''}$), 124.29, 121.44 (2 C, C_3, $C_{3''}$), 116.72 (2 C, $C_{3'}$, $C_{5'}$), 82.62 (C_{016}), 69.50 (C_{015}), 61.39 (C_7), 59.84 (C_{014}), 53.98 (C_{03}), 53.29 (C_{05}), 51.91 (C_{012}), 51.35 , 47.86 (C_{02}), 46.52, 41.90, 18.40 (C_{013}), 17.95 (C_{06}). ESI-MS: *m/z* (fragment) 272.6939 ([M+H-Br]$^{2+}$), 544.3924 ([M-Br]$^+$).

[(ttp)Ru(ptmtb)](PF$_6$)$_3$

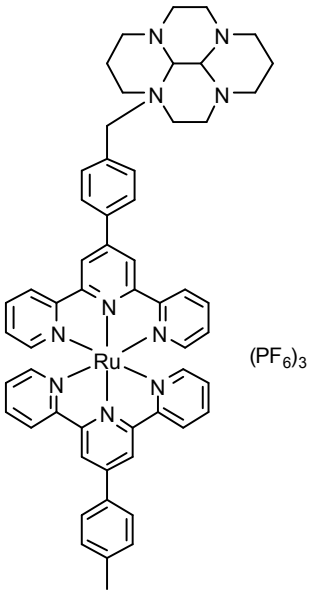

To a solution of 0.02 g [Ru(ttp)Cl$_3$] in MeOH was added an equimolar amount of ptmtb and 10 drops *N*-methylmorpholine. The solution was heated at reflux for 1h under Ar. The deep red solution was cooled to room temperature before it was filtered to remove any unreacted materials and excess methanolic solution of ammonium hexafluorophosphate was added to the filtrate to precipitate the product complexes. The dark red precipitate was dissolved in CH_3CN, then the solution was taken to dryness under vacuum and the residue was purified by column chromatography (SiO_2 eluting with CH_3CN-saturated KNO_3 solution-H_2O, 14 :0.5 :1). An excess of NH_4PF_6 was added to the major red fraction and the solution was reduced in volume under vacuum. The precipitate was collected by filtration over Celite, before it was dissolved in CH_3CN, and evaporated to dryness *in vacuo* to give [(ttp)Ru(ptmtb)](PF$_6$)$_3$ as a red powder. Yield 0.043 g, 78%. ^{13}C NMR (75 MHz; solvent CD_3CN) δ 159.21, 159.10, 156.69, 156.28, 153.42, 149.43, 147.56, 141.99, 140.10, 139.02, 135.40, 134.88, 134.82, 131.27, 129.66, 129.48, 129.30, 128.67, 128.54, 128.42, 125.63, 125.53, 122.68, 122.35, 84.35, 71.13, 62.23, 61.10, 55.43, 55.06, 53.28, 53.21, 49.87, 47.69, 43.46, 21.43, 19.83, 19.67. ESI-MS: *m/z* (fragment) 557.2206 ([M-2(PF$_6$)]$^{2+}$), 323.1544 ([M-3(PF$_6$)]$^{3+}$). IR (KBr): $\tilde{\nu}$/cm^{-1} = 3651 w, 2949 w, 2843 w, 1655 w, 1607 m, 1524 w, 1477 m, 1466 m, 1431 m, 1406 m, 1384 m, 1356 w, 1246 w, 1196 w, 1144 w, 1086 w, 1030 w, 845 ssh, 789 s, 754 m, 735 w, 656 w, 557 ssh, 492 w, 480 w, 448 w, 421 w. UV-vis (CH_3CN): λ_{max} = 285.0, 295.0, 305.0, 490.0 nm.

[(ttp)Ru(mptmtb)](I)$(PF_6)_3$

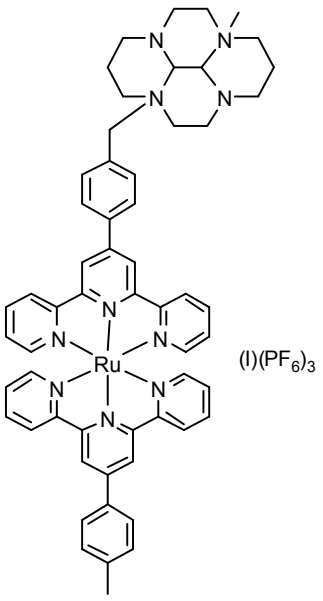

To the complex [(ttp)Ru(ptmtb)]$(PF_6)_3$, (0.5368 g, 0.38 mmol) in CH_3CN (50ml) was added CH_3I (0.5ml). The solution was stirred at room temperature for 72 hours. The remaining CH_3I and solvent were removed on a rotary evaporator to give a red solid. Yield 0.5547g, 95%.^{1}H NMR (500MHz; solvent CD_3CN) δ 9.086 (d, 4 H), 8.729 (t, 4 H), 8.419 (d, 2 H), 8.185 (d, 2 H), 8.01-7.9 (m, 6 H), 7.646 (d, 2 H), 7.5-7.48 (m, 4 H), 7.249 (m, 4 H), 5.288 (d, 1 H), 4.81 (d, 1 H), 4.35 (s, 2 H), 3.8-2.8 (m, 20 H, cyclam), 3.411 (s, 3 H), 2.64 (s, 3 H). ESI-MS: *m/z* (fragment) 637.27 ($[M-(PF_6)-(I)]^{2+}$), 376.49 ($[M-2(PF_6)-(I)]^{3+}$).

8.2. Chapter 3

1,10-phenanthroline-5,6-dione

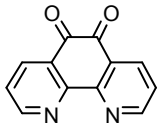

6.13 g of 1,10-phenanthroline and 6.25 g of KBr were placed in a 250 ml round bottomed flask. A cooled 0 °C mixture of 60 ml H_2SO_4 and 30 ml HNO_3 was then slowly added. After addition of the acid mixture the solution was heated at reflux for 3 h before being cooled to room temperature. The condenser was then removed from the round bottom flask and the solution allowed to stand for 5 to 10 mins. The solution was then poured over 600 ml of ice and carefully neutralised with NaOH until either neutral or slightly acidic. The bright yellow product was obtained by extraction with $CHCl_3$. Yield 6.27 g (87%). ^{1}H NMR (500MHz; solvent $CDCl_3$) δ 9.131 (dd, 1 H), 8.517 (dd, 1 H), 7.600 (dd, 1 H).

1,10-phenanthroline-1-oxide[125]

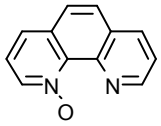

6 ml of 30% H_2O_2 is added to a solution of 10 g 1,10-phenanthroline in 60 ml glacial acetic acid. The solution was heated at 70 – 75 °C for 3 h before addition of another 6 ml H_2O_2; heating was then continued for another 3 h. The solution was then concentrated to ~15 ml on a rotary evaporator, 15 ml of H_2O added and the concentration continued until ~10 ml. The concentrated solution was then neutralised with a sodium carbonate-water paste before being extracted multiple times with several portions of chloroform. The extracts were taken to dryness and then further dried overnight in a 50 °C oven. The dried product was ground into a fine powder and reextracted with chloroform. The extracts were dried over sodium sulfate; boiled with decolourising charcoal and evaporated to give the crude product which was then recrystallised from chlorobenzene. Yield 5.53 g (51%).

^{1}H NMR (500MHz; solvent D_2O) δ 8.671 (d, 1 H), 8.297 (d, 1 H), 7.823 (d, 1 H), 7.526 (d, 1 H), 7.414 (dd, 1 H), 7.287 (t, 1 H), 7.146 (d, 1 H), 7.061 (d, 1 H)

2-cyano-1,10-phenanthroline [125]

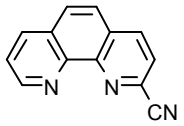

3 ml benzoyl chloride was added drop wise over 15 mins to a solution of 2.98 g 1,10-phenanthroline-1-oxide and 3 g KCN in 50 ml H_2O. The solution was then stirred for an additional 15 mins. The resulting precipitate was collected by suction filtration and washed with water. The crude product was then recrystallised from ethanol. Yield 1.920 g (61 %). Mp 240-242 °C (lit: 237-238 °C). ^{1}H NMR (500MHz; solvent $CDCl_3$) δ 9.276 (d, 1 H), 8.404 (d, 1 H), 8.316 (d, 1 H), 7.965 (m, 2 H), 7.851 (d, 1 H), 7.740 (dd, 1 H)

1,10-phenanthroline-2-carbohydrazonamide[126]

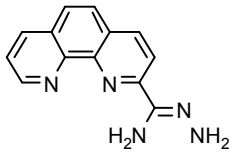

0.97 g 2-cyano-1,10-phenanthroline and 8 ml hydrazine hydrate were placed in 10 ml ethanol and stirred at room temperature for 3 h. Evaporation of the ethanol and remaining hydrazine gave the final product. Yield 1.09 g (98 %). ^{1}H NMR (500MHz; solvent DMSO) δ 9.126 (dd, 1 H), 8.434 (dd, 1 H), 8.399 (d, 1 H), 8.288 (d, 1 H), 7.982 (m, 2 H), 7.790 (dd, 1 H), 6.138 (s, 2 H), 5.599 (br s, 2 H)

Pyridine-2-carbohydrazonamide

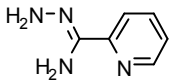

2.2 g 2-cyanopyridine and 1.5 g hydrazine hydrate were placed in a round bottomed flask with a minimal amount of ethanol, to aid dissolution. The flask was stoppered and the solution stirred overnight. The yellow precipitate was filtered from the solution and washed with ether. Yield 1.69 g (60 %). ^{1}H NMR (500MHz; solvent $CDCl_3$) δ 8.517 (d, 1 H), 8.011 (d, 1 H), 7.691 (t, 1 H), 7.265 (t, 1 H), 5.273 (s, 2 H), 4.544 (br s, 2 H)

Pyrazine-2-carbohydrazonamide

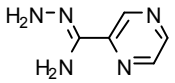

2.2 g 2-cyanopyrazine and 1.5 g hydrazine hydrate were placed in a round bottomed flask with a minimal amount of ethanol, to aid dissolution. The flask was stoppered and the solution stirred overnight. The yellow precipitate was filtered from the solution and washed with ether. Yield 2.04 g (72 %). ^{1}H NMR (500MHz; solvent $CDCl_3$) δ 9.282 (s, 1 H), 8.525 (d, 1 H), 8.450 (m, 1 H), 5.118 (s, 2 H), 4.709 (br s, 2 H).

Phtp[114]

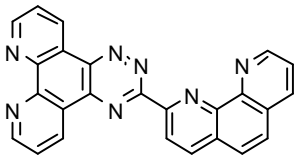

0.5 g 1,10-phenanthroline-5,6-dione and 0.57 g 1,10-phenanthroline-2-carbohydazonamide were heated at reflux for 6 h in 40 ml of ethanol. The bright yellow product was collected by vacuum filtration and washed with cold ethanol before being dried for 16 h at 80 °C. The final product was then recrystallised from DMF. Yield 0.75 g (77%).

Pytp[114]

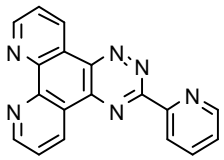

0.32 g of pyridine-2-carbohydrazonamide and 0.5 g of 1,10-phenanthroline-5,6-dione were refluxed for 6 hours in 40 ml EtOH. The solution was cooled and the yellow product filtered off and dried for 16 hours at 80 ^{o}C under reduced pressure. Yield 0.51 g (69 %). ^{1}H NMR ($CDCl_3$) δ 9.78 (1 H), 9.75 (1 H), 9.38 (1 H), 9.35 (1 H), 9.00 (1 H), 8.88 (1 H), 8.02 (1 H), 7.89 (1 H), 7.85 (1 H), 7.56 (1 H).

Pztp[114]

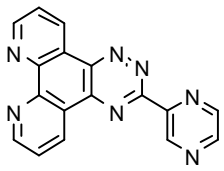

0.6 g of pyridine-2-carbohydrazonamide and 0.9 g of 1,10-phenanthroline-5,6-dione were refluxed for 6 hours in 40 ml EtOH. The solution was cooled and the yellow product filtered off and dried for 16 hours at 80 ^{o}C under reduced pressure. Yield 1.3 g (97%). ^{1}H NMR ($CDCl_3$) δ 10.060 (s, 1 H), 9.780 (s, 1 H), 9.701 (d, 1 H), 9.369 (d, 2 H), 8.935 (d, 1 H), 8.842 (d, 1 H), 7.880 (m, 2 H).

3,6-di(pyridin-2-yl)-1,4-dihydro-1,2,4,5-tetrazine[122]

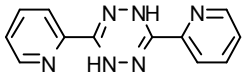

1 g of 2-cyanopyradine was placed in a round bottomed flask with 2 ml ethanol and 2 g of hydrazine hydrate. The solution was then heated at reflux for 4-5 hours. The solution was then cooled to room temperature and the orange precipitate isolated by vacuum filtration. Yield 0.71 g (80%). ^{1}H NMR (500MHz; solvent DMSO) δ 8.978 (s, 2 H), 8.640 (d, 2 H), 7.946 (m, 4 H), 7.534 (t, 2 H)

Pytz[122]

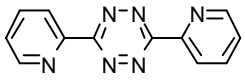

1.71 g of 3,6-di(pyridin-2-yl)-dihydro-1,2,4,5-tetrazine was dissolved in 200 ml of glacial acetic acid and 140 ml of water. The solution was placed in an ice bath and to this was slowly added a solution of 16.8 g $NaNO_2$ dissolved in 50 ml H_2O. Once the entire solution had been added the mixture was stirred at 0 ºC for 1 hour before being neutralised with ammonia. The final bright pink product was isolated by filtration. Yield 1.33 g (78%). ^{1}H NMR (500MHz; solvent DMSO) δ 8.947 (s, 2 H), 8.621 (d, 2 H), 8.168 (t, 2 H), 7.742 (t, 2 H)

3,6-di(pyrazin-2-yl)-dihydro-1,2,4,5-tetrazine[121]

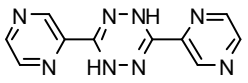

5.65 g of 2-cyanopyrazine was placed in a round bottomed flask with 90 ml THF and 9 ml c. HCl. To this solution was added 10.6 g of hydrazine hydrate and then the combined solution was heated at reflux for 5 hours. The solution was then cooled to room temperature and the orange precipitate isolated by vacuum filtration. Yield 5.76 g (88%). ^{1}H NMR (500MHz; solvent DMSO) δ 9.389 (s, 2 H), 8.867 (m, 2 H), 8.833 (m, 2 H), 7.035 (s, 2 H)

Pztz[122]

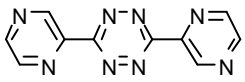

0.7 g of 3,6-di(pyrazin-2-yl)-dihydro-1,2,4,5-tetrazine was dissolved in 100 ml of glacial acetic acid and 70 ml of water. The solution was placed in an ice bath and to this was slowly added a solution of 6.9 g $NaNO_2$ dissolved in 20 ml H_2O. Once the entire solution had been added the mixture was stirred at 0 ºC for 1 hour before being neutralised with ammonia. The final bright pink product was isolated by filtration. Yield 0.43 g (61%). ^{1}H NMR (500MHz; solvent $CDCl_3$) δ 9.897 (s, 2 H), 8.905 (s, 2 H), 8.854 (s, 2 H)

$[(bpy)_2Ru(pytz)](PF_6)_4$

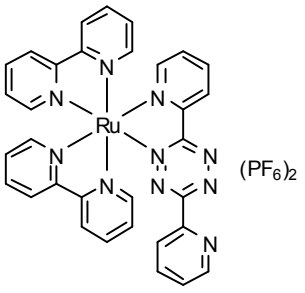

0.200 g of pytz (0.84 mmol) was placed in 10 ml of methanol. 0.300 g of $[Ru(bpy)_2Cl_2].2H_2O$ (0.6 mmol) was dissolved in 20 ml of methanol. The pytz solution was heated to reflux and the ruthenium solution then slowly added to the refluxing solution. The combined reaction mixture was then heated at reflux for an additional 5 hours before being cooled to room temperature. The solution was concentrated to give a dark slurry and purified by column chromatography over silica gel using CH_3CN: saturated aqueous KNO_3 solution:

water (7:2:2) as elutant. The major purple-red band was collected and the product precipitated out by addition of saturated methanolic NH_4PF_6. Yield 0.2368 g (42%). ^{1}H NMR (500MHz; solvent CD_3CN) δ 8.947 (d, 1 H), 8.787 (d, 1 H), 8.656 (d, 1 H), 8.595 (d, 1 H), 8.492 (m, 3 H), 8.237 (m, 2 H), 8.152 (m, 4 H), 8.010 (d, 1 H), 7.918 (t, 1 H), 8.365 (d, 1 H), 7.773 (d, 1 H), 7.705 (t, 1 H), 7.580 (m, 3 H), 7.508 (t, 1 H), 7.435 (m, 2 H). ESI-MS: *m/z* (fragment) 795.12 ($[M-(PF_6)]^+$), 325.08 ($[M-2(PF_6)]^{2+}$). UV-vis (CH_3CN): λ_{max} = 514 nm.

$[(bpy)_2Ru(pytz)Ru(bpy)_2](PF_6)_4$

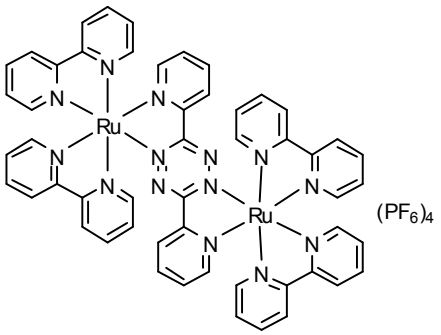

0.5 g of $[Ru(bpy)_2Cl_2].2H_2O$ (1 mmol) and 0.236 g pytz (1 mmol) were heated together at reflux in a solution of 18 ml ethylene glycol and 2 ml water for 3 hours. The solution was then cooled to room temperature and an additional 20 ml of water added. The product was precipitated out by addition of a saturated methanolic solution of NH_4PF_6. Yield 0.39 g (48%). ^{1}H NMR (500MHz; solvent CD_3CN) δ 8.743 – 8.442 (m, 10 H), 8.304 – 8.011 (m, 12 H), 7.835 – 7.437 (m, 18 H). UV-vis (CH_3CN): λ_{max} = 700 nm (Lit 688 nm)[128]

$[(bpy)_2Ru(phendione)](PF_6)_2.H_2O$

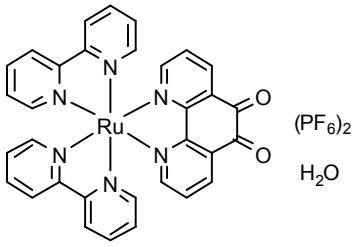

1 g of $[Ru(bpy)_2Cl_2].2H_2O$ and .4 g 1,10-phenanthroline-5,6-dione were heated at reflux in 50 ml of ethanol. The solution was concentrated to ~20 ml followed by addition of 50 ml H_2O. The product was precipitated by addition of 1 ml saturated methanolic solution of NH_4PF_6. The precipitate was collected by vacuum filtration and washed with 0 °C ethanol. Yield 0.54 g (30 %). ^{1}H NMR (CD_3CN) δ 8.518 (m, 6 H), 8.095 (t, 4 H), 7.986 (s, 2

H), 7.845 (d, 2 H), 7.753 (d, 2 H), 7.613 (t, 2 H), 7.433 (t, 4 H). Anal. Calc. for $C_{32}H_{22}F_{12}N_6O2Ru.H_2O$ (931.57): C 41.26, H 2.60, N 9.02%; found: C 41.49, H 2.63, N 9.08.

$[(bpy)_2Ru(pytp)](PF_6)_2$

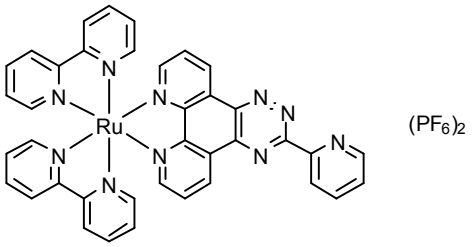

0.5 g $[(bpy)_2Ru(phendione)](PF_6)_2.H_2O$ was dissolved in 15 ml of CH_3CN. 0.076 g of pyridine-2-carbohydrazonamide was dissolved in 5 ml of EtOH and then added to the acetonitrile solution. The reaction mixture was heated at reflux for 1 h after which it was filtered over celite and taken to dryness. The pure product was obtained by column chromatography on silica gel, eluting with an EtOH and 10% NaCl H_2O solution (50:50). The major red band was collected and the ethanol removed under vacuum. The addition of a few drops of a methanolic saturated solution of NH_4PF_6 precipitated out the product which was filtered and washed with 0 °C water, 0 °C EtOH and ether. Yield 0.30 g (52 %). ^1H NMR (500MHz; solvent CD_3CN) δ 9.806 (dd, 1 H, phen), 9.721 (dd, 1 H, phen), 8.963 (d, 1 H, py), 8.927 (d, 1 H, py), 8.543 (m, 4 H, bpy), 8.302 (dd, 1 H, phen), 8.263 (dd, 1 H, phen), 8.140 (m, 1 H, py), 8.127 (m, 2 H, bpy), 8.030 (m, 2 H, bpy), 7.957 (m, 2 H, py), 7.848 (d, 2 H, bpy), 7.717 (d, 1 H, py), 7.682 (m, 2 H, bpy), 7.475 (m, 2 H, bpy), 7.269 (m, 2 H, bpy). ESI-MS: *m/z* (fragment) 869.38 ($[M-(PF_6)]^+$), 362.32 ($[M-2(PF_6)]^{2+}$). UV-vis (CH_3CN): λ_{max} = 440.0 nm.

$[(bpy)_2Ru(pztp)](PF_6)_2.2H_2O$

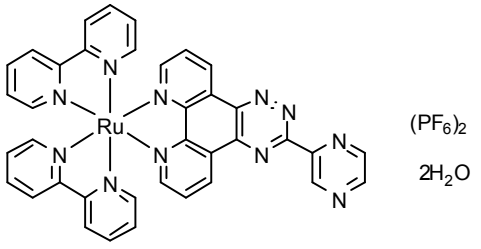

0.5 g $[(bpy)_2Ru(phendione)](PF_6)_2.H_2O$ was dissolved in 15 ml of CH_3CN. 0.08 g of pyridine-2-carbohydrazonamide was dissolved in 5 ml of EtOH and then added to the acetonitrile

solution. The reaction mixture was heated at reflux for 1 h after which it was filtered over celite and taken to dryness. The pure product was obtained by column chromatography on silica gel, eluting with an EtOH and 10% NaCl H_2O solution (50:50). The major red band was collected and the ethanol removed under vacuum. The addition of a few drops of a methanolic saturated solution of NH_4PF_6 precipitated out the product which was filtered and washed with 0 °C water, 0 °C EtOH and ether. Yield 0.24 g (42 %). ^{1}H NMR (500MHz; solvent CD_3CN) δ 10.069 (m, 1 H), 9.817 (m, 1 H), 9.724 (m, 1 H), 8.961 (m, 1 H), 8.904 (m, 1 H), 8.542 (m, 4 H), 8.313 (m, 1 H), 8.277 (m, 1 H), 8.126 (m, 2 H), 8.031 (m, 2 H), 7.964 (m, 2 H), 7.848 (m, 2 H), 7.703 (m, 2 H), 7.476 (m, 2 H), 7.269 (m, 2 H), . Anal. Calc. for $C_{37}H_{25}F_{12}N_{11}P_2Ru.2H_2O$ (1050.70): C 42.30, H 2.78, N 14.66%; found: C 42.57, H 2.96, N 14.56. UV-vis (CH_3CN): λ_{max} = 439 nm.

8.3. Chapter 4

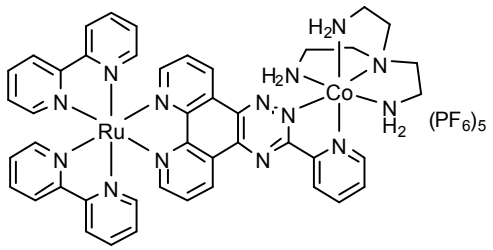

$[(bpy)_2Ru(pytp)Co(tren)](PF_6)_5$

0.0586 g of $[(bpy)_2Ru(pytp)]^{2+}$ and 0.0377g $[Co(tren)(OTf)_2](OTf)$ were placed in a 25 ml round bottom flask. The flask was wrapped in aluminium foil and 2 ml of acetonitrile added. The flask was then stoppered and the solution stirred for 3 hours at room temperature. The product was precipitated out as the PF_6^- salt by drop wise addition to a stirred solution of 60 ml water and 3 ml of saturated solution of NH_4PF_6 in methanol. Yield 0.0515g ^{1}H NMR (500MHz; solvent CD_3CN) δ 9.856 (dd, 1 H, phen), 9.589 (dd, 1 H, phen), 9.333 (dd, 1 H, py), 8.880 (d, 1 H, py), 8.693 (t, 1 H, py), 8.562 (m, 4 H, bpy), 8.490 (dd, 1 H, phen), 8.409 (dd, 1 H, phen), 8.232 (m, 1 H, py), 8.143 (m, 2 H, bpy), 8.092 – 8.032 (m, 4 H, phen, bpy), 7.846 (m, 2 H, bpy), 7.750 (dd, 1 H, bpy), 7.689 (dd, 1 H, bpy), 7.490 (m, 2 H, bpy), 7.294 (m, 2 H, bpy), 5.299 (br s, 2 H, tren, NH_2), 4.637 (m, 2 H, tren), 4.364 (br s, 2 H, tren, NH_2), 4.115 (m, 2 H, tren, NH_2), 3.637 (m, 4 H, tren), 3.166 (m, 6 H, tren). ^{13}C NMR (75 MHZ; solvent CD_3CN) δ 165.166, 159.777 (phen), 158.013 (bpy), 157.818 (phen), 157.785, 155.528 (py), 154.595, 153.096 (bpy), 152.991 (bpy), 152.466, 151.849, 148.527, 147.127, 144.772 (py), 139.280 (bpy), 139.259 (bpy), 139.217 (bpy), 139.187 (bpy), 136.405 (phen), 135.046 (phen), 132.958 (py), 130.379 (py), 128.679 (bpy), 128.630 (bpy), 128.583 (bpy), 127.814, 127.766, 125.403 (bpy), 65.248 (tren), 61.879 (tren), 47.867 (tren), 44.969 (tren). Anal. Calc. for $C_{44}H_{44}F_{30}N_{14}P_5CoRu.H_2O$ (1653.74): C 31.96, H 2.68, N 11.86%; found: C 31.70, H 3.50, N 11.05. ESI-MS: *m/z* (fragment) 1509.31 ($[M-(PF_6)]^+$), 362.32 ($[M-2(PF_6)]^{2+}$). UV-vis (CH_3CN): λ_{max} = 445 nm.

$[(bpy)_2Ru(pytp)Co(en)](PF_6)_5$

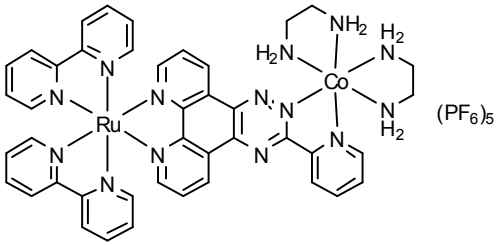

0.0586 g of $[(bpy)_2Ru(pytp)]^{2+}$ and 0.0377g $[Co(en)(OTf)_2](OTf)$ were placed in a 25 ml round bottom flask. The flask was wrapped in aluminium foil and 2 ml of acetonitrile added. The flask was then stoppered and the solution stirred for 3 hours at room temperature. The product was precipitated out as the PF_6^- salt by drop wise addition to a stirred solution of 60 ml water and 3 ml of saturated solution of NH_4PF_6 in methanol. Yield 0.0515g ^{1}H NMR (500 MHz; solvent CD_3CN) δ 9.851 (m, 1 H), 9.781 (m, 1 H), 9.304 (d, 1 H), 8.830 (d, 1 H), 8.714 (t, 1 H), 8.554 (m, 4 H), 8.470 (m, 1 H), 8.412 (m, 1 H), 8.268 (m, 1 H), 8.144 (m, 2 H), 8.061 (m, 4 H), 7.842 (m, 2 H), 7.742 (t, 1 H), 7.688 (t, 1 H), 7.489 (m, 2 H), 7.300 (m, 2 H), 3.156 (m, 4 H), 3.758 (m, 4 H). Anal. Calc. for $C_{42}H_{42}F_{30}N_{14}P_5CoRu.H_2O$ (1627.70): C 30.99, H 2.60, N 12.05%; found: C 30.32, H 3.26, N 11.59. UV-vis (CH_3CN): λ_{max} = 445 nm.

$[(bpy)_2Ru(pztp)Co(en)](PF_6)_5$

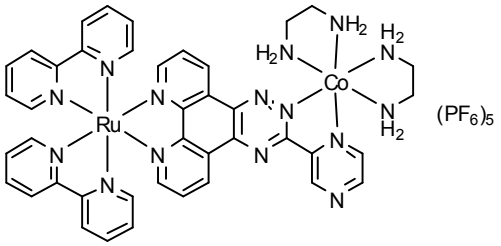

0.0364 g of $[(bpy)_2Ru(pztp)]^{2+}$ and 0.0377g $[Co(en)(OTf)_2](OTf)$ were placed in a 25 ml round bottom flask. The flask was wrapped in aluminium foil and 2 ml of acetonitrile added. The flask was then stoppered and the solution stirred for 24 hours at room temperature. The product was precipitated out as the PF_6^- salt by drop wise addition to a stirred solution of 60 ml water and 3 ml of saturated solution of NH_4PF_6 in methanol. Yield 0.0199g ^{1}H NMR (500 MHz; solvent CD_3CN) δ 9.634 (s, 1 H), 9.170 (d, 1 H), 9.130 (m, 1 H), 8.708 (d, 1 H), 8.313 (t, 1 H), 7.847 (m, 4 H), 7.788 (dd, 1 H), 7.728 (m, 1 H), 7.678 (dd, 1 H), 7.435 (m, 2 H),

7.383 – 7.314 (m, 4 H), 7.137 (m, 2 H), 6.915 (m, 1 H), 6.777 (m, 2 H), 6.602 (m, 1 H), 6.511 (m, 1 H). UV-vis (CH_3CN): λ_{max} = 445 nm.

$[(bpy)_2Ru(pytz)Co(tren)](PF_6)_5$

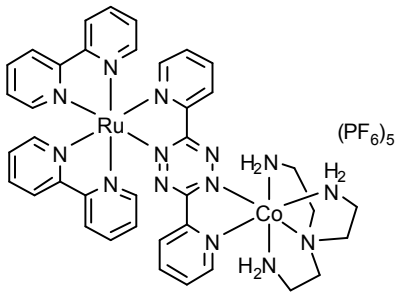

0.1 g of $[(bpy)_2Ru(pytz)]^{2+}$ and 0.07g $[Co(tren)(OTf)_2](OTf)$ were placed in a 25 ml round bottom flask. The flask was wrapped in aluminium foil and 2 ml of acetonitrile added. The flask was then stoppered and the solution stirred for 3 hours at room temperature. The product was precipitated out as the PF_6^- salt by drop wise addition to a stirred solution of 60 ml water and 3 ml of saturated solution of NH_4PF_6 in methanol. Yield 0.0809 g. ^1H NMR (500 MHz; solvent CD_3CN) δ 8.042 (d, 1 H), 8.809 (d, 1 H), 8.770 (d, 1 H), 8.732 (d, 1 H), 8.661 (d, 1 H), 8.557 (d, 1 H), 8.481 (m, 2 H), 8.393 (t, 1 H), 8.303 (m, 1 H), 8.249 (t, 1 H), 8.158 (m, 1 H), 8.101 (m, 1 H), 7.817 (m, 2 H), 7.754 (m, 2 H), 7.703 (m, 2 H), 7.597 (m, 2 H), 7.468 (m, 2 H), 7.275 (d, 1 H), 5.268 (br s, 2 H), 4.509 (m, 2 H), 4.357 (m, 2 H), 4.007 (m, 1 H), 3.596 (m, 5 H), 3.294 (m, 1 H), 3.098 (m, 1 H). UV-vis (CH_3CN): λ_{max} = 570 nm.

8.4. Chapter 5

N,N′-diethylethane-1,2-diamine

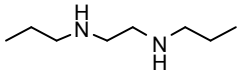

5 g $LiAlH_4$ was dissolved in 200 ml of ether. To this was added a slurry of N,N′-(ethane-1,2-diyl)diacetamide in 50 ml of ether. The solution was heated at reflux overnight under N_2; any unreacted $LiAlH_4$ was then decomposed by the slow addition of water. The solution was then filtered and the precipitate washed with ether. The ether layer of the filtrate was combined with the ether washings and evaporated to give N,N′-diethylethane-1,2-diamine as an oil. Yield 3.0845 g (39%) ^{1}H NMR (500 MHz; solvent $CDCl_3$) δ 2.671 (s, 2 H), 2.595 (q, 2 H), 1.426 (br s, 2 H), 1.048 (t, 3 H)

N,N′-bis(2-hydroxyethyl)ethane-1,2-diamine

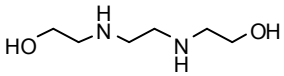

8.5 g of 2-chloroethanol was added to a suspension of 8 g Na_2CO_3 in 10.4 g 2-(2-aminoethylamino)ethanol. The solution was stirred at 120 °C for 29 hours before being cooled to room temperature. 150 ml of methanol was then added and the solution filtered. The methanol was then evaporated from the filtrate to give a viscous yellow oil. The oil was titurated in 150 ml boiling THF for 30 minutes after which the supernatant fluid was decanted off and placed in the fridge overnight. The product was then obtained by filtration as a white solid (2.4 g). Repeating the trituration of the yellow oil gave a second crop of product (1.1 g). Yield 3.5 g (24%) ^{1}H NMR (500 MHz; solvent CD_3OD) δ 3.653 (t, 4 H), 2.757 (s, 4 H), 2.729 (t, 4 H)

_N_,_N_,_N′_,_N′_-Tetrakis(2-hydroxyethyl)ethane-1,2-diamine[150]

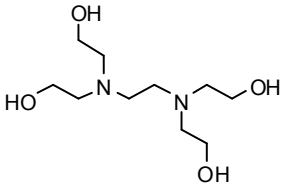

3 g diethanolamine and 2 g 1,2-dibromoethane were dissolved in 50 ml of ethanol. 1 ml of triethyl amine was then added and the solution heated at reflux for 40 hours. The solution was cooled to room temperature and filtered. Any unreacted starting material was then removed under vacuum to give the product as a yellow oil. Yield 3.47 g (92%) ^{1}H NMR (500 MHz; solvent $CDCl_3$) δ 5.322 (s, 4 H, OH), 3.659 (t, 8 H), 2.652 (s, 4 H), 2.615 (t, 8 H)

$[Co(heen)_2(NO_2)_2](NO_3).H_2O$

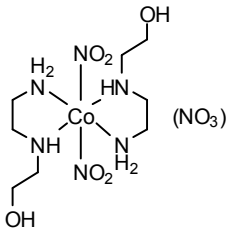

11.64 g $Co(NO_3)_2.6H_2O$ and 6 g $NaNO_2$ were dissolved in 20 ml H_2O and placed in a bubbler. To this was added 8.3 g heen dissolved in 10 ml H_2O and 3 ml conc. HNO_3. A vigorous stream of air was drawn through the solution for 1 hour after which the solution was placed in the freezer overnight. The yellow-orange crystalline product was then isolated by filtration. Yield 11.7 g (67%) ^{1}H NMR (500 MHz; solvent DMSO) δ 6.672 (m, 2 H, NH, NH_2), 5.125 (s, 1 H, OH), 5.082 (m, 1 H, NH_2), 3.706 (m, 1 H, HOCH_2), 3.519 (m, 1 H, HOCH_2), 2.936 (m, 1 H), 2.817 (m, 1 H), 2.671 (m, 1 H, C$H_2$$NH_2$), 2.322 (m, 1 H), 2.241 (m, 1 H, C$H_2$$NH_2$), 2.171 (m, 1 H). ^{13}C NMR (126 MHz solvent DMSO) 56.455 ($HOCH_2$), 53.094 ($HOCH_2CH_2$), 51.175 ($NHCH_2$) 42.706 (CH_2NH_2). Anal. Calc. for $C_8H_{24}N_7O_9Co.H_2O$ (439.27): C 21.87, H 5.97, N 22.32%; found: C 22.18, H 6.01, N 22.69.

$[Co(ceen)_2(NO_2)Cl]Cl$

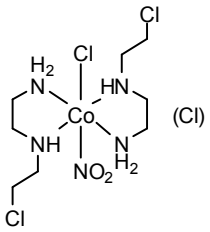

1.8 g of $[Co(heen)_2(NO_2)_2](NO_3).H_2O$ was placed in a 50 ml round bottomed flask. 20 ml of $SOCl_2$ was then slowly added with stirring. 1 ml of DMF was then added drop wise to facilitate dissolution of the solid. The reaction mixture was stirred for 30 minutes after which the thionyl chloride was removed under a stream of nitrogen. The resulting dark pink slurry was recrystallised from a mixture of water and ethanol. Yield 1.23 g (71%) ^{13}C NMR (126 MHz solvent DMSO) δ 52.488, 51.476, 42.705, 40.094. Anal. Calc. for $C_8H_{22}N_5Cl_4O_2Co$ (421.04): C 22.82, H 5.27, N 16.63%; found: C 22.73, H 5.44, N 16.49.

$[Co(ceen)_2(OTf)Cl]OTf$

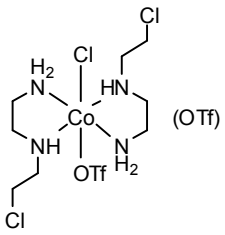

$[Co(ceen)_2(NO_2)Cl]Cl$ was placed in a 25 ml round bottom flask and cooled in a salt-ice bath. HOTf was then added drop wise with stirring, until the solid was just covered. The reaction mixture was stirred under vacuum in the salt-ice bath for 45 minutes. 100 ml of ether was placed in a second salt-ice bath to which the reaction mixture was slowly added by drop wise addition. Trituration aids solidification of the product which was isolated by filtration and then dried under vacuum to give a green solid. ^1H NMR (500 MHz; solvent CD_3CN) δ 5.723 (br m, 2 H), 5.179 (br s, 1 H), 4.011 - 3.908 (m, 2 H), 3.122 (m, 3 H), 3.006 (m, 2 H), 2.715 (m, 1 H).

8.5. Chapter 6

4,4′-dimethyl-2,2′-bipyridine

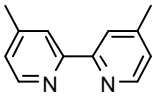

10 g of 4-methylpyridine was flushed with nitrogen for 30 minutes, after which 0.5 g of 10% Pd/C was added and the mixture heated at reflux for 1 week. 50 ml of chloroform was then added and the solution filtered through celite. The chloroform was then removed from the filtrate under vacuum and the remaining solution was filtered again to give the product as a white solid. Yield 2.23 g (22.6%). ^{1}H NMR (500 MHz; solvent $CDCl_3$) δ 8.459 (d, 2 H), 8.150 (s, 2 H), 7.055 (d, 2 H), 2.362 (s, 6 H)

2,2′-bipyridine-4,4′-dicarboxylic acid

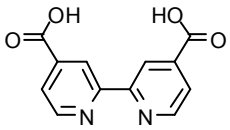

0.046 g of 4,4′-dimethyl-2,2′-bipyridine was placed in a 23 ml Teflon bomb with 8 ml H_2O and 0.5 ml c.HNO_3. The solution was stirred for 10 minutes before being sealed and heated to 200 °C for 36 hours. The sample was then slowly cooled back to room temperature at a rate of 5 °C/hr. Filtration gave the product as a white crystalline solid. Yield 0.0239 g (39%). ^{1}H NMR (500 MHz; solvent DMSO) δ 8.905 (m, 2 H), 8.825 (m, 2 H), 7.906 (m, 2 H)

$[Co(en)_2(phen)]Br_3$

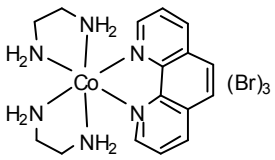

1 g of 1,10-phenanthroline was dissolved in 6 ml of ethanol. 1.43 g of $[Co(en)_2Cl_2]Cl$ and 3 g of NaBr were dissolved in 5 ml of water. The ethanolic solution of 1,10-phenanthroline was the added to the aqueous solution, which was then heated on a water bath until dark yellow. The mixture was then cooled in ice and the precipitate filtered off and recrystallised from water. Yield 0.70 g (21%).

$[Co(en)_2(phendione)](ClO_4)_3$

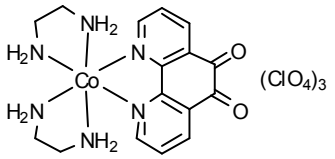

0.95 g of $[Co(en)_2(phen)]Br_3$ and 0.54 g of NaBr were placed in a round bottom flask and then placed in an ice bath. 6 ml of H_2SO_4 was then slowly added, followed by the slow addition of HNO_3. The mixture was then heated at reflux for 40 minutes after which the heat was reduced and the condenser removed for 5 mins. The solution was then cooled to 0 °C and added drop wise to a solution of 2.13 g $NaClO_4.H_2O$ in 40 ml water, which was placed in the freezer overnight. The product was obtained by filtration and washed twice with 5 ml of 0 °C HCl, and 5 ml EtOH before being dried under vacuum. ^1H NMR (500MHz; solvent D_2O) δ 9.046 (d, 1 H), 8.943 (m, 1 H), 8.864 (t, 1 H), 8.706 (t, 1 H), 8.292 (m, 1 H), 8.210 (m, 1 H), 5.991 – 5.578 (m, 8 H), 3.292 (m, 2 H), 3.184 (m, 2 H), 3.037 (m, 4 H).

Appendices

Appendix 1: X-Ray Crystal Data

[Ru(6′-p-tolyl-2,2′:4′,2″-terpyridine)$_2$Cl$_2$]

Identification code	[Ru(6′-p-tolyl-2,2′:4′,2″-terpyridine)$_2$Cl$_2$]	
Empirical formula	C48 H46 Cl2 N6 O2 Ru	
Formula weight	910.88	
Temperature	108(2) K	
Wavelength	0.71073 Å	
Crystal system	Triclinic	
Space group	P -1	
Unit cell dimensions	a = 11.1012(4) Å	α= 110.958(2)°.
	b = 13.8935(4) Å	β= 93.182(2)°.
	c = 16.8503(8) Å	γ = 111.078(2)°.
Volume	2213.43(15) Å^3	
Z	2	
Density (calculated)	1.367 Mg/m^3	
Absorption coefficient	0.520 mm^{-1}	
F(000)	940	
Crystal size	0.25 x 0.15 x 0.10 mm^3	
Theta range for data collection	1.32 to 35.73°.	
Index ranges	-17<=h<=17, -21<=k<=22, -25<=l<=26	
Reflections collected	57750	
Independent reflections	18228 [R(int) = 0.0432]	
Completeness to theta = 25.04°	99.9 %	
Absorption correction	Semi-empirical from equivalents	
Max. and min. transmission	1 and 0.895017	
Refinement method	Full-matrix least-squares on F^2	
Data / restraints / parameters	7819 / 1 / 521	
Goodness-of-fit on F^2	1.078	
Final R indices [I>2sigma(I)]	R1 = 0.0615, wR2 = 0.1757	
R indices (all data)	R1 = 0.0722, wR2 = 0.1901	
Largest diff. peak and hole	4.241 and -1.029 e.Å^{-3}	

pytp.2HCl.H_2O

Identification code	pytp.2HCl.H_2O	
Empirical formula	C18 H14 Cl2 N6 O	
Formula weight	401.25	
Temperature	118(2) K	
Wavelength	0.71073 Å	
Crystal system	Triclinic	
Space group	P-1	
Unit cell dimensions	a = 8.3203(2) Å	α= 112.3820(10)°.
	b = 9.8047(3) Å	β= 93.764(2)°.
	c = 11.3191(4) Å	γ = 93.041(2)°.
Volume	848.93(4) $Å^3$	
Z	2	
Density (calculated)	1.570 Mg/m^3	
Absorption coefficient	0.406 mm^{-1}	
F(000)	412	
Crystal size	0.24 x 0.19 x 0.17 mm^3	
Theta range for data collection	1.95 to 30.99°.	
Index ranges	-12<=h<=12, -14<=k<=14, -16<=l<=16	
Reflections collected	24101	
Independent reflections	5311 [R(int) = 0.0324]	
Completeness to theta = 30.99°	98.4 %	
Absorption correction	Semi-empirical from equivalents	
Max. and min. transmission	0.9595 and 0.9435	
Refinement method	Full-matrix least-squares on F^2	
Data / restraints / parameters	5311 / 2 / 256	
Goodness-of-fit on F^2	1.139	
Final R indices [I>2sigma(I)]	R1 = 0.0332, wR2 = 0.0941	
R indices (all data)	R1 = 0.0396, wR2 = 0.1086	
Largest diff. peak and hole	0.514 and -0.297 $e.Å^{-3}$	

[(bpy)Ru(pztp)]$(PF_6)_2$.2CH_3CN

Identification code	$[(bpy)_2Ru(pztp)](PF_6)_2$	
Empirical formula	C41 H31 F12 N13 P2 Ru	
Formula weight	1096.80	
Temperature	136(2) K	
Wavelength	0.71073 Å	
Crystal system	Triclinic	
Space group	P -1	
Unit cell dimensions	a = 11.8919(7) Å	α= 81.000(4)°.
	b = 12.3372(7) Å	β= 77.789(4)°.
	c = 15.9036(10) Å	γ = 66.668(4)°.
Volume	2087.1(2) $Å^3$	
Z	2	
Density (calculated)	1.745 Mg/m^3	
Absorption coefficient	0.558 mm^{-1}	
F(000)	1100	
Crystal size	0.35 x 0.11 x 0.02 mm^3	
Theta range for data collection	1.31 to 26.51°.	
Index ranges	-14<=h<=14, -15<=k<=15, -19<=l<=19	
Reflections collected	38662	
Independent reflections	8631 [R(int) = 0.1187]	
Completeness to theta = 26.51°	99.5 %	
Absorption correction	Semi-empirical from equivalents	
Max. and min. transmission	0.9889 and 0.8286	
Refinement method	Full-matrix least-squares on F^2	
Data / restraints / parameters	8631 / 0 / 612	
Goodness-of-fit on F^2	1.001	
Final R indices [I>2sigma(I)]	R1 = 0.0655, wR2 = 0.1564	
R indices (all data)	R1 = 0.1494, wR2 = 0.2207	
Largest diff. peak and hole	1.044 and -0.846 $e.Å^{-3}$	

Glycolated $[(bpy)_2Ru(Phendione)](PF_6)_2$

Identification code	Glycolated $[(bpy)_2Ru(phendione)](PF_6)_2$	
Empirical formula	C36 H30 F12 N6 O4 P2 Ru	
Formula weight	1001.67	
Temperature	136(2) K	
Wavelength	0.71073 Å	
Crystal system	Monoclinic	
Space group	P21/c	
Unit cell dimensions	a = 13.3982(11) Å	α= 90°.
	b = 22.3433(19) Å	β= 98.509(6)°.
	c = 13.6758(12) Å	γ = 90°.
Volume	4048.9(6) $Å^3$	
Z	4	
Density (calculated)	1.643 Mg/m^3	
Absorption coefficient	0.569 mm^{-1}	
F(000)	2008	
Crystal size	0.13 x 0.12 x 0.04 mm^3	
Theta range for data collection	2.19 to 25.05°.	
Index ranges	-15<=h<=15, -26<=k<=26, -16<=l<=16	
Reflections collected	75165	
Independent reflections	7157 [R(int) = 0.4831]	
Completeness to theta = 25.05°	99.9 %	
Absorption correction	Semi-empirical from equivalents	
Max. and min. transmission	0.9776 and 0.9297	
Refinement method	Full-matrix least-squares on F^2	
Data / restraints / parameters	7157 / 0 / 550	
Goodness-of-fit on F^2	0.738	
Final R indices [I>2sigma(I)]	R1 = 0.0738, wR2 = 0.1720	
R indices (all data)	R1 = 0.3318, wR2 = 0.2288	
Largest diff. peak and hole	0.650 and -0.504 $e.Å^{-3}$	

$[Co(heen)_2(NO_2)_2](NO_3).H_2O$

Identification code	$[Co(heen)2(NO_2)_2](NO_3).H_2O$	
Empirical formula	C8 H26 Co N7 O10	
Formula weight	439.29	
Temperature	136(2) K	
Wavelength	0.71073 Å	
Crystal system	Triclinic	
Space group	P-1	
Unit cell dimensions	a = 9.3740(9) Å	α= 69.965(4)°.
	b = 9.5745(9) Å	β= 87.315(4)°.
	c = 11.5103(10) Å	γ = 62.039(4)°.
Volume	849.16(14) $Å^3$	
Z	2	
Density (calculated)	1.718 Mg/m^3	
Absorption coefficient	1.079 mm^{-1}	
F(000)	460	
Crystal size	0.56 x 0.19 x 0.01 mm^3	
Theta range for data collection	2.48 to 25.05°.	
Index ranges	-11<=h<=11, -11<=k<=11, -13<=l<=13	
Reflections collected	16406	
Independent reflections	3013 [R(int) = 0.0320]	
Completeness to theta = 25.05°	99.9 %	
Absorption correction	Semi-empirical from equivalents	
Max. and min. transmission	0.9851 and 0.5833	
Refinement method	Full-matrix least-squares on F^2	
Data / restraints / parameters	3013 / 0 / 245	
Goodness-of-fit on F^2	0.975	
Final R indices [I>2sigma(I)]	R1 = 0.0222, wR2 = 0.0564	
R indices (all data)	R1 = 0.0240, wR2 = 0.0575	
Largest diff. peak and hole	0.279 and -0.246 $e.Å^{-3}$	

Appendix 2: P388 IC_{50} Data

PC388 IC_{50} data for $[(bpy)_2Ru(pytp)]^{2+}$:

Submitted concentration: 69 mg/ml

% Cell	90.45	92.09	87.06	69.94	73.99	25.43	20.23	27.30
Log ID50	1.989	2.290	2.591	2.892	3.193	3.494	3.796	4.097

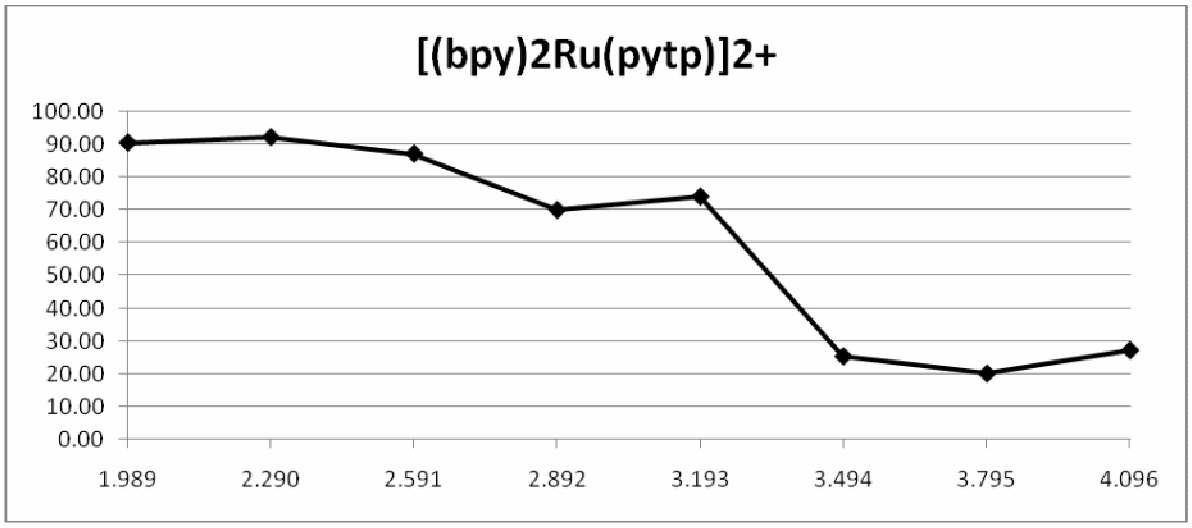

IC_{50}: 47 µmol/L

PC388 IC_{50} data for $[(bpy)_2Ru(pytp)Co(tren)]^{5+}$:

Submitted concentration: 65 mg/ml

% Cell	85.84	80.31	92.10	101.79	86.78	75.07	38.75	24.44
Log ID50	1.989	2.290	2.591	2.892	3.193	3.494	3.796	4.097

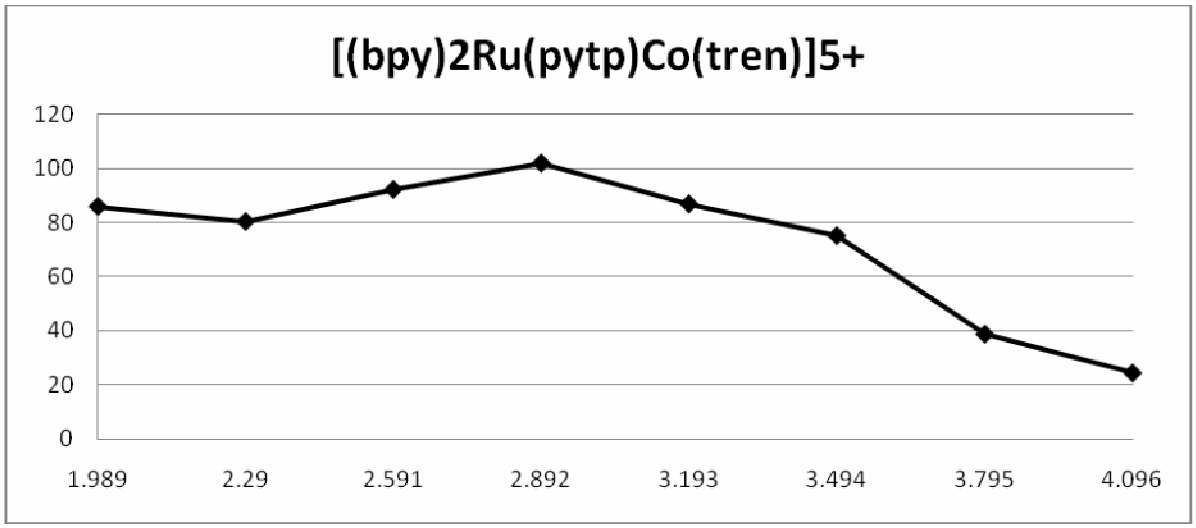

IC_{50}: 195 µmol/L

PC388 IC_{50} data for $[(bpy)_2Ru(pztp)]^{2+}$

Submitted concentration: 56 mg/ml

% Cell	93.81	85.69	83.59	77.92	29.95	24.35	11.59	14.83
Log ID50	1.989	2.290	2.591	2.892	3.193	3.494	3.796	4.097

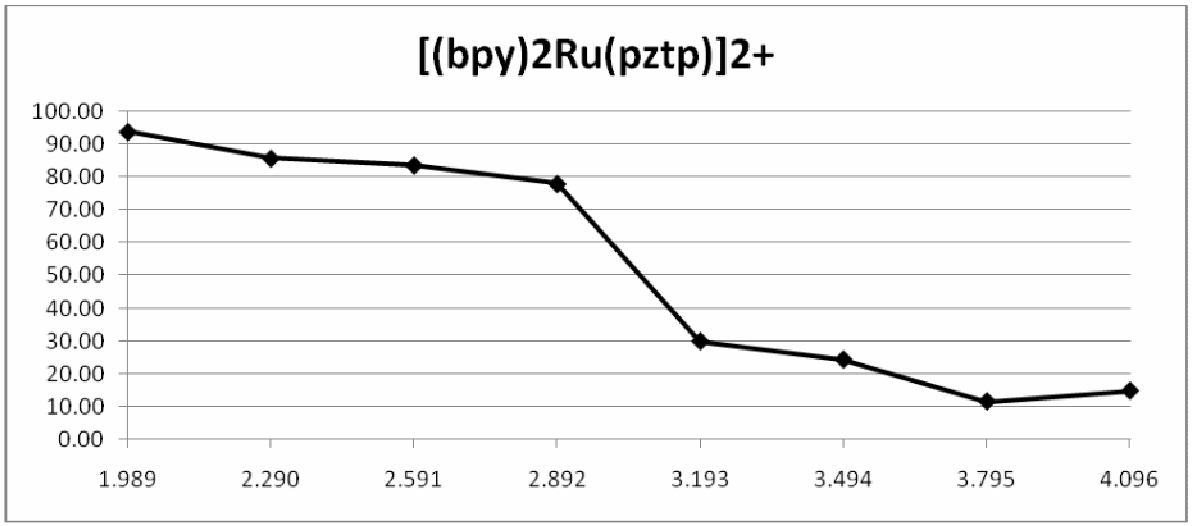

IC_{50}: 66 µmol/L

PC388 IC_{50} data for $[(tbpy)_2Ru(pytp)]^{2+}$

Submitted concentration: 69 mg/ml

% Cell	88.94	100.89	88.08	93.57	76.19	46.13	19.88	1.37
Log ID50	1.989	2.290	2.591	2.892	3.193	3.494	3.796	4.097

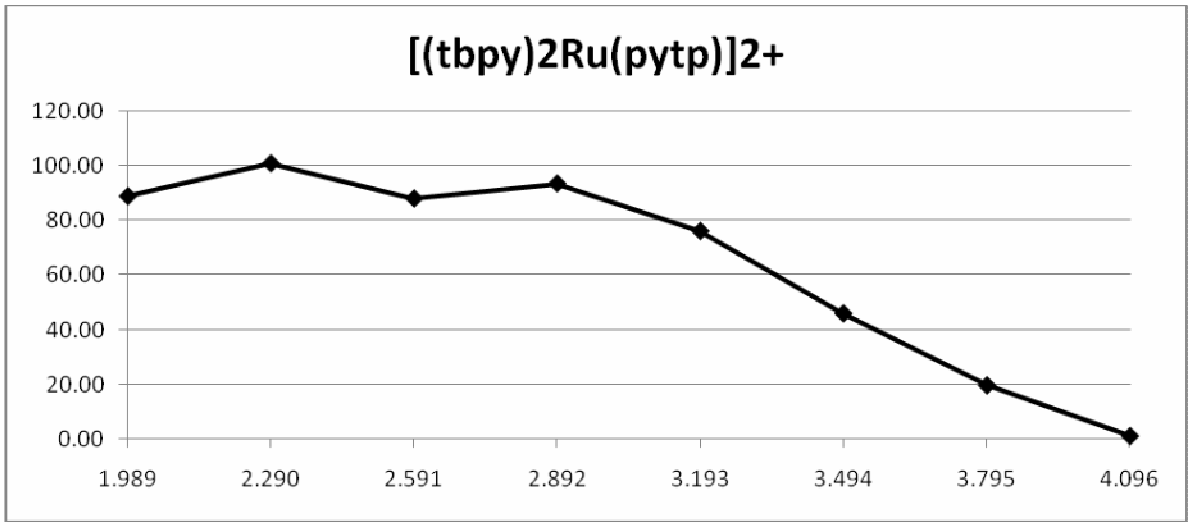

IC_{50}: 166 µmol/L

PC388 IC_{50} data for $[(phen)_2Ru(pytp)]^{2+}$

Submitted concentration: 67 mg/ml

% Cell	93.92	91.02	78.84	23.16	23.04	35.77	24.89	6.09
Log ID50	1.989	2.290	2.591	2.892	3.193	3.494	3.796	4.097

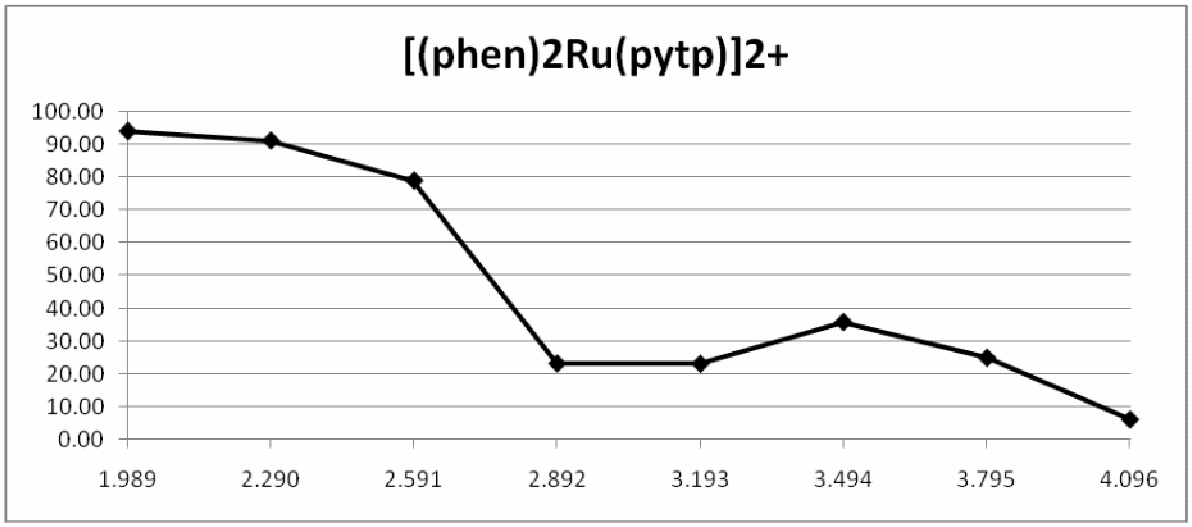

IC_{50}: 38 µmol/L

PC388 IC_{50} data for $[(bpy)_2Ru(pytz)]^{2+}$

Submitted concentration: 73 mg/ml

% Cell	92.09	93.05	88.10	95.49	92.49	97.88	40.41	-18.85
Log ID50	1.989	2.290	2.591	2.892	3.193	3.494	3.796	4.097

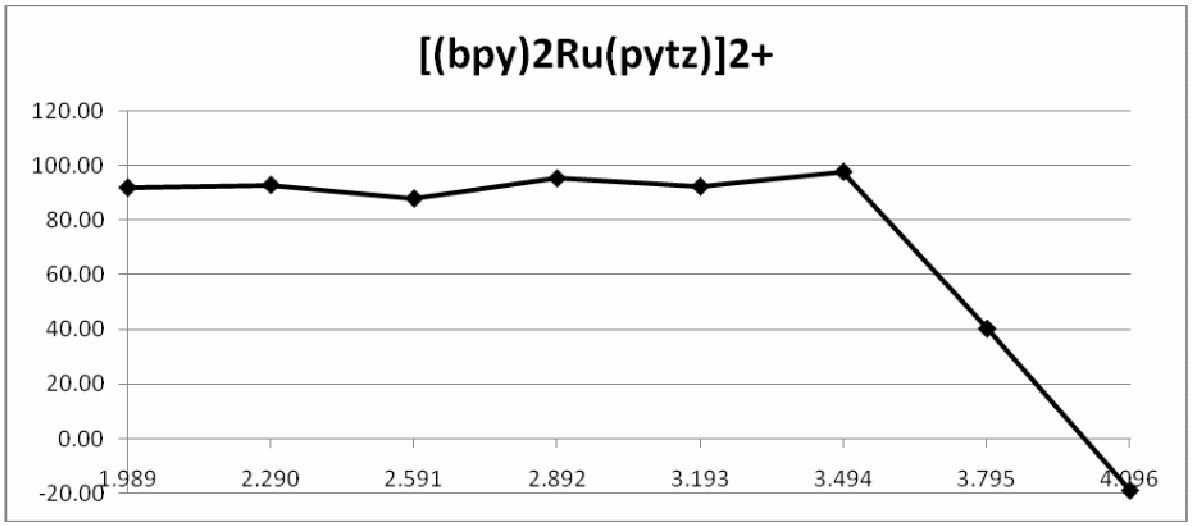

IC_{50}: 472 µmol/L

PC388 IC_{50} data for $[(bpy)_2Ru(pztz)]^{2+}$

Submitted concentration: 53 mg/ml

% Cell	82.82	95.92	92.18	92.84	88.46	82.66	76.15	25.83
Log ID50	1.989	2.290	2.591	2.892	3.193	3.494	3.796	4.097

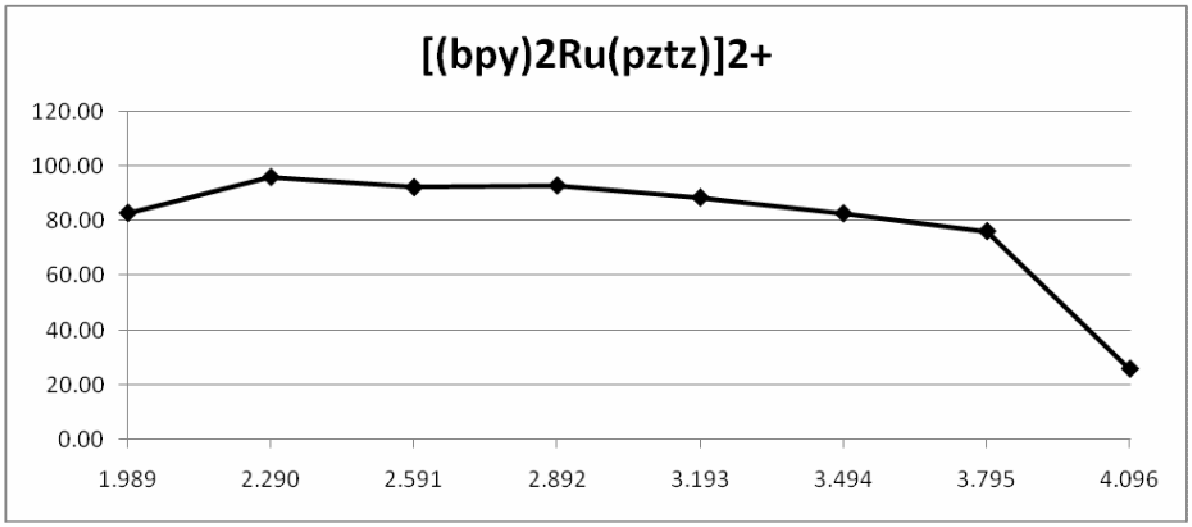

IC_{50}: 547 µmol/L

PC388 IC_{50} data for $[(bpy)_2Ru(pytz)Co(tren)]^{5+}$

Submitted concentration: 81 mg/ml

% Cell	107.40	98.09	95.95	99.69	109.65	98.97	93.60	88.35
Log ID50	1.989	2.290	2.591	2.892	3.193	3.494	3.796	4.097

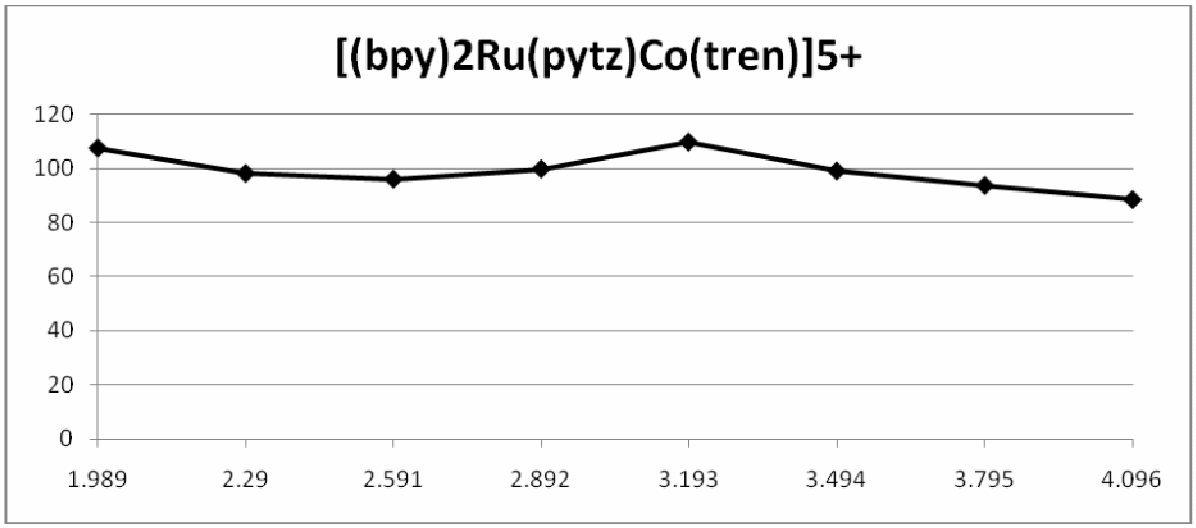

IC_{50}: >641 µmol/L

PC388 IC_{50} data for $[(bpy)_2Ru(pytz)Co(ceen)]^{5+}$

Submitted concentration: 94 mg/ml

% Cell	110.43	90.53	83.22	78.23	70.85	52.73	35.24	5.25
Log ID50	1.989	2.290	2.591	2.892	3.193	3.494	3.796	4.097

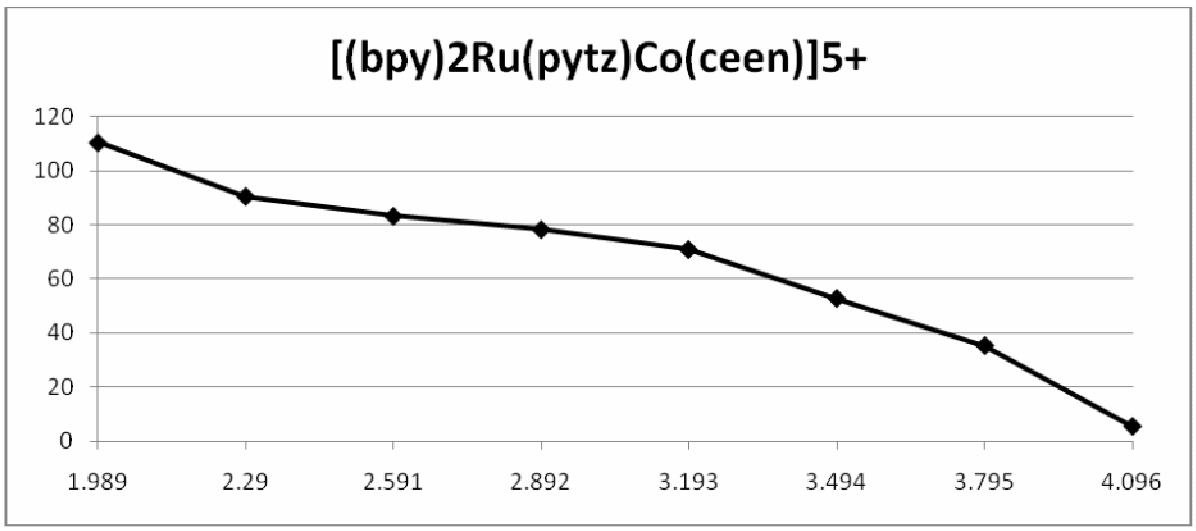

IC_{50}: 181 µmol/L

PC388 IC_{50} data for $[(bpy)_2Ru(pytz)Ru(bpy)_2]^{4+}$

Submitted concentration: 111 mg/ml

% Cell	116.92	116.88	108.79	114.61	114.14	122.06	93.16	23.62
Log ID50	1.989	2.290	2.591	2.892	3.193	3.494	3.796	4.097

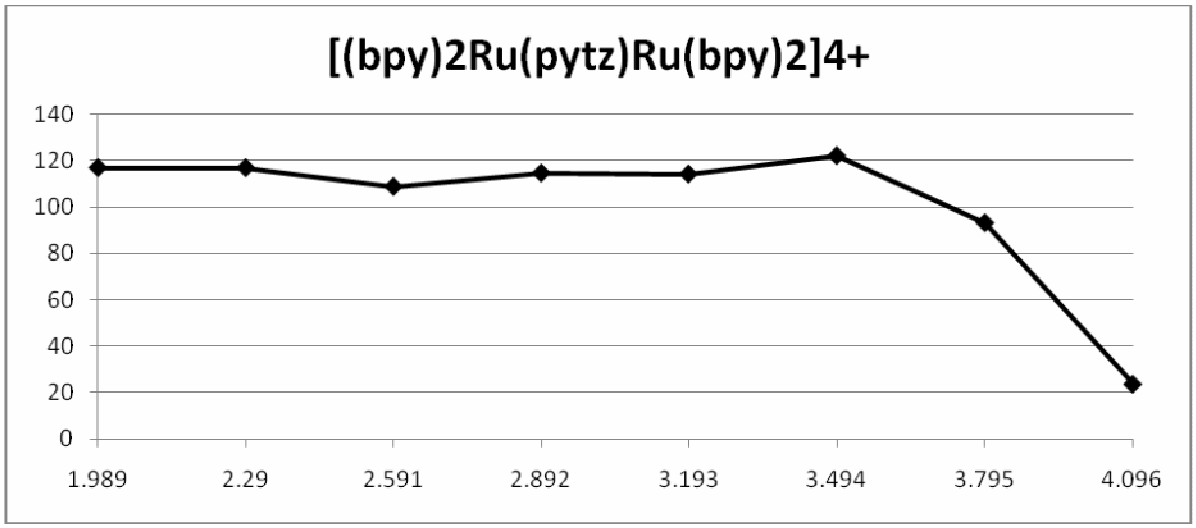

IC_{50}: 660 µmol/L

PC388 IC_{50} data for $[Co(en)_2(OTf)_2](OTf)$

Submitted concentration: 36 mg/ml

% Cell	101.10	107.22	96.36	95.25	93.28	75.73	41.86	10.50
Log ID50	1.989	2.290	2.591	2.892	3.193	3.494	3.796	4.097

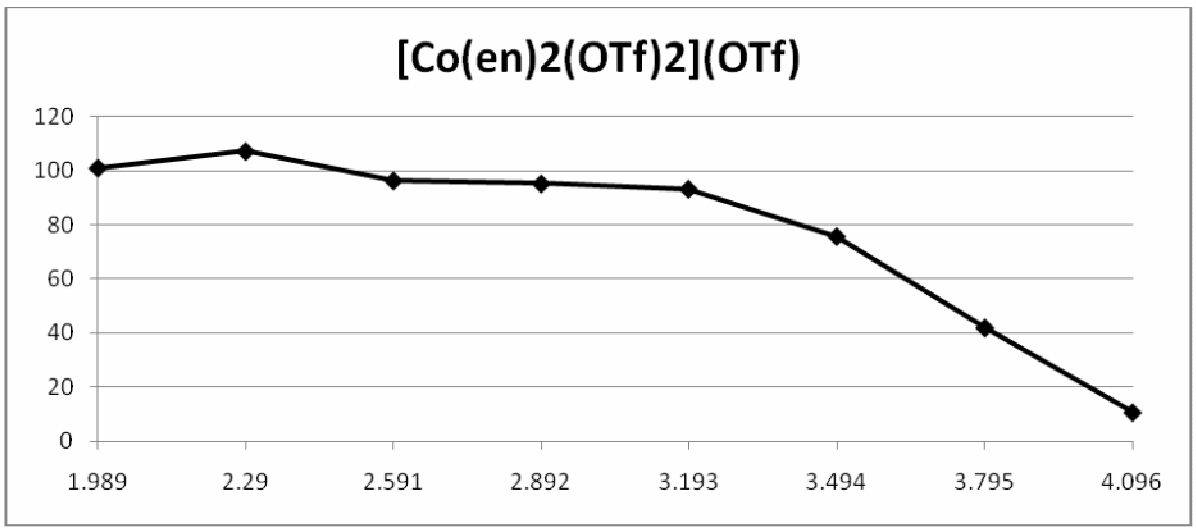

IC_{50}: 303 µmol/L

PC388 IC_{50} data for $[Co(ceen)_2(OTf)Cl](OTf)$

Submitted concentration: 35 mg/ml

% Cell	112.22	107.22	94.85	71.74	89.99	77.26	61.54	27.24
Log ID50	1.989	2.290	2.591	2.892	3.193	3.494	3.796	4.097

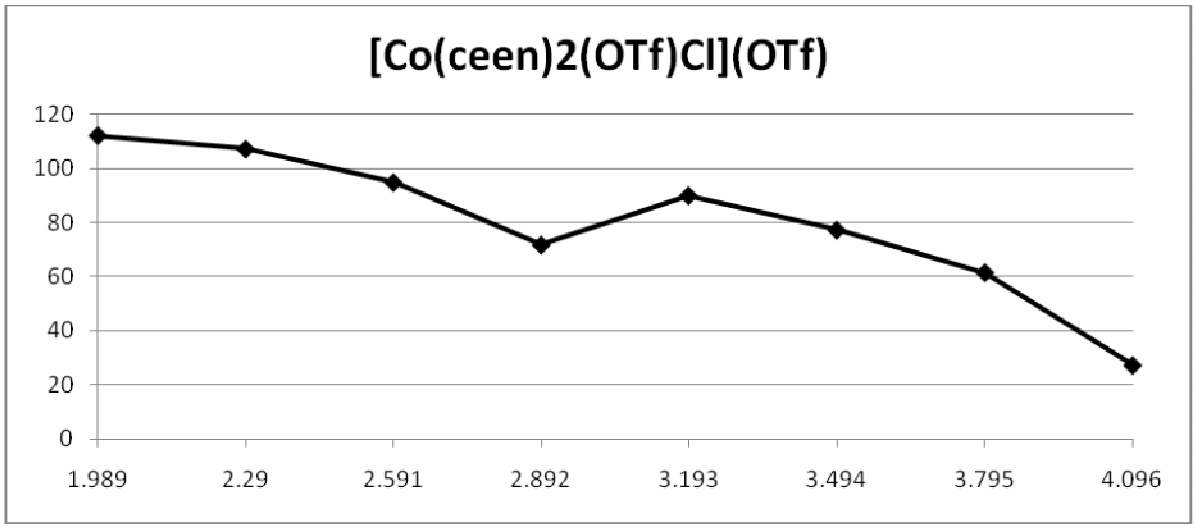

IC_{50}: 349 µmol/L

References

[1] Ministry of Health. 2009. *Cancer: New Registrations and Deaths 2005: Revised edition.* Wellington: Ministry of Health.
[2] J. M. Brown and A. J. Giaccia, *Cancer Res* **1998**, *58*, 1408-1416.
[3] T. W. Hambley, *Australian Journal of Chemistry* **2008**, *61*, 647-653.
[4] I. F. Tannock and D. Rotin, *Cancer Res* **1989**, *49*, 4373-4384.
[5] M. Kraus and B. Wolf, *Tumor Biology* **1996**, *17*, 133-154.
[6] N. Raghunand, X. He, R. v. Sluis, B. Mahoney, B. Baggett, C. W. Taylor, G. Paine-Murrieta, D. Roe, Z. M. Bhujwalla and R. J. Gillies, *Br J Cancer* **1999**, *80*, 1005-1011.
[7] O. Tredan, C. M. Galmarini, K. Patel and I. F. Tannock, *J. Natl. Cancer Inst.* **2007**, *99*, 1441-1454.
[8] F. Yuan, M. Dellian, D. Fukumura, M. Leunig, D. A. Berk, V. P. Torchilin and R. K. Jain, *Cancer Res* **1995**, *55*, 3752-3756.
[9] G. Scherphof, F. Roerdink, J. Dijkstra, H. Ellens, R. Dezanger and E. Wisse, *Biology of the Cell* **1983**, *47*, 47-57.
[10] R. Altman and M. Sarg, *The Cancer Dictionary*, Facts on File, New York, **1992**, p. xi, 334.
[11] S. A. Schepartz in *Cancer Chemotherapeutic Agents*, (Ed. W. O. Foye), American Chemical Society, Washington, DC, **1995**.
[12] L. S. Goodman, M. M. Wintrobe, W. Dameshek, M. J. Goodman, A. Gilman and M. T. McLennan, *J Am Med Assoc* **1946**, *132*, 126-132.
[13] J. Hirsch, *JAMA* **2006**, *296*, 1518-1520.
[14] A. A. Nelson and G. Woodard, *Archives of Pathology* **1949**, *48*, 387-394.
[15] A. M. Hutter and D. E. Kayhoe, *American Journal of Medicine* **1966**, *41*, 581-&.
[16] B. K. Keppler in *Metal complexes in cancer chemotherapy*, (Ed. B. K. Keppler), Vch, Weinheim ; New York, **1993**.
[17] Rosenber.B, L. Vancamp and T. Krigas, *Nature* **1965**, *205*, 698-&.
[18] Rosenber.B, L. Vancamp, E. B. Grimley and A. J. Thomson, *Journal of Biological Chemistry* **1967**, *242*, 1347-&.
[19] Rosenber.B, L. Vancamp, J. E. Trosko and V. H. Mansour, *Nature* **1969**, *222*, 385-&.
[20] W. A. Denny in *Cancer Chemotherapeutic Agents*, (Ed. W. O. Foye), American Chemical Society, Washington, DC, **1995**.
[21] W. A. Denny in *The Chemistry of Antitumour Agents*, (Ed. D. E. V. Wilman), Blackie ; Chapman and Hall, Glasgow
New York, **1990**.
[22] J. Anastassopoulou, *Journal of Molecular Structure* **2003**, *651-653*, 19-26.
[23] A. R. Mustafina, V. V. Skripacheva, V. P. Gubskaya, M. Gruner, S. E. Solv'eva, I. S. Antipin, E. K. Kazakova, A. I. Konovalov and W. D. Habicher, *Russian Chemical Bulletin* **2004**, *53*, 1511-1519.
[24] K. W. Kohn, A. Orr, P. M. O'Connor, L. J. Guziec and F. S. Guziec, *Journal of Medicinal Chemistry* **1994**, *37*, 67-72.
[25] M. E. Heim in *Metal complexes in cancer chemotherapy*, (Ed. B. K. Keppler), Vch, Weinheim ; New York, **1993**.

[26] N. Farrell, *Transition metal complexes as drugs and chemotherapeutic agents*, Kluwer Academic Publishers, Dordrecht ; Boston, **1989**, p. xii, 291.
[27] R. B. Weiss and D. S. Poster, *Cancer Treatment Reviews* **1982**, *9*, 37-56.
[28] T. W. Hambley, *Journal of the Chemical Society-Dalton Transactions* **2001**, 2711-2718.
[29] M. J. Clarke in *Metal complexes in cancer chemotherapy*, (Ed. B. K. Keppler), Vch, Weinheim ; New York, **1993**.
[30] R. E. Yasbin, C. R. Matthews and M. J. Clarke, *Chemico-Biological Interactions* **1980**, *31*, 355-365.
[31] J. K. Barton, *Pure and Applied Chemistry* **1989**, *61*, 563-564.
[32] B. M. Zeglis, V. C. Pierre and J. K. Barton, *Chemical Communications* **2007**, 4565-4579.
[33] F. R. Keene, J. A. Smith and J. G. Collins, *Coordination Chemistry Reviews* **2009**, *253*, 2021-2035.
[34] A. Wee Han and J. D. Paul, *European Journal of Inorganic Chemistry* **2006**, 4003-4018.
[35] A. D. Richards and A. Rodger, *Chemical Society Reviews* **2007**, *36*, 471-483.
[36] M. Groessl, E. Reisner, C. G. Hartinger, R. Eichinger, O. Semenova, A. R. Timerbaev, M. A. Jakupec, V. B. Arion and B. K. Keppler, *Journal of Medicinal Chemistry* **2007**, *50*, 2185-2193.
[37] W. A. Denny, *European Journal of Medicinal Chemistry* **2001**, *36*, 577-595.
[38] J. L. Cohen and J. Y. Jao, *Journal of Pharmacology and Experimental Therapeutics* **1970**, *174*, 206-&.
[39] L. W. Anderson, T. L. Chen, O. M. Colvin, L. B. Grochow, J. M. Collins, M. J. Kennedy and J. M. Strong, *Clinical Cancer Research* **1996**, *2*, 1481-1487.
[40] J. A. Montgomery in *Cancer Chemotherapeutic Agents*, (Ed. W. O. Foye), American Chemical Society, Washington, DC, **1995**.
[41] M. P. Hay, K. O. Hicks, K. Pchalek, H. H. Lee, A. Blaser, F. B. Pruijn, R. F. Anderson, S. S. Shinde, W. R. Wilson and W. A. Denny, *Journal of Medicinal Chemistry* **2008**, *51*, 6853-6865.
[42] D. Katsaros, M. V. Oletti, I. A. Rigault de la Longrais, A. Ferrero, A. Celano, S. Fracchioli, M. Donadio, R. Passera, L. Cattel and C. Bumma, *Ann Oncol* **2005**, *16*, 300-306.
[43] About DOXIL, *http://www.doxil.com/learn_doxil/about_doxil.jsp*, Last Accessed: **16/11/2009**
[44] D. C. Ware, W. R. Wilson, W. A. Denny and C. E. F. Rickard, *Journal of the Chemical Society-Chemical Communications* **1991**, 1171-1173.
[45] D. C. Ware, B. D. Palmer, W. R. Wilson and W. A. Denny, *Journal of Medicinal Chemistry* **1993**, *36*, 1839-1846.
[46] D. C. Ware, B. G. Siim, K. G. Robinson, W. A. Denny, P. J. Brothers and G. R. Clark, *Inorganic Chemistry* **1991**, *30*, 3750-3757.
[47] B. D. Palmer, W. R. Wilson, G. J. Atwell, D. Schultz, X. Z. Xu and W. A. Denny, *Journal of Medicinal Chemistry* **1994**, *37*, 2175-2184.
[48] B. D. Palmer, W. R. Wilson, R. F. Anderson, M. Boyd and W. A. Denny, *Journal of Medicinal Chemistry* **1996**, *39*, 2518-2528.
[49] G. A. Lawrance, *Advances in inorganic chemistry* **1989**, *34*, 145 - 194.
[50] N. Shinohara and J. Lilie, *Inorganic Chemistry* **1990**, *29*, 3812-3815.
[51] T. J. Dougherty in *Cancer Chemotherapeutic Agents*, (Ed. W. O. Foye), American Chemical Society, Washington, DC, **1995**.
[52] C. Patoux, J. P. Launay, M. Beley, S. Chodorowski-Kimmes, J. P. Collin, S. James and J. P. Sauvage, *Journal of the American Chemical Society* **1998**, *120*, 3717-3725.

[53] S. Ernst, V. Kasack and W. Kaim, *Inorganic Chemistry* **1988**, *27*, 1146-1148.
[54] V. N. Pitchkov, *Platinum Metal Reviews* **1996**, *40*, 181-188.
[55] E. A. Seddon and K. R. Seddon, *The Chemistry of Ruthenium*, Elsevier, Amsterdam ; New York, **1984**, p. 1373.
[56] J. G. Vos and J. M. Kelly, *Dalton Transactions* **2006**, 4869-4883.
[57] M. Srnec, J. Chalupsky and L. Rulisek, *Collection of Czechoslovak Chemical Communications* **2008**, *73*, 1231-1244.
[58] K. R. Hyde, E. W. Hooper, J. Waters and J. M. Fletcher, *Journal of the Less-Common Metals* **1965**, *8*, 428-&.
[59] A. S. Polo, M. K. Itokazu and N. Y. Murakami Iha, *Coordination Chemistry Reviews* **2004**, *248*, 1343-1361.
[60] C. A. Bignozzi, R. Argazzi and C. J. Kleverlaan, *Chemical Society Reviews* **2000**, *29*, 87-96.
[61] M. Grâtzel, *Accounts of Chemical Research* **2009**, *42*, 1788-1798.
[62] A. J. Bard and M. A. Fox, *Accounts of Chemical Research* **1995**, *28*, 141-145.
[63] M. Yoshida, S. Masaoka and K. Sakai, *Chemistry Letters* **2009**, *38*, 702-703.
[64] A. E. Friedman, J. C. Chambron, J. P. Sauvage, N. J. Turro and J. K. Barton, *Journal of the American Chemical Society* **1990**, *112*, 4960-4962.
[65] C. Hiort, P. Lincoln and B. Norden, *Journal of the American Chemical Society* **1993**, *115*, 3448-3454.
[66] P. T. Chou and Y. Chi, *European Journal of Inorganic Chemistry* **2006**, 3319-3332.
[67] S. Campagna, F. Puntoriero, F. Nastasi, G. Bergamini and V. Balzani, *Topics in Current Chemistry* **2007**, *280*, 117-214.
[68] E. A. Medlycott and G. S. Hanan, *Chemical Society Reviews* **2005**, *34*, 133-142.
[69] A. Harriman, A. Khatyr and R. Ziessel, *Dalton Transactions* **2003**, 2061-2068.
[70] P. W. Atkins, P. W. Atkins and J. De Paula, *Atkins' Physical chemistry*, Oxford University Press, Oxford ; New York, **2002**, p. xxi, 1149.
[71] E. M. Kober and T. J. Meyer, *Inorganic Chemistry* **1982**, *21*, 3967-3977.
[72] K. Mandal, T. D. L. Pearson, W. P. Krug and J. N. Demas, *Journal of the American Chemical Society* **1983**, *105*, 701-707.
[73] A. W. Adamson, *Journal of Chemical Education* **1983**, *60*, 797.
[74] S. J. Wang, *Jom* **2006**, *58*, 47-50.
[75] N. N. Greenwood and A. Earnshaw, *Chemistry of the Elements*, Pergamon Press, Oxford [Oxfordshire] ; New York, **1984**, p. xxi, 1542.
[76] D. F. Shriver and P. W. Atkins, *Inorganic chemistry*, Oxford University Press, New York, **1999**, p. xvii, 763 p.
[77] S. Kremer, W. Henke and D. Reinen, *Inorganic Chemistry* **1982**, *21*, 3013-3022.
[78] A. D. McNaught, A. Wilkinson and International Union of Pure and Applied Chemistry., *Compendium of chemical terminology : IUPAC recommendations*, Blackwell Science, Oxford [Oxfordshire] ; Malden, MA, **1997**, p. vii, 450.
[79] D. E. Richardson and H. Taube, *Coordination Chemistry Reviews* **1984**, *60*, 107-129.
[80] D. M. D'Alessandro and F. R. Keene, *Pure and Applied Chemistry* **2008**, *80*, 1-16.
[81] D. M. D'Alessandro and F. R. Keene, *Chemical Society Reviews* **2006**, *35*, 424-440.
[82] S. K. S. Zawacky and H. Taube, *Journal of the American Chemical Society* **1981**, *103*, 3379-3387.
[83] K. Rieder and H. Taube, *Journal of the American Chemical Society* **1977**, *99*, 7891-7894.

[84] H. Fischer, G. M. Tom and H. Taube, *Journal of the American Chemical Society* **1976**, *98*, 5512-5517.
[85] S. S. Isied and H. Taube, *Journal of the American Chemical Society* **1973**, *95*, 8198-8200.
[86] C. Creutz, *Journal of Physical Chemistry B* **2007**, *111*, 6713-6717.
[87] R. Zibaseresht, *Approaches to Photoactivated Cytotoxins*, University of Canterbury, Christchurch, **2006**.
[88] R. Zibaseresht and R. M. Hartshorn, *Dalton Trans* **2005**, 3898-3908.
[89] R. M. Hartshorn, R. Zibaseresht and W. T. Robinson, *Acta Crystallographica Section E-Structure Reports Online* **2005**, *61*, M981-M983.
[90] R. Zibaseresht and R. M. Hartshorn, *Australian Journal of Chemistry* **2005**, *58*, 345-353.
[91] R. M. Hartshorn and R. Zibaseresht, *Arkivoc* **2006**, 104-126.
[92] R. Zibaseresht, W. T. Robinson and R. M. Hartshorn, *Acta Crystallographica Section E-Structure Reports Online* **2006**, *62*, M1150-M1153.
[93] R. Zibaseresht and R. M. Hartshorn, *Acta Crystallographica Section E-Structure Reports Online* **2006**, *62*, I19-I22.
[94] H. Hofmeier and U. S. Schubert, *Chemical Society Reviews* **2004**, *33*, 373-399.
[95] F. Kröhnke, *Synthesis* **1976**, 1-24.
[96] R.-A. Fallahpour, *Synthesis* **2003**, 155-184.
[97] M. Heller and U. S. Schubert, *European Journal of Organic Chemistry* **2003**, 947-961.
[98] A. Thompson, *Coordination Chemistry Reviews* **1997**, *160*, 1-52.
[99] J. P. Collin, S. Guillerez, J. P. Sauvage, F. Barigelletti, L. De Cola, L. Flamigni and V. Balzani, *Inorg. Chem.* **1991**, *30*, 4230-4238.
[100] J. H. Wang and G. S. Hanan, *Synlett* **2005**, 1251-1254.
[101] R. Ballardini, V. Balzani, M. Clemente-Leon, A. Credi, M. T. Gandolfi, E. Ishow, J. Perkins, J. F. Stoddart, H.-R. Tseng and S. Wenger, *Journal of the American Chemical Society* **2002**, *124*, 12786-12795.
[102] J. S. Field, R. J. Haines, D. R. McMillin and G. C. Summerton, *Journal of the Chemical Society-Dalton Transactions* **2002**, 1369-1376.
[103] E. C. Constable, M. D. Ward and S. Corr, *Inorganica Chimica Acta* **1988**, *141*, 201-203.
[104] Q. Jiang, Z. Y. Wu, Y. M. Zhang, A. C. G. Hotze, M. J. Hannon and Z. J. Guo, *Dalton Transactions* **2008**, 3054-3060.
[105] Q. H. Wei, S. P. Argent, H. Adams and M. D. Ward, *New Journal of Chemistry* **2008**, *32*, 73-82.
[106] F. Dumur, C. R. Mayer, E. Dumas, F. Miomandre, M. Frigoli and F. Secheresse, *Organic Letters* **2008**, *10*, 321-324.
[107] H. Bertrand, D. Monchaud, A. De Cian, R. Guillot, J.-L. Mergny and M.-P. Teulade-Fichou, *Organic & Biomolecular Chemistry* **2007**, *5*, 2555-2559.
[108] B. Bosnich, C. K. Poon and M. L. Tobe, *Inorganic Chemistry* **1965**, *4*, 1102-1108.
[109] T. F. Lai and C. K. Poon, *Inorg. Chem.* **1976**, *15*, 1562-1566.
[110] C. K. Poon and M. L. Tobe, *Inorg. Chem.* **1968**, *7*, 2398-2404.
[111] E. H. Wong, G. R. Weisman, D. C. Hill, D. P. Reed, M. E. Rogers, J. S. Condon, M. A. Fagan, J. C. Calabrese, K.-C. Lam, I. A. Guzei and A. L. Rheingold, *Journal of the American Chemical Society* **2000**, *122*, 10561-10572.
[112] K. P. Wainwright, *Inorganic Chemistry* **1980**, *19*, 1396-1398.
[113] D. J. Bray, J. K. Clegg, K. A. Jolliffe, L. F. Lindoy and G. Wei, *Journal of Coordination Chemistry* **2008**, *61*, 3 - 13.
[114] G. R. Pabst, O. C. Pfuller and J. Sauer, *Tetrahedron Letters* **1998**, *39*, 8825-8828.

[115] G. R. Pabst and J. Sauer, *Tetrahedron Letters* **1998**, *39*, 6687-6690.
[116] G. R. Pabst and J. r. Sauer, *Tetrahedron Letters* **1998**, *39*, 8817-8820.
[117] G. R. Pabst, K. Schmid and J. Sauer, *Tetrahedron Letters* **1998**, *39*, 6691-6694.
[118] O. C. Pfu¨ller and J. r. Sauer, *Tetrahedron Letters* **1998**, *39*, 8821-8824.
[119] X. H. Zou, B. H. Ye, H. Li, J. G. Lin, Y. Xiong and L. N. Ji, *Journal of the Chemical Society-Dalton Transactions* **1999**, 1423-1428.
[120] Y. F. Suen, H. Hope, M. H. Nantz, M. J. Haddadin and M. J. Kurth, *Journal of Organic Chemistry* **2005**, *70*, 8468-8471.
[121] B. Sarkar, W. Kaim, T. Schleid, I. Hartenbach and J. Fiedler, *Zeitschrift Fur Anorganische Und Allgemeine Chemie* **2003**, *629*, 1353-1357.
[122] H. Bakkali, C. Marie, A. Ly, C. Thobie-Gautiera, J. Graton, M. Pipelier, S. Sengmany, E. Leonel, J. Y. Nedelec, M. Evain and D. Dubreuil, *European Journal of Organic Chemistry* **2008**, 2156-2166.
[123] B. Sarkar, S. Frantz, W. Kaim and C. Duboc, *Dalton Transactions* **2004**, 3727-3731.
[124] S. D. Ernst and W. Kaim, *Inorganic Chemistry* **1989**, *28*, 1520-1528.
[125] E. J. Corey, A. L. Borror and T. Foglia, *Journal of Organic Chemistry* **1965**, *30*, 288-&.
[126] H. Chao, G. Yang, G.-Q. Xue, H. Li, H. Zang, I. D. Williams, L.-N. Ji, X.-M. Chen and X.-Y. Li, *Journal of the Chemical Society, Dalton Transactions* **2001**, 1326-1331.
[127] M. Erez and B. Fuchs, *Tetrahedron Letters* **1971**, *12*, 4931-4934.
[128] S. Kohlmann, S. Ernst and W. Kaim, *Angewandte Chemie International Edition in English* **1985**, *24*, 684-685.
[129] D. P. Rillema, G. Allen, T. J. Meyer and D. Conrad, *Inorganic Chemistry* **1983**, *22*, 1617-1622.
[130] W. Kaim, S. Ernst, S. Kohlmann and P. Welkerling, *Chemical Physics Letters* **1985**, *118*, 431-434.
[131] E. C. Constable, H. Eriksson, C. E. Housecroft, B. M. Kariuki, E. Nordlander and J. Olsson, *Inorganic Chemistry Communications* **2001**, *4*, 749-752.
[132] H. Chao, Z.-R. Qiu, L.-R. Cai, H. Zhang, X.-Y. Li, K.-S. Wong and L.-N. Ji, *Inorganic Chemistry* **2003**, *42*, 8823-8830.
[133] H. Ozawa, Y. Yokoyama, M.-a. Haga and K. Sakai, *Dalton Transactions* **2007**, 1197-1206.
[134] N. Isoda, Y. Torii, T. Okada, M. Misoo, H. Yokoyama, N. Ikeda, M. Nojiri, S. Suzuki and K. Yamaguchi, *Dalton Transactions* **2009**, 10175-10177.
[135] H. Torieda, K. Nozaki, A. Yoshimura and T. Ohno, *The Journal of Physical Chemistry A* **2004**, *108*, 4819-4829.
[136] H. Torieda, A. Yoshimura, K. Nozaki, S. Sakai and T. Ohno, *The Journal of Physical Chemistry A* **2002**, *106*, 11034-11044.
[137] J. E. Baggott, G. K. Gregory, M. J. Pilling, S. Anderson, K. R. Seddon and J. E. Turp, *Journal of the Chemical Society-Faraday Transactions Ii* **1983**, *79*, 195-210.
[138] J. Van Houten and R. J. Watts, *Journal of the American Chemical Society* **1976**, *98*, 4853-4858.
[139] H.-J. Kim, W. Kim, A. J. Lough, B. M. Kim and J. Chin, *Journal of the American Chemical Society* **2005**, *127*, 16776-16777.
[140] H. Yoneda, *Bulletin of the Chemical Society of Japan* **1967**, *40*, 2442-&.
[141] L. G. Reiter, S. A. Bobyr', T. E. Shubina and V. N. Rodionov, *Theoretical and Experimental Chemistry (Translation of Teoreticheskaya i Eksperimental'naya Khimiya)* **2005**, *41*, 7-12.

[142] B. Das Sarma, G. J. Tennenhouse and J. C. Bailar, *Journal of the American Chemical Society* **1968**, *90*, 1362-1363.
[143] B. Das Sarma and J. C. Bailar, *Journal of the American Chemical Society* **1969**, *91*, 5958-5963.
[144] A. S. d. Sousa, S. A. Reisinger, M. A. Fernandes, C. B. Perry, P. R. Varadwaj and H. M. Marques, *Dalton Transactions* **2009**, 10208-10218.
[145] R. Bagai, K. A. Abboud and G. Christou, *Chemical Communications* **2007**, 3359-3361.
[146] N. Friis, PCT Int. Appl. (**1988**), WO8805041
[147] L. M. Rice, B. H. Armbrecht, C. H. Grogan and E. E. Reid, *Journal of the American Chemical Society* **1953**, *75*, 1750-1750.
[148] H. Maeda, S. Furuyoshi, Y. Nakatsuji and M. Okahara, *Bulletin of the Chemical Society of Japan* **1983**, *56*, 3073-3077.
[149] U. Asseline, M. Chassignol, J. Draus, M. Durand and J. C. Maurizot, *Bioorganic & Medicinal Chemistry* **2003**, *11*, 3499-3511.
[150] P. Paul, B. Tyagi and P. Natarajan, *Indian Journal of Chemistry, Section A Inorganic, Bio-inorganic, Physical, Theoretical & Analytical Chemistry* **2003**, *42A*, 2283-2289.
[151] J. A. Broomhead, *Journal of the American Chemical Society* **1968**, *90*, 4480-4482.
[152] N. E. Dixon, W. G. Jackson, M. J. Lancaster, G. A. Lawrance and A. M. Sargeson, *Inorganic Chemistry* **1981**, *20*, 470-476.
[153] N. E. Dixon, W. G. Jackson, G. A. Lawrance and A. M. Sargeson, *Inorganic Syntheses* **1983**, *22*, 103-107.
[154] F. Galsboel, C. H. Petersen and K. Simonsen, *Acta Chemica Scandinavica* **1996**, *50*, 567-570.
[155] P. Comba, N. J. Curtis, W. G. Jackson and A. M. Sargeson, *Australian Journal of Chemistry* **1986**, *39*, 1297-1306.
[156] J. Liu, X.-H. Zou, Q.-L. Zhang, W.-J. Mei, J.-Z. Liu and L.-N. Ji, *Metal-Based Drugs* **2000**, *7*, 343-348.
[157] L. S. Kelso, D. A. Reitsma and F. R. Keene, *Inorganic Chemistry* **1996**, *35*, 5144-5153.
[158] P. Kruger, *Personal Communication*.
[159] A. Mihailovic, I. Vladescu, M. McCauley, E. Ly, M. C. Williams, E. M. Spain and M. E. Nunez, *Langmuir* **2006**, *22*, 4699-4709.
[160] D. M. D'Alessandro, A. C. Topley, M. S. Davies and F. R. Keene, *Chemistry - A European Journal* **2006**, *12*, 4873-4884.
[161] J. A. Zampese, F. R. Keene and P. J. Steel, *Dalton Transactions* **2004**, 4124-4129.
[162] J. A. Broomhead, F. P. Dwyer and J. W. Hogarth, *Inorganic Syntheses* **1960**, *6*, 183-186.
[163] J. A. Broomhead, F. P. Dwyer and J. W. Hogarth, *Inorganic Syntheses* **1960**, *6*, 186-188.
[164] C. M. Dupureur and J. K. Barton, *Inorganic Chemistry* **1997**, *36*, 33-43.
[165] I. Haq, P. Lincoln, D. Suh, B. Norden, B. Z. Chowdhry and J. B. Chaires, *Journal of the American Chemical Society* **1995**, *117*, 4788-4796.
[166] A. M. Funston, C. Cullinane, K. P. Ghiggino, W. D. McFadyen, S. S. Stylli and P. A. Tregloan, *Australian Journal of Chemistry* **2005**, *58*, 206-212.
[167] A. M. Funston, R. W. Gable, W. D. McFadyen and P. A. Tregloan, *Australian Journal of Chemistry* **1999**, *52*, 817-822.
[168] E. Kimura, S. Young and J. P. Collman, *Inorganic Chemistry* **1970**, *9*, 1183-1191.
[169] B. Bosnich, J. M. Harrowfield and H. Boucher, *Inorganic Chemistry* **1975**, *14*, 815-828.
[170] N. Shinohara and J. Lilie, *Inorganic Chemistry* **1979**, *18*, 434-438.

[171] Bruker (2007) APEX2 (Version 2.1-4), SAINT (Version 7.34A), SADABS (Version 2004/1) Bruker ASX Inc. Madison, Wisconsin, USA
[172] O. V. Dolomanov, L. J. Bourhis, R. J. Gildea, J. A. K. Howard and H. Puschmann, *Journal of Applied Crystallography* **2009**, *42*, 339-341.
[173] D. D. Perrin and W. L. F. Armarego, *Purification of Laboratory Chemicals. 3rd Ed*, **1988**, p. 391 pp.
[174] E. K. Barefield, F. Wagner, A. W. Herlinger and A. R. Dahl, *Inorganic Syntheses* **1976**, *16*, 220-225.